

# **DESIGN AND ANALYSIS OF MULTILEVEL CONVERTER FOR GRID APPLICATIONS**

**by**

**JYOTI KULKARNI**

**(2K13/PhD/EE/01)**

**Department of Electrical Engineering**

*Submitted*

*In fulfillment of the requirements of the degree of*

**DOCTOR OF PHILOSOPHY**

In

**Electrical Engineering**



Under the Supervision of:  
**Prof. Narendra Kumar and Prof. Bhim Singh**

**DEPARTMENT OF ELECTRICAL ENGINEERING  
DELHI TECHNOLOGICAL UNIVERSITY  
DELHI-110042, INDIA**

**December, 2020**

## **CERTIFICATE**

It is certified that the thesis entitled “**Design and Analysis of Multilevel Converter for Grid Applications,**” being submitted by **Mrs. Jyoti Kulkarni** for award of the degree of **Doctor of Philosophy** in the Department of Electrical Engineering, Delhi Technological University, Delhi, is a record of the student work carried out by her under our supervision and guidance. The matter embodied in this thesis has not been submitted for the award of any other degree or diploma.

**Dated:**

**(Dr. Narendra Kumar)**  
**Professor**  
**Electrical Engineering Department**  
**Delhi Technological University**  
**Main Bawana Road,**  
**Shahbad Daultpur,**  
**Delhi – 110042, India**

**(Dr. Bhim Singh)**  
**Professor**  
**Electrical Engineering Department**  
**Indian Institute of Technology Delhi**  
**Hauz Khas, New Delhi-110016, India**

## ACKNOWLEDGEMENT

Completion of Ph.D. research work is a cherished milestone. It is not the end of research, rather it is opening up of the world of research. From here on, you can think of a way forward, which may be guided or not. Till now this journey has been under supervision, help was available when needed. There was a route which had defined stops. There were people to tell, whether the journey is reaching the destination or how far you are. I feel privileged to have undertaken this journey under two able persons. Now is the right time and place to express my gratitude towards them.

First, I wish to express my sincere gratitude to my supervisor **Prof. Narendra Kumar** for guiding me and being a pillar of strength during this journey right from the course work to completion of the Ph.D. work. It is because of him that I got to work with Prof. Bhim Singh. He has always been there to support and guide me throughout. I will always remain indebted to him.

I wish to express my deepest gratitude and indebtedness to **Prof. Bhim Singh** for providing me guidance and constant supervision to carry out the Ph.D. work. Working under him has been a wonderful experience, which has provided deep insight into the world of research. Determination, dedication, innovativeness, resourcefulness, and discipline of **Prof. Bhim Singh** have been the inspiration for me to complete this work. His consistent encouragement, continuous monitoring and commitments to excellence have always motivated me to improve my work and use the best of my capabilities. Due to his blessing, I have earned various experiences other than research, which will help me throughout my life. His early morning phone calls used to set the tone for the whole day and kept me alert. His eye for details and knack of spotting the errors which went unnoticed till then, sets him apart from others. It speaks volumes about his involvement.

I wish to thank my SRC Members – **Prof. Madhusudan Singh** (Chairman, DRC, EED and Departmental expert, DTU), **Prof. Neeta Pandey** (Expert outside the department, DTU), **Prof. S. P. Srivastava** (IIT Roorkee, Expert outside DTU) for their constant motivation and whole-hearted support during my Ph.D. research work.

I also wish to express my gratitude to Head of the Department, EED, DTU **Prof. Uma Nangia** and ex-HoD **Prof. Madhusudan Singh** and other DRC members for their continued guidance and help during the entire Ph.D. research work.

I also wish to thank **all the Faculty members and staff of Electrical Engineering Department, DTU** for their direct and indirect help during the tenure of my research work.

I also wish to thank **Dr. Manoj Badoni, Dr. Md. Tausif Ahmad, Dr. Ambrish Devanshu and Mr. Hemant Saxena** from EED, DTU and **Dr. Piyush Kant and Mr. Shivam Kumar Yadav, EED, IIT Delhi** for extending all the help and support. Special thanks are due to Mr. Shivam Kumar Yadav for helping in OPAL-RT simulation.

I wish to thank **my family** for all the support extended during the course of this research work. Special thanks to my son **Shubham** for keeping his patience during the writing of the thesis and entire research work. I whole-heartedly thank my husband **Sh. Ashish R. Kulkarni** for his constant full support for the entire duration of my research work. Without his help I would not have been able to complete the research work.

I wish to thank my Father **late Sh, Shayam Mohan Nigam** for his constant motivation and guidance. It was his wish to see me complete the Ph.D. research work. I dedicate this thesis to him. I wish to thank my mother **Smt. Kunti Nigam** for all the help, support and numerous prayers she has offered for me. Thanks are due to my elder sister **Dr. Priti Nigam**, brother **Sh. Anoop Nigam** and sister -in-law **Mrs. Anjana** for all the help, support and patience shown and also being on my side when required the most. I would

like to thank them all for giving me the inner strength and wholehearted support. Their trust in my capabilities had been a key factor to all my achievements.

I also thank the **Principal, and HoD of GNDIT, Rohini**, Delhi for helping me during the course of my Ph.D. research work.

Last I would like to thank the God Almighty for guiding me through-out and keeping me blessed.

Dt.:

**Jyoti Kulkarni**

## ABSTRACT

A lot of research is being carried out on power converters employed for grid interfacing applications and multilevel converter is perceived as gen-next technique for grid integration. Multilevel converters are advantageous over the traditional two-level converter due to increased scalability, lower harmonics content, reduced filter components, low switching frequency, less voltage stress across switching device and an increased efficiency. Multilevel converters are widely used in recent years for high voltage and high power grid applications such as integration of renewable energy sources, FACT devices, HVDC, STATCOM and BESS. In the proposed work, the grid integration of photovoltaic source is considered. Solar energy provides the clean, ever available, reliable and environment-friendly electricity generation near the load centre. Many multilevel converters (MLC) topologies like, diode clamped, flying capacitor and cascaded H-bridge converter are reported in the literature. In the proposed work, cascaded H-bridge multilevel converter is employed as it is the best suitable configuration for photovoltaic (PV) power generation because multistring PV plant naturally provides the isolated DC source for each bridge of the CHB converter.

A set of 7-level, 9-level, 19-level and 43-level multilevel converters for integration of large photovoltaic system are investigated in the proposed work.

Multilevel converter has the advantage of direct interfacing with high and medium voltage grid. Hence transformerless integration with the grid is employed in the proposed work to avoid a bulky and expensive step-up transformer. This system is a single-stage converter to eliminate DC-DC stage, for reducing the cost, losses and also control complexity in the system.

The selection of optimum number of levels for given voltage rating is investigated in the proposed work to obtain the proper ratio of performance versus cost and complexity. The

number of levels in the multilevel converter is selected in proposed work, considering all design considerations like the cost of IGBTs, arithmetic and logical operations (ALOs), THDs, and device voltage utilization factor (DVUF).

As well-known algorithms converge fast, so these algorithms like perturb and observe (P&O), and incremental conductance (INC) methods are employed in proposed work. Each PV array is provided with a separate maximum power point tracking (MPPT) algorithm to overcome the unpredictable irradiance level variations, ambient temperature, shading effect, and other relevant factors in proposed work. Decoupled current control with SRF-PLL is used for VSC control in the proposed work.

This work focuses on investigation of a suitable modulation technique with improved THD of MLC output voltage and grid current, and low switching frequency for the symmetrical CHB multilevel converter. The phase shifted PWM, SHE-PWM and NLM modulation techniques are investigated in this work. The major focus of this research work is on the investigations of high power converter based PV grid tied system for photovoltaic application, while satisfying the IEEE standards. The lower switching frequency employed for switching the converter, reduces the switching losses and reduces the acoustic noise. It ultimately reduces the size, hence the cost of the filter. The reduction of switching losses at higher power rating system is significant.

# TABLE OF CONTENTS

Certificate		i
Acknowledgement		ii
Abstract		v
Table of Contents		vii
List of Figures		xv
List of Tables		xxi
List of Abbreviations		xxii
List of Symbols		xxiii
<b>CHAPTER-I INTRODUCTION</b>		
1.1	GENERAL	1
1.2	STATE OF ART	4
1.3	GRID INTERFACED PHOTOVOLTAIC CONVERTERS	6
1.4	MULTILEVEL CONVERTERS	9
	1.4.1 Multilevel Converter Topologies	9
	1.4.2 Multilevel Converter Applications	10
1.5	SCOPE OF WORK	10
	1.5.1 System Configuration	11
	1.5.2 MPPT Algorithm	12
	1.5.3 VSC Control Algorithm	12
	1.5.4 PWM Control	12
1.6	OUTLINE OF CHAPTERS	13
<b>CHAPTER-II LITERATURE REVIEW</b>		
2.1	GENERAL	16
2.2	LITERATURE SURVEY	16
	2.2.1 Review of Two Level VSCs for Grid Connected Converter	17



2.2.2	Review of MPPT Techniques for Grid Connected Converter	18
2.2.3	Review of Multilevel and Multipulse VSC for Grid Connected Converter	20
2.2.3.1	Review of multilevel converter topologies	21
2.2.3.2	Review of optimum selection of numbers of levels in multilevel converter	22
2.2.3.3	Review of VSC control scheme	24
2.2.3.4	Review of PWM techniques	25
2.3	IDENTIFIED RESEARCH AREAS	28
2.4	PROBLEM FORMULATION	29
2.5	CONCLUSIONS	30
<b>CHAPTER-III CONTROL AND DESIGN OF SEVEN LEVEL CASCADED MULTI LEVEL CONVERTER</b>		
3.1	INTRODUCTION	31
3.2	SYSTEM CONFIGURATION	32
3.3	DESIGN OF 7-LEVEL SYMMETRICAL CHB MULTILEVEL CONVERTER FOR GRID INTEGRATED PV SYSTEM	33
3.3.1	Selection of $V_{dc}$ Voltage for 7-Level Converter	33
3.3.2	Design Calculations and Selection of PV Array for 7-Level Converter	33
3.3.3	Design of Capacitor for 7-Level Converter	34
3.3.4	Design of Interfacing Inductor	35
3.4	CONTROL OF 7- LEVEL SYMMETRICAL CHB MULTILEVEL CONVERTER FOR GRID INTEGRATED PV SYSTEM	36
3.4.1	Implementation of Improved P&O MPPT Algorithm	36
3.4.2	Implementation of VSC Algorithm	37
3.4.3	Implementation of Phase Shifted Multi-Carrier PWM Control 7-Level Converter	39
3.5	MATLAB MODELLING OF 7-LEVEL SYMMETRICAL CHB MULTILEVEL CONVERTER FOR GRID INTEGRATED PV SYSTEM	41

3.5.1	MATLAB Model of Grid Connected Converter	41
3.5.2	MATLAB Model of PV Array Connected Seven-Level H-Bridge Converter	42
3.5.3	MATLAB Model of the Control	44
3.5.4	MATLAB Model of the MPPT Controller	45
3.5.5	MATLAB Model of Phase-shifted PWM	46
3.6	RESULTS AND DISCUSSION	47
3.6.1	Steady state performances for 7-level converter	47
3.6.2	Dynamic performances for 7-level converter	48
3.6.3	Power quality performances for 7-level converter	51
3.6.4	Validation of Results in HIL on OPAL-RT Simulator	52
3.7	CONCLUSIONS	55
<b>CHAPTER-IV</b>	<b>CONTROL AND DESIGN OF NINE LEVEL CASCADED MULTI LEVEL CONVERTER BASED PV SYSTEM</b>	
4.1	GENERAL	56
4.2	SYSTEM CONFIGURATION	57
4.3	DESIGN OF 9-LEVEL SYMMETRICAL CHB MULTILEVEL CONVERTER FOR GRID INTEGRATED PV SYSTEM	58
4.3.1	Selection of $V_{dc}$ Voltage for 9-Level Converter	58
4.3.2	Design Calculations and Selection of PV Array for 9-Level Converter	58
4.3.3	Design of DC-Link Capacitor for 9-Level Converter	60
4.3.4	Design of Interfacing Inductor	60
4.4	CONTROL OF 9-LEVEL SYMMETRICAL CHB MULTILEVEL CONVERTER FOR GRID INTEGRATED PV SYSTEM	61
4.4.1	Implementation of Improved P&O MPPT Algorithm	61
4.4.2	Implementation of VSC Algorithm	61
4.4.3	Implementation of PWM Control for 9-Level Converter	63

	4.4.3.1	Phase shifted multi carrier PWM	63
	4.4.3.2	SHE-PWM	64
	4.4.3.3	NLM	67
4.5		MODELLING OF 9-LEVEL SYMMETRICAL CHB MULTILEVEL CONVERTER FOR GRID INTEGRATED PV SYSTEM	69
	4.5.1	Model of Grid Connected Converter	70
	4.5.2	Model of PV Array Connected Nine-Level H-Bridge Converter	71
	4.5.3	Model of the Control Algorithm	72
	4.5.4	Model of the MPPT Controller	72
	4.5.5	Model of PWM Technique	73
	4.5.6	Model of Phase-shifted PWM	74
	4.5.7	Model of SHE-PWM	75
	4.5.8	Model of NLM	76
4.6		RESULTS AND DISCUSSION	77
	4.6.1	Steady state performance for 9-level converter	77
	4.6.2	Dynamic performance for 9-level converter	77
	4.6.3	Power quality performance for 9-level converter	81
	4.6.4	Validation of Results of SHE-PWM in HIL on OPAL-RT Simulator Platform	81
4.7		CONCLUSIONS	89
<b>CHAPTER-V CONTROL AND DESIGN OF NINETEEN LEVEL CASCADED MULTI LEVEL CONVERTER BASED PV SYSTEM</b>			
5.1		GENERAL	91
5.2		SELECTION CRITERIA OF OPTIMUM NUMBERS OF LEVELS	92
5.3		SYSTEM CONFIGURATION	94

5.4	DESIGN OF 19-LEVEL SYMMETRICAL CHB MULTILEVEL CONVERTER FOR GRID INTEGRATED PV SYSTEM	95
5.4.1	Selection of $V_{dc}$ Voltage for 19-Level Converter	96
5.4.2	Design Calculations and Selection of PV Array for 19-Level Converter	96
5.4.3	Design of Capacitor for 19-Level Converter	97
5.4.4	Design of Interfacing Inductor	98
5.5	CONTROL OF 19- LEVEL SYMMETRICAL CHB  MULTILEVEL CONVERTER FOR GRID  INTEGRATED PV SYSTEM	98
5.5.1	Implementation of Improved P&O MPPT Algorithm	99
5.5.2	Implementation of VSC Control Algorithm	99
5.5.3	Implementation of Phase Shifted Multi- Carrier PWM Control for 19-Level Converter	101
5.6	MODELLING OF 19-LEVEL SYMMETRICAL CHB MULTILEVEL CONVERTER FOR GRID INTEGRATED PV SYSTEM	102
5.6.1	Model of Grid Connected Converter	102
5.6.2	Model of PV Array Connected Nineteen- Level H-Bridge Converter	102
5.6.3	Model of the Control Algorithm	103
5.6.4	Model of the MPPT Controller	104
5.6.5	Model of Phase-shifted PWM	104
5.7	RESULTS AND DISCUSSION	106
5.7.1	Steady state performance for 19-level converter	109
5.7.2	Dynamic performance for 19-level converter	110
5.7.3	Power quality performance for 19-level converter	112
5.7.4	Validation of Results in HIL on OPAL-RT Simulator	114
5.8	CONCLUSIONS	117

**CHAPTER-VI CONTROL AND DESIGN OF FORTY THREE LEVEL  
CASCADED MULTI LEVEL CONVERTER BASED PV  
SYSTEM**

6.1	GENERAL	118
6.2	SELECTION CRITERIA OF OPTIMUM NUMBERS OF LEVELS	119
6.3	SYSTEM CONFIGURATION	121
6.4	DESIGN OF 43-LEVEL SYMMETRICAL CHB MULTILEVEL CONVERTER FOR GRID INTEGRATED PV SYSTEM	123
	6.4.1 Selection of $V_{dc}$ Voltage for 43-Level Converter	123
	6.4.2 Design Calculations and Selection of PV Array for 43-Level Converter	123
	6.4.3 Design of Capacitor for 43-Level Converter	124
	6.4.4 Design of Interfacing Inductor	125
6.5	CONTROL OF 43- LEVEL SYMMETRICAL CHB MULTILEVEL CONVERTER FOR GRID INTEGRATED PV SYSTEM	126
	6.5.1 Implementation of Incremental Conductance MPPT Algorithm	127
	6.5.2 Implementation of VSC Control Algorithm	127
	6.5.3 Implementation of Phase Shifted Multi- Carrier PWM Control for 43-Level Converter	129
6.6	MODELLING OF 43-LEVEL SYMMETRICAL CHB MULTILEVEL CONVERTER FOR GRID INTEGRATED PV SYSTEM	130
	6.6.1 Model of Grid Connected Converter	130
	6.6.2 Model of PV Array Connected 43-Level H-Bridge Converter	130
	6.6.3 Model of the Control Algorithm	132
	6.6.4 Model of the MPPT Controller	133
	6.6.5 Model of Phase-shifted PWM	133
6.7	RESULTS AND DISCUSSION	133
	6.7.1 Steady state performance for 43-level converter	135
	6.7.2 Dynamic performance for 43-level converter	136

6.7.3	Power quality performance for 43-level converter	139
6.7.4	Validation of Results in HIL on OPAL-RT Simulator	141
6.8	CONCLUSIONS	144
<b>CHAPTER-VII COMPARATIVE STUDY OF DIFFERENT CONVERTERS FOR PV SYSTEMS</b>		
7.1	GENERAL	145
7.2	COMPARISON OF CONVERTERS FOR DIFFERENT LEVELS	146
7.3	COMPARISON OF CONVERTER ON DIFFERENT PWM TECHNIQUES	147
7.3.1	Frequency Based Comparison	147
7.3.2	THD Based Comparison	148
7.3.3	Complexity Based Comparison	148
7.4	RESULTS AND DISCUSSION	148
7.4.1	Different Number of Levels	149
7.4.2	Different Modulation Techniques	152
	7.4.2.1 PWM strategies	152
	7.4.2.2 Power quality	154
7.4.3	Reduction in Filter Size	157
7.5	CONCLUSIONS	157
<b>CHAPTER-VIII MAIN CONCLUSIONS AND SUGGESTIONS FOR FURTHER WORK</b>		
8.1	GENERAL	159
8.2	MAIN CONCLUSIONS	160
8.3	SUGGESTIONS FOR FURTHER WORK	163
	<b>REFERENCES</b>	164
	<b>APPENDIX</b>	176
	<b>LIST OF PUBLICATIONS</b>	178



## LIST OF FIGURES

- Fig. 1.1 Source wise installed power generation capacity (MW) in India as on 31-12-2019
- Fig. 1.2 Source-wise cumulative renewable energy generation (MW as on 31-12-2019)
- Fig. 1.3 Top 10 states solar Installation (capacity in MW as of 31-12-2019)
- Fig. 1.4 Inverter configurations for Solar PV array connection (a) Central (a-c) Inverter, (b) Double-stage multi-string, (c) Single stage multi-string
- Fig. 1.5 Control block diagram for SPV generation system
- Fig. 3.1 Seven level grid interfaced converter PV system
- Fig. 3.2 Control algorithm for 7-level converter
- Fig. 3.3 Flowchart for improved P&O MPPT algorithm
- Fig. 3.4 Control algorithm for generating  $I_{dc}^*$  for 7-level converter
- Fig. 3.5 Generation of pulses for 7-level converter
- Fig. 3.6 Phase shifted PWM scheme for 7-level converter
- Fig. 3.7 MATLAB implementation of Grid-connected converter for 7-level converter
- Fig. 3.8 PV array fed 7-level CHB multilevel converter
- Fig. 3.9 Single H-bridge module
- Fig. 3.10 MATLAB implementation of control algorithm for 7-level converter
- Fig. 3.11 MATLAB implementation of MPPT controller for 7-level converter
- Fig. 3.12 MATLAB model of phase shifted PWM for 7-level
- Fig. 3.13 Steady-state performance at insolation level  $1000 \text{ W/m}^2$  and temperature  $25^\circ\text{C}$  for 7-level symmetrical CHB grid-tied system
- Fig. 3.14 Dynamic performance when insolation level is changed from 1000 to (a-b)  $400 \text{ W/m}^2$  at 0.6 sec for 7-level symmetrical CHB grid-tied system
- Fig. 3.14 Dynamic performance when insolation level is changed from 400 to (c-d)  $1000 \text{ W/m}^2$  at 0.6 sec for 7-level symmetrical CHB grid-tied system
- Fig. 3.15 Waveform and harmonic spectra of (a) line voltage (b) line current (a-c) (c) converter current
- Fig. 3.16 Steady state performance of  $V_{pv}$ ,  $I_{pv}$ ,  $i_{sa}$  and converter voltage at  $25^\circ\text{C}$



- and  $1000\text{W/m}^2$
- Fig. 3.17 Steady state performance of  $V_{ca}$ ,  $V_{cb}$  and  $V_{cc}$  voltage at  $25^\circ\text{C}$  and  $1000\text{W/m}^2$
- Fig. 3.18 Steady state performance of  $i_{sa}$ ,  $i_{sb}$  and  $i_{sc}$  at converter  $25^\circ\text{C}$  and  $1000\text{W/m}^2$
- Fig. 3.19 Dynamic performance of  $V_{pv}$ ,  $I_{pv}$ ,  $i_{sa}$  and voltage at irradiance change from  $1000\text{W/m}^2$  to  $500\text{W/m}^2$
- Fig. 3.20 Dynamic performance of  $V_{pv}$ ,  $I_{pv}$ ,  $i_{sa}$  and converter voltage at irradiance change from  $500\text{W/m}^2$  to  $1000\text{W/m}^2$
- Fig. 3.21 Converter phase voltage THD
- Fig. 3.22 Converter line voltage THD
- Fig. 3.23 Grid current THD
- Fig. 4.1 9-Level Grid Interfaced Converter PV System
- Fig. 4.2 Control algorithm for 9-level CHB converter
- Fig. 4.3 control algorithm for generating  $I_{dc}^*$  for 9-level converter
- Fig. 4.4 Pulse generation for PSPWM of 9-level CHB multilevel converter
- Fig. 4.5 Staircase waveform generation
- Fig. 4.6 Flowchart for SHE-PWM
- Fig. 4.7 Flowchart for NLM
- Fig. 4.8 MATLAB implementation of grid-connected 9-level CHB multilevel converter
- Fig. 4.9 PV array fed 9-level CHB multilevel converter
- Fig. 4.10 MATLAB implementation of control algorithm of 9-level CHB multilevel converter
- Fig. 4.11 MATLAB model for MPPT controller of 9-level CHB multilevel converter
- Fig. 4.12 MATLAB model for Phase shifted PWM of 9-level CHB multilevel converter
- Fig. 4.13 MATLAB model for SHE-PWM of 9-level CHB multilevel converter
- Fig. 4.14 MATLAB model for NLM of 9-level CHB multilevel converter
- Fig. 4.15 Steady state response for phase shifted PWM
- Fig. 4.16 Steady state response for SHE-PWM
- Fig. 4.17 Steady state response for NLM

- Fig. 4.18 (a-d) Dynamic response for the SHE-PWM technique for (a) and (b) decrease in insolation level from  $1000 \text{ W/m}^2$  to  $400 \text{ W/m}^2$ , (c) and (d) increase in insolation level from  $400 \text{ W/m}^2$  to  $1000 \text{ W/m}^2$  at  $0.6 \text{ s}$
- Fig. 4.19 (a-c) Waveforms and harmonic spectra for converter side voltage for (a) SHE-PWM (b) PSPWM (c) NLM
- Fig. 4.20 (a-c) Waveforms and harmonic spectra for supply Voltage for (a) SHE-PWM (b) NLM (c) PSPWM
- Fig. 4.21 (a-c) Waveforms and harmonic spectra for supply current for (a) SHE (b) PSPWM (c) NLM
- Fig.4.22 (a-b) Steady-state response (a) PV voltage, PV current, grid current and grid voltage (b) Converter voltage
- Fig.4.23 (a-b) Dynamic response (a) PV voltage for three phase array1 (b) PV current for three phase array1
- Fig.4.24 (a-d) Converter voltage THDs (a) SHE-PWM phase voltage (b) SHE-PWM line voltage (c) NLM-PWM phase voltage and (d) PS PWM phase voltage
- Fig.4.25 Grid current THD
- Fig. 4.26 (a-d) OPAL-RT results (a) & (b) Converter line voltage THD of NLM-PWM and PS PWM, (c) and (d) Grid current THD for NLM-PWM and PS PWM
- Fig. 5.1 19-level grid interfaced converter PV system
- Fig. 5.2 Control algorithm for 19-level CHB multilevel converter
- Fig. 5.3 Generation of  $I_{dc}^*$  for 19-level CHB multilevel converter
- Fig.5.4 Scheme for the generation of PWM signals for 19-level CHB multilevel converter
- Fig. 5.5 MATLAB model of PV array fed 19-level CHB multilevel converter
- Fig. 5.6 PV array fed 19-level CHB multilevel converter
- Fig. 5.7 MATLAB model of control algorithm for 19-level CHB multilevel converter
- Fig. 5.8 MATLAB model of MPPT controller for 19-level converter
- Fig. 5.9 MATLAB model for Phase shifted PWM for 19-level CHB multilevel converter

- Fig. 5.10 Steady-state response of the system of the 19-level CHB multilevel converter
- Fig. 5.11 Dynamic response for the SHE-PWM technique for (a) and (b) decrease in insolation level from  $1000 \text{ W/m}^2$  to  $500 \text{ W/m}^2$ , (c) and (d) increase in insolation level from  $500 \text{ W/m}^2$  to  $1000 \text{ W/m}^2$  at 0.7 s
- Fig. 5.12 Waveform and harmonic spectra of 19-level and 11kV system (a) line voltage (b) line current (c) converter voltage
- Fig. 5.13 Steady state performance of  $V_{pv}$ ,  $I_{pv}$ ,  $i_{sa}$ ,  $v_{ca}$  at  $25^\circ\text{C}$  and  $1000\text{W/m}^2$
- Fig. 5.14 Steady state performance of  $i_{sa}$ ,  $v_{sa}$ ,  $I_{pv}$ , and converter voltage at  $25^\circ\text{C}$  and  $1000\text{W/m}^2$
- Fig. 5.15 Steady state performance of  $i_{sa}$ ,  $i_{sb}$  and  $i_{sc}$  at  $25^\circ\text{C}$  and  $1000\text{W/m}^2$
- Fig. 5.16 Dynamic performance of  $v_{ca}$ ,  $v_{cb}$  and  $v_{cc}$  voltage at irradiance change from  $1000\text{W/m}^2$  to  $500 \text{ W/m}^2$
- Fig. 5.17 Dynamic performance of  $V_{pv}$ ,  $I_{pv}$ ,  $i_{sa}$  and  $v_{ca}$  at irradiance change from  $500\text{W/m}^2$  to  $1000 \text{ W/m}^2$
- Fig. 5.18 Dynamic performance of  $i_{sa}$ ,  $i_{sb}$  and  $i_{sc}$  at irradiance change from  $500\text{W/m}^2$  to  $1000 \text{ W/m}^2$
- Fig. 5.19 Dynamic performance of  $i_{sa}$ ,  $i_{sb}$  and  $i_{sc}$  at irradiance change from  $500\text{W/m}^2$  to  $1000 \text{ W/m}^2$  and  $1000\text{W/m}^2$  to  $500\text{W/m}^2$  and  $25^\circ\text{C}$
- Fig. 5.20 Dynamic performance of  $i_{sa}$ ,  $v_{sa}$ ,  $I_{pv}$  and converter voltage at irradiance change from  $1000\text{W/m}^2$  to  $500 \text{ W/m}^2$  and  $25^\circ\text{C}$
- Fig. 5.21 Dynamic performance of  $i_{sa}$ ,  $v_{sa}$ ,  $I_{pv}$  and converter voltage at irradiance change from  $500\text{W/m}^2$  to  $1000 \text{ W/m}^2$  and  $1000\text{W/m}^2$  to  $500\text{W/m}^2$  and  $25^\circ\text{C}$
- Fig. 5.22 Converter phase voltage THD
- Fig. 5.23 Converter line voltage THD
- Fig. 5.24 Grid current THD
- Fig. 6.1 43-level grid interfaced CHB multilevel converter
- Fig. 6.2 Control algorithm for 43-level CHB multilevel converter
- Fig. 6.3 Control algorithm for generating  $I_{dc}^*$  for 43-level CHB multilevel converter
- Fig.6.4 Flowchart for incremental conductance algorithm

- Fig. 6.5 Scheme for the generation of PWM signals for 43-level CHB multilevel converter
- Fig. 6.6 PV array fed 43-level CHB multilevel converter
- Fig. 6.7 MATLAB model of Single PV array with H-bridge
- Fig. 6.8 MATLAB model of Control algorithm of 43-level CHB multilevel converter
- Fig. 6.9 Single module of separate MPPT algorithm with the controller
- Fig. 6.10 Pulse generation of single H-bridge
- Fig. 6.11 System performance at constant insolation level  $1000 \text{ W/m}^2$
- Fig. 6.12 System response to an insolation change from  $1000$  to  $400 \text{ W/m}^2$  at  $0.5$  (a-b) sec
- Fig. 6.12 System response to an insolation change from  $400$  to  $1000 \text{ W/m}^2$  at  $0.5$  (c-d) sec
- Fig. 6.13 Waveform and harmonic spectra of 43-level and  $33 \text{ kV}$  system (a) line (a-c) voltage ( $v_{sabc}$ ) (b) line current ( $i_{sabc}$ ) (c) converter side voltage ( $v_{cabc}$ ) at  $1000 \text{ W/m}^2$  and  $25^\circ\text{C}$
- Fig. 6.14 Steady state performance of  $V_{pv}$ ,  $I_{pv}$ ,  $i_{sa}$  and converter voltage at  $25^\circ\text{C}$  and  $1000 \text{ W/m}^2$
- Fig. 6.15 Steady state performance of  $v_{ca}$ ,  $v_{cb}$  and  $v_{cc}$  voltage at  $25^\circ\text{C}$  and  $1000 \text{ W/m}^2$
- Fig. 6.16 Steady state performance of  $i_{sa}$ ,  $i_{sb}$  and  $i_{sc}$  at converter  $25^\circ\text{C}$  and  $1000 \text{ W/m}^2$
- Fig. 6.17 Dynamic performance of  $V_{pv}$ ,  $I_{pv}$ ,  $i_{sa}$  and voltage at irradiance change from  $1000 \text{ W/m}^2$  to  $500 \text{ W/m}^2$
- Fig. 6.18 Dynamic performance of  $V_{pv}$ ,  $I_{pv}$ ,  $i_{sa}$  and converter voltage at irradiance change from  $500 \text{ W/m}^2$  to  $1000 \text{ W/m}^2$
- Fig. 6.19 Dynamic performance of  $V_{pv}$ ,  $I_{pv}$ ,  $i_{sa}$  and converter voltage at irradiance change from  $1000 \text{ W/m}^2$  to  $500 \text{ W/m}^2$
- Fig. 6.20 Dynamic performance of  $V_{pv}$ ,  $I_{pv}$ ,  $i_{sa}$  and voltage at irradiance change from  $500 \text{ W/m}^2$  to  $1000 \text{ W/m}^2$  and  $25^\circ\text{C}$
- Fig. 6.21 Dynamic performance of  $i_{sa}$ ,  $i_{sb}$  and  $i_{sc}$  at irradiance change from  $1000 \text{ W/m}^2$  to  $500 \text{ W/m}^2$  and  $25^\circ\text{C}$

- Fig. 6.22 Dynamic performance of  $i_{sa}$ ,  $i_{sb}$  and  $i_{sc}$  at irradiance change from 500 W/m<sup>2</sup> to 1000 W/m<sup>2</sup> and 25°C
- Fig. 6.23 Converter phase voltage THD
- Fig. 6.24 Converter line voltage THD
- Fig. 6.25 Grid current THD
- Fig 7.1 Converter output voltage and harmonic spectra for (a)7-level, (b) 9-level, (c)11-level, (d) 19-level, (e) 25-level and (f) 43-level
- Fig.7.2 Grid current waveform and harmonic spectra for (a)7-level, (b) 9-level, (a-f) (c)11-level, (d) 19-level, (e) 25-level and (f) 43-level
- Fig.7.3 Graph of (a) converter voltage and (b) grid current THD versus (a-b) number of levels
- Fig.7.4 Switching pulses generated in PSPWM
- Fig. 7.5 Waveforms and harmonic spectra for converter side voltage for (a) (a-c) SHE-PWM (b) PSPWM (c) NLM
- Fig.7.6 Waveforms and harmonic spectra for supply Voltage for (a) SHE- (a-c) PWM (b) NLM (c) PSPWM
- Fig. 7.7 Waveforms and harmonic spectra for supply current for (a) SHE (b) (a-c) PSPWM (c) NLM
- Fig.7.8 Graph of (a) grid voltage (b) grid current (c) converter voltage versus (a-c) PWM techniques

## LIST OF TABLES

Table 1.1	Classification of the grid-tied converter based on power processing
Table 3.1	Component specifications
Table 4.1	Component specifications of grid tied 9-level CHB multilevel converter for photovoltaic application
Table 4.2	Look-up Table
Table 5.1	DVUF in an 11 kV system for different levels
Table 5.2	An 11kV system
Table 5.3	Normalized index for 11kV system
Table 5.4	Component specifications for a 19 level system
Table 6.1	DVUF in a 33 kV system for different levels
Table 6.2	A 33kV system
Table 6.3	Normalized index for 33kV system
Table 6.4	Component specifications for 43-level system
Table 6.5	THD Values (%) at the insolation level of $1000 \text{ W/m}^2$ and ambient temperature $25^\circ\text{C}$
Table 7.1	THD for different number of levels
Table 7.2	Modulation techniques and corresponding THD values for a 9-level converter
Table 7.3	Inductor value (p.u.) corresponding to number of levels

## **List of Abbreviations**

AC	Alternating Current
ALO	Arithmetic and Logical Operations
CHB	Cascaded H-Bridge
DC	Direct Current
DVUF	Device Voltage Utilization Factor
FFT	Fast Fourier Transform
HVDC	High Voltage Direct Current
IEEE	Institute of Electrical and Electronics Engineers
IGBT	Insulated Gate Bi-polar Transistor
InC	Incremental Conductance
MLC	Multi Level Converter
MPPT	Maximum Power Point Tracking
NLM	Nearest Level Method
PF	Power Factor
PI	Proportional- Integral
PLL	Phase-Locked-Loop
PSPWM	Phase Shifted carrier Pulse Width Modulation
PV	Photo Voltaic
PWM	Pulse Width Modulation
P&O	Perturb and Observe
SHE-PWM	Selective Harmonic Elimination - Pulse Width Modulation
SPV	Solar Photo Voltaic
SPWM	Sinusoidal Pulse Width Modulation
SRF	Synchronous Reference Frame
STATCOM	STATic COMPensator
THD	Total Harmonic Distortion
VOC	Voltage Oriented Control
VSC	Voltage Source Converter

## List of Symbols

$V_{rms}$	Three-phase rms voltage of grid (kV)
$P$	The power rating of the grid (MW)
$V_{dc}$	DC-link voltage (V)
$C_{dc}$	DC-link capacitance ( $\mu$ F)
$V_{oc}$	Open circuit voltage of PV array (V)
$I_{sc}$	Short circuit current of PV array (A)
$V_{mpp}$	The voltage of the PV array at maximum power (V)
$I_{mpp}$	The current of PV array at maximum power (A)
$P_{mpp}$	Power at maximum power point(kW)
$N_s$	No of series paths in SPV array
$N_p$	No of parallel paths in SPV array
$L_c$	Coupling inductance (mH)
$V_{pv}$	Photovoltaic voltage (V)
$I_{pv}$	Photovoltaic current (A)
$v_{sabc}$	Grid voltage (V)
$i_{sabc}$	Grid current (A)
$v_{cabc}$	Converter voltage (V)
$a$	Overloading factor
$\alpha$	Switching angle
$\theta$	Grid detection angle
$G$	Number of positive steps
$R_p$	Predefined Steps
$F_c$	Carrier frequency
$f$	Grid Frequency
$I_{dv}$	Device current
$I_d^*$	Active current loss component
$I_d$	Direct axis current
$I_q$	Quadrature axis current
$V_d$	
$V_e$	Error voltage



$k_p$	Proportional constant for PI-controller
$k_i$	Integral constant for PI-controller
$k_{p2}$	Proportional gain of direct axis current controller
$k_{i2}$	Integral gain of direct axis current controller
$k_{p3}$	Proportional gain of quadrature axis current controller
$k_{i3}$	Integral gain of quadrature axis current controller
$P_{\text{loss\_ivr}}$	Inverter section losses
$P_{\text{c\_ivr}}$	Inverter section conduction losses
$P_{\text{c\_swi}}$	Conduction losses for switching devices
$P_{\text{c\_Dv}}$	Conduction losses for antiparallel diodes
$P_{\text{sw\_ivr}}$	Inverter section switching losses

# **CHAPTER-I**

## **INTRODUCTION**

### **1.1 GENERAL**

Today, the world is at crossroads for energy scenarios. Every country wants to be a developed one. The per capita energy consumption is one key index to assess the progress of a nation. Hence, developing nations are investing more in power generation. Most of the nation's, developed or developing, are focusing on increasing the percentage of renewable energy generation in their countries overall energy generation. Renewable energy is perceived as the solution to the future energy crisis and restoration of the environment to its maximum pure form.

Developing nations want socio-economic growth without harm to the environment and India is showing the path to them. Rather India is a sort of world leader on this front. Currently, most of the investment is preferred in conventional energy sources. The source wise installed power generation capacity in India as given in MNRES [1] is shown in fig. 1.1. The critical challenge now is to balance progress and the environment [1-6]. Rapidly vanishing conventional energy sources have put an alarming energy crisis for the world. Moreover it increases the greenhouse gases and the pollution due to fuel used in conventional power plants [7]. The fuels used in a conventional power plant are depleting and polluting in nature. Hence to obtain clean, ever available, reliable, and environment-friendly electricity generation, the use of renewable energy sources, like solar and wind, are increasing for the last two decades. The source-wise cumulative renewable energy generation as given in MNRES report (31-12-2019) is shown in Fig.1.2 [1].

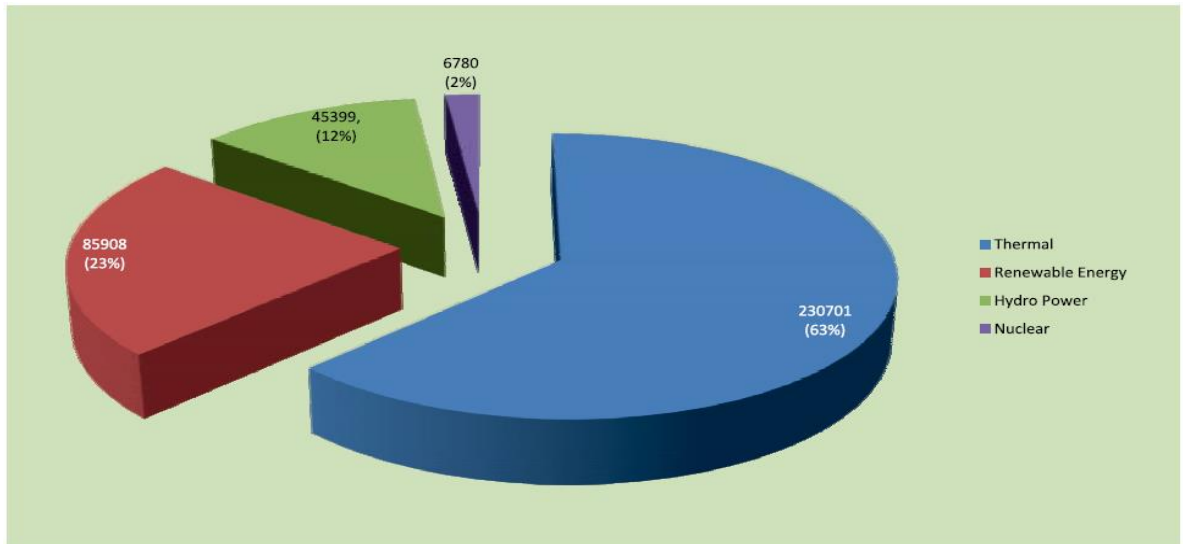


Figure 1.1 Source wise installed power generation capacity (MW) in India as on 31-12-2019 (source: MNRES annual report) [1]

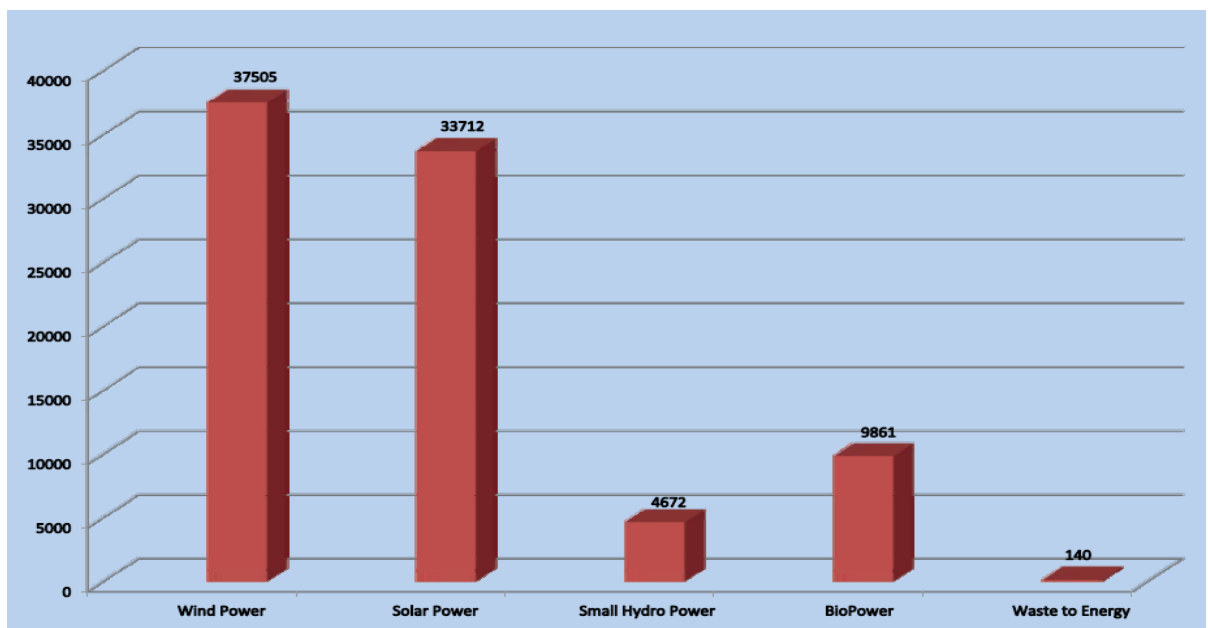


Figure 1.2 Source-wise cumulative renewable energy generation (MW as on 31-12-2019) (Source: MNRES annual report) [1]

After the Paris agreement (International Solar Alliance) 2016, in the United Nations Framework Convention on Climate Change (UNFCCC), each signatory nation is bound to reduce its carbon footprint. SPV power's unit cost has gone down with recent

development in power converters and SPV (Solar Photovoltaic) generation. The SPV power generating system is widely used to provide neat, clean, and maintenance-free energy near the load centre [1, 3]. The best way is to utilize solar energy – the most pristine of all renewable energy sources (RESs). Out of this concern, an International Solar Alliance (ISA) has been established in 2016. ISA's focus is to provide affordable solar power for every domestic household by the year 2030 [1-2, 4]. For example, India has set an ambitious target to have 100 GW installed solar capacity by 2022 and reduce emission intensity by 33-35 % by 2030 [1, 3]. With an objective to make India a global leader in solar energy, National Solar mission (NSM) has been launched in January 2010. It is the first mission operationalized under the National Action Plan on Climate Change (NAPCC). Mission has adopted a three-phase approach for quick diffusion of solar technology throughout the country by implementing conducive policy conditions. The top states of India in solar installation as given in MNRES annual report (31-12-2019) are shown in Fig. 1.3 [1].

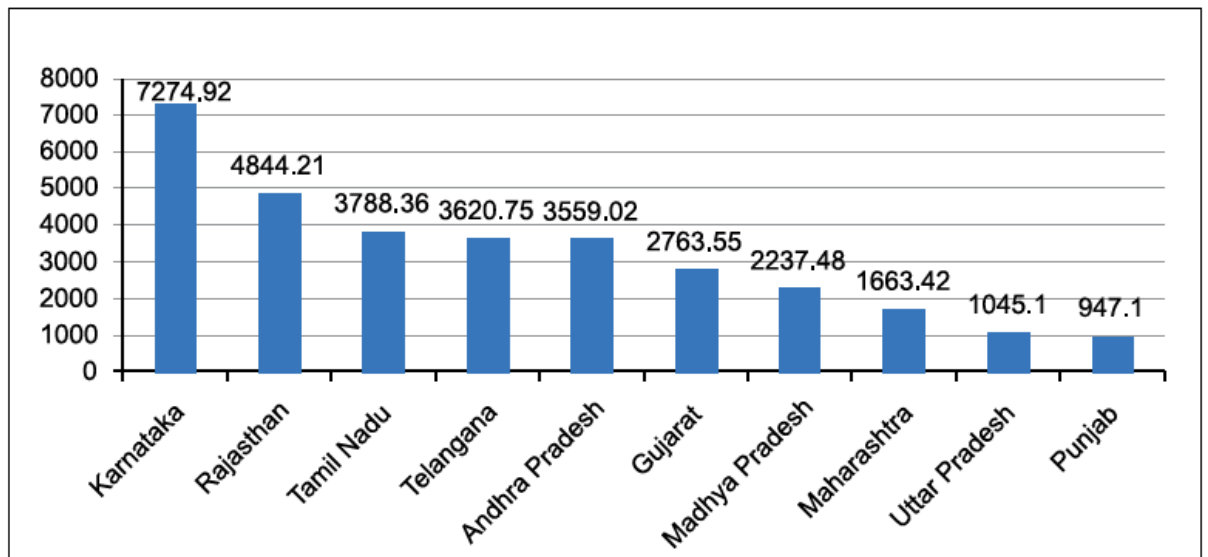


Figure 1.3 Top 10 states solar Installation (capacity in MW as of 31-12-2019) (source: MNRES annual report) [1]

In 2015, India has set an ambitious target to have 175 GW renewable energy installed capacity including all renewable sources by 2022. In just four years, the cumulative renewable installed capacity stands at 85.90 GW as of December, 2019. This amounts to almost 24 percent of total installed capacity of India, which is phenomenal. Over a period of 5 years from 2013-14, the renewable energy capacity of India has doubled. Solar energy being the biggest contributor as solar power installation has increased 14 times in last five years, with total installed solar power capacity at 37739 MW as of August, 2020 [1].

## **1.2 STATE OF ART**

The research on power converters for interfacing the renewable generation system to the grid has gained an importance to maintain good power quality, reliability, and stability of the grid [7-25]. The literature reports substantial research on the single-stage and double stage grid interfaced two-level converters to integrate the photovoltaic system [26-40]. For tracking the maximum power from the PV array, various MPPT techniques are reported in the literature [41-62]. For a multi-string SPV system, each string is provided with a separate MPPT, each controlled by a separate controller to overcome the unpredictable irradiance level variations, ambient temperature, shading effect, and other relevant factors [63-65].

However, in a conventional two-level converter for improving the THD of output current waveform of the system to enhance the power quality, one has to increase the switching frequency, which significantly increases the switching losses and the acoustic noise in the system. For filtering this high acoustic noise, the filter size is increased, increasing the system's cost. Multipulse converters are used in large solar PV grid-connected systems to minimize harmonics in the voltage waveform resulting in good power quality,

lower switching losses, and good reliability compared to the two-level topologies. This requires a good design of the transformer and interfacing magnetic for proper operation of a multi-pulse-based system [66-67].

The higher voltage rating devices used in conventional 2-level inverter topology are costly. On the other hand, the cascaded connection of low-voltage rated IGBT can be a cost-effective solution for medium or high-voltage inverter applications; they are also mature in construction [68-72]. The increased numbers of levels mean that medium or high-voltage is attainable, and it is possible to connect the SPV plant to the medium or high voltage AC network directly. This direct connection with the grid avoids a bulky and expensive step-up transformer. The transformerless converter has a reduced cost, weight, and size and improves conversion efficiency, reducing overall installation and maintenance costs of converter and interfacing transformers [73-75].

An increased number of levels in a multilevel inverter leads to the output voltage having more steps. The generated output voltage has a staircase waveform and harmonics distortions are reduced. More number of levels increases the number of switches and other circuitry around it like the snubber circuits and passive components. Accordingly the control complexity increases and may create voltage-imbalance in the string. Therefore, the optimal selection of the number of inverter levels is essential to achieve the best performance versus cost ratio of the PV systems. Extensive coverage of the topologies of the multilevel converter is reported in the literature [76-87]. These are extensively used for interfacing the renewable energy sources with the grid, and in STATCOM, back-to-back HVDC transmission, high voltage drives, and traction applications [88-100]. However, due to naturally available separate DC sources in the multi-string SPV system, CHB is most suitable for a large photovoltaic system [84].

VSCs are controlled to feed the current to the grid at the unity PF. The number of control scheme's for the VSC's are reported in the literature [101-128].

The continuous research is going on for a better modulation technique [129-160]. While devising control schemes for the controllers, the main challenge is to use suitable modulation techniques, which improves the THD as per limits specified in the IEEE-519 standard. Selecting modulation techniques with lower switching frequency reduces the switching losses and also contributes to reducing acoustic noise. As multilevel converters are used for medium or high power applications; hence switching losses are the significant parameter for selecting the appropriate multilevel converter.

### **1.3 GRID TIED PHOTOVOLTAIC INVERTERS**

Given the above, one of the critical challenges for engineers is the grid integration of renewable energy sources. The increasing number of renewable energy sources and distributed generators require new strategies for the grid's operation and management to maintain and to improve the power quality and reliability. Power-electronic technology plays a vital role in the distributed generation and integrates renewable energy sources into the electrical grid.

The large-scale grid integration of solar power plants, is the key focus area as the targets cannot be met without it. The generation of bulk solar power using the available solar panels, requires a series-parallel connection of solar panels to achieve the desired current and voltage ratings [3]. Usually, two types of configurations are employed for connecting the inverter with the PV array: central inverter and multi-string inverter, as shown in Fig.1.4.[12] In the central inverter, the single inverter controls the whole PV array, and a single MPPT tracks the maximum power [12-14, 19-26] from the PV array.

Hence in case of fault and shading in the part of PV array, the complete system is to be affected. A converter is connected to a single string in a multi-string converter, and a separate MPPT tracks the maximum power. Only that particular string is to be affected under fault and partial shading conditions instead of the whole system. The control block diagram of the grid interfaced converter [26] is shown in Fig.1.5. To extract the maximum power from a PV array, it must operate the voltage and current on PV characteristic at maximum power point under all varying environmental conditions,

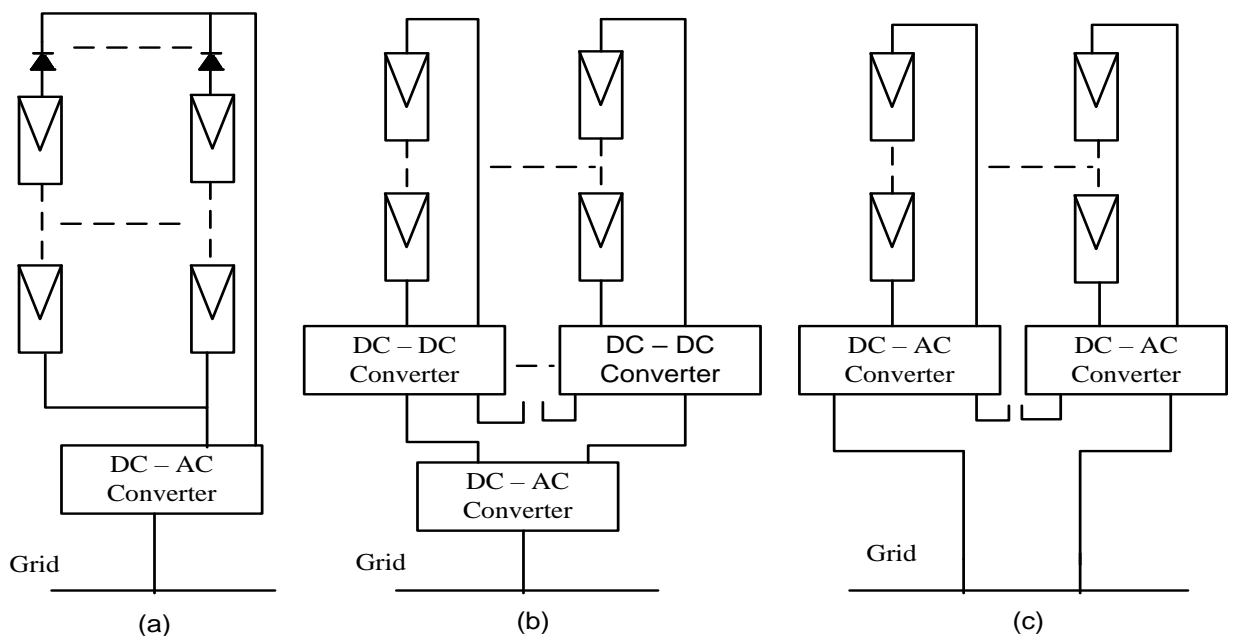


Fig. 1.4 Inverter configurations for solar PV array connection (a) Central inverter, (b) Double-stage multi-string, (c) Single stage multi-string [12]

insolation level change, and partial shading. This can be achieved using the maximum power point tracking (MPPT) algorithm [41-43]. The maximum power extracted from the PV array is fed to the inverter after boosting the DC voltage by a DC to DC converter. The DC-AC converter feeds extracted power from the PV array to the grid at unity PF [26].



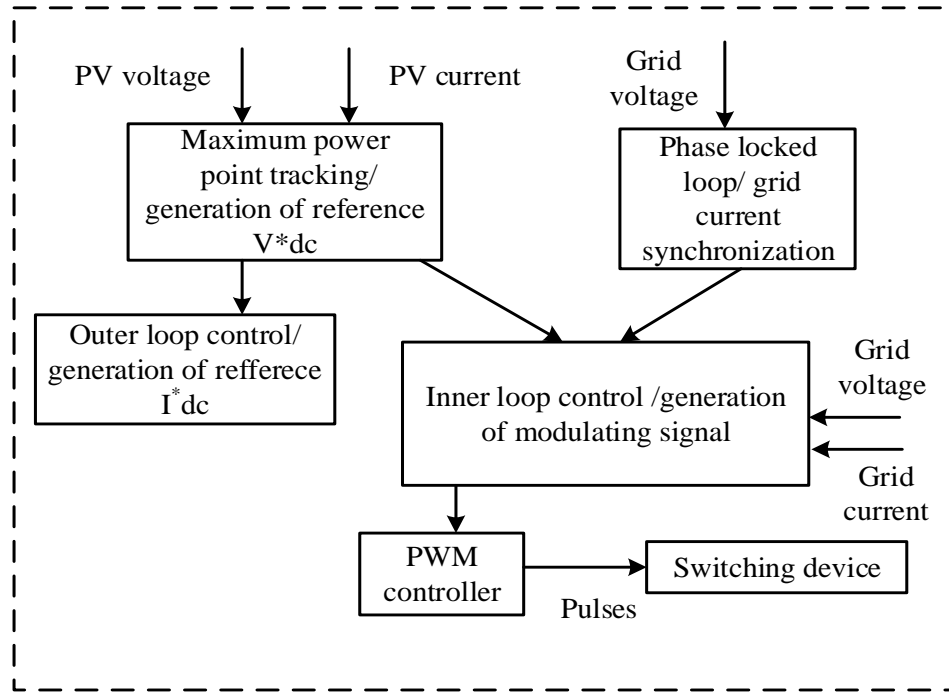


Fig 1.5 Control block diagram for SPV generation system [26]

The grid interfaced SPV generating system can be classified into two categories depending on the power processing stages as given in Table 1.1.

Table-1.1 Classification of grid-tied converter based on power processing

Stage	Converter Used	Task Performed
Single-stage	DC-AC Inverter	1. MPPT control 2. It feeds extracted power to the grid at unity PF.
Double Stage	DC-DC Inverter	MPPT control
	DC-AC Inverter	It feeds extracted power to the grid at unity PF.

In double stage PV inverter, the DC to DC converter boosts up the DC voltage generated by the PV array and also provides the galvanic isolation for protection against the leakage current (The uncontrolled leakage current results in the risk of electrical shock, increased

power loss, and reduced reliability). Moreover, the cost of the system and control complexity are increased. Hence it is preferable to use a single-stage SPV generation system and galvanic isolation in case of a single-stage system may be provided through a low frequency isolating transformer [27-40].

## **1.4 MULTILEVEL CONVERTERS**

The power-electronics has undergone a fast evolution. Multilevel inverters are presented as the solutions of choice for high-power and medium-voltage applications and the grid interfacing. The conventional two level inverters have inherent shortcomings on account of limitations due to increased switching losses at high frequency and device rating constraints. In contrast, multilevel inverters work as a group of switching devices and DC voltage supplies. They are capable of producing stepped output voltage and also keep harmonics distortion at a low value. Main appealing factor in multilevel converter topologies, is increased power rating with lower device ratings, reduced voltage stress on the switching devices, high quality output voltages, and sinusoidal currents with less distortion [76-82].

### **1.4.1 Multilevel Converter Topologies**

Many multilevel converter topologies are proposed in the literature. Nevertheless, mainly, three topologies of MLCs are preferably used [76-82].

- (i) CHB with separate DC sources,
- (ii) Diode clamped (or neutral clamped), and
- (iii) Flying capacitors (or capacitor clamped).

Among various MLCs topologies reported in the literature [5-8], for large photovoltaic applications, cascaded H-bridge (CHB) topology is an exciting topology as separate DC sources for each H-bridge in CHB multilevel converter are naturally provided in the multi-string solar PV system. Despite the increased hardware cost and complexity, multi-string topology allows individual MPPT control of each string. It also provides increased modularity, improves power output from the solar module despite possible module mismatch and partial shading [10].

#### **1.4.2 Multilevel Converter Applications**

Multilevel converters can be used in the following applications in high power and medium voltage grid applications [88-100].

- (1) Interfacing of renewable energy sources,
- (2) Battery energy storage system,
- (3) STATCOM,
- (4) VSC based HVDC back to back connection.

Only the first of the above applications, is considered in this work and also in interfacing of renewable energy sources, only solar interface is investigated in this work.

### **1.5 SCOPE OF WORK**

After carrying out the detailed literature review on the grid interfaced converters, it has been identified that the conventional two-level converter cannot be applied for high or medium voltage due to an increased per device voltage stress. The use of a multilevel converter instead of two converters gives the lower per device voltage stress, improved THD, scalability, and lower switching frequency, providing reliable, efficient, and

enhanced power quality of grid interfacing systems. The performance of the system is verified on the MATLAB Simulink platform.

The main objectives of this proposed work are as follows.

- To select the optimum number levels of multilevel converter corresponding to the high voltage rating of systems interfaced to the grid.
- To model and design the grid integrated multilevel converter.
- To select distributed MPPT algorithm.
- To develop the control algorithm for grid interfaced multilevel converter.
- To choose a suitable modulation technique with improved THD and low switching frequency.
- To obtain both dynamic and steady-state performances of the system on MATLAB Simulink.
- To find the power quality improvement by using the FFT Tool of MATLAB Simulink.

This proposed research work has been carried out on following objectives.

### **1.5.1 System Configurations**

The multilevel converters are designed and modelled for different levels depending on the voltage rating of the grid. The 7- and 9- level CHB multilevel converters are designed for the 3.3 kV AC grid. The 19-level CHB multilevel converter is designed for 11 kV grid. The 43-level multilevel converter is designed for a 33 kV grid. Because of the natural availability of independent DC sources in the multi-string photovoltaic system, CHB multilevel converter is employed in this research work.

### **1.5.2 MPPT Algorithm**

As the well-known MPPT algorithms converge fast, these algorithms are employed in this research work. Among various known methods, therefore, a perturb and observe (P&O), and an incremental conductance (INC) methods are used for tracking maximum power from the PV array. Both techniques introduce small disturbances (perturbations) to track the MPP and to determine the voltage at which, the PV array is able to deliver its maximum power. Each PV array is provided with a separate MPPT algorithm and separate controller to overcome the unpredictable irradiance level variations, ambient temperature, shading effect, and other relevant factors.

### **1.5.3 VSC Control Algorithm**

VSC feeds the extracted power from the PV array to the grid at unity power factor. The decoupled current control based on SRF-PLL is applied for the VSC control. The voltage oriented control with SRF-PLL is also used for the VSC control. PLL is used for synchronization to the grid. The performance is tested on MATLAB/Simulink software. Both, the steady-state and dynamic performances are studied. The power quality improvement is observed using the FFT tool of the MATLAB. The THD of output voltage and current waveforms for various levels are also compared in detail. Results are also validated in hardware-in-loop (HIL) on OPAL-RT simulator.

### **1.5.4 PWM Control**

The modulation schemes suitable for CHB multilevel converter are employed in this thesis. Three modulation techniques are used, and their THD's are compared. Firstly, a simple and straightforward phase-shifted multicarrier sinusoidal is applied to a 7, 9, 19, and 43- level CHB multilevel converters. The number of carrier signals and phase-

shifting between them are calculated for different number of levels. Moreover, NLM, and SHE PWM techniques are applied to the 9-level converter. Accordingly, the comparison of different modulation techniques employed is also made for the output voltage and current waveforms THDs in detail.

## **1.6 OUTLINE OF CHAPTERS**

This thesis consists of eight chapters, including introduction, literature review, design and development of grid interfaced multilevel converters, control algorithm, PWM strategies, their comparison, MATLAB modelling, results and discussion, main conclusions, and suggestions for further work followed by references.

**Chapter-I:** This chapter summarizes the shortcomings of the conventional sources and the need for renewable energy and India's statistics. Solar energy statistics in India and the mission launched to increase solar energy generation are discussed in brief. It covers the grid interfaced photovoltaic converter and introduces the multilevel converters, its topologies, and applications. The scope of the work includes system configurations of multilevel converters for the given specifications of the grid, MPPT techniques, VSC control, and PWM control. The scope of the work is discussed and the outline of chapters is presented here.

**Chapter-II:** The detailed literature review on MPPT control algorithms for grid interfaced converters, is described in this chapter. Further, a comprehensive review of multi-pulse and multilevel converters for a large photovoltaic system is carried out in detail. A review of PWM controls for obtaining improved THD and the low switching frequency is also discussed in this chapter. Based on the exhaustive literature review, the research areas are identified, and problem formation is presented at the end of the chapter.

**Chapter-III:** This chapter presents the design, modeling and control of grid interfaced transformerless single stage 7-level CHB multilevel converter for photovoltaic system. The maximum power is tracked from the PV array using an improved P&O algorithm. The decoupled SRF-PLL control is used for VSC control to feed current to the grid at unity P.F. Phase shifted PWM method is implemented for the modulation of multilevel converter. MATLAB simulative results are presented out for validating the steady state and dynamic performances. The THDs of converter voltage, grid voltage and current are tested on FFT tool of MATLAB. The performance of the designed system is also tested on the OPAL RT simulator.

**Chapter-IV:** This chapter includes the design, modeling and control of grid interfaced transformerless single stage 9-level CHB multilevel converter for photovoltaic system with phase shifted PWM, SHE (Selective Harmonics Elimination)-PWM and NLM (Nearest level modulation)-PWM modulation method. The control scheme comprises an improved P&O MPPT algorithm and decoupled current control with SRF-PLL. The steady state and dynamic performances and THDs are presented and validated on MATLAB Simulink and OPAL RT simulator.

**Chapter-V:** This chapter presents the design, modeling and control of grid interfaced transformerless single stage 19-level CHB multilevel converter for photovoltaic system. The number of levels in multilevel converter in this system is selected with all design considerations like the cost of IGBTs, arithmetic and logical operations (ALOs), THDs and device voltage utilization factor (DVUF). The control scheme comprises an improved P&O MPPT algorithm and decoupled current control with SRF-PLL. Phase shifted PWM is used for modulation of MLC. The steady state and dynamic performances and THDs are presented and validated on MATLAB Simulink and OPAL RT simulator.

**Chapter-VI:** This chapter deals with the design, modeling and control of grid interfaced transformerless single stage 43-level CHB multilevel converter for large photovoltaic system. The number of optimum levels in multilevel converter in this system is selected with all design considerations. The maximum power is tracked by using an incremental conductance algorithm. The control scheme used for VSC control is SRF-PLL based VOC control. Performances and THDs are simulated on MATLAB Simulink and validated using the OPAL RT simulator.

**Chapter-VII:** This chapter present of the comparative analysis of different multilevel converters on the basis of number of levels used and also on modulation techniques implemented in detail.

**Chapter-VIII:** A brief summary of the conclusions drawn for the different level MLCs, various control algorithms, using a variety of PWM schemes and their comparative analysis is provided in this chapter. At the end of the chapter, some suggestions are also given for the further work in the areas covered in the thesis.



## **CHAPTER-II**

### **LITERATURE REVIEW**

#### **2.1 GENERAL**

The integration of distributed renewable energy resources with the grid provides the substitute to the large conventional central power stations and give neat, clean, pollution-free and non-depleting power generation. The specifications of a power electronic interface are related not only to the renewable energy source itself but also to its effects on the power system operation. Substantial research is being carried out for power electronics used on the grid interfaced converters, and several related research publications are available in the literature [19-25]. The extensive literature survey is done for a grid-connected converters, maximum power point techniques, multilevel inverters, their control, and modulation techniques. The multilevel converter provides efficient, economical (without a transformer and with a low-size filter), a reliable interface for medium or high voltage grid with enhanced power quality. This chapter deals with the detailed literature review of renewable energy sources integration to the grid, multilevel converters, maximum power point tracking for PV array, PWM control, and VSC control for feeding power from the SPV generation system to the grid at unity PF.

#### **2.2 LITERATURE SURVEY**

The grid integration of renewable energy sources covers various aspects like choice of converter topology, energy source and modulation techniques etc. In case of solar PV systems, choice of appropriate algorithm for harnessing maximum power from the PV arrays is also important. A detailed review of various aspects, is presented here in the following sub-sections, covering the basic two level converter to the multilevel converters for high voltage and power applications.

### **2.2.1 Review of Two-Level VSC for Grid Connected Converters**

Solar photovoltaic (PV) energy generation systems can be broadly classified into two main categories that are standalone and grid interfaced systems. Several standalone systems for PV power generation systems considering rural electrification, three-port converters for PV application, PV-based battery charging station, and battery energy management are shown in [8]. The batteries are an integral part of a standalone PV-based system. However, they require frequent maintenance and timely replacement. Therefore, battery-less grid interfaced PV generation systems are preferred where the grid is available. There are many challenges in integrating SPV generation with the grid-like efficiency, power quality, stability, cost of the energy conversion, load management, fault ride through, and reliability. However, while integrating renewable energy of any source to the electric grid, it has to fulfil standard power quality requirements so that the grid is not polluted due to such interface [26].

Several single-stage and double stage grid interfaced two-level converters are reported in the literature [27-40]. Various single-stage grid-connected SPV systems given in the literature are UVT based control described in [28] and decoupled adaptive neural network [29]. Various controls of double stage grid interfaced SPV systems reported in the literature are as follows: adaptive noise cancellation based harmonic elimination presented in [30], adaptive noise reduction control presented in [31], modified EPLL based control discussed in [32], Takagi–Sugeno–Kang probabilistic fuzzy neural network control reported in [33], Luenberger observer based control algorithm explained in [34], ANF based control approach described in [35], adaptive DC link voltage for CPI voltage variations given in [36], an adjustable DC-Link voltage-based control is reported in [37], damped-SOGI-based control algorithm given in [38], a decoupled adaptive noise

detection based control approach presented in [39], and adaptive pseudo-linear control reported in [40].

### **2.2.2 Review of MPPT Techniques for Grid Connected Converters**

As the output of solar PV array is highly dependent on parameters such as insolation level and surrounding temperature, hence its V-I characteristic is non-linear. Only a single operating point on V-I characteristic provides maximum power output from a given PV array. However, the operating point varies with the variation in surrounding conditions. To track maximum power point even in varying surrounding conditions, MPPT (Maximum Power Point Tracking) techniques are used. Extracting maximal power from the solar PV array is a big challenge, and researchers have tried different techniques reported in the literature for implementing the concept of MPPT. Various conventional and intelligent algorithms for varying characteristics are developed and reported in the literature [41-62]. An incremental conductance, P&O method, improved P&O method, curve-fitting technique, fractional open-circuit voltage (FOCV) technique, fractional short-circuit current (FSCI) technique, linearization-based MPPT technique, parasitic capacitance technique, current sweep technique, forced oscillation technique are various conventional MPPT algorithms are reported in the literature [41-43]. Particle swarm optimization-based MPPT (PSO-MPPT) technique, artificial neural network (ANN)-based MPPT technique, adaptive perturb and observe, estimated perturb and observe, fuzzy logic (FL)-based MPPT technique, adaptive fuzzy and particle swarm optimization (PSO) techniques are various intelligent techniques are also reported in the literature [41-43]. A combination of fractional open circuit voltage [47] and fuzzy-based MPPT technique is given in [50] wherein a constant offset is added at the fuzzy controller's

output to improve the MPPT performance. The application of the sliding mode controller to the MPPT algorithm is reported in [52].

An intelligent algorithm gives an improved accuracy but the converged time is more. As a conventional algorithm converges fast, so usually well-known algorithms are employed. Among well-known methods, perturb and observe (P&O), and an incremental conductance (INC) methods are popular and find wide acceptance in commercial products [53]. Both introduce small disturbances (perturbations) to track the MPP and to determine the voltage at which, the PV array is able to deliver its maximum power. Its simplicity and ease of implementation characterize the P&O algorithm. However, it tends to oscillate around the maximum power point. The improved P&O algorithm is a modification of the P&O algorithm, which considerably reduces the ripple in the PV voltage. At the insolation change, the standard P&O technique fails to differentiate between variation in the power on account of insolation variation and the perturbation, which is taken care of by an improved P&O algorithm [54-57].

These improvements in the P&O algorithm have resulted in a slower response, especially under rapid weather changes. It is reported that tracking is improper. During cloudy weather, the efficiency is dragged down. In contrast, the InC algorithm has fast tracking and better accuracy, as reported in the literature [58-62].

It is essential to ensure extraction of maximum power from a PV array under all weather conditions and during steady-state as well. Failure to do so may render all efforts of maximizing efficiency of an inverter fruitless. The available literature reports many MPPT algorithms, which are optimized for extracting maximum power from the PV array. Despite this maximum extraction of power is seldom achieved due to PV array mismatch. This is especially true for medium and large scale PV plants. They are very sensitive to partial shading owing to long nature of PV strings. It is reported that even a

passing cloud or nearby hindrances may affect the performance as they create conditions for partial shading. Hence, each PV array is provided with a separate MPPT algorithm to overcome the unpredictable irradiance level variations, ambient temperature, shading effect, and other relevant factors [63-65].

### **2.2.3 Review of Multilevel and Multipulse VSCs for Grid Connected Converter**

The main problem with a large SPV connected grid system is to design the voltage source converter (VSC) using high rating components with lower switching losses. Multilevel and multi-pulse converters are generally used to feed large photovoltaic power into the grid. Multipulse converters are used in large solar PV grid-connected system to minimize harmonics in the voltage waveform resulting in good power quality, lower switching losses, and reliability in comparison to the two-level topologies, but the excellent designs of the transformer and interfacing magnetic are required for proper operation of multi-pulse based system [66-67].

Since the multilevel converter is designed for high voltage and power applications, it can efficiently, reliably, and economically be employed to integrate the large solar plant with the grid. The low switching frequency employed in multilevel converters used for high power applications reduces the switching losses and reduces the acoustic noise, which reduces the size of filter and further contributes to the reduction of cost of the system [84-87].

As a multilevel converter is designed for high or medium voltage applications, it can directly connect to the medium voltage grid. It eliminates the need for a large size, heavyweight expensive step-up transformer for grid interfacing. Only a low-frequency transformer is sufficient for providing galvanic isolation to limit the leakage current. The

transformerless converter has reduced cost, weight, size and improved conversion efficiency [68-71].

### **2.2.3.1 Review of multilevel converter topologies**

A substantial literature has reported many multilevel converter topologies [78-82]. The use of CHB multilevel converters for applications such, as an interface with renewable energy sources, STATCOM and battery energy storage system (BESS) have been proposed in [84-90]. Peng *et.al.* [88] have reported a prototype CHB multilevel converter based STATCOM connected in parallel with the electrical system. It has been reported that it is capable of supplying or drawing reactive current from an electrical system. Through proper control, this converter can either regulate the power factor of the current drawn from the source or the bus voltage of the electrical system where the inverter is connected. Peng *et.al.*[88] and Joos *et.al.*[89] have demonstrated direct series connection of CHB multilevel converter with the electrical system for STATCOM. A cascaded converter system for HVDC application is used in [90].

Nabae *et. al.* [91] in 1981 have proposed the neutral point converter, which has essentially a three-level diode-clamped inverter. In diode clamped multilevel converter, all phases share a common DC bus so the converter's capacitance requirements are minimized. Therefore, a back-to-back connected topology can be realized for the use in a back-to-back high-voltage inter-connection or an adjustable speed drive. Post 1990, many researchers have reported experimentally backed results for four to six level diode clamped converters. They have used MLCs in applications like STATCOM and high-voltage system interconnections [93-97]. Other reported applications of the multilevel diode-clamped inverters are an interface between a high-voltage DC transmission line and an AC transmission line [93] and STATCOM [94]. Many other applications are

variable speed drives for high-power medium-voltage (2.4 kV to 13.8 kV) motors [95-97]. The quadratic relationship between number of levels and clamping diodes required, makes the scheme very cumbersome for higher number of levels.

Meynard and Foch [98] have introduced a flying-capacitor-based inverter in 1992. In case of a flying-capacitor-based inverter, the output voltage can be synthesized using any valid switch combination due to inner voltage redundancies. Moreover, there is no requirement for the conducting switches to be in series like the diode-clamped inverter. Whereas, the diode-clamped inverter has only line-line redundancies, the flying-capacitor inverter has phase redundancies [76]. This allows the choice of specific capacitors for charging / discharging and helps in designing the control scheme for voltage balancing across various levels.

With increasing number of levels, the flying capacitor topology becomes bulky and expensive and packaging also becomes difficult owing to large number of capacitors. One application for medium-voltage motor drive is given in [99]. For electric aircraft applications, the design of a GaN-based interleaved nine-level flying capacitor multilevel inverter is described in [100].

### **2.2.3.2 Review of optimum selection of numbers of levels in multilevel converters**

In high voltage range (3.3, 4.5, 6.5 kV), costly IGBTs are available in the market, but lower voltage (0.6, 0.9, 1.2, 1.7, and 2.5 kV) IGBTs are comparatively lower in cost and have better technology. Hence, a cascaded connection of low voltage IGBTs for achieving medium voltage can be used for developing a low-cost inverter, and the designed system can facilitate a direct connection to a medium voltage AC network, with an improved output power quality. At the same time, this leads to a linear increase in component number and control complexity. Hence, to realize a better performance versus

price and control complexity ratio, finding the optimum value for the number of levels is essential.

The following factors should be considered for selecting the optimum number of levels for the given voltage rating of the system [68-72].

- As the cost of a semiconductor device is significant for a medium voltage system, a higher device voltage utilization factor (DVUF) is necessary for making the system design a cost-effective one.
- The count of arithmetic and logical operations (ALOs), which are required in a switching section and count of IGBTs for different levels.
- In semiconductor devices, the inverter section losses are the sum of conduction losses and switching losses. As one increases the number of levels in a multilevel converter, the carrier frequency reduces, and the active switching device count increases linearly. Hence, switching losses are reduced, and at the same time, conduction losses are increased. Moreover, the device voltage ratings determine an IGBT's on-state voltage drops and diode's forward voltage. For these reasons, total losses in the inverter section are almost constant and, therefore, despite the change in the number of levels, multilevel inverter's efficiency remains almost constant. Therefore, the efficiency is not a consideration in the selection of levels while designing a multilevel inverter.
- For comparing a variety of the inverter systems based on performance and control complexity comprehensively, a normalized index which is defined as [68],

$$I_{dw} = (w - w_{\min}) / (w_{\max} - w_{\min})$$

is considered. Where  $w$  is scored value and  $w_{\min}$  and  $w_{\max}$  are the lowest and highest values of the indicator. The normalized index should be lowest for the number of the level selected for the system's given voltage rating. Choosing the number of levels



beyond the selected, one provides negligible power quality improvements and the reduction in semiconductor cost and only increases the part (component) count and control complications.

### **2.2.3.3 Review of VSC control scheme**

In grid interfaced converters, the VSC should be controlled such that it should feed power to the grid at unity PF and works stably both in steady-state and dynamic conditions. The PLL is used for grid synchronization for operation at unity power factor as required by grid standards or by some other method as described in [101]. Various control schemes for VSC are reported in the literature [102-128]. For CHB multilevel grid-tied PV system, the sliding mode control based power balancing is described in [102] and energy sampled data modelling is given in [103]. The control scheme is discussed in [104] for energy balance control modelling of a cascaded H-bridge multilevel converter for single-phase grid-connected H-bridge multilevel inverter linking  $n$  independent photovoltaic (PV) arrays to the grid. The model predictive control suitable for multilevel CHB converters is presented in [105-107]. However, it has a fast dynamic response, easy inclusion of nonlinearities and constraints of the system, and the flexibility to include other system requirements in the controller. Moreover, this control scheme is complex in implementation. Some single-phase grid interfaced system is considered in [109-112]. The decoupled current control with PLL-SRF for a single-phase grid is reported in [109-110]. The SRF theory is simple control scheme in the implementation. In control scheme based on SRF theory, detection of real power component of load current is done in a coupled manner. Under unbalance condition of the load currents, this results in oscillations of second harmonic. These oscillations can be suppressed using a low-pass filter. Hence, SRF-control provides zero steady-state error with a good dynamic performance [108]. Some literature has also described the control of CHB multilevel

converter for grid interfaced PV system [113-122]. The grid integrated large PV plant with CHB multilevel convert has been given in [122-128].

#### **2.2.3.4 Review of PWM techniques**

While devising control schemes for the MLCs, the main challenge is to use a suitable modulation technique, which controls the rectangular output pulses to realize the desired waveform as it generates the voltage at the required frequency as per limitations specified in IEEE-519 standard [17]. Various high switching frequency PWM methods such as sinusoidal PWM, space vector PWM, and fundamental switching frequency modulation techniques such as selective harmonic elimination modulation, selective harmonic mitigation (SHM), space vector control, synchronous optimal pulse width modulation, etc. are reported in the literature [129-130]. The high switching frequency SPWM method is simple in implementation, the modular multilevel converters with phase-shifted carrier SPWM are given [129-130]. The level shifting SPWM for the asymmetric 7-level converter is used in [110,114-115]. The level-shifting SPWM has phase redundancy, hence not suitable for symmetric CHB. Usually, phase-shifted SPWM is employed for the CHB multilevel converter [130]. As in these converters, the output voltage of individual H-bridges is almost identical, the rotation of switching patterns is not required and also switching devices operate at the same switching frequency and conduction time. Ilves et al. [131] have discussed the modular multilevel converters with phase-shifted carrier PWM. A 27-level symmetric CHB multilevel converter is described in [116]. A simplified phase shift PWM- based feedforward method is given in [132] for grid-connected cascaded PV inverter. The generalized theory of phase-shifted carrier PWM is given in [133], and modified SPWM for cascaded CHB is presented in [134]. Pa and Peng [135] have discussed "a novel PWM method with voltage capability for multilevel

rectifier and inverter system". However, high-frequency PWM techniques suffer from two disadvantages like the inability for the complete elimination of the low order harmonics and high switching losses owing to high switching frequency operation [15]. For medium and high power applications, the switching losses are the crucial parameter for design consideration; hence the low switching frequency method is preferred [15]. The space-vector PWM method, a fundamental frequency method, has good utilization of the DC-link voltage, low current ripple, and low losses due to fundamental switching frequency [137]. Yi Deng et al. [138] have presented a fast and generalized space vector modulation scheme to obtain "the switching states, duty cycles, and switching sequences by simple calculation scheme, no lookup table is needed, and the scheme is computationally fast". Ahmed et al. [139] have proposed "simplified space vector modulation techniques for multilevel inverters". However, space vector modulation suffers from dramatic increase in redundant switching states and switching state selection complexity with an increase in the number of levels [15,136].

SHE-PWM technique, which is developed based on the harmonics elimination theory proposed by Patel *et. al.*[140-141], is used for modulation in given work as it has better THD as compared to other modulation technique with lower rating switches. The power quality can also be improved by using several switching per quarter cycle, but the increased switching frequency increases the switching losses. SHE is a fundamental switching frequency method, and the fundamental frequency employed reduces the switching losses. Reduced THD and low switching frequency employed in SHE further reduce the size and, hence, the filter's cost. In this method, the non-linear transcendental equations are written to implement SHE-PWM from Fourier analysis of output waveform to eliminate various order harmonics. The main challenge in SHE-PWM method is to solve transcendental equations for the determination of switching angles. Several

methods, iterative, algebraic, evolutionary, and intelligent, have been proposed in the literature for the solution of these equations [15, 143-149]. Al-Hitmi et al. [142] have given selective harmonic elimination method in multilevel inverter using modified Newton-Raphson method. Ahmad et al. [143] have described “the derivative-free iterative method under varying voltage conditions”. The iterative procedure requires a good initial guess. Moreover, the solution is not guaranteed, which renders it non-feasible to calculate a large number of switching angles in the absence of good initial guess [143]. The evolution and swarm based optimization techniques are reported in the literature such as “harmonics optimization of multilevel using genetic algorithms” in [144], “modified species-based particle swarm optimization” in [145]. “genetic algorithm and artificial neural network angle generation” is used in [146], “harmonic elimination through a colony of continuously exploring ants” is presented in [147], “application of the Bee algorithm” is given in [148]. “Hopfield neural network” is discussed in [149] and “new fundamental modulation technique with SHE using shuffled frog leaping algorithm” in [150]. The evolution and swarm-based optimization techniques are dependent on various parameters (objective function, number of evolution, initial population, number of particles, the number for generation, accuracy in the solution) selected for implementation of the technique. They may fail to converge sometimes [143]. Ahmed et al. [151] have provided “real-time solution and implementation of SHE” and Kundu et al. [152] have given “comparative study between different optimization techniques for finding precise switching angle” for SHE-PWM.

For solving non-linear transcendental equations, the resultant theory method is employed in the proposed work. The resultant theory method is an algebraic method that converts the transcendental equations into polynomial equations for calculating switching angles corresponding to each voltage source and efficiently removing the lower order harmonics

[153]. Higher-order harmonics are easily filtered using a low-value inductive filter. The third harmonic and its multiples are cancelled out in line voltages. No initial guess is required in this method and also not dependent on so many parameters [143]

The nearest level modulation (NLM) given in the literature, is also a suitable and more straightforward modulation technique for symmetric CHB multilevel converter. It is a fundamental switching modulation strategy that is simpler than SHE-PWM method. In order to implement NLM strategy for cascaded inverter, the solution of the complex transcendental equations is not required to get turn ON and OFF angles. Because of the fundamental switching frequency employed in NLM, switching losses are also reduced. This modulation scheme can be easily implemented for any number of levels [154-160].

### **2.3 IDENTIFIED RESEARCH AREAS**

After surveying the available literature on multilevel converters, controls, and applications for SPV energy generation systems, the following research areas have been identified to be explored in the present research work:

- To design a multilevel converter for optimum level in order to improve the current and voltage THDs. An optimum level needs to be decided as increasing the number of levels in the multilevel inverter, the number of switching devices, gate amp, diodes, and other passive elements increases, leading to increased control complexity in inverter and creates possible voltage unbalance.
- To design a cascaded multilevel converter without transformer interfacing, with the same DC voltage source. To perform simulation, implementation, and analysis in detail.
- Design and simulation of a SPV energy generation system with suitable MPPT are to be carried out to achieve distributed maximum power point tracking for all-weather

and transient condition and feeding power extracted from PV array to grid at unity PF with lowest THD.

- To select a suitable modulation control strategy for the multilevel converter to achieve low THD (adhering to IEEE-519 standard specifications) and low switching frequency.

## **2.4 PROBLEM FORMULATION**

The design, analysis, and control of grid tied multilevel converters for SPV generating system are carried out with keeping in view research gaps, and the following features are selected for investigations.

- Shading effect or any other mismatch of PV array.
- THDs of the output voltage and current.
- Converter switching frequency.
- Feeding power to the grid at unity pf.
- Suitable PWM technique for MLC.
- Reduced cost and complexity.

The design, analysis, and control of grid integrated multilevel converters for SPV generating system are considered in the presented research work in the following manner.

- Distributed MPPT for each PV array to mitigate the issue of shading effect and mismatch or unbalance of PV cell.
- Design for the optimum number of levels to reduce the THDs of output voltage and current.
- Control the VSC to feed power to the grid at unity pf.

- Selection of the modulation technique with improving THD and low switching frequency, which reduces switching losses and also acoustic noise (which consequently reduce the size of filter and cost).
- This use single-stage SPV generating system to reduce the cost and control complexity
- Transformerless grid interface to reduce the cost, size, and weight of system and conversion efficiency, and
- Lower acoustic noise because of the lower switching frequency.

## **2.5 CONCLUSIONS**

An exhaustive literature review has revealed that the research work carried out in integration of MLCs to the grid, good power quality and reliability in grid are mainly influenced by the technical developments in power electronics, control algorithms and modulation strategies. The main focus of this work is to develop topologies for the multilevel converters in a cost-effective way with simple controlled manner and an improved power quality for the grid interfacing of large SPV energy generation systems.

## **CHAPTER-III**

### **CONTROL AND DESIGN OF SEVEN LEVEL CASCADED MULTILEVEL CONVERTER BASED PV SYSTEM**

#### **3.1 INTRODUCTION**

In this chapter, the design, modelling, and control of three-phase seven-level symmetrical CHB multilevel converter are carried out for the grid integration of the photovoltaic (PV) system without bulky line frequency step-up transformer. The presented work is implemented with a single-stage photovoltaic converter to reduce cost and control complexity. The control algorithm employed in this work consists of the MPPT algorithm and VSC control. The outer loop of the control algorithm comprises a different maximum power point techniques (MPPT) controller for each PV array. The improved perturb and observe (P&O) MPPT algorithm is used to track the PV array's maximum power. VSC control comprises a decoupled current control with synchronous reference frame (SRF) transformation and phase-locked loop (PLL) with low switching frequency phase-shifted pulse width modulation (PWM) technique to feed the current to the grid at unity pf with a low THD output current waveform. PLL achieves synchronization to the grid. A low-value inductive filter is sufficient for filtering in this work because of the reduced THD of output voltages and currents, and lower switching frequency (lower acoustic noise). Simulations are carried out in MATLAB/Simulink and validated in HIL on OPAL RT simulator. Both the steady-state and dynamic performances are validated, and the THDs of output voltage and the current waveforms are verified as per the IEEE-519 standard by using the FFT tool of MATLAB and results of OPAL RT simulator. The system configuration, design, modelling, control, simulation, and results are discussed in detail in different sections of this chapter.



### 3.2 SYSTEM CONFIGURATION

As shown in Fig. 3.1, the system is designed for a 1.48 MW, 3.3 kV, 50Hz, 3- $\Phi$  seven-level cascaded H-bridge (CHB) converter with a low switching frequency of 500Hz. The SPV system is connected to the grid through an interfacing inductor for reducing ripple content in the current. As the PV system is designed for medium and higher power rating, this is feeding power to the grid only for power transmission purposes. If the  $L$  is the number of levels in the cascaded multilevel converter, the H-bridge number per phase selected is calculated as [10].

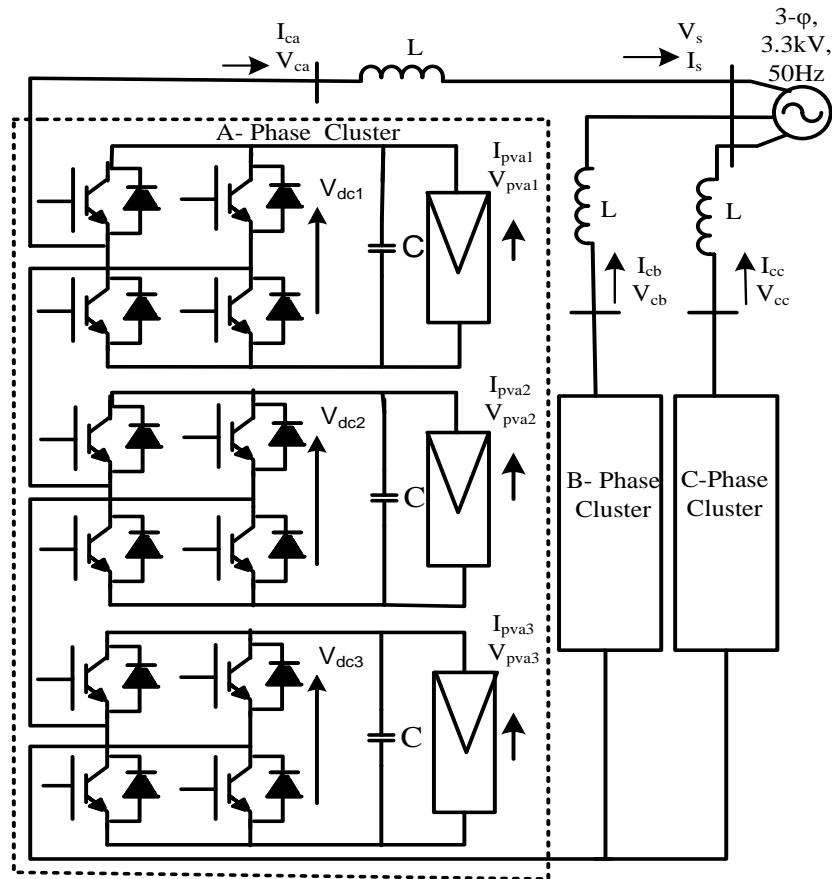


Fig. 3.1 Seven level grid interfaced converter PV system

$$L = (2 * \text{number of H-bridge per phase} + 1) = 7 \quad (3.1)$$

Number of H-bridges per phase ( $s$ ) = 3

So for a 7-level symmetric CHB converter, 3 H-bridges per phase are required, and each H-bridge is fed by the separate and equal PV array, which is easily available in a large multi-string SPV system.

The variables measured for implementing the control algorithm are grid voltages ( $v_{sabc}$ ), grid currents ( $i_{sabc}$ ), converter voltages ( $v_{cabc}$ ), converter currents ( $i_{cabc}$ ), DC link voltage ( $V_{dc}$ ), photovoltaic array voltage ( $V_{pv}$ ), and photovoltaic array current ( $I_{pv}$ ).

### **3.3 DESIGN OF 7-LEVEL SYMMETRICAL CHB MULTILEVEL CONVERTER FOR GRID INTEGRATED PV SYSTEM**

The system design includes the design and modeling of the PV array, DC link capacitor, DC link voltage, and coupling inductor for a seven-level of the multilevel converter. As per the parameters obtained, the PV array is selected from the PV library. Depending on the PV module chosen, the number of series and parallel connected PV modules in a PV array is selected. The other design specifications of the system are given in Table 3.1.

#### **3.3.1 Selection of $V_{dc}$ Voltage for 7-Level Converter**

For L-level CHB multilevel converter, the DC-link voltage ( $V_{dc}$ ) for each H-bridge connected to the PV array is calculated as [10],

$$V_{rms} = 0.612*(L-1)*V_{dc} \quad (3.2)$$

$$V_{dc} = 898.692V.$$

$V_{dc}$  is taken as 905V.

#### **3.3.2 Design Calculations and Selection of PV Array for 7-Level Converter**

The required power rating of each PV array for a 7-level CHB converter consisting of nine PV arrays (i.e. three per phase) for feeding 1.48MW power to the grid is calculated as,

$$P_{mmp} = \frac{\text{(power rating of the system)}}{\text{(number of total PV array)}} \quad (3.3)$$

$$= 1.48\text{MW}/9 = 164.44 \text{ kW}$$

To obtain the PV array of 164.44 kW power ( $P_{mmp}$ ) and  $V_{dc}$  of 905V, a Sharp ND H230Q2 model is chosen from the PV array library. The numbers of PV modules connected in parallel and series in PV array are selected as,

$$N_s = V_{dc}/V_{mmp} \quad (3.4)$$

$$= 30$$

$$N_p = P_{mmp}/(N_s * I_{mmp} * V_{mmp}) \quad (3.5)$$

$$= 23$$

### 3.3.3 Design of DC-link Capacitor for 7-Level Converter

The DC-link capacitor ( $C_{dc}$ ) for each H-bridge connected to the PV array is obtained following the principle of conservation of energy. As per this principle, for  $V_{dc}$  recovery in 5 ms and 1.2 overloading factor 'a', as [11],

$$\frac{1}{2} * C_{dc} (V_{dc}^2 - V_{dc1}^2) = K_1 * 3 * V * a * I * t \quad (3.6)$$

Where  $K_1$  denotes variation of energy during dynamics, taken as 10% ( $K_1 = 0.1$ ).

Therefore, from eqn. (3.6) the DC link capacitor value is found as,

$$C_{dc} = (0.1 * 164444 * 0.005) / (0.5 * (905 * 905 - 898.7 * 898.7))$$

$$C_{dc} = 14471.5 \mu\text{F}$$

It is selected as,  $C_{dc}(C) = 14500 \mu\text{F}$

### 3.3.4 Design of Interfacing Inductor for 7-Level Converter

Interfacing inductor is essentially a low-pass filter, which should satisfy ripple current requirements and cause a low voltage drop. Keeping this in consideration, a 4.5mH inductor is selected for getting the required result of THD of grid current waveform for 7-level as per IEEE-519 standard. The per unit value of inductor corresponding to 4.5mH is calculated as [13]

$$\begin{aligned}
 L_c(\text{p.u.}) &= (2 \cdot \pi \cdot f \cdot L \cdot P) / V_s^2 \\
 &= (314 \times 4.5 \times 10^{-3} \times 1.48 \times 10^6) / (3.3 \times 10^3 \times 3.3 \times 10^3) \\
 &= 0.192 \text{ p.u.}
 \end{aligned}$$

Table-3.1 Component specifications

Component	Value
Power	1.48 MW
Voltage( $V_{\text{rms}}$ )	3.3 kV
Frequency	50 Hz
Switching Frequency	500 Hz
Inductor ( $L_c$ )	4.5mH
No of parallel paths in SPV array ( $N_p$ )	23
No of series paths in SPV array ( $N_s$ )	30
The voltage of the PV module at maximum power ( $V_{\text{mmp}}$ )	30.2 V
The current of PV module at maximum power ( $I_{\text{mmp}}$ )	7.95 A
Open circuit voltage of PV module ( $V_{\text{oc}}$ )	37.5 V
Short circuit current of PV module ( $I_{\text{sc}}$ )	8.61 A
DC-link voltage ( $V_{\text{dc}}$ )	905 V
DC-link capacitor ( $C_{\text{dc}}$ )	14500 $\mu$ F

### 3.4 CONTROL OF 7- LEVEL SYMMETRICAL CHB MULTILEVEL CONVERTER FOR GRID INTEGRATED PV SYSTEM

The control algorithm used for controlling the SPV system tied to the three-phase AC grid is shown in Fig. 3.2. The maximum power developed by the PV array is tracked, employing an improved P&O algorithm. The decoupled current controller has a feed-forward term, separate controller for each DC-link capacitor, SRF and PLL to control the voltage source converter (VSC) [115-116].

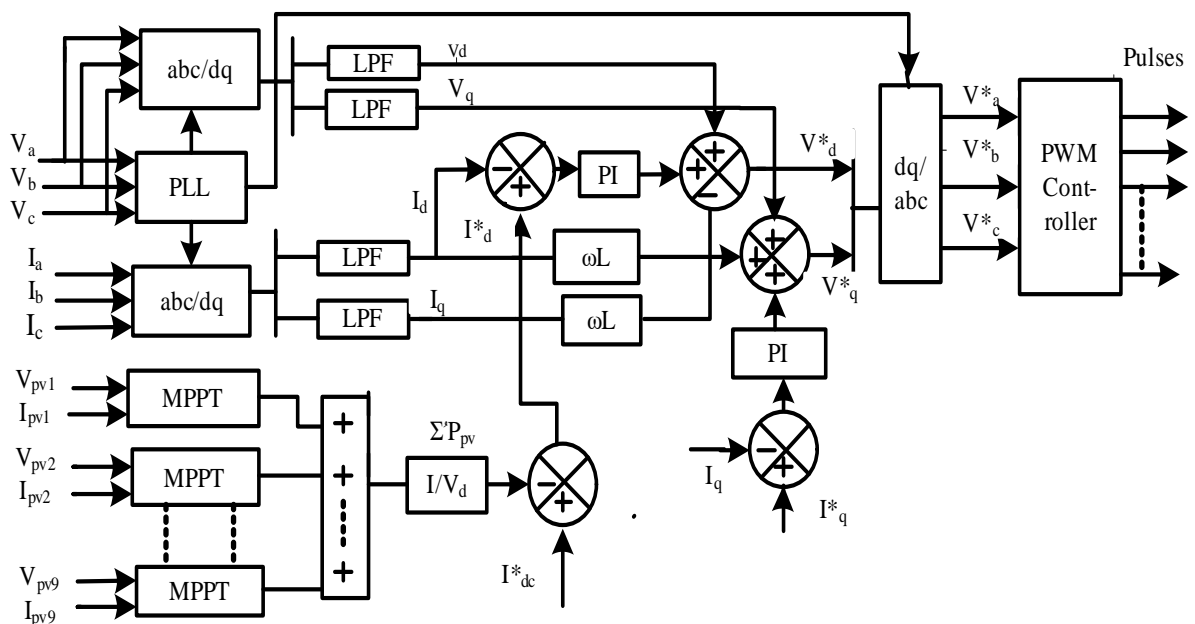


Fig. 3.2 Control algorithm

#### 3.4.1 Implementation of Improved P&O MPPT Algorithm

By using an improved P&O MPPT algorithm, the maximum power is extracted from the PV array, and a suitable reference DC voltage ( $V_{dc\_ref}$ ) is generated in this work. In the improved P&O MPPT algorithm, the detail of variation in PV current ( $\Delta I_{pv}$ ) is also

considered along with the variation in PV voltage ( $\Delta V_{pv}$ ) and PV power ( $\Delta P_{pv}$ ).  $V_{dc\_ref}$  is generated by an improved P&O using logic, as shown in the flowchart shown in Fig. 3.3.

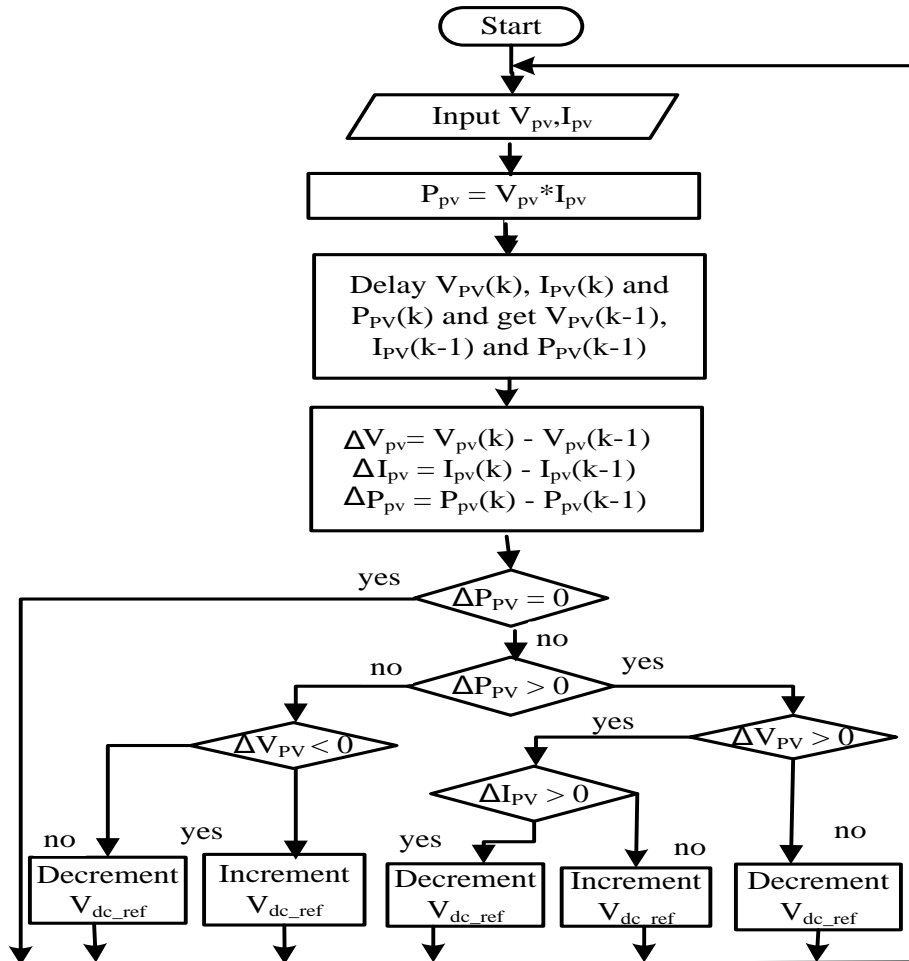


Fig. 3.3 Flowchart for improved P&O MPPT algorithm

### 3.4.2 Implementation of VSC Algorithm

The voltage measured from each DC link of H-bridge is compared with the individual  $V_{dc\_ref}$  obtained by each MPPT algorithm, as shown in Fig.3.4. A proportional-integral (PI) controller processes the error voltage (the difference between the two). The output of the PI controller provides the active current loss component  $I^*_a$ , through the DC link, which is given as,

$$I_d^*(k) = I_d^*(k-1) + K_p\{V_e(k) - V_e(k-1)\} + K_i V_e(k) \quad (3.7)$$

Where  $V_e(k)$  and  $V_e(k-1)$  are the error voltages at given sampling instants  $k$  and  $(k-1)$ . The  $K_p$  &  $K_i$  are proportional and integral gain constants. The sum of all reference DC-link currents and the feed-forward term are compared with the direct current component ( $I_d$ ).  $I_d$  is obtained by Park's transform from the grid currents as,

$$\begin{bmatrix} I_d \\ I_q \\ I_0 \end{bmatrix} = \frac{2}{3} \begin{bmatrix} \sin(\theta) & \sin\left(\theta - \frac{2\pi}{3}\right) & \sin\left(\theta + \frac{2\pi}{3}\right) \\ \cos & \cos\left(\theta - \frac{2\pi}{3}\right) & \cos\left(\theta + \frac{2\pi}{3}\right) \\ \frac{1}{2} & \frac{1}{2} & \frac{1}{2} \end{bmatrix} \begin{bmatrix} I_a \\ I_b \\ I_c \end{bmatrix} \quad (3.8)$$

The grid detection angle ( $\theta$ ) for Park's transformation is obtained from three-phase PLL.  $I_q^*$ , the reference quadrature current is set to zero for feeding grid current at unity power factor. It is compared with the quadrature current component obtained from Park's transformation.

Similarly, using Park's transformation, direct and quadrature components of grid voltages ( $V_d$  &  $V_q$ ) are calculated as follows.

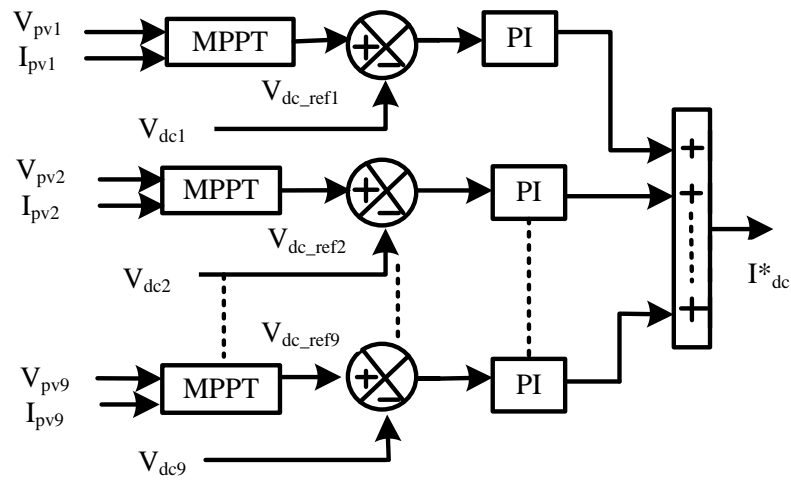


Fig.3.4 Control algorithm for generating  $I_{dc}^*$

$$\begin{bmatrix} V_d \\ V_q \\ V_0 \end{bmatrix} = \frac{2}{3} \begin{bmatrix} \sin(\theta) & \sin\left(\theta - \frac{2\pi}{3}\right) & \sin\left(\theta + \frac{2\pi}{3}\right) \\ \cos(\theta) & \cos\left(\theta - \frac{2\pi}{3}\right) & \cos\left(\theta + \frac{2\pi}{3}\right) \\ \frac{1}{2} & \frac{1}{2} & \frac{1}{2} \end{bmatrix} \begin{bmatrix} V_a \\ V_b \\ V_c \end{bmatrix} \quad (3.9)$$

The reference direct-axis voltage and quadrature-axis voltage are calculated as,

$$V_d^*(k) = V_d^*(k-1) + K_{p2} \{ I_{de}(k) - I_{de}(k-1) \} + K_{i2} * I_{de}(k) + V_d - I_q^* \omega L \quad (3.10)$$

$$V_q^*(k) = V_q^*(k-1) + K_{p3} \{ I_{qe}(k) - I_{qe}(k-1) \} + K_{i3} * I_{qe}(k) + V_q + I_d^* \omega L \quad (3.11)$$

Where  $I_{de} = (I_d^* - I_d)$ ,  $I_{qe} = (I_q^* - I_q)$ , and  $\omega L$  is the coupling reactance.  $K_{p2}$ ,  $K_{i2}$ , denote the direct-axis current controller's proportional and integral gains, and  $K_{p3}$  and  $K_{i3}$  are the proportional and integral gains of the quadrature-axis current controller. The reference voltages (modulating signal) for the PWM controller are obtained using the inverse Park's transform.

### 3.4.3 Implementation of Phase Shifted Multi-Carrier PWM Control 7-Level Converter

For the PWM controller, a phase-shifted modulation technique is used. In phase-shifted SPWM, the gate signals are generated by comparing the modulating signal with the triangular carrier waves, as shown in Fig.3.5. A multilevel converter with L-levels in output staircase waveform requires (L-1) triangular carrier's waveform having the same frequency and amplitude (unit amplitude). The phase shift between two adjacent carrier waves is calculated as in [10]

$$\varphi_{cr} = 360^\circ / (L-1) \quad (3.12)$$

$$= 360^\circ / 6 = 60^\circ$$



Each carrier ( $V_{cr1}$  to  $V_{cr6}$ ) is compared with  $V_{ref}$  signal to generate pulses, as shown in Fig.3.6. The bipolar phase-shifted SPWM method is used for modulation [8,10].

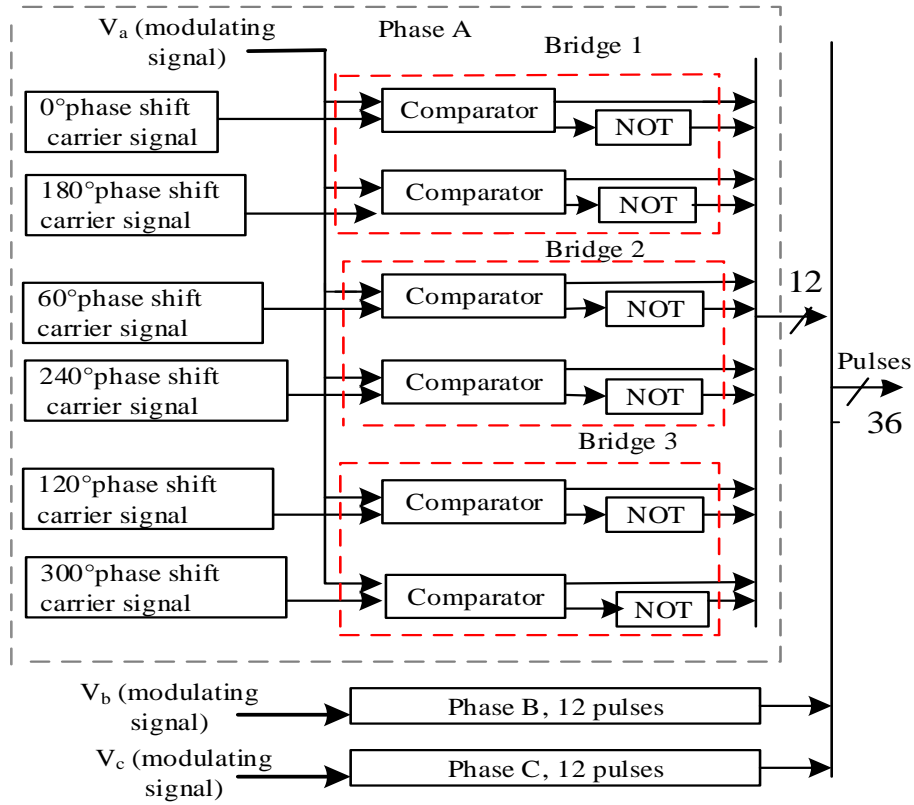


Fig.3.5 Generation of pulses for 7-level converter

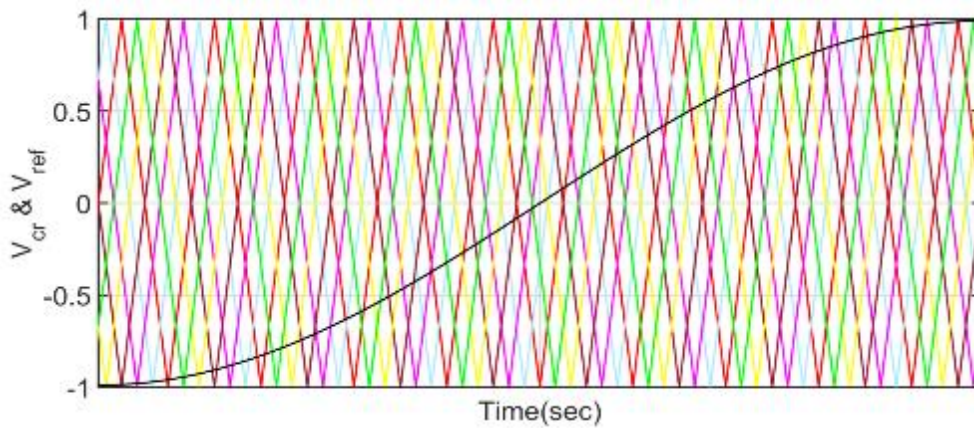


Fig.3.6 Phase shifted PWM scheme for 7-level converter

### **3.5. MATLAB BASED MODELLING OF 7-LEVEL SYMMETRICAL CHB MULTILEVEL CONVERTER FOR GRID INTEGRATED PV SYSTEM**

This section presents the MATLAB based modelling of a seven-level CHB multilevel converter for grid interfaced SPV system. MATLAB R2015a is used for simulation. MATLAB modeling of the grid-connected converter, PV array fed 7-level CHB multilevel converter for phase A (remaining phase modeling is the same as phase A), single H-bridge module, MATLAB model for MPPT block, control algorithm, and phase-shifted sinusoidal PWM is also developed. MATLAB model is implemented by selecting a block from both Simulink and Simscape SimPowerSystems specialized technology library of MATLAB.

#### **3.5.1 MATLAB Model of Grid Connected Converter**

The developed MATLAB model of grid-connected multilevel converter for three-phase system is shown in Fig. 3.7. The system is interfaced through the coupling inductor. The grid voltages ( $v_{sabc}$ ), grid currents ( $i_{abc}$ ), converter voltages ( $v_{cabc}$ ), and converter currents ( $i_{cabc}$ ) are sensed from three-phase VI-measurement. Phase to neutral and phase to phase voltage of 7-level CHB multilevel converter are also measured. Discrete powergui environmental block is selected from Simscape SimPowerSystems specialized technology library. Three-phase sources block of rating 3.3kV is chosen from the same library for the grid.

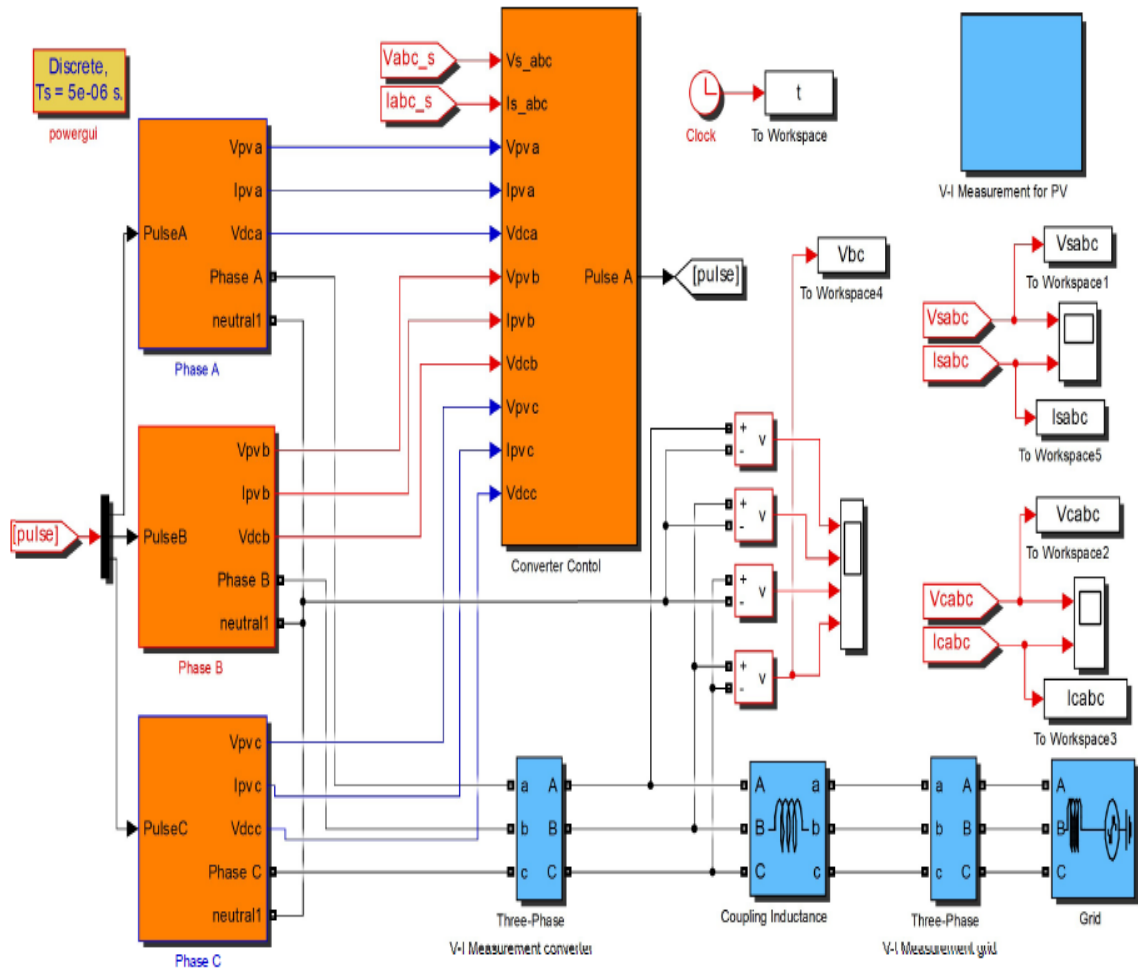


Fig. 3.7 MATLAB implementation of Grid-connected converter

### 3.5.2 MATLAB Model of PV Array Connected Seven-Level H-Bridge Converter

For getting a seven-level converter, three H-bridges are connected in a cascade. Each PV array is fed by separate H-bridge as shown in Fig. 3.8. A single H-bridge module is shown in Fig.3.9. For the photovoltaic system, the insolation level is taken as  $1000\text{W}/\text{m}^2$  and at a temperature of  $25^\circ\text{C}$ . The insolation level's value is given to the PV array through a limiter block, and the temperature is provided through a saturation block, selected from the Simulink library. A Sharp ND H230Q2 PV array is selected from simscape simpowersystems specialized technology PV array library. The photovoltaic voltage and

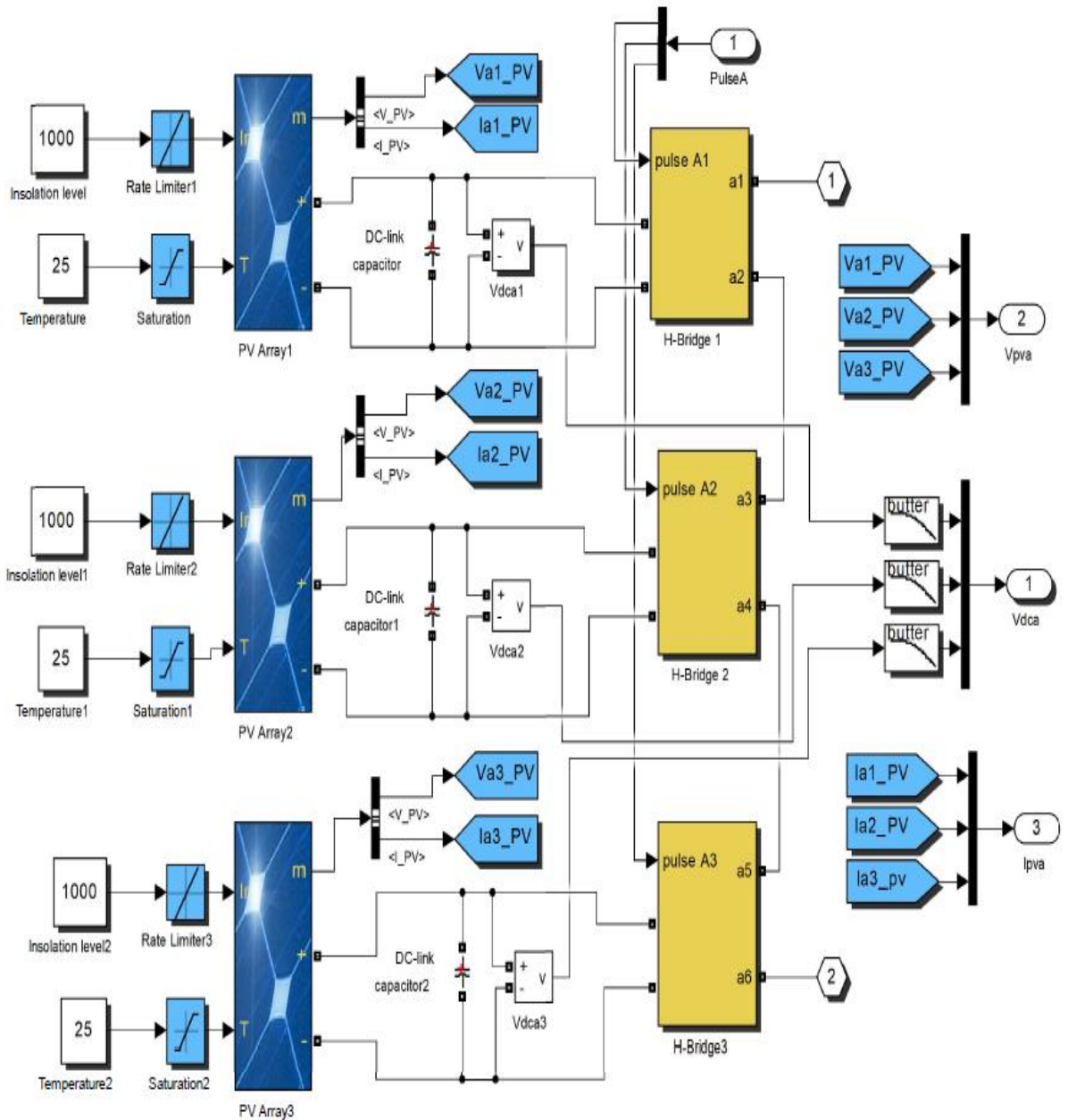


Fig. 3.8 PV array fed 7-level CHB multilevel converter

current of array1 ( $V_{a1\_PV}$  &  $I_{a1\_PV}$ ), array2 ( $V_{a2\_PV}$  &  $I_{a2\_PV}$ ) and array 3 ( $V_{a3\_PV}$  &  $I_{a3\_PV}$ ) are measured for MPPT.  $V_{dc1}$ ,  $V_{dc2}$ , and  $V_{dc3}$  are the DC-link voltages across the DC link capacitor, measured to control the DC-link and give  $I_d^*$  for active power loss component.

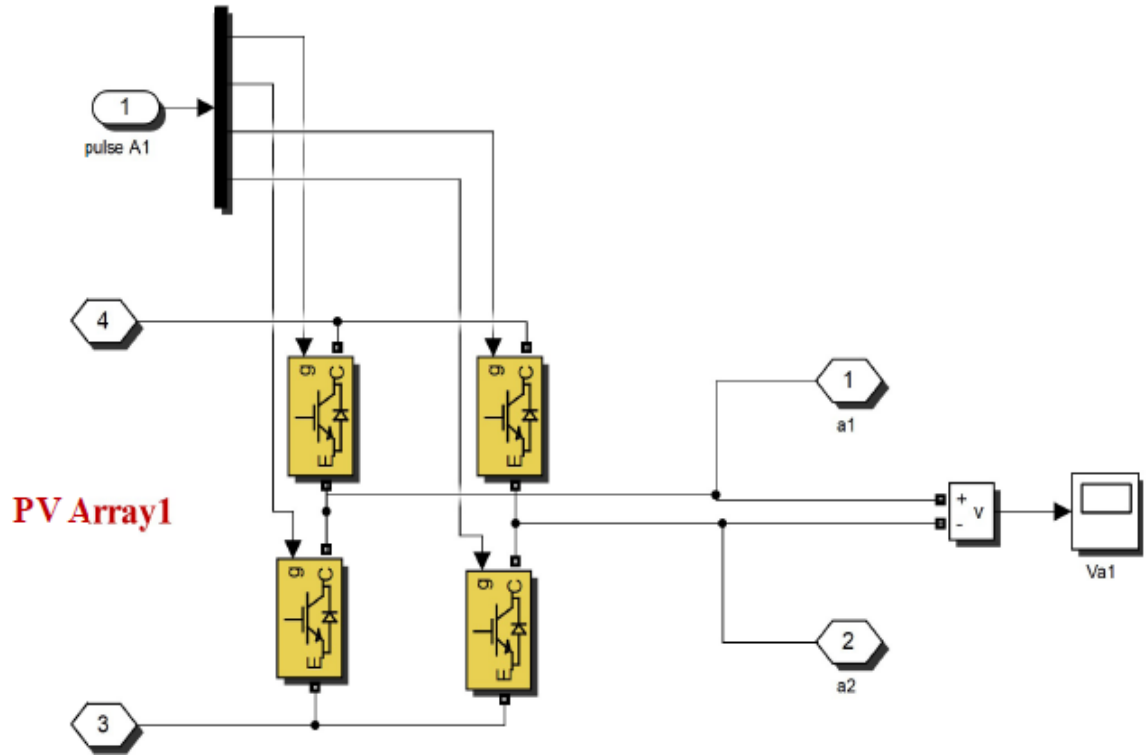


Fig. 3.9 Single H-bridge module

### 3.5.3 MATLAB Model of the Control Algorithm

Fig.3.10 shows the control algorithm for VSC control. To implement the decoupled current scheme, the abc to dq0 transformation block and PLL block are selected from simpower systems specialized technology library. The measured value of grid currents ( $i_{sabc}$ ) and grid voltage ( $v_{sabc}$ ) are input to abc to the dq0 transformation block. The dq-components of voltage and currents obtained from transformation are filtered by 2<sup>nd</sup> order Butterworth filter of 12 Hz frequency. The reference direct current obtained from the MPPT block and the feed-forward term are compared by a comparator block selected from Simulink library with direct current  $I_d$  and error signal given to PI-controller. A saturation limit is fixed on the output of the controller to avoid unwanted oscillation. Similarly, the quadrature-component of current is compared with zero-reference and the

error voltage is passed through a PI-controller with saturation limit fixed at the output. The reference dq-components of voltages so obtained is transformed to  $V^*_{abc}$  (modulation signal) and given to the PWM block. The synchronous signal ( $\omega t$ ) is provided by the PLL to abc to dq0 and dq0 to abc. The synchronous signal ( $\omega t$ ) is provided by the PLL to abc to dq0 and dq0 to abc.

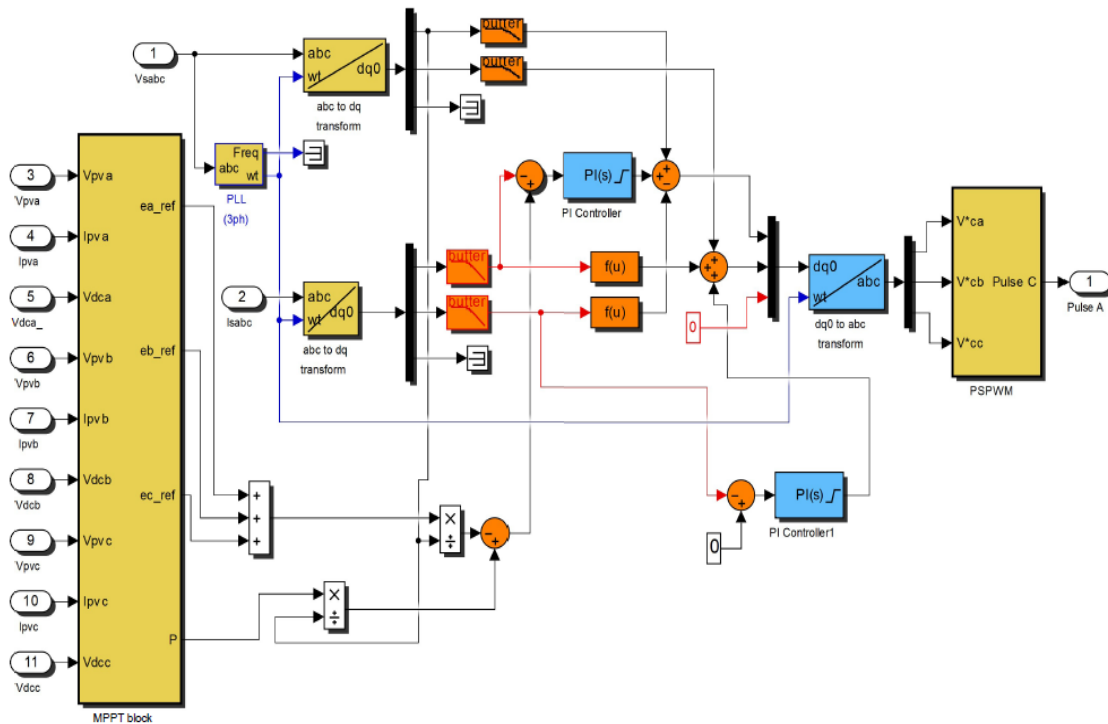


Fig.3.10 MATLAB implementation of Control algorithm for 7-level converter

Each PV array is provided with a separate MPPT algorithm as shown in Fig.3.11, and every MPPT algorithm is controlled by a separate PI-controller with a saturation limit. The MPPT algorithm is implemented by writing the MPPT algorithm on a user-defined block of Simulink library of MATLAB. Param block gives the upper and lower limit of  $V_{dc\_ref}$  and increment step for algorithm. The MPPT algorithm provides the  $V_{dc\_ref}$  for controlling each DC-link of PV array. It also provides power generated by each PV array for finding the feed-forward term.

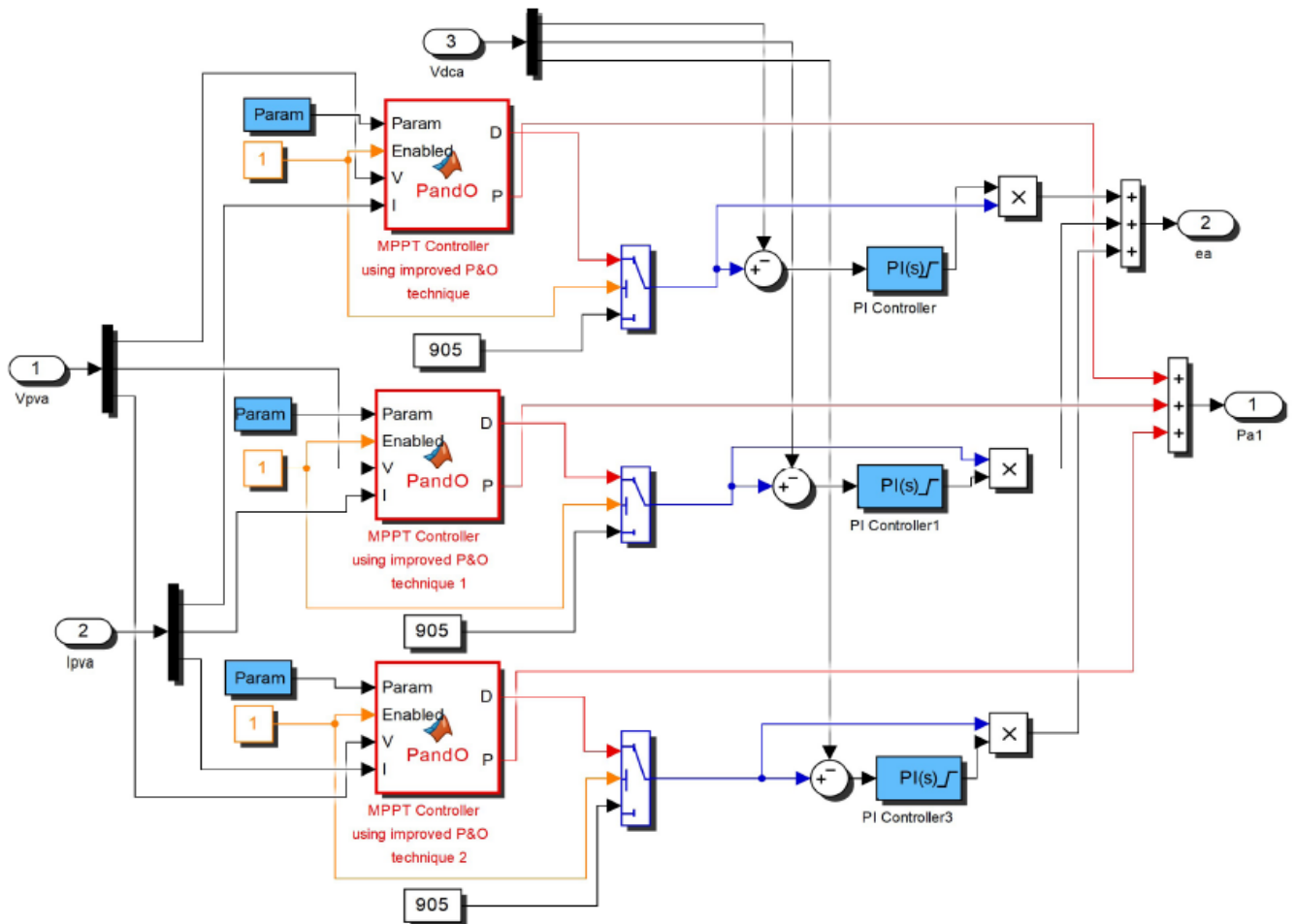


Fig. 3.11 MATLAB implementation of MPPT controller for 7-level converter

### 3.5.5 MATLAB Model of Phase-shifted PWM

The six carrier signals of 500 Hz switching frequency are generated by selecting a triangle generator block from simpowersystems specialized technology control and signal generation library for implementing the phase-shifted PWM. The triangle generator block generates a symmetrical triangle waveform with a peak amplitude of  $\pm 1$ . These carrier signals are compared with the modulating signal, as shown in Fig. 3.12, and pulses are generated. Comparator and NOT-gate block are selected from the Simulink library for the generation of pulses.

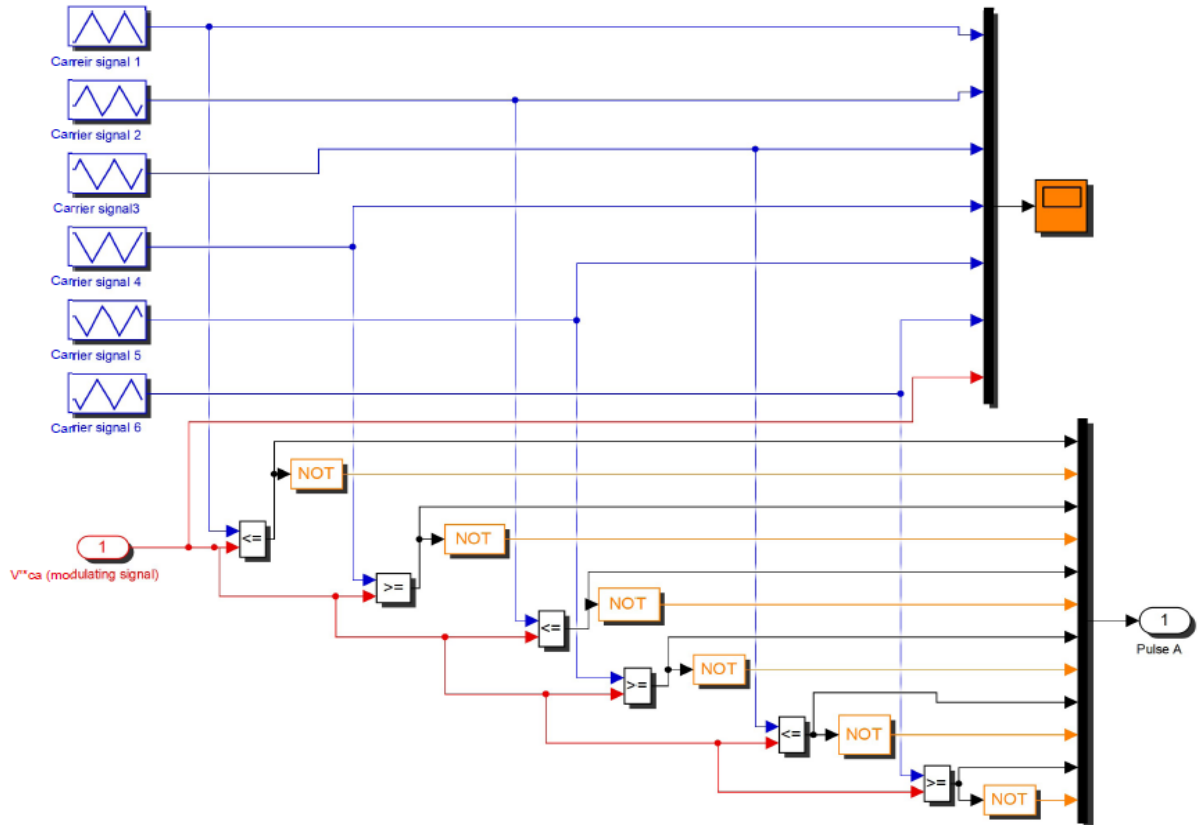


Fig. 3.12 MATLAB model of Phase shifted PWM for 7-level

### 3.6 RESULTS AND DISCUSSION

The three-phase grid-tied SPV system, as shown in Fig.3.1, is designed, modeled, and controlled with a seven-level H-bridge multilevel converter. This system is simulated in MATLAB/Simulink and OPAL RT simulator, and the results are discussed as follows.

#### 3.6.1 Steady-State Performances for 7-level Converter

The steady-state response of the system is studied at an insolation level of  $1000 \text{ W/m}^2$  and temperature  $25^\circ\text{C}$  and the results are depicted in Fig.3.13. For validating the system performance, the simulated results are consisting of the grid voltages ( $v_{sabc}$ ), converter voltages ( $v_{cabc}$ ), SPV voltage ( $V_{pv}$ ), SPV current ( $I_{pv}$ ) and power (P). The grid voltage



and the grid current are in phase in steady-state response, so the maximum active power transfer is evident at a power factor of unity. The PV array generates almost constant voltage and delivers almost constant current and power as shown in figure.

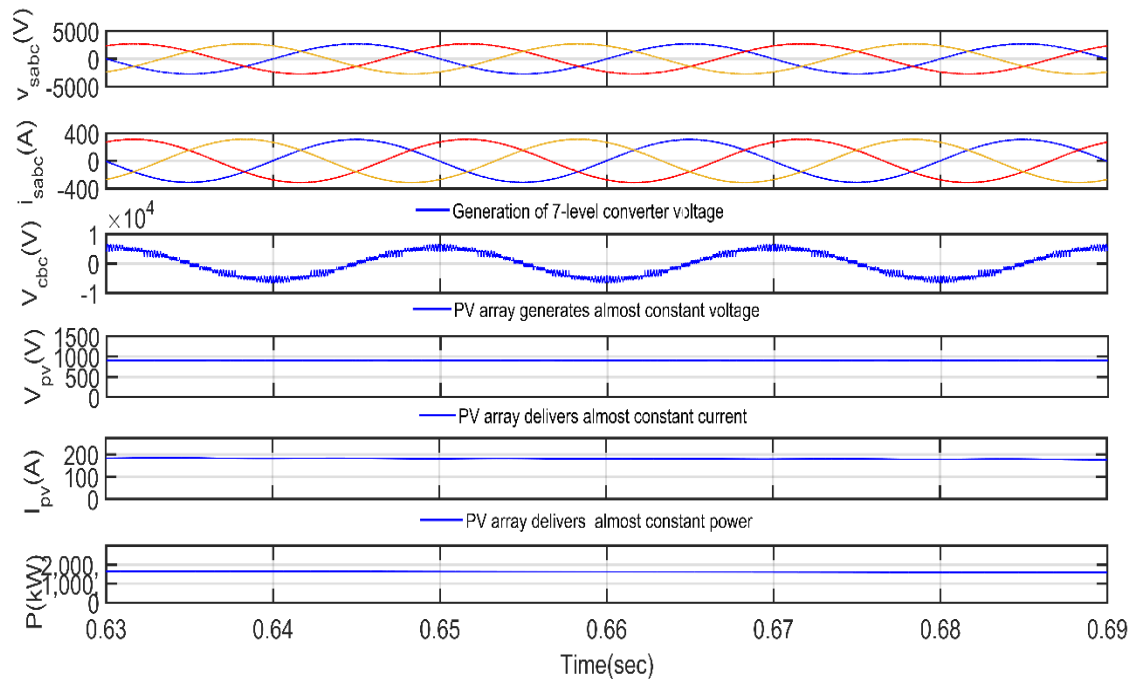
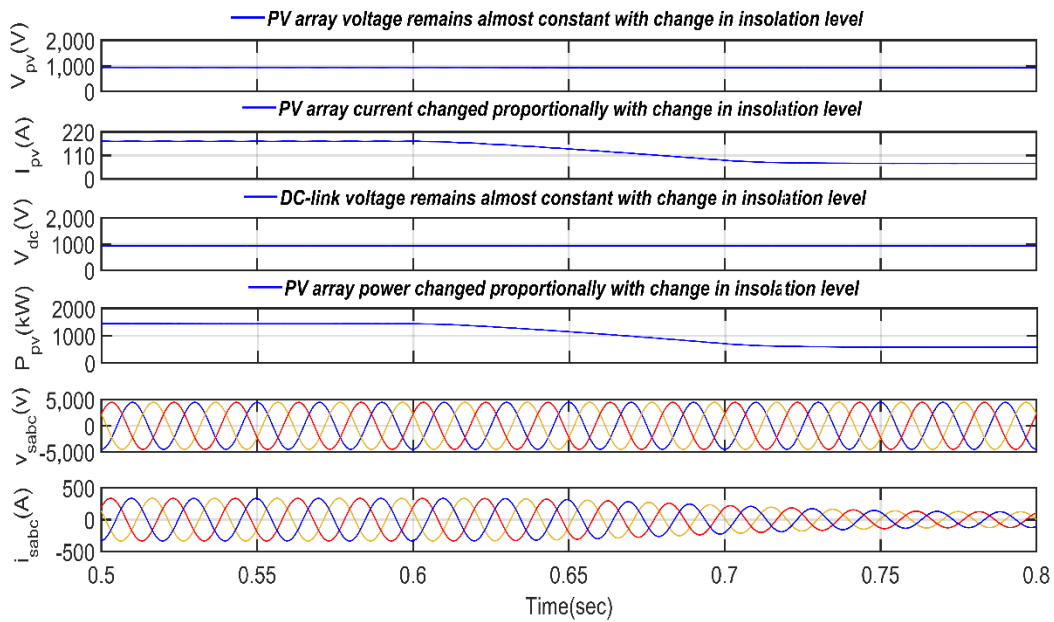


Fig.3.13 Steady-state performance at insolation level  $1000 \text{ W/m}^2$  and temperature  $25^\circ\text{C}$  for 7-level symmetrical CHB grid-tied system

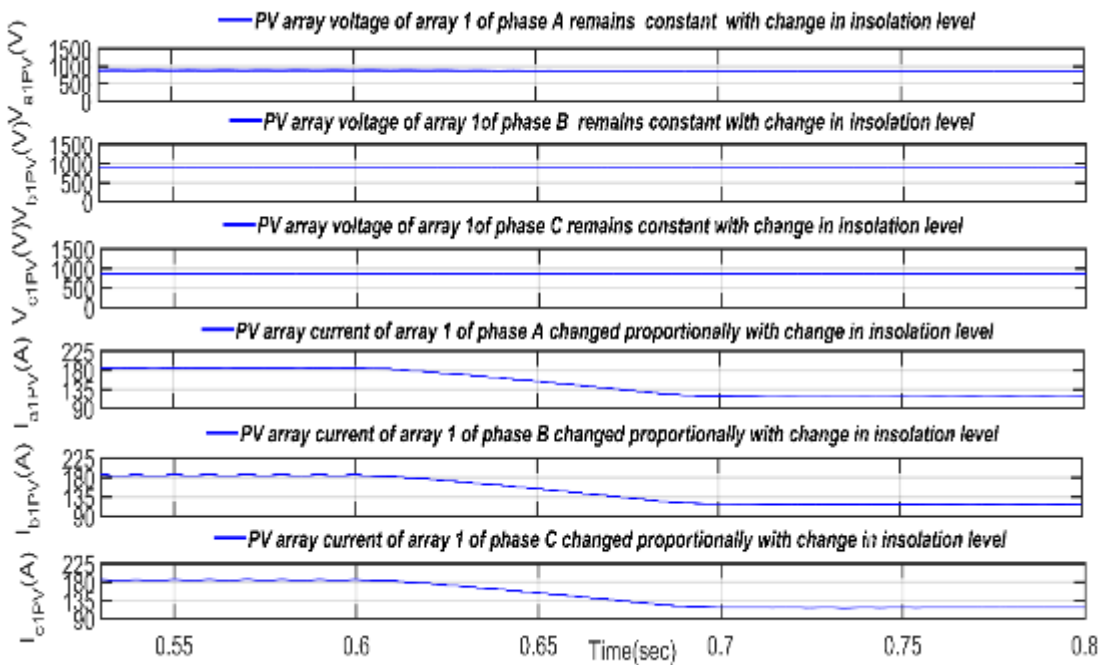
### 3.6.2 Dynamic Performances of 7-level Converter

The dynamic response is studied with constant temperature of  $25^\circ\text{C}$  and an insolation change from  $1000 \text{ W/m}^2$  to  $400 \text{ W/m}^2$  at 0.6 sec, as shown in Figs. 3.14 (a) and (b). Simulated results consist of the voltages & the currents for a PV array 1 of A-phase ( $V_{a1pv}$  &  $I_{a1pv}$ ), B- phase ( $V_{b1pv}$  &  $I_{b1pv}$ ), C- phase ( $V_{c1pv}$  &  $I_{c1pv}$ ). In dynamic response, with the decrease of the insolation level, the remarkable change in the PV current is observed, while there is no significant change seen in the PV voltage. The PV voltage and the change in PV array current are same for three phase array 1, which verifies that the distributed MPPT control of each array is achieved as shown in Fig. 3.14 (b). The grid

current, PV array power and PV array current change proportionally and PV voltage and grid voltage remain constant with the change in insolation level as shown in Fig. 3.14 (a).



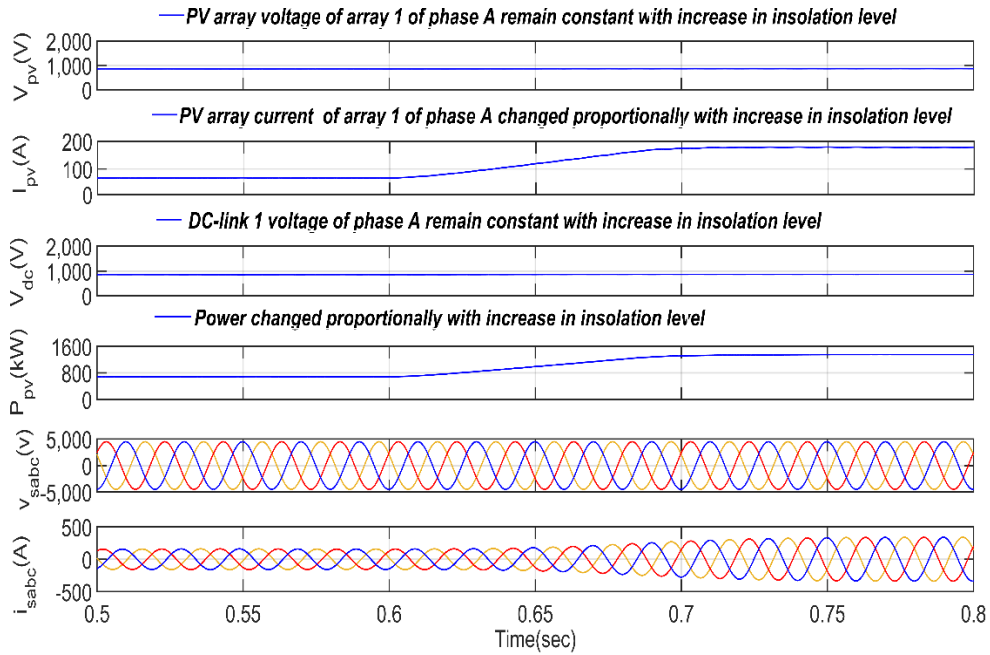
(a)



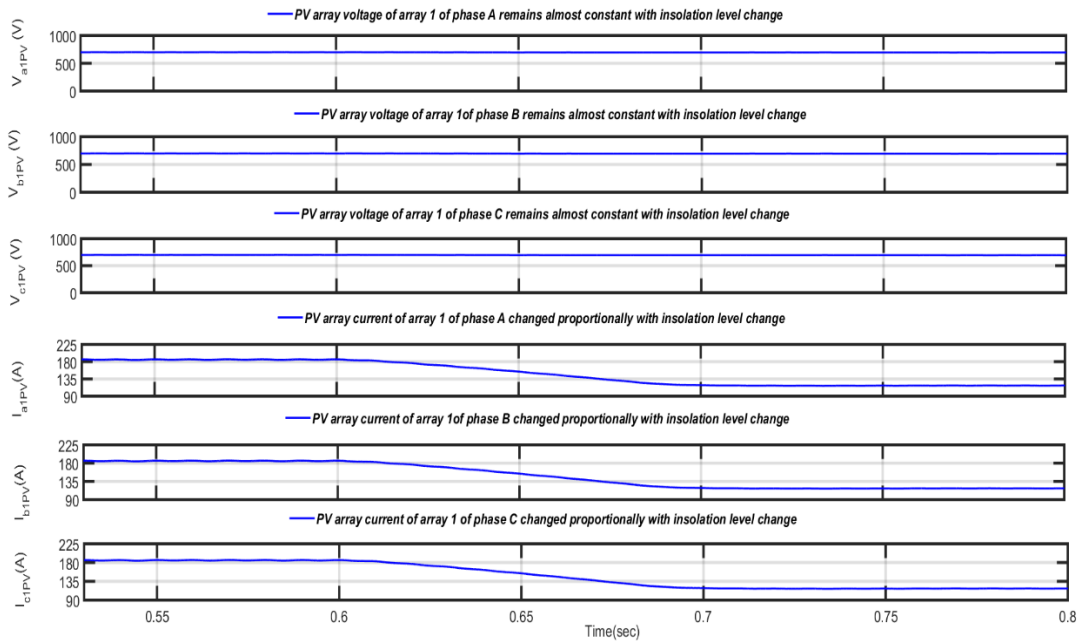
(b)

Fig.3.14(a) and (b) Dynamic performance when insolation level is changed from 1000 to 400 W/m<sup>2</sup> at 0.6 sec for 7-level symmetrical CHB grid-tied system

Fig.3.14 (c) and (d) show the value of  $I_{pv}$ ,  $V_{pv}$ ,  $i_{sabc}$ ,  $v_{sabc}$ ,  $P$  and  $V_{dc}$  with the increase in insolation level from  $400\text{W/m}^2$  to  $1000\text{ W/m}^2$  at 0.6 sec.



(c)

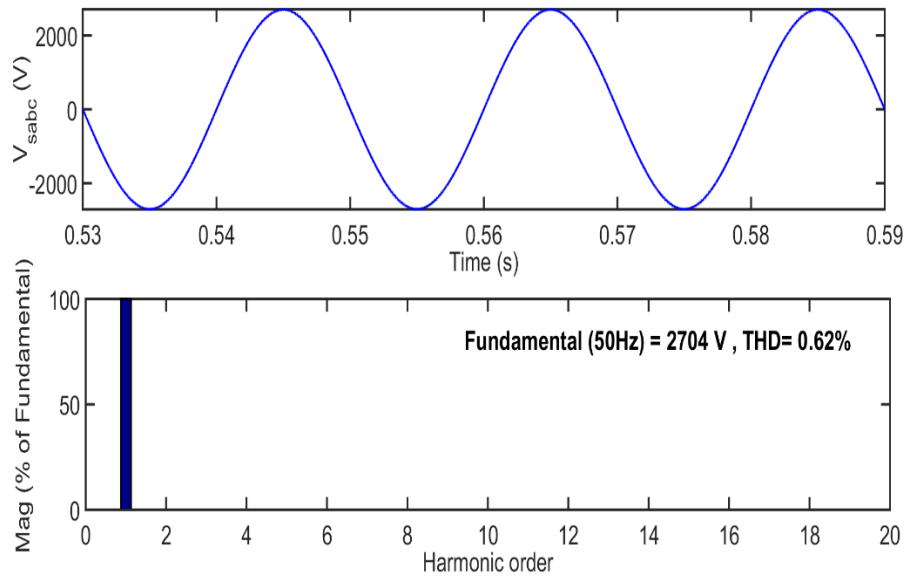


(d)

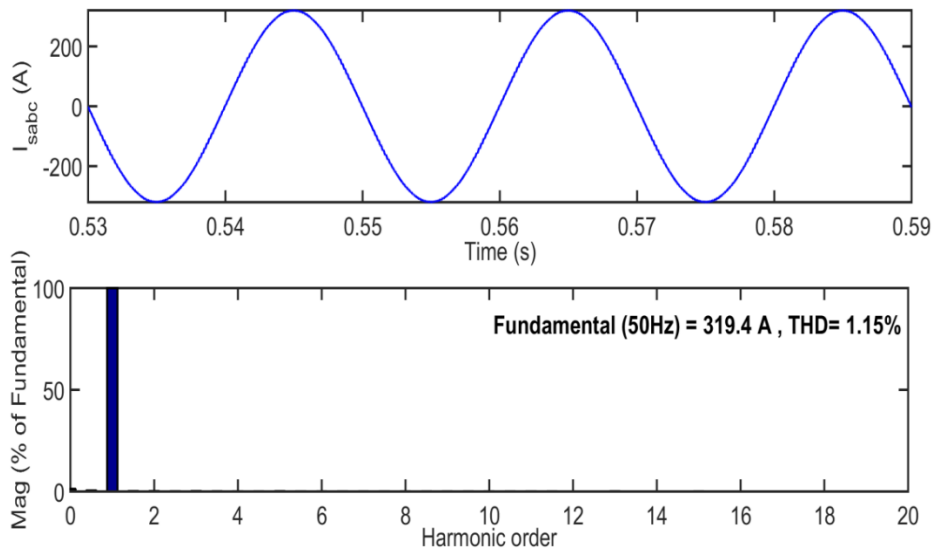
Fig.3.14(c) and (d) Dynamic performance when insolation level is changed from 400 to 1000  $\text{W/m}^2$  at 0.6 sec for 7-level symmetrical CHB grid-tied system

### 3.6.3 Power Quality Performances for 7-level Converter

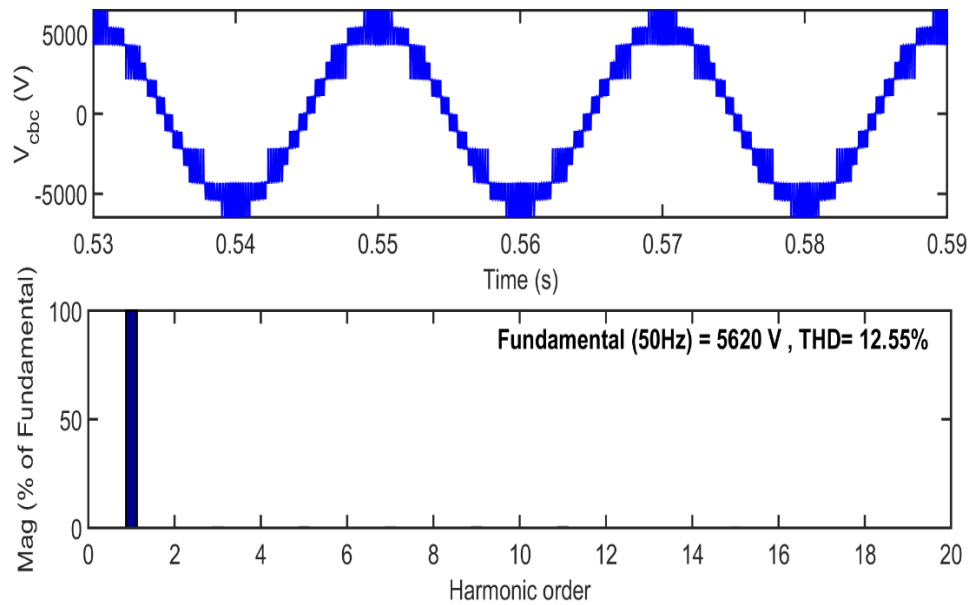
Fig. 3.15 shows the waveforms for the line voltage, line current ( $i_a$ ), and converter line voltage ( $v_{cabc}$ ) and harmonic spectra along with THD levels at 1000 W/m<sup>2</sup> level. The THD values of 0.62 %, 1.15%, and 12.55% at insolation of 1000 W/m<sup>2</sup> and temperature



(a)



(b)



(c)

Fig. 3.15 Waveform and harmonic spectra of (a) line voltage (b) line current  
(c) converter current

of 25°C, respectively, are observed for line voltage, line current and converter line voltage. The THD of the supply current is observed to be within limits set by the IEEE-519 standard [17]. A minor variance is seen, though; the power factor is also close to unity.

### 3.6.4 Validation of Results in HIL on OPAL-RT Simulator

Simulation results obtained in previous section are validated in hardware-in-loop (HIL) on OPAL-RT platform. The procedure and parameter settings and other system details for using OPAL-RT are shared in the appendix. Fig.3.16 to Fig.3.18 show the steady state performance of the system at 1000W/m<sup>2</sup> and 25°C temperature. Fig. 3.16 gives the steady state performance of PV array1 voltage of phase A ( $V_{pv}$ ), PV array1 current of phase A ( $I_{pv}$ ), phase A grid current ( $i_{sa}$ ) and converter voltage ( $v_{ca}$ ). Fig. 3.17 and Fig. 3.18 give

the steady state performance of phase A, B and C of converter voltages ( $v_{ca}$ ,  $v_{cb}$  and  $v_{cc}$ ) and grid currents ( $i_{sa}$ ,  $i_{sb}$  and  $i_{sc}$ ) respectively. Fig. 3.19 and Fig.3.20 show the dynamic performance of the system with increase and decrease in irradiance and show the change in  $V_{pv}$ ,  $I_{pv}$ ,  $i_{sa}$  and converter voltage with the change in irradiance.  $V_{pv}$  and converter voltage remains constant and  $I_{pv}$  and  $i_{sa}$  changes with change in irradiance as shown in Fig. 3.19 and Fig. 3.20. THD of converter phase voltage, converter line voltage and grid current are 17.31%, 12% and 1.2% respectively, as shown in Fig. 3.21, Fig.3.22 and Fig.3.23. Above values of the THDs validate the results obtained in MATLAB/Simulink environment.

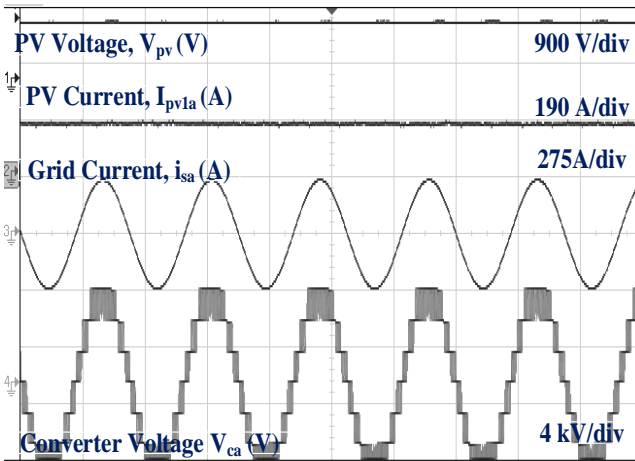


Fig. 3.16 Steady state performance of  $V_{pv}$ ,  $I_{pv}$ ,  $i_{sa}$  and converter voltage at 25°C and 1000W/m<sup>2</sup>

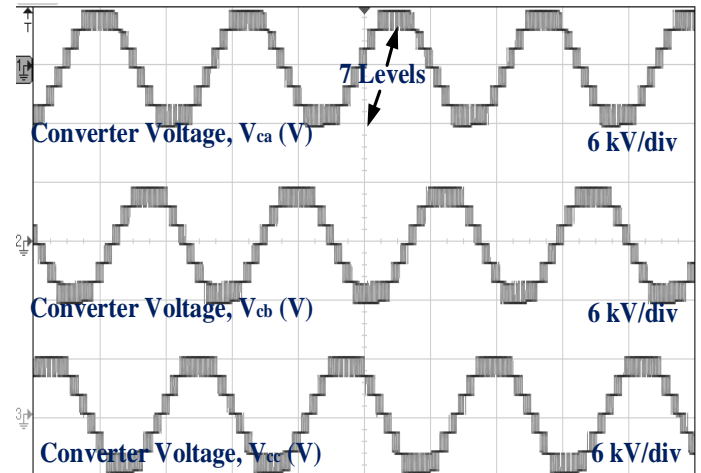


Fig. 3.17 Steady state performance of  $v_{ca}$ ,  $v_{cb}$  and  $v_{cc}$ , voltage at 25°C and 1000W/m<sup>2</sup>

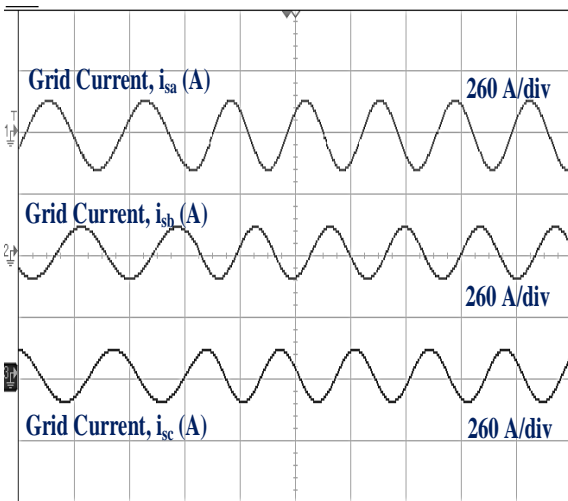


Fig. 3.18 Steady state performance of  $i_{sa}$ ,  $i_{sb}$  and  $i_{sc}$  at 25°C and 1000W/m<sup>2</sup>

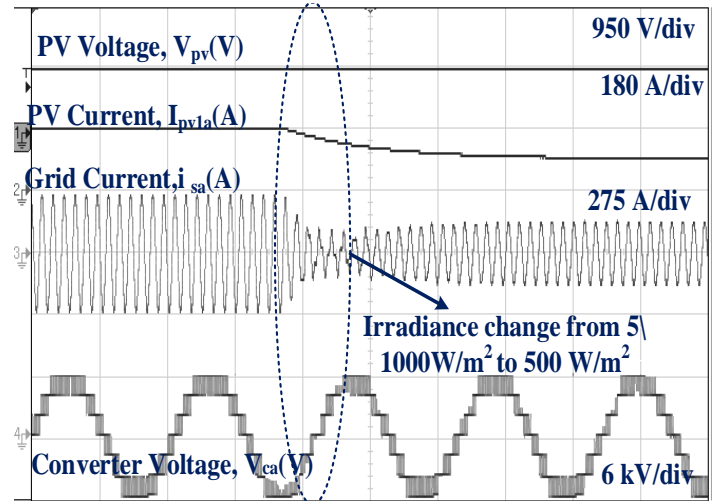


Fig. 3.19 Dynamic performance of  $V_{pv}$ ,  $I_{pv}$ ,  $i_{sa}$  and converter voltage at irradiance change from 1000W/m<sup>2</sup> to 500 W/m<sup>2</sup>

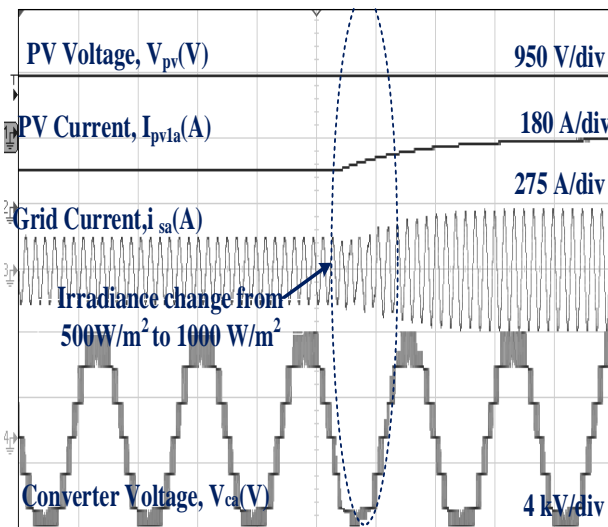


Fig. 3.20 Dynamic performance of  $V_{pv}$ ,  $I_{pv}$ ,  $i_{sa}$  and converter voltage at irradiance change from 500W/m<sup>2</sup> to 1000 W/m<sup>2</sup>

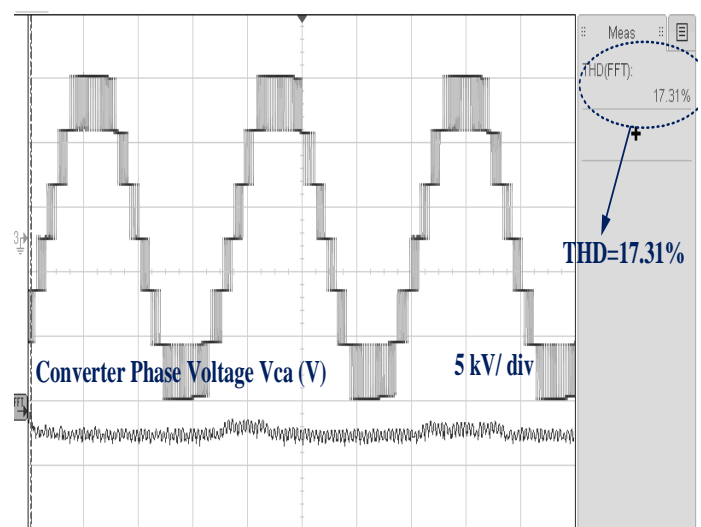
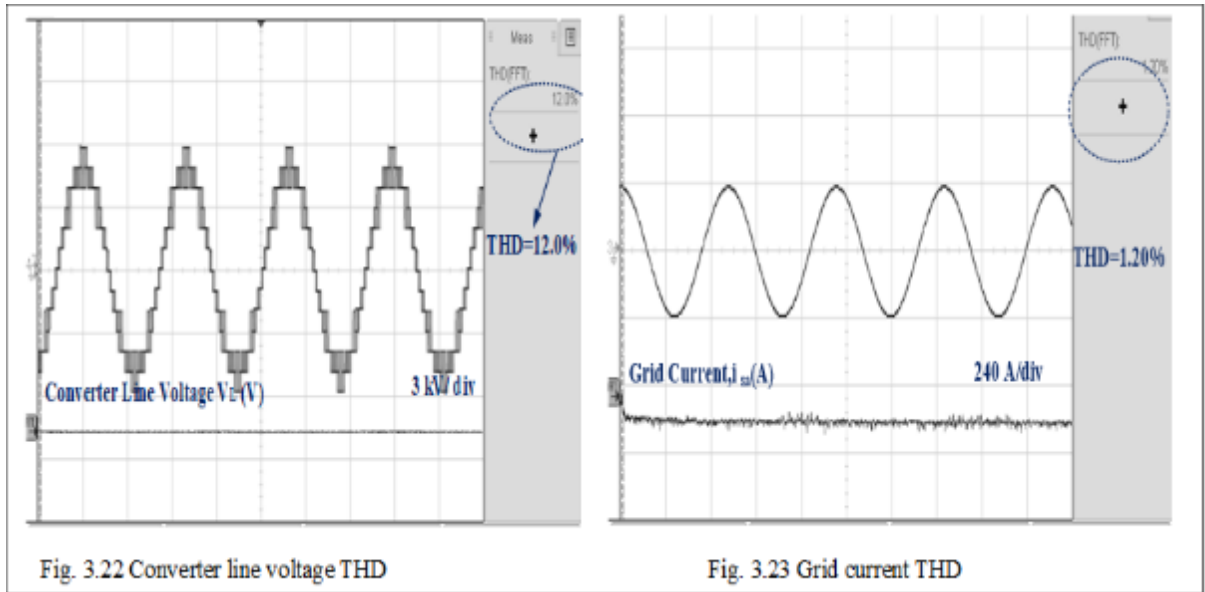


Fig. 3.21 Converter phase voltage THD



### 3.7 CONCLUSIONS

The design, modelling and control of transformerless single-stage seven-level H-bridge cascaded multilevel converters have been carried out with the improved P&O MPPT, decoupled current controller based on SRF-PLL, and phase-shifted SPWM at 500 Hz switching frequency for the photovoltaic grid-tied plant. Enhanced power quality is observed because of the increased output multilevel converter voltage waveform steps compared to a two-level converter. It has attributed to the reduction in the supply current THD. Only an inductive filter is used for filtrating, which further results in a reduction of the cost. The system's performance is observed satisfactory at  $1000 \text{ W/m}^2$  insolation level and  $25^\circ\text{C}$  temperature and has been validated in accordance with the IEEE-519 standard [17].



## CHAPTER-IV

### CONTROL AND DESIGN OF NINE LEVEL CASCADED MULTILEVEL CONVERTER BASED PV SYSTEM

#### 4.1 GENERAL

The design, modeling, and control of nine-level symmetrical CHB MLC for transformerless grid integration of the photovoltaic system with SHE-PWM, NLM, and phase-shifted multicarrier PWM are given in this chapter. Power quality improvement is the major issue in grid integrated converters as they inject harmonics into the grid. Many modulation techniques are developed for a multilevel converter (used for medium or high voltage grid) to meet the challenge of eliminating harmonics. Selective harmonic elimination–pulse width modulation (SHE-PWM) method, nearest level method (NLM), and phase-shifted PWM are investigated in this chapter for a 9-level cascaded H-bridge (CHB) multilevel converter for the grid integration of a large PV (Photovoltaic) system. The SHE-PWM method is applied to eliminate its fifth, seventh, and eleventh order harmonic contents. The converter's control scheme comprises a decoupled current control with a synchronous rotating frame- phase-locked loop (SRF-PLL). Separate improved perturb and observe (P&O) maximum power point tracking (MPPT) algorithm is used to track maximum power from each PV array to overcome the unpredictable irradiance level variations, ambient temperature, and shading effect, and other relevant factors of multi-string SPV system. The system steady-state performance and dynamic performance at different insolation levels are simulated in the MATLAB software platform. The performance is validated as per the IEEE-519 standard by using the FFT tool of MATLAB. The 9-level CHB converter with SHE-PWM technique is also tested and validated using OPAL-RT simulator platform. Hardware in loop (HIL) validated results obtained on OPAL-RT system are in conformity with simulated results obtained in

MATLAB/Simulink environment. The system configuration, design, modelling, control, simulation, and results are discussed in detail in different sections of this chapter.

## 4.2 SYSTEM CONFIGURATION

As shown in Fig. 4.1, the system is designed for a 1.48 MW, 3.3 kV, 50Hz, 3- $\Phi$  nine-level cascaded H-bridge (CHB) converter. The SPV system is connected to the grid through an interfacing inductor for reducing ripple content in the current. If the  $L$  is the number of levels in the cascaded multilevel converter, the H-bridge number per phase selected is calculated as [10].

$$L = (2 * \text{number of H-bridge per phase} + 1) = 9 \quad (4.1)$$

Number of H-bridges per phase ( $s$ ) = 4

So for a 9-level symmetric CHB converter, 4 H-bridges per phase are required, and each H-bridge is fed by the separate and similar PV array, which is easily available in a

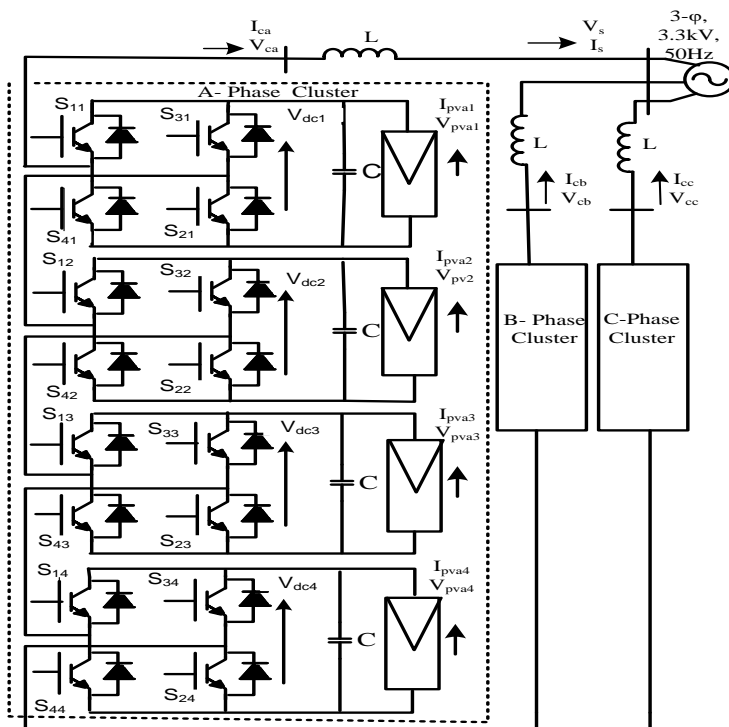


Fig.4.1 9-Level Grid Interfaced Converter PV System

large multi-string SPV system. The variables measured for implementing the control algorithm are grid voltages ( $v_{sabc}$ ), grid currents ( $i_{sabc}$ ), converter voltages ( $v_{cabc}$ ), converter currents ( $i_{cabc}$ ), DC link voltage ( $V_{dc}$ ), photovoltaic array voltage ( $V_{pv}$ ), and photovoltaic array current ( $I_{pv}$ ).

### **4.3 DESIGN OF 9-LEVEL SYMMETRICAL CHB MULTILEVEL CONVERTER FOR GRID INTEGRATED PV SYSTEM**

The system designed includes the design and modeling of the PV array, DC-link capacitor, DC-link voltage, and coupling inductor for a nine-level of the multilevel converter. As per the parameters obtained, the PV module is selected from the PV library. Depending on the PV module chosen, the number of series and parallel connected PV modules in a PV array is selected. The other design specifications of the system are given in Table 4.1.

#### **4.3.1 Selection of $V_{dc}$ Voltage for 9-Level converter**

For L-level CHB multilevel converter, the DC-link voltage ( $V_{dc}$ ) for each H-bridge connected to the PV array is calculated as [10],

$$V_{rms} = 0.612*(L-1)*V_{dc} \quad (4.2)$$

$$V_{dc} = 674.02V.$$

$V_{dc}$  is taken as 680 V.

#### **4.3.2 Design Calculations and Selection of PV Array for 9-Level converter**

The required power rating of each PV array for a 9-level CHB converter consisting of twelve PV array for feeding 1.48MW power to the grid is calculated as,

$$P_{mmp} = \frac{(\text{power rating of the system})}{(\text{number of total PV array})} \quad (4.3)$$

$$= 1.48MW/12 = 123.334 \text{ kW}$$

**TABLE-4.1** Component specifications of grid tied 9-level CHB multilevel converter for photovoltaic application

<b>Component</b>	<b>Value</b>
Power	1.48 MW
Voltage( $V_{rms}$ )	3.3 kV
Frequency	50 Hz
PSPWM switching frequency	500 Hz
SHE-PWM switching frequency	50 Hz
NLM switching frequency	50 Hz
Inductor for SHE-PWM & NLM ( $L_c$ )	2.5 mH
Inductor for PSPWM ( $L_c$ )	4mH
No of parallel paths in SPV array ( $N_p$ )	36
No of series paths in SPV array ( $N_s$ )	19
Voltage of PV module at maximum power ( $V_{mmp}$ )	35.86 V
Current of PV module at maximum power ( $I_{mmp}$ )	5.02 A
Open circuit voltage of PV module ( $V_{oc}$ )	44.8 V
Short circuit current of PV module ( $I_{sc}$ )	5.6 A
DC-link voltage ( $V_{dc}$ )	680 V
DC-link capacitor ( $C_{dc}$ )	15240 $\mu$ F

To obtain the PV array of 123.334 kW power ( $P_{mmp}$ ) and  $V_{dc}$  of 680V, a Sharp NT-180U1 model is chosen from the PV array library. The numbers of PV modules connected in parallel and series in PV array are selected as,

$$\begin{aligned}
 N_s &= V_{dc}/V_{mmp} & (4.4) \\
 &= 680/35.86
 \end{aligned}$$

=19

$$N_p = P_{mmp} / (N_s * I_{mmp} * V_{mmp}) \quad (4.5)$$

$$= 123.334 * 1000 / 19 * 35.86 * 5.02$$

=36

### 4.3.3 Design of DC-Link Capacitor for 9-Level converter

The DC-link capacitor ( $C_{dc}$ ) for each H-bridge connected to the PV array is obtained following the principle of conservation of energy. As per this principle, For  $V_{dc}$  recovery in 5 ms and 1.2 overloading factor 'a', as [11],

$$\frac{1}{2} * C_{dc} (V_{dc}^2 - V_{dc1}^2) = K_1 * 3 * V * a * I * t \quad (4.6)$$

Where  $K_1$  denotes variation of energy during dynamics, taken as 10% ( $K_1 = 0.1$ ).

Therefore,

$$C_{dc} = (0.1 * 123334 * 0.005) / (0.5 * (680 * 680 - 674.02 * 674.02))$$

$$C_{dc} = 15231.9867 \mu F$$

It is selected as,  $C_{dc}(C) = 15240 \mu F$

### 4.3.4 Design of Interfacing Inductor for 9-Level converter

#### Inductor selection for phase shifted PWM modulation

A 4mH inductor is selected for getting the required result of THD of grid current waveform for 9-level as per IEEE-519 standard for phase shifted PWM modulation. The per unit value of inductor corresponding to 4 mH is calculated as [13]

$$L_c(\text{p.u.}) = (2 * \pi * f * L * P) / V_s^2$$

$$= (314 \times 4 \times 10^{-3} \times 1.48 \times 10^6) / (3.3 \times 10^3 \times 3.3 \times 10^3)$$

$$= 0.17 \text{ p.u.}$$

#### Inductor selection for SHE-PWM and NLM-PWM

The 2.5mH inductor is selected for getting the required result of THD of grid current waveform for 9-level as per IEEE-519 standard for selective harmonic elimination modulation and nearest level modulation. The per unit value of inductor corresponding to 2.5mH is calculated as [13]

$$L_c(\text{p.u.}) = (2 * \pi * f * L * P) / V_s^2$$

$$= (314 \times 2.5 \times 10^{-3} \times 1.48 \times 10^6) / (3.3 \times 10^3 \times 3.3 \times 10^3)$$

$$= 0.1 \text{ p.u.}$$

### **4.4 CONTROL OF 9-LEVEL SYMMETRICAL CHB MULTILEVEL CONVERTER FOR GRID INTEGRATED PV SYSTEM**

The algorithm for the control of the PV inverter system connected to the three-phase AC grid is as shown in Fig.4.2. The maximum power developed by the array is tracked using the improved P&O algorithm. The decoupled current controller has a feed-forward term, separate controller for each DC-link capacitor, SRF, and PLL used to control the voltage source converter (VSC) [115-116].

#### **4.4.1 Implementation of Improved P&O MPPT Algorithm**

By using an improved P&O MPPT algorithm, the maximum power is extracted from the PV array, and a suitable  $V_{dc\_ref}$  is generated, as apart from the benefits of the P&O algorithm, it also takes care of drift effect owing to increased insolation by taking into account the change in current apart from change in voltage and power [54-57]. The governing equations for MPPT are as follows.

$$V_{pv}^*(k) = V_{pv}^*(k-1) + \Delta V_{pv}, \text{ if } dP_{pv} < 0 \text{ and } dV_{pv} < 0 \text{ or } dP_{pv} > 0, dV_{pv} > 0 \text{ and } dI_{pv} < 0 \quad (4.7)$$

$$V_{pv}^*(k) = V_{pv}^*(k-1) - \Delta V_{pv}, \text{ if } dP_{pv} < 0 \text{ and } dV_{pv} > 0 \text{ or } dP_{pv} > 0, dV_{pv} > 0 \text{ and } dI_{pv} > 0 \text{ or } dP_{pv} > 0 \text{ and } dV_{pv} < 0 \quad (4.8)$$

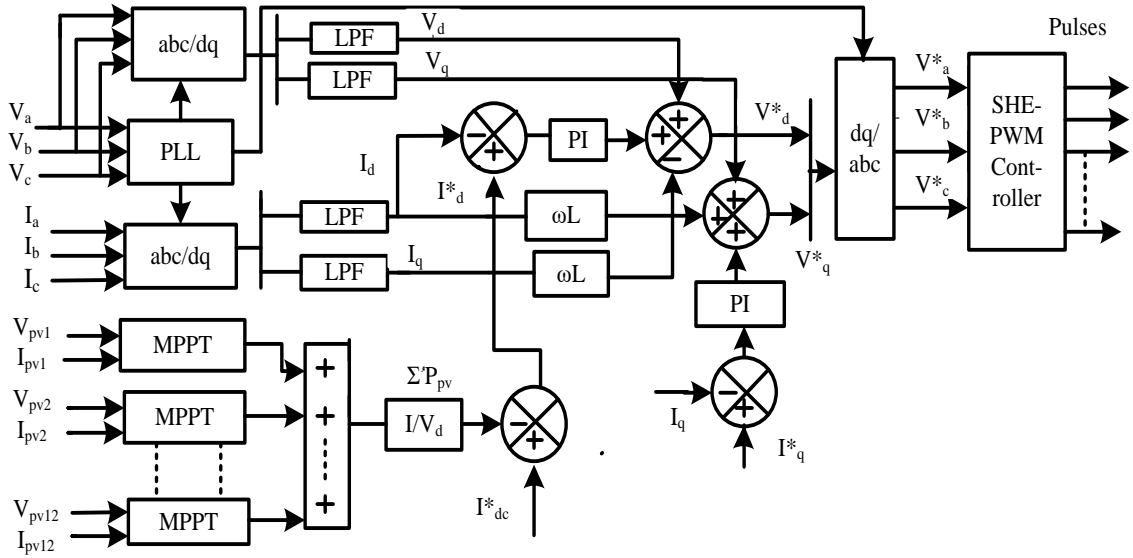


Fig. 4.2 Control algorithm for 9-level CHB converter

#### 4.4.2 Implementation of VSC Algorithm

The voltage measured from each DC link is compared with the individual  $V_{dc\_ref}$  given by each MPPT algorithm, as shown in Fig.4.3. The error voltage (the difference between the two) is processed by a proportional-integral (PI) controller to provide the active current loss component  $I^*_d$ , through the DC link, which is given as,

$$I^*_d(k) = I^*_d(k-1) + K_p \{V_e(k) - V_e(k-1)\} + K_i V_e(k) \quad (4.9)$$

Where  $V_e(k)$  and  $V_e(k-1)$  are the error voltages at given sampling instants  $k$  &  $(k-1)$  and  $K_p$  &  $K_i$  are proportional and integral gain constants. The sum of all reference DC-link currents along with the feed-forward term is compared with the direct current component obtained by Park's transformation from the grid current as [115-116],

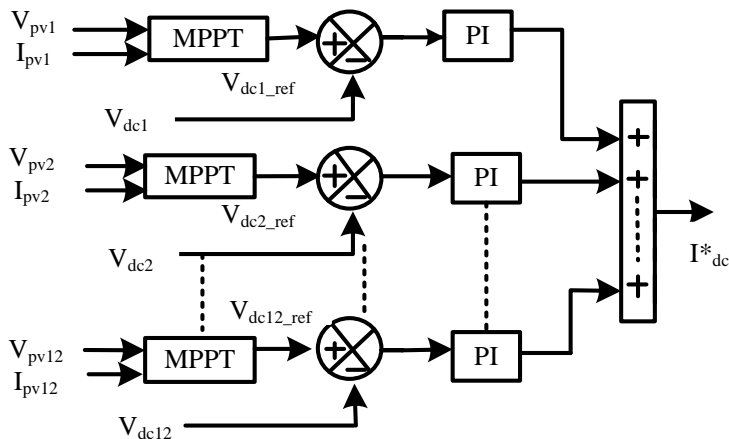


Fig. 4.3 Control algorithm for generating  $I^*_d$  for 9-level CHB converter

The grid detection angle ( $\theta$ ) for Park's transformation is obtained from three-phase PLL.  $I_q^*$ , the reference quadrature current (set to zero for feeding grid current at unity power factor), is compared with the quadrature current component obtained from Park's transformation. Similarly, using Park's transformation, direct and quadrature components of grid voltages ( $V_d$  &  $V_q$ ) are calculated. The reference direct-axis voltage and quadrature-axis voltage are calculated as follows.

$$V_d^*(k) = V_d^*(k-1) + K_{p2} \{ I_{de}(k) - I_{de}(k-1) \} + K_{i2} * I_{de}(k) + V_d - I_q^* \omega L \quad (4.10)$$

$$V_q^*(k) = V_q^*(k-1) + K_{p3} \{ I_{qe}(k) - I_{qe}(k-1) \} + K_{i3} * I_{qe}(k) + V_q + I_d^* \omega L \quad (4.11)$$

Where  $I_{de} = (I_d^* - I_d)$ ,  $I_{qe} = (I_q^* - I_q)$ , and  $\omega L$  is the coupling reactance.  $K_{p2}$ ,  $K_{i2}$ , and  $K_{p3}$ ,  $K_{i3}$  denote the direct axis current controller and quadrature axis current controller's proportional and integral gains, respectively. The reference voltage (modulating signal) for the PWM controller is obtained using the inverse Park's transform.

#### 4.4.3 Implementation of PWM Control for 9-Level Converter

For devising the control scheme for a multilevel converter, the selection of an appropriate modulation scheme improves both THD and switching frequency. Three modulation techniques are implemented for the 9-level converter.

##### 4.4.3.1 Phase-shifted multi carrier PWM

In phase-shifted SPWM, the gate signal is generated by comparing the modulating signal with the triangular carrier waves, as shown in Fig. 4.4. The modulating signal is a sinusoidal signal of adjustable amplitude and frequency. A multilevel converter with  $L$ -levels in output staircase waveform requires  $(L-1)$  triangular carriers waveform having the same frequency and amplitude. The phase shift between two adjacent carrier waves is calculated as in [10]

$$\Phi_{cr} = 360^\circ / (L-1) \quad (4.12)$$

$$= 360 / (9-1)$$

$$= 45^\circ$$



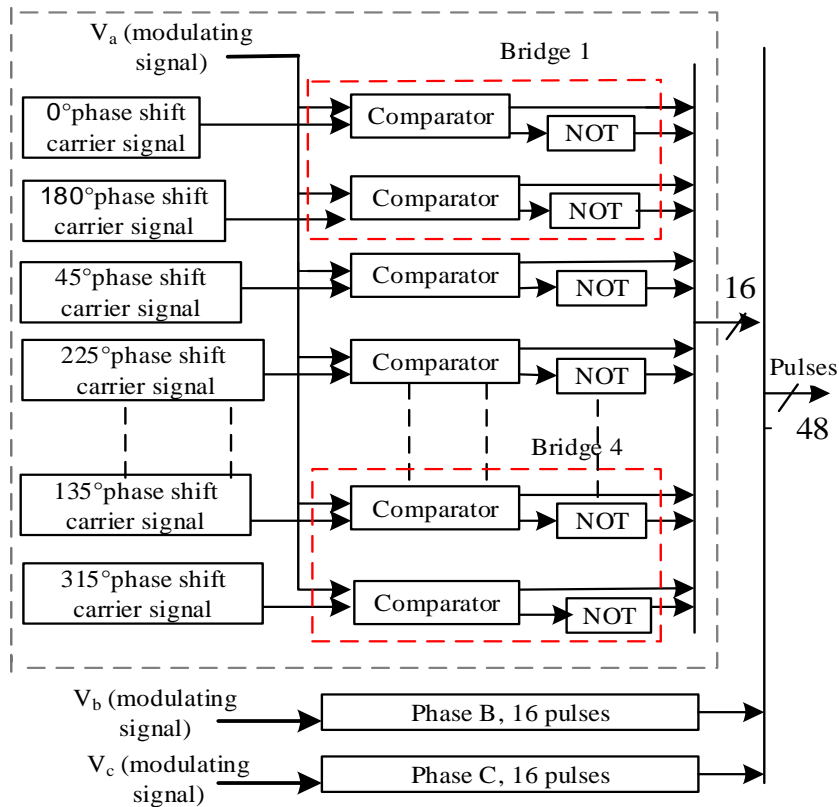


Fig. 4.4 Pulse generation for PSPWM of 9-level CHB multilevel converter

#### 4.4.3.2 SHE-PWM

SHE-PWM switches the switching devices at the fundamental frequency and eliminates lower order harmonics present in output voltage waveform. A series of switching angles are calculated for a multilevel converter to obtain the desired output voltage waveform, depending on the number of levels. A 9-level CHB multilevel converter produces a staircase voltage waveform by synthesizing the number of DC voltages, as shown in Fig. 4.5 [15]. Fourier series expansion of staircase waveform for equal DC voltage sources is given as [15],

$$V(\omega t) = \sum_{n=1,3,5}^{\infty} (4 * V_{dc}/n * \pi) * (\cos(n * \alpha_1) + \cos(n * \alpha_2) + \cos(n * \alpha_3) + \dots + \cos(n * \alpha_s)) * \sin(\omega t) \quad (4.13)$$

Where 's' (s =4) is the number of H-bridges in the multilevel converter, the switching angles must satisfy the condition  $0 < \alpha_1 < \alpha_2 < \alpha_3 < \dots < \pi/2$  for applicability of this method. This results in a narrow band of possible modulation index [15].

In a three-phase system, the third harmonic and its multiples need not be eliminated for each phase voltage as they are cancelled in the line voltage on its own. Only low order harmonics are eliminated by the SHE-PWM method, and the higher-order harmonics can be eliminated by connecting an inductive filter. For eliminating lower order harmonics 5<sup>th</sup>, 7<sup>th</sup>, and 11<sup>th</sup>, the following equations are formulated in terms of Fourier series as [15, 153],

$$\begin{aligned}
 \cos(\alpha_1) + \cos(\alpha_2) + \cos(\alpha_3) + \cos(\alpha_4) &= m \\
 \cos(5\alpha_1) + \cos(5\alpha_2) + \cos(5\alpha_3) + \cos(5\alpha_4) &= 0 \\
 \cos(7\alpha_1) + \cos(7\alpha_2) + \cos(7\alpha_3) + \cos(7\alpha_4) &= 0 \\
 \cos(11\alpha_1) + \cos(11\alpha_2) + \cos(11\alpha_3) + \cos(11\alpha_4) &= 0
 \end{aligned} \quad \left. \vphantom{\begin{aligned} \cos(\alpha_1) + \cos(\alpha_2) + \cos(\alpha_3) + \cos(\alpha_4) = m \\ \cos(5\alpha_1) + \cos(5\alpha_2) + \cos(5\alpha_3) + \cos(5\alpha_4) = 0 \\ \cos(7\alpha_1) + \cos(7\alpha_2) + \cos(7\alpha_3) + \cos(7\alpha_4) = 0 \\ \cos(11\alpha_1) + \cos(11\alpha_2) + \cos(11\alpha_3) + \cos(11\alpha_4) = 0 \end{aligned}} \right\} \quad (4.14)$$

Where m is the modulating index. For converting these transcendental equations into the polynomial form, one can consider  $\cos \alpha_1 = C_1$ ,  $\cos \alpha_2 = C_2$ ,  $\cos \alpha_3 = C_3$  and  $\cos \alpha_4 = C_4$  and the cosine terms can be expanded as,

$$\begin{aligned}
 \cos 5\alpha &= 16 \cos^5 \alpha - 20 \cos^3 \alpha + 5 \cos \alpha \\
 \cos 7\alpha &= 64 \cos^7 \alpha - 112 \cos^5 \alpha + 56 \cos^3 \alpha - 7 \cos \alpha \\
 \cos 11\alpha &= 1024 \cos^{11} \alpha - 2816 \cos^9 \alpha + 2816 \cos^7 \alpha - 1232 \cos^5 \alpha + 220 \cos^3 \alpha - 11 \cos \alpha
 \end{aligned} \quad \left. \vphantom{\begin{aligned} \cos 5\alpha = 16 \cos^5 \alpha - 20 \cos^3 \alpha + 5 \cos \alpha \\ \cos 7\alpha = 64 \cos^7 \alpha - 112 \cos^5 \alpha + 56 \cos^3 \alpha - 7 \cos \alpha \\ \cos 11\alpha = 1024 \cos^{11} \alpha - 2816 \cos^9 \alpha + 2816 \cos^7 \alpha - 1232 \cos^5 \alpha + 220 \cos^3 \alpha - 11 \cos \alpha \end{aligned}} \right\} \quad (4.15)$$

Substituting the eqn. (4.15) in eqn. (4.14), one gets,

$$\begin{aligned}
 C_1 + C_2 + C_3 + C_4 &= m \\
 16C_1^5 - 20C_1^3 + 5C_1 + 16C_2^5 - 20C_2^3 + 5C_2 + 16C_3^5 - 20C_3^3 + 5C_3 + 16C_4^5 - 20C_4^3 \\
 + 5C_4 &= 0 \\
 64C_1^7 - 112C_1^5 + 56C_1^3 - 7C_1 + 64C_2^7 - 112C_2^5 + 56C_2^3 - 7C_2 + 64C_3^7 - 112C_3^5 + 56C_3^3 - \\
 7C_3 + 64C_4^7 - 112C_4^5 + 56C_4^3 - 7C_4 &= 0 \\
 1024C_1^{11} - 2816C_1^9 + 2816C_1^7 - 1232C_1^5 + 220C_1^3 - 11C_1 + 1024C_2^{11} - 2816C_2^9 + \\
 2816C_2^7 - 1232C_2^5 + 220C_2^3 - 11C_2 + 1024C_3^{11} - 2816C_3^9 + 2816C_3^7 - 1232C_3^5 + 220C_3^3 - \\
 11C_3 + 1024C_4^{11} - 2816C_4^9 + 2816C_4^7 - 1232C_4^5 + 220C_4^3 - 11C_4 &= 0
 \end{aligned} \quad \left. \vphantom{\begin{aligned} 16C_1^5 - 20C_1^3 + 5C_1 + 16C_2^5 - 20C_2^3 + 5C_2 + 16C_3^5 - 20C_3^3 + 5C_3 + 16C_4^5 - 20C_4^3 \\ + 5C_4 = 0 \\ 64C_1^7 - 112C_1^5 + 56C_1^3 - 7C_1 + 64C_2^7 - 112C_2^5 + 56C_2^3 - 7C_2 + 64C_3^7 - 112C_3^5 + 56C_3^3 - \\ 7C_3 + 64C_4^7 - 112C_4^5 + 56C_4^3 - 7C_4 = 0 \end{aligned}} \right\} \quad (4.16)$$

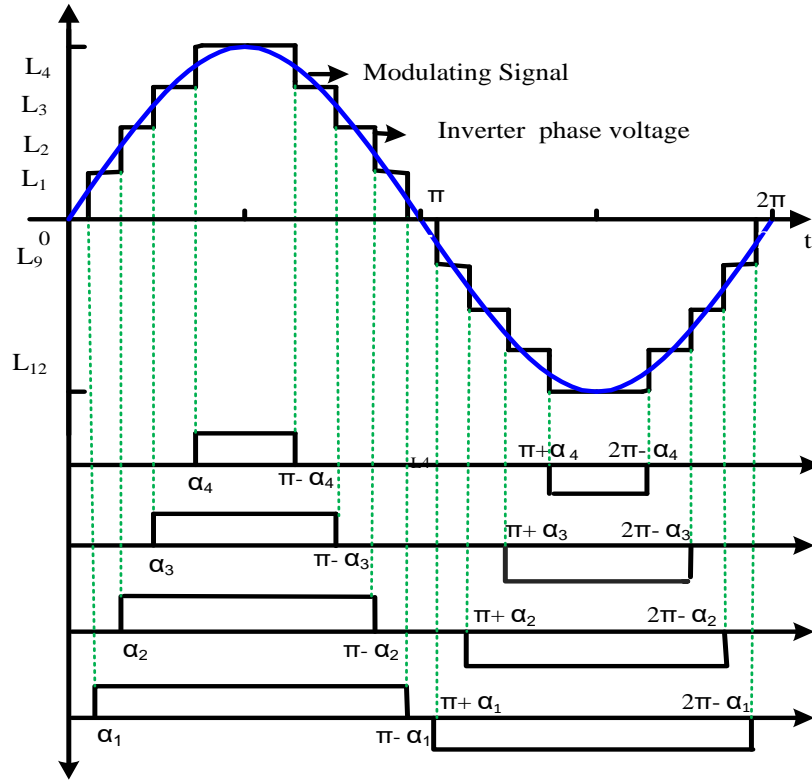


Fig.4.5 Staircase waveform generation[153]

By solving these polynomial equations for unity modulation index by resultant theory method, the switching angles are obtained as  $\alpha_1 = 10.0154$ ,  $\alpha_2 = 22.1424$ ,  $\alpha_3 = 40.7521$  and  $\alpha_4 = 61.7681$  [15,153]. Remaining switching angles  $\alpha_5$ , to  $\alpha_{16}$  are calculated by quarter-wave symmetry of staircase waveform as shown in (Figure 4.5) and given as,  $\alpha_5 = (180 - \alpha_4)$ ,  $\alpha_6 = (180 - \alpha_3)$ ,  $\alpha_7 = (180 - \alpha_2)$ ,  $\alpha_8 = (180 - \alpha_1)$ ,  $\alpha_9 = (180 + \alpha_1)$ ,  $\alpha_{10} = (180 + \alpha_2)$ ,  $\alpha_{11} = (180 + \alpha_3)$ ,  $\alpha_{12} = (180 + \alpha_4)$ ,  $\alpha_{13} = (360 - \alpha_4)$ ,  $\alpha_{14} = (360 - \alpha_3)$ ,  $\alpha_{15} = (360 - \alpha_2)$  and  $\alpha_{16} = (360 - \alpha_1)$ . After these angles calculation, the magnitude of  $L_1, L_2, L_3, \dots, L_{16}$ , as shown in Fig.4.5, are calculated as,  $L_1 = \sin(\alpha_1)$ ,  $L_2 = \sin(\alpha_2)$ ,  $L_3 = \sin(\alpha_3)$ , similarly for  $L_4$  to  $L_{16}$ . The value of the modulating signal ( $m_{ref}$ ) is compared with the calculated magnitude ( $L_1$  to  $L_{16}$ ) for selecting corresponding switching sequence for a level as shown in flowchart given in Fig. 4.6. From this flowchart, it is observed that, if  $L_1 < m_{ref} < L_2$  then first level is essential and switching sequence for first level is chosen from Table 4.2. The selection of other levels is done based on the value of  $m_{ref}$  from Table 4.2 as per the flowchart. The switching combination for the other two phases is given similarly.

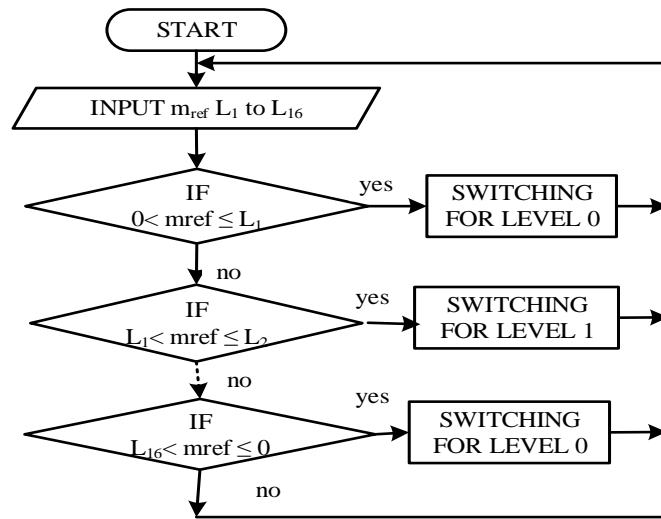


Fig. 4.6 Flowchart for SHE-PWM

TABLE-4.2 Look-up Table for Switching Sequence Corresponding to Output Level

Outputs	Sequence	Outputs	Sequence
0	$S_{11}S_{13}S_{21}S_{23}S_{31}S_{33}S_{41}S_{43}$	$-V_{dc}$	$S_{13}S_{14}S_{21}S_{23} S_{31}S_{33}S_{41}S_{43}$
$V_{dc}$	$S_{11}S_{12}S_{21}S_{23}S_{31}S_{33}S_{41}S_{43}$	$-2V_{dc}$	$S_{13}S_{14}S_{23}S_{24} S_{31}S_{33}S_{41}S_{43}$
$2V_{dc}$	$S_{11}S_{12}S_{21}S_{22}S_{31}S_{33}S_{41}S_{43}$	$-3V_{dc}$	$S_{13}S_{14}S_{23}S_{24}S_{33}S_{34}S_{41}S_{43}$
$3V_{dc}$	$S_{11}S_{12}S_{21}S_{22}S_{31}S_{32}S_{41}S_{43}$	$-4V_{dc}$	$S_{13}S_{14}S_{23}S_{24}S_{33}S_{34}S_{43}S_{44}$
$4 V_{dc}$	$S_{11}S_{12}S_{21}S_{22}S_{31}S_{32}S_{41}S_{42}$		

#### 4.4.3.3 Nearest level modulation (NLM)

In the case of NLM-PWM, an online calculation is performed to obtain the required predefined level. The required level for a specific time duration is found first by taking the ratio of the value of the modulating signal at the particular instant and a predefined step. After determining the required level, an appropriate switching sequence is selected from the corresponding look-up table. Table 4.2 specifies the switching sequence for a particular level. Switching sequences for the other two phases are determined similarly [154-160]. The required predefined step is found as,

$$GR_p = 1 \text{ and } G = (L - 1)/2 \quad (4.17)$$

Where “G” is the number of positive steps in a 9-level inverter, “R<sub>p</sub>” is predefined steps, and “L” is the number of levels. From eqn. (4.17), R<sub>p</sub> = 1/G. After this, the ratio of the instantaneous values of the modulating signal (m<sub>ref</sub>) and predefined step (R<sub>p</sub>) is obtained. The quotient of this ratio gives the required level for that particular value of the modulating signal. The above steps are illustrated graphically through a flowchart depicted in Fig. 4.7. If the value of N is between zero and one, then Level ‘0’ is selected, if N is between one and two, Level ‘1’ is selected, and so on. The corresponding switching sequence for the selected level is picked from Table 4.2 [154].

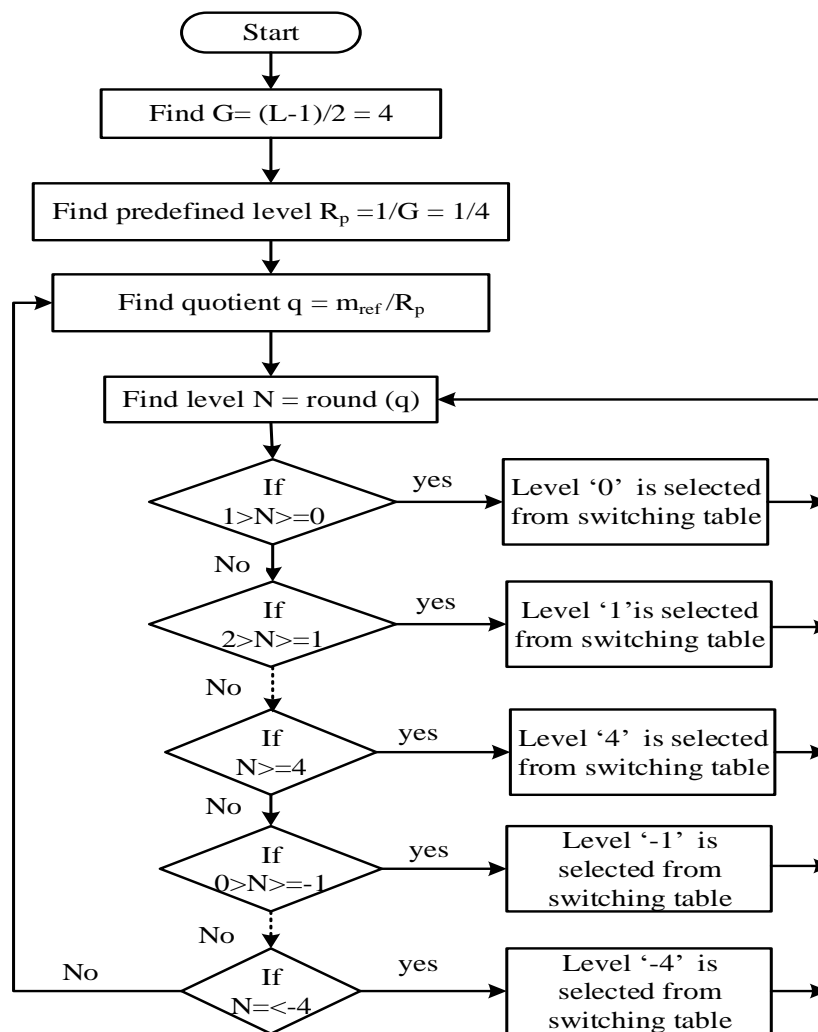


Fig.4.7 Flowchart for NLM

#### 4.5 MODELLING OF 9-LEVEL SYMMETRICAL CHB MULTILEVEL CONVERTER FOR GRID INTEGRATED PV SYSTEM

This section presents the MATLAB based modelling of a nine-level CHB multilevel converter for grid interfaced SPV system. MATLAB R2015a is used for simulation. MATLAB modeling of the grid-connected converter, PV array fed 9-level CHB multilevel converter for phase A (remaining phase modeling is the same as phase A), MATLAB model for MPPT block, control algorithm, and phase-shifted sinusoidal PWM is also developed. MATLAB model is implemented by selecting a block from both Simulink and Simscape Simpowersystems specialized technology library of MATLAB.

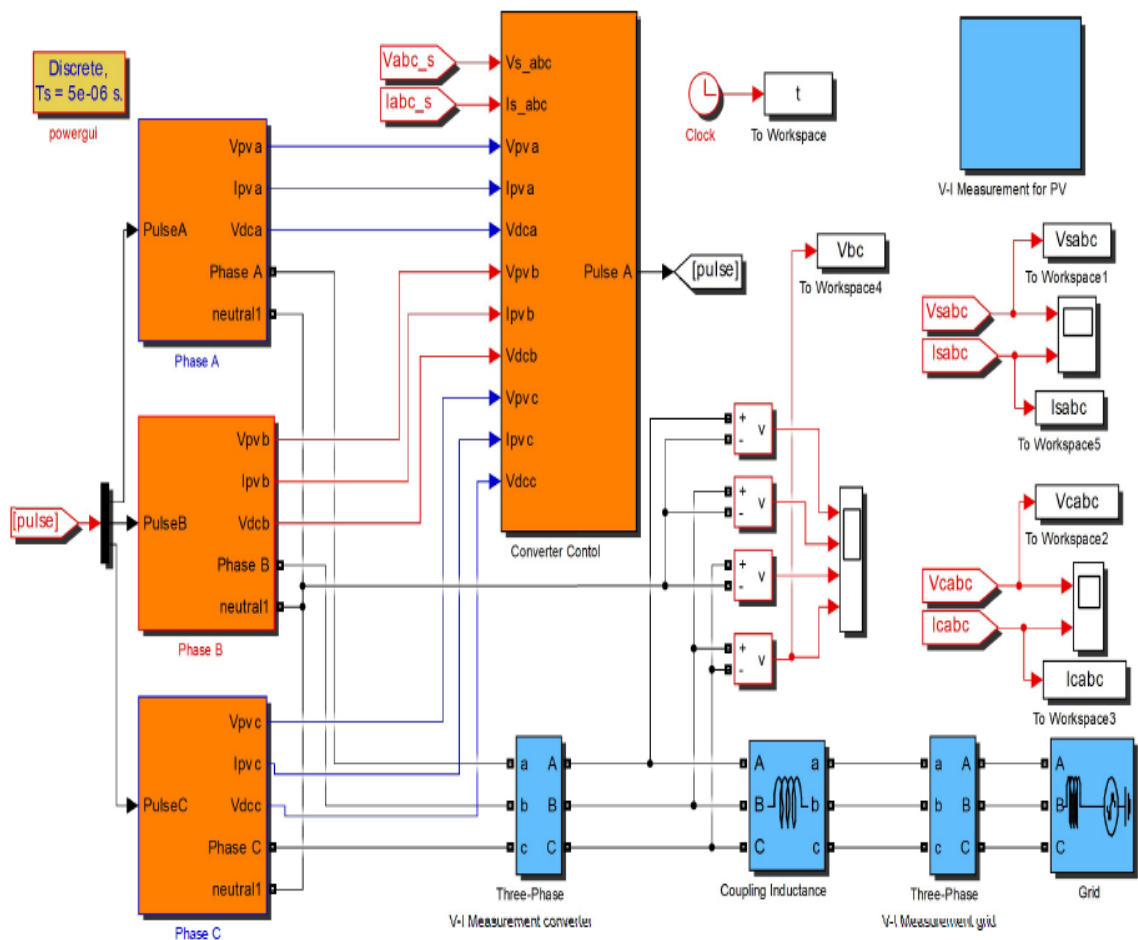


Fig. 4.8 MATLAB model of grid interfaced 9-level CHB multilevel converter

### 4.5.1 Model of Grid Connected Converter

The developed MATLAB model of grid-connected multilevel converter for the three-phase system is shown in Fig.4.8. The grid voltages ( $v_{sabc}$ ), grid currents ( $i_{sabc}$ ), converter voltages ( $v_{cabc}$ ), and converter currents ( $i_{cabc}$ ) are measured from three-phase VI-measurement. A three-phase source block of rating 3.3kV is chosen from the same library for the grid. Discrete powergui environmental block is selected from simscape insolation level

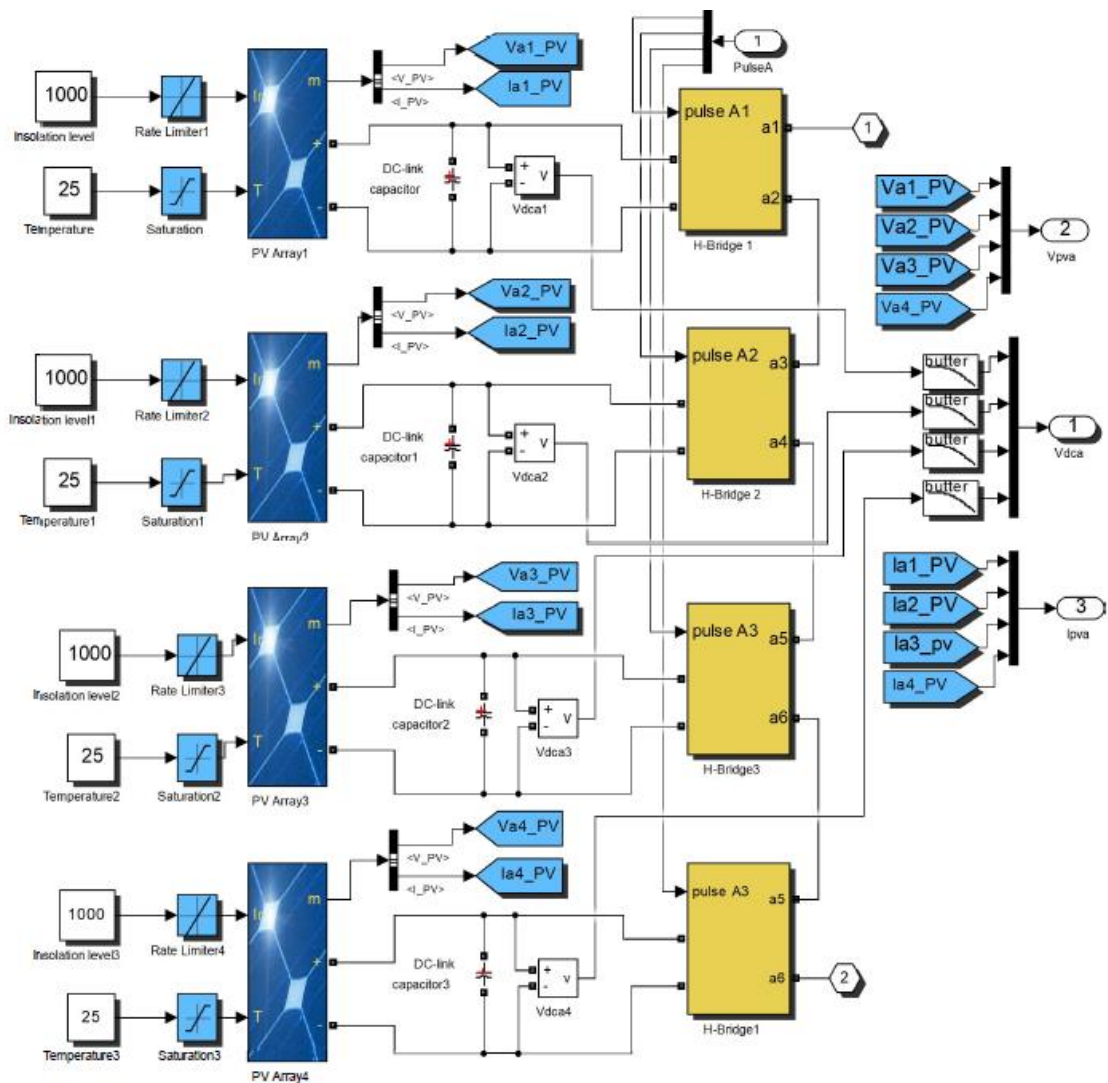


Fig. 4.9 PV array fed 9-level CHB multilevel converter

#### 4.5.2 Model of PV Array Connected Nine-level H-Bridge Converter

For getting a nine-level converter, four H-bridges are connected in a cascade. Each PV array is fed by a separate H-bridge, as shown in Fig. 4.9. For the photovoltaic system, the insolation level is taken as  $1000\text{W/m}^2$  and given through a limiter block, and temperature  $25^\circ\text{C}$  is provided through a saturation block, selected from the Simulink library. A Sharp NT-180U1 PV array is selected from Simscape SimPowerSystems specialized technology PV array library. The photovoltaic voltage and current of array1 ( $V_{a1\_PV}$  &  $I_{a1\_PV}$ ), array2 ( $V_{a2\_PV}$  &  $I_{a2\_PV}$ ), array 3 ( $V_{a3\_PV}$  &  $I_{a3\_PV}$ ) and array 4 ( $V_{a4\_PV}$  &  $I_{a4\_PV}$ ) are measured for MPPT.  $V_{dc1}$ ,  $V_{dc2}$ ,  $V_{dc3}$  and  $V_{dc4}$  are the DC-link voltages across the DC link capacitor, measured to control the DC-link and give  $I_d^*$  for active power loss component.

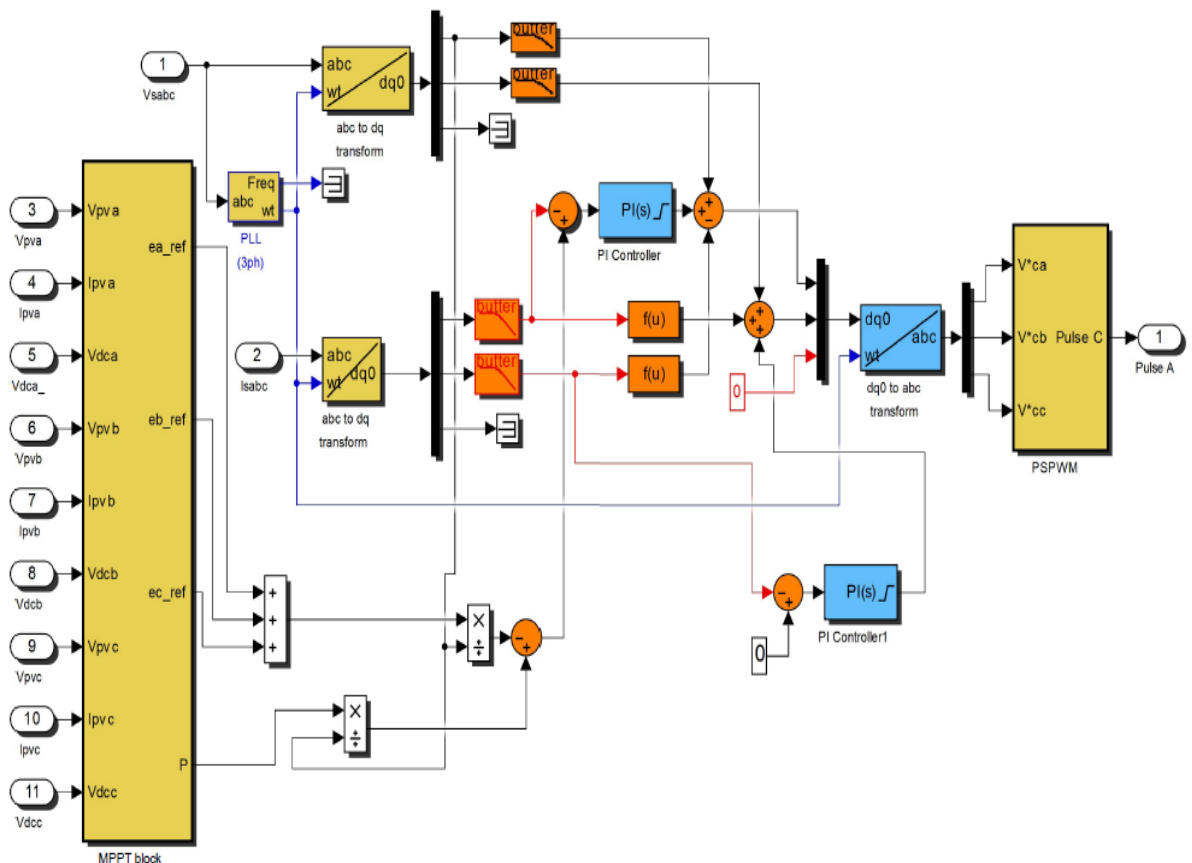


Fig.4.10 MATLAB model of Control algorithm of 9-level CHB multilevel converter



### 4.5.3 Model of Control Algorithm

Fig.4.10 shows the developed model of the control algorithm for VSC control. To implement the decoupled current scheme, the abc to dq0 transformation block and PLL block are selected from simpower systems specialized technology library. The reference direct current obtained from the MPPT block and the feed-forward term are compared by a comparator block selected from Simulink library with direct current  $I_d$  and error signal given to a PI-controller. Similarly, the quadrature-component of current is compared with zero-reference (unity pf), and the error voltage is passed through a PI-controller with a saturation limit fixed at the output. The reference dq-components of voltages so obtained are transformed to  $V_{abc}^*$  (modulation signal) by a dq0 to abc transformation block and given to the PWM block. The synchronous signal ( $\omega t$ ) is provided by the PLL to abc to dq0 and dq0 to abc transformation.

### 4.5.4 Model of MPPT Controller

Each array is provided with a separate MPPT algorithm controlled by a separate PI-controller, as shown in Fig.4.11. The MPPT algorithm is implemented by writing the algorithm on a user-defined block of the Simulink library. Param block gives the upper and lower limit of  $V_{dc\_ref}$  and increment step for implementing the algorithm.

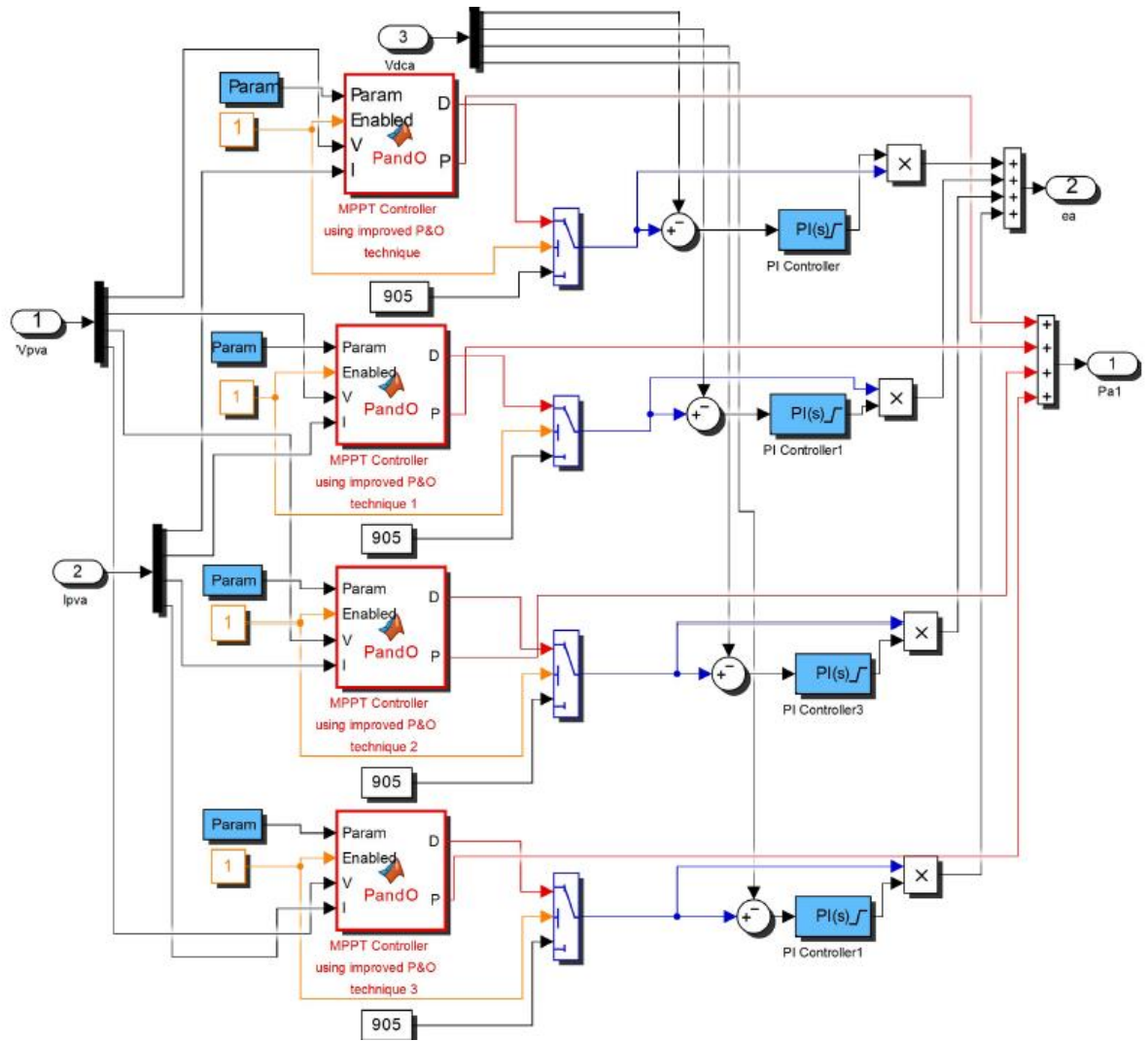


Fig.4.11 MATLAB model for MPPT controller of 9-level CHB multilevel converter

#### 4.5.5 Model of PWM Technique

The three PWM techniques, phase-shifted PWM, SHE-PWM, and NLM, are investigated for modulation of a 9-level symmetrical CHB multilevel converter. The MATLAB model of these algorithms is described in the following given section.

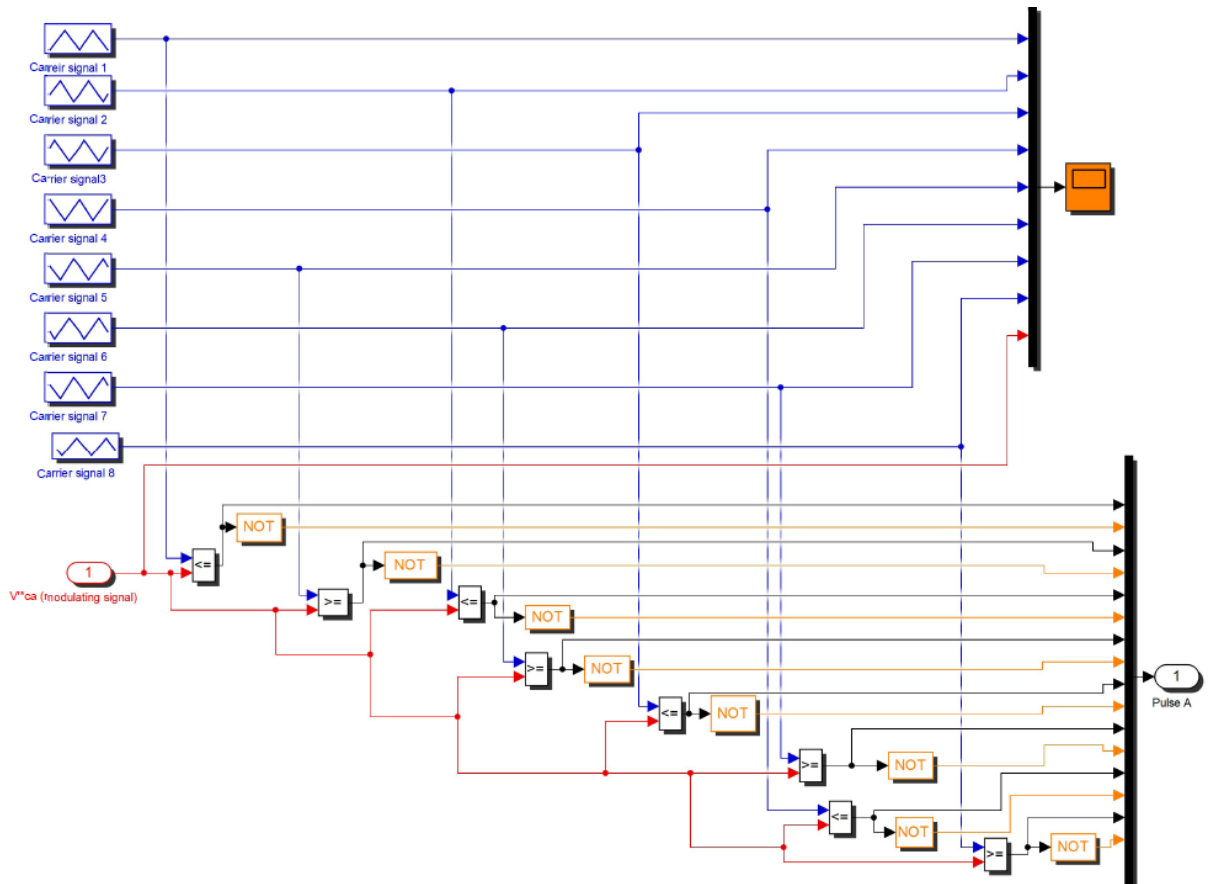


Fig. 4.12 MATLAB model for Phase shifted PWM of 9-level CHB multilevel converter

#### 4.5.6 Model of Phase-shifted PWM

The eight carrier signals of 500 Hz switching frequency are generated by selecting a triangle generator block from Simpower systems specialized technology control and signal generation library for implementing the phase-shifted PWM. The triangle generator block generates a symmetrical triangle waveform with a peak amplitude of +/- 1 for implementing carrier signal. These carrier signals are compared with the modulating signal, as shown in Fig. 4.12, and pulses are generated. Comparator and NOT-gate block are selected from the Simulink library for the generation of pulses.

### 4.5.7 Model of SHE-PWM

The developed MATLAB model of SHE-PWM is shown in Fig.4.13. The model of SHE-PWM is developed by comparing the modulating signal, as per switching Table 4.2, obtained from the control algorithm with a constant for generating the pulse signal. The value of the constant is obtained by switching angles calculated offline for eliminating the selected harmonics.

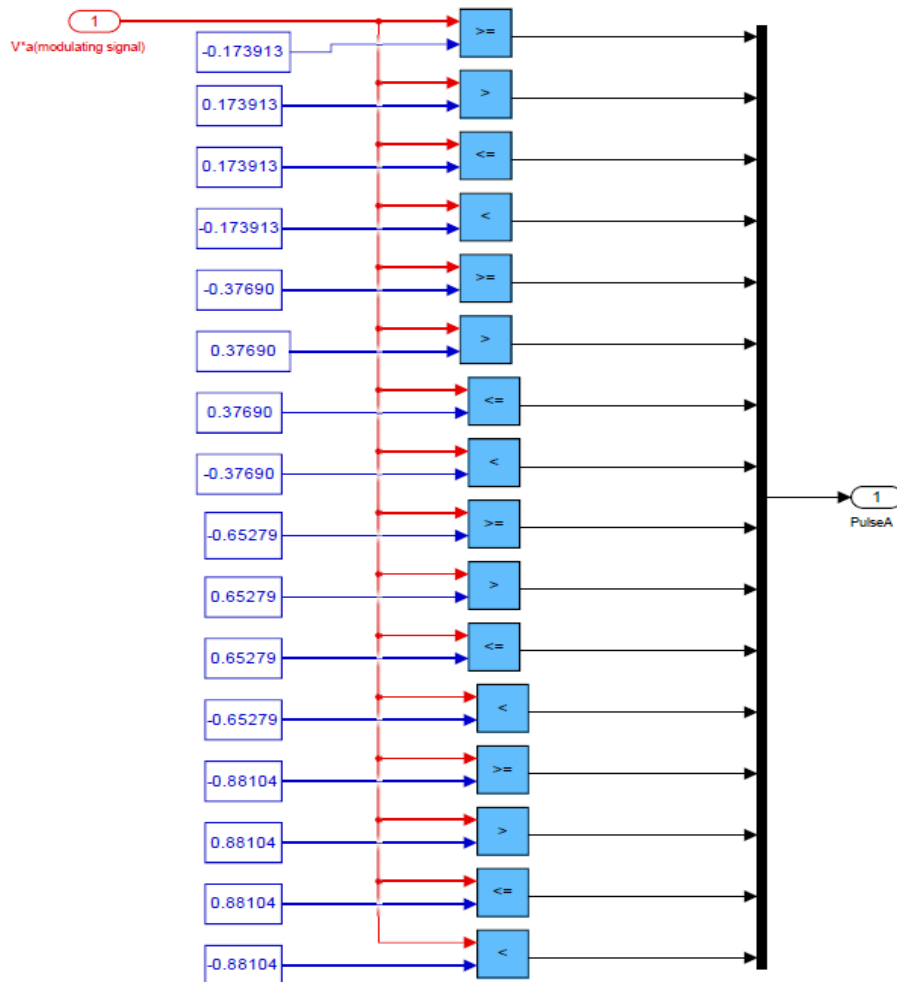


Fig. 4.13 MATLAB model for SHE-PWM of 9-level CHB multilevel converter

### 4.5.8 Model of Nearest Level Modulation (NLM)

The MATLAB model is developed by comparing the modulating signal with a constant, as per switching Table 4.2, for generating the pulses as shown in Fig.4.14 of NLM-PWM, an online calculation is performed to obtain the required predefined level for finding the constant value.

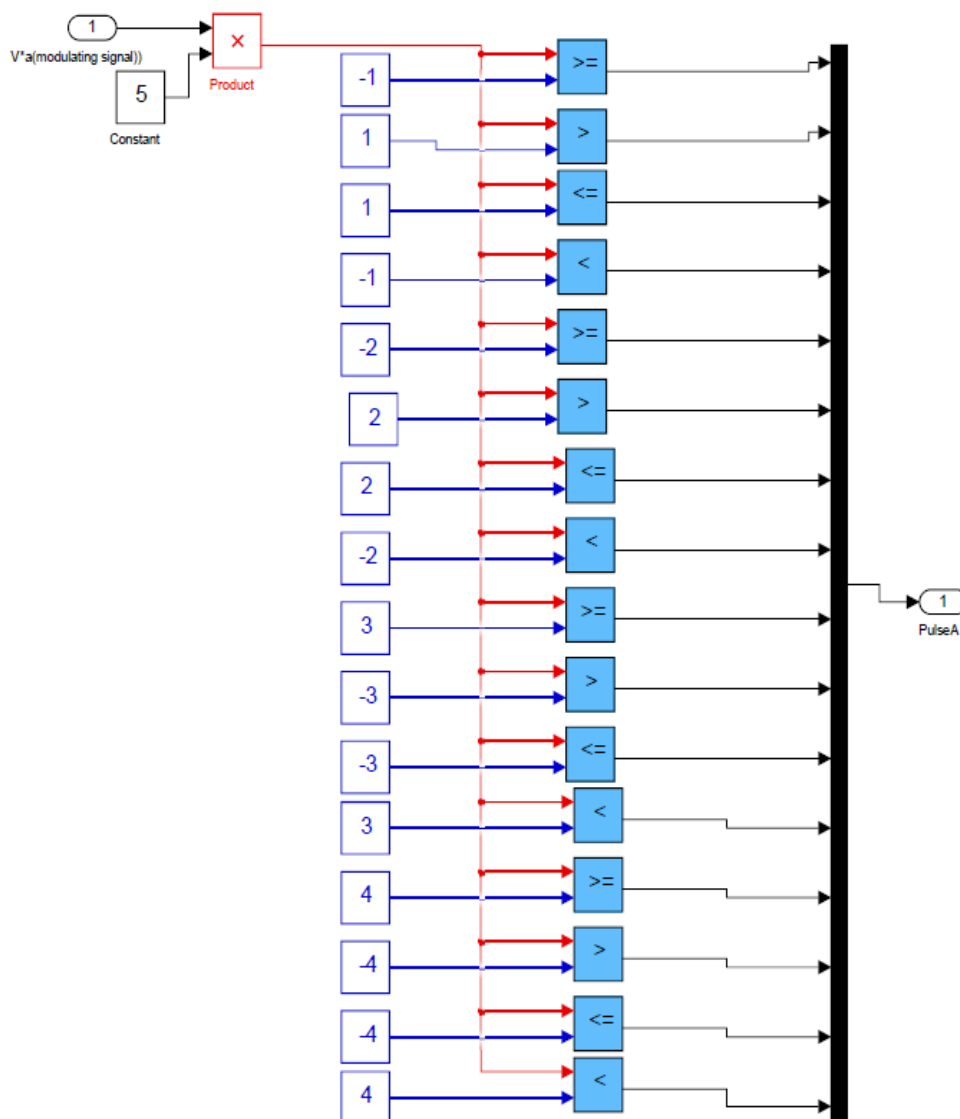


Fig. 4.14 MATLAB model for NLM of 9-level CHB multilevel converter

## 4.6. RESULTS AND DISCUSSION

The three-phase grid-tied SPV system, as shown in Fig.4.1, is designed, modelled, and controlled with a nine-level H-bridge multilevel converter. This system is modelled and its performance is simulated in MATLAB/Simulink, and the results are discussed here. Moreover, a 9-level CHB converter with SHE-PWM technique is tested on OPAL-RT simulator platform to validate the results obtained in MATLAB/Simulink.

### 4.6.1 Steady-State Performance for 9-Level Converter

The system's steady-state response is studied at an insolation level of  $1000 \text{ W/m}^2$  and  $25^\circ\text{C}$  temperature. Simulated results consisting of the grid voltages ( $v_{sabc}$ ), the grid currents ( $i_{sabc}$ ), the AC line voltages of VSC ( $v_{cabc}$ ), SPV voltage ( $V_{pv}$ ), SPV current ( $I_{pv}$ ), and power (P) are obtained to validate the system performance. The steady-state response for the three modulation techniques, phase-shifted PWM, SHE-PWM, and NLM, are shown in Figs. 4.15, 4.16 and 4.17. As the grid voltages and the grid currents are in phase in the steady-state response hence the maximum active power transfer is evident at a power factor of unity. PV array generates almost constant voltage and delivers almost constant current and power as shown in figure.

### 4.6.2. Dynamic Performance for 9-Level Converter

Fig.4.18 shows the dynamic response of SHE-PWM only. The dynamic response is studied with a constant temperature of  $25^\circ\text{C}$  and an insolation change from  $1000 \text{ W/m}^2$  to  $400 \text{ W/m}^2$  at 0.6sec. as shown in Fig. 4.18 (a) and (b). Whereas reverse change is studied in Fig. 4.18 (c) and (d). Simulated results consist of the voltage and the current for a PV array 1 of A-phase ( $V_{a1pv}$  &  $I_{a1pv}$ ), B- phase ( $V_{b1pv}$  &  $I_{b1pv}$ ), C- phase ( $V_{c1pv}$  &  $I_{c1pv}$ ). In dynamic response, with the decrease of the insolation level, remarkable change in the PV current is observed, while there is no significant change seen in the PV voltage. As the dynamic response shows a change in PV voltage and current with insolation level, for the same PV array and insolation level change, the dynamic response for all three modulation techniques is almost similar. The PV voltage and the change in PV current is

similar for three phase array 1, which verifies that the distributed MPPT control of each array is achieved as shown in Fig. 4.18 (a). The grid current, PV array power and PV current are changed proportionally and PV voltage and grid voltage remains constant with change in insolation level as shown in Fig. 4.18 (b)

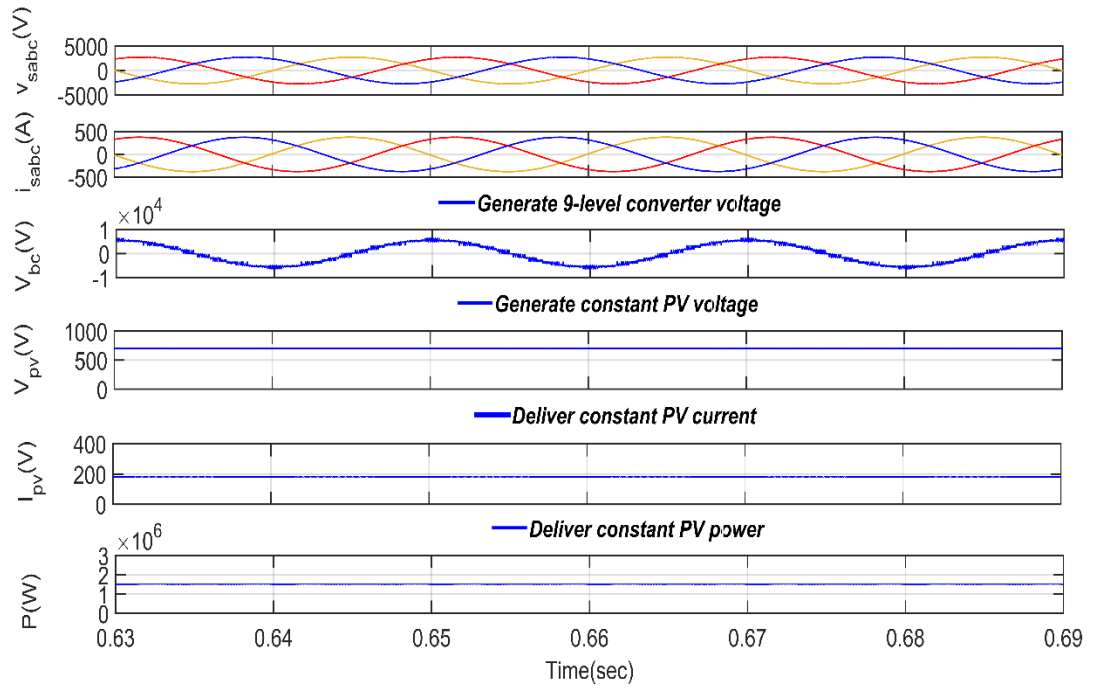


Fig. 4.15 Steady state response for phase shifted PWM

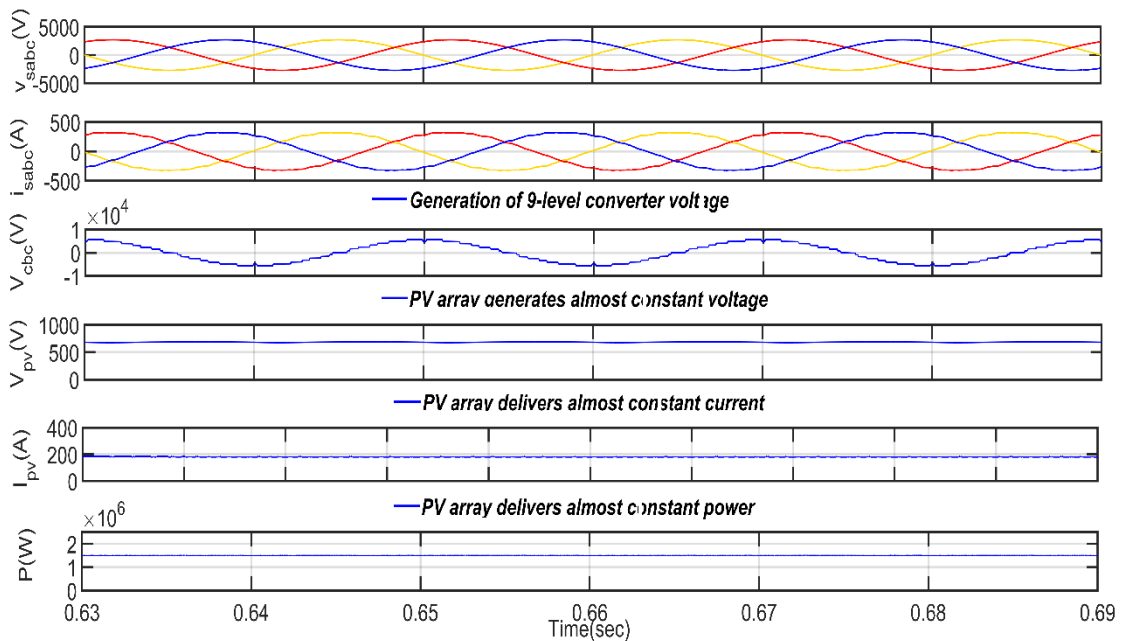


Fig. 4.16 Steady state response for SHE-PWM

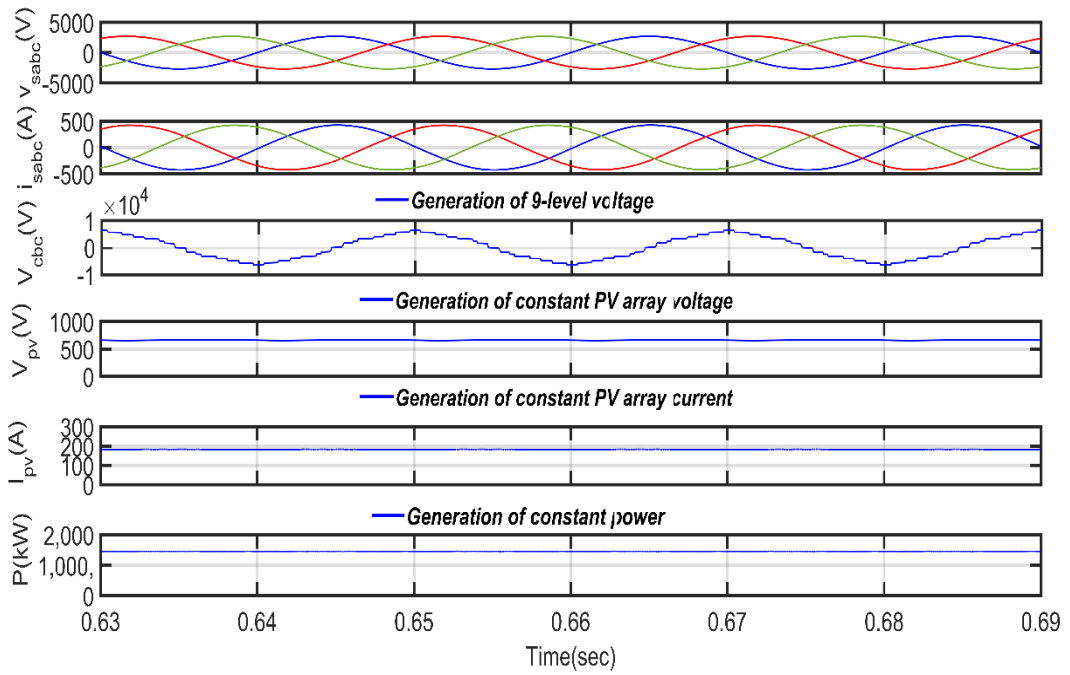
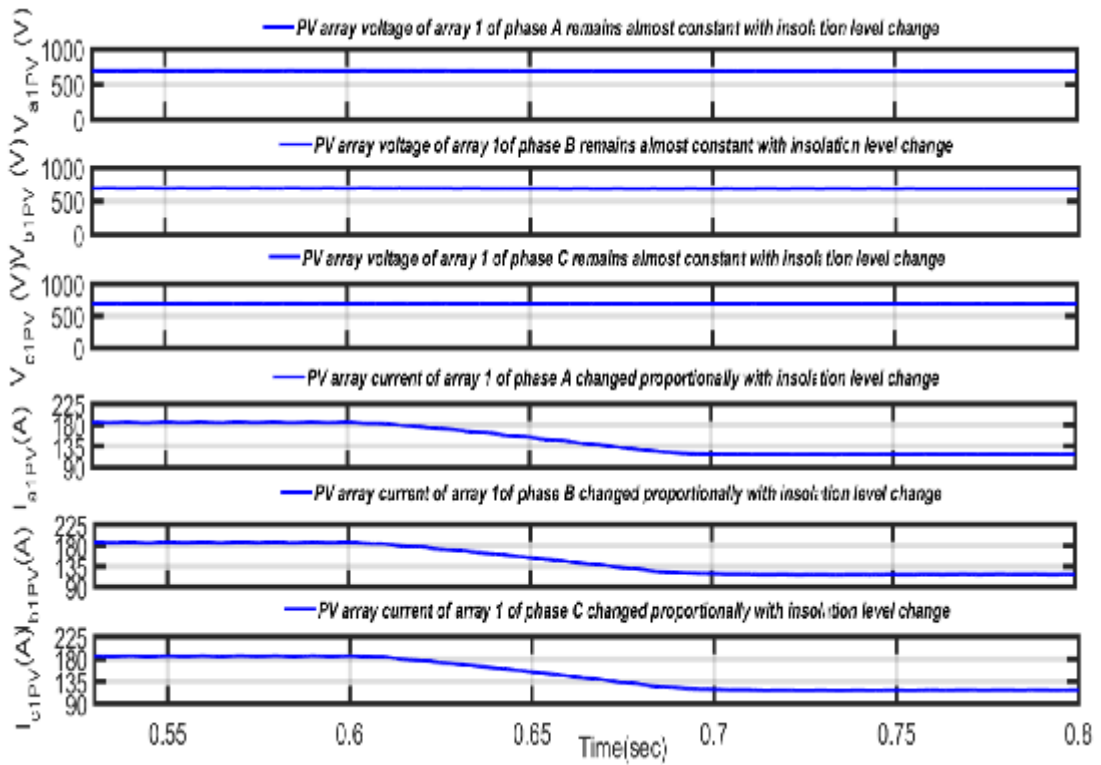
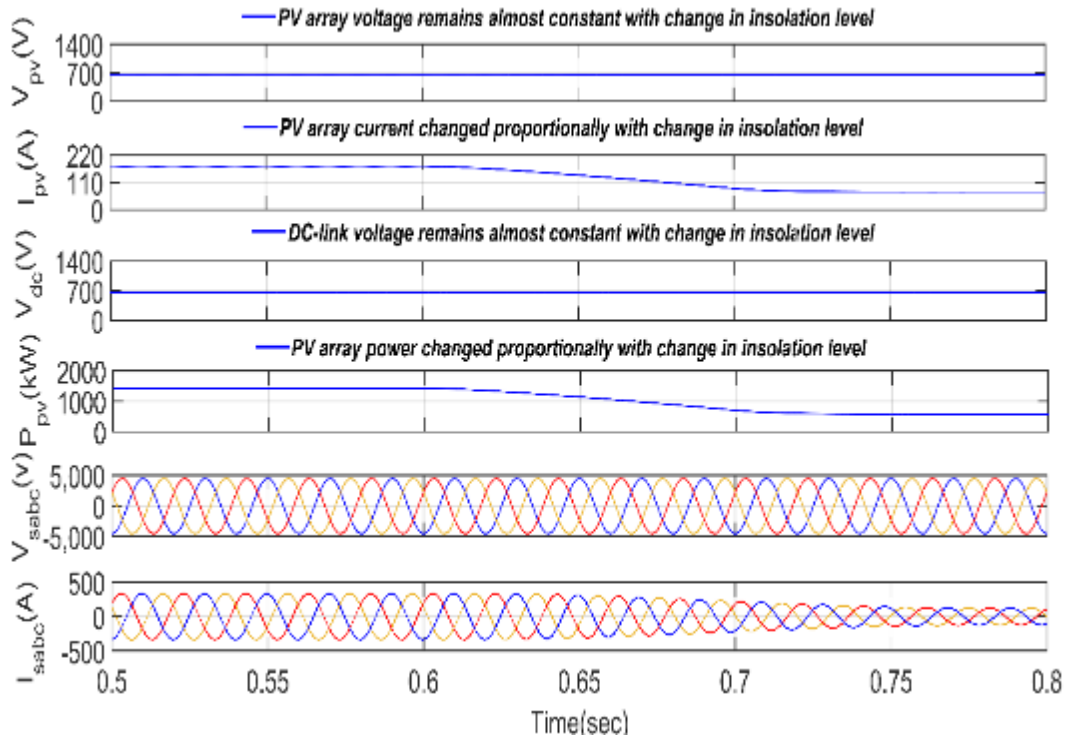


Fig. 4.17 Steady state response for NLM

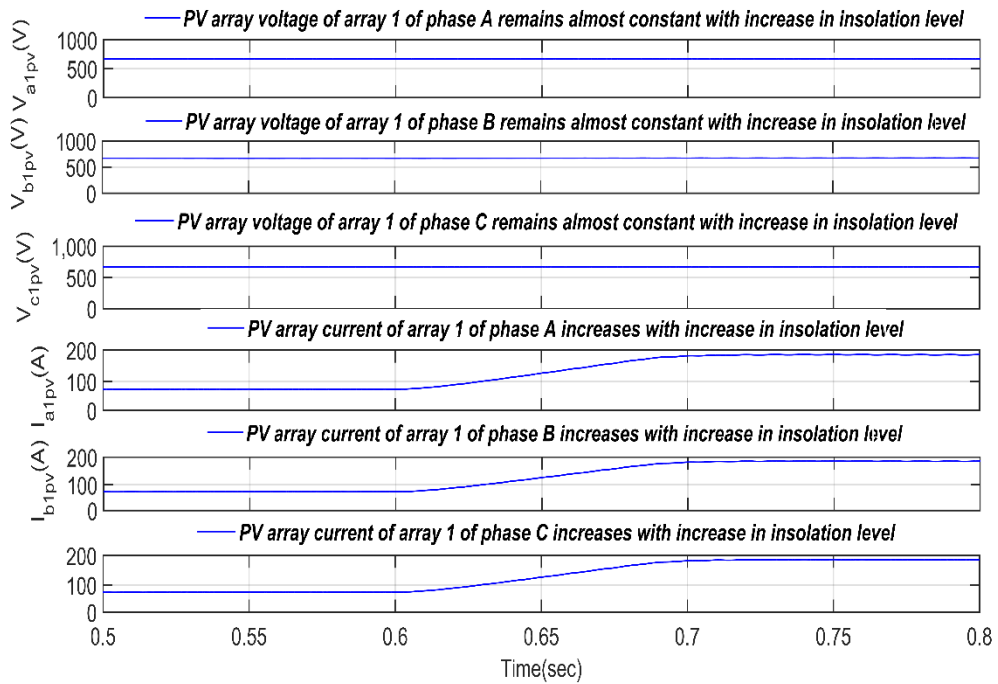


(a)

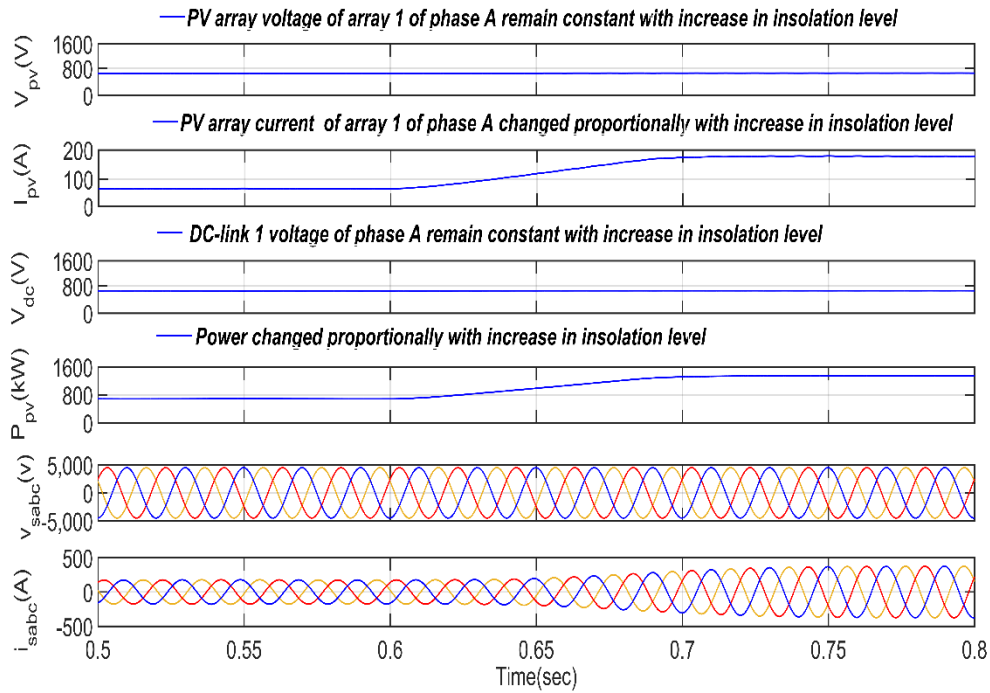




(b)



(c)



(d)

Fig. 4. 18 Dynamic response for the SHE-PWM technique for (a) and (b) decrease in insolation level from  $1000 \text{ W/m}^2$  to  $400 \text{ W/m}^2$ , (c) and (d) increase in insolation level from  $400 \text{ W/m}^2$  to  $1000 \text{ W/m}^2$  at 0.6 s

#### 4.6.3 Power Quality Performance for 9-level Converter

Fig.4.19 shows waveform of the converter line voltages ( $v_{cabc}$ ), and harmonic spectra along with THD levels at  $1000 \text{ W/m}^2$  levels by using the fast Fourier transform tool in MATLAB for (a) SHE-PWM (b) PSPWM (c) NLM. The converter voltage THD values of 6.96%, 11.70 %, and 9.18% at insolation of  $1000 \text{ W/m}^2$  and temperature of  $25^\circ\text{C}$  respectively, are observed for 9-level grid interfaced 3.3 kV SPV system with modulation index of unity.

Fig.4.20 shows waveform of the supply voltages ( $v_{sabc}$ ), and harmonic spectra along with THD levels at  $1000 \text{ W/m}^2$  levels by using the fast Fourier transform tool in MATLAB for (a) SHE-PWM (b) NLM (c) PSPWM. The grid voltage THD values of 0.32%, 0.39

%, and 0.62% at insolation of 1000 W/m<sup>2</sup> and temperature of 25°C, respectively, are observed for 9-level grid interfaced 3.3 kV SPV system with modulation index of unity.

Fig.4.21 shows waveform of the supply currents ( $i_{sabc}$ ), and harmonic spectra along with THD levels at 1000 W/m<sup>2</sup> levels by using the fast Fourier transform tool in MATLAB for (a) SHE-PWM (b) PSPWM (c) NLM. The grid current THD values of 0.47%, 0.80%, and 0.58% at insolation of 1000 W/m<sup>2</sup> and temperature of 25°C, respectively, are observed for 9-level grid interfaced 3.3 kV SPV system with at modulation index of unity. Therefore, obtained results confirm the elimination of lower-order harmonic fifth, seventh, and eleventh order harmonic for which, the SHE-PWM transcendental equation is written.

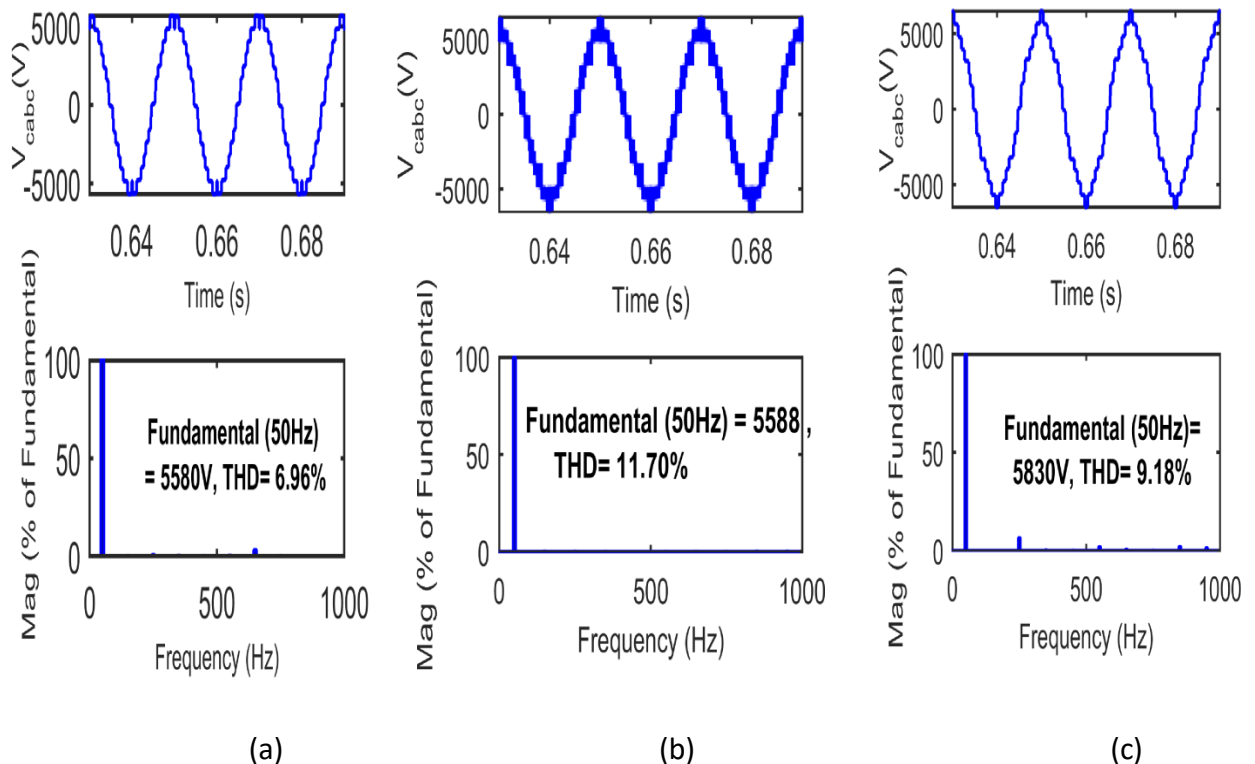


Fig. 4.19 Waveforms and harmonic spectra for converter line voltage for (a) SHE-PWM (b) PSPWM (c) NLM

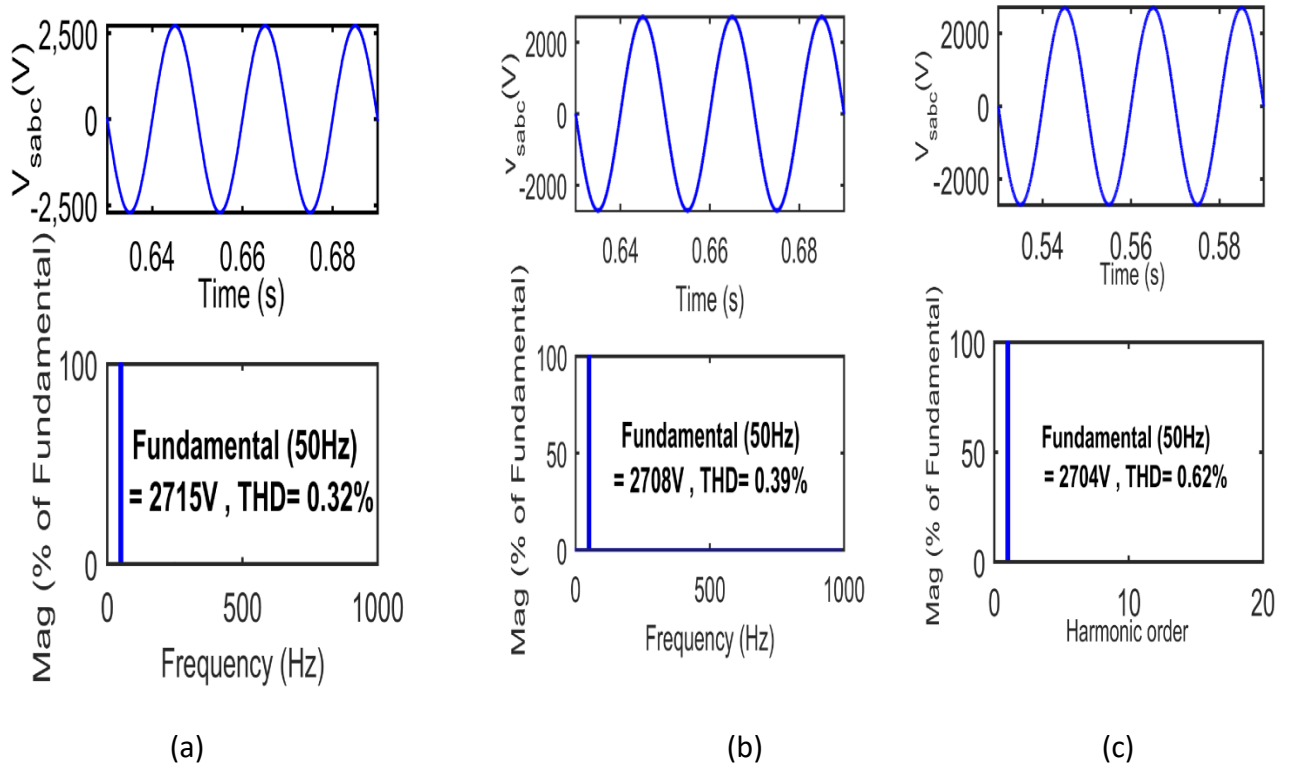


Fig. 4.20 Waveforms and harmonic spectra for supply voltage for (a) SHE-PWM (b) NLM (c) PSPWM

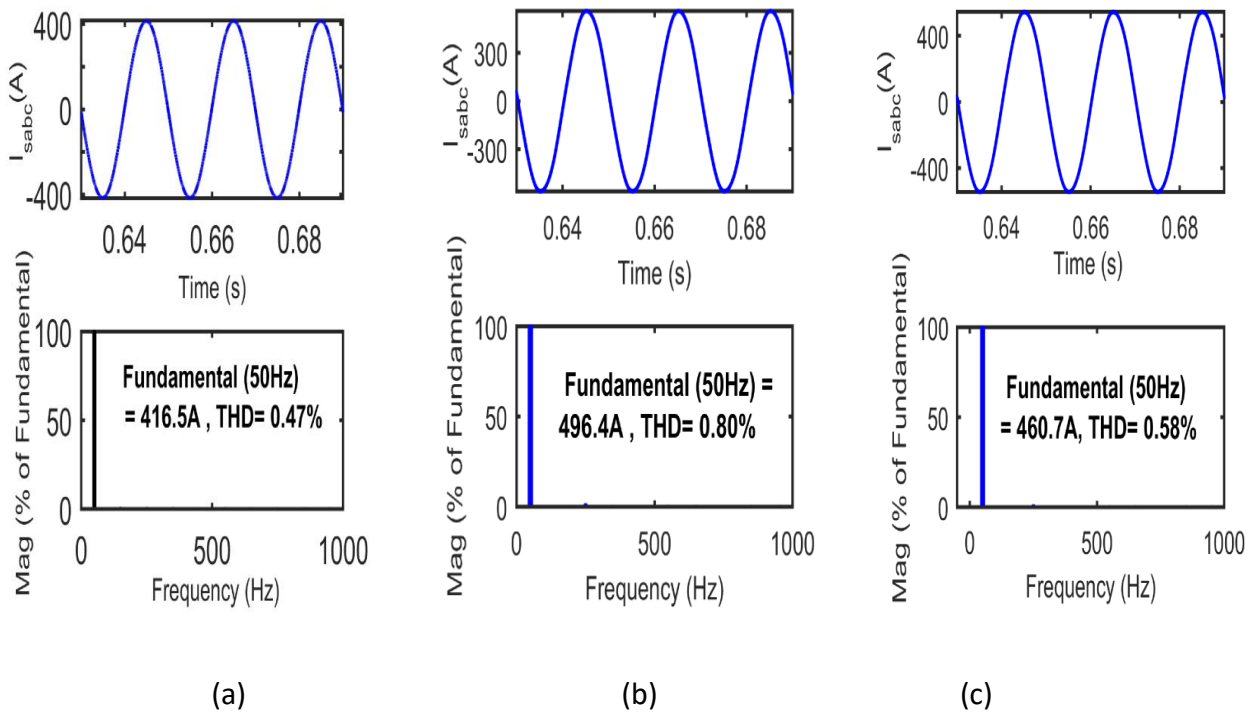
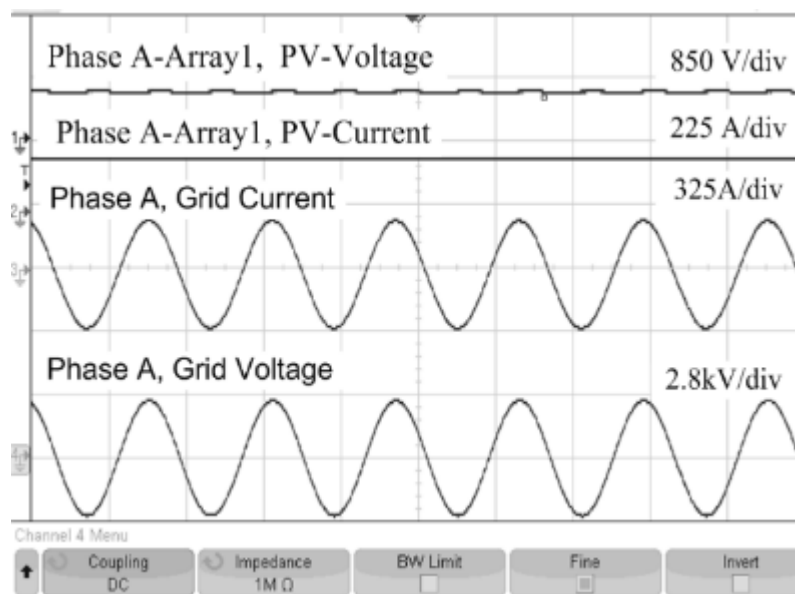
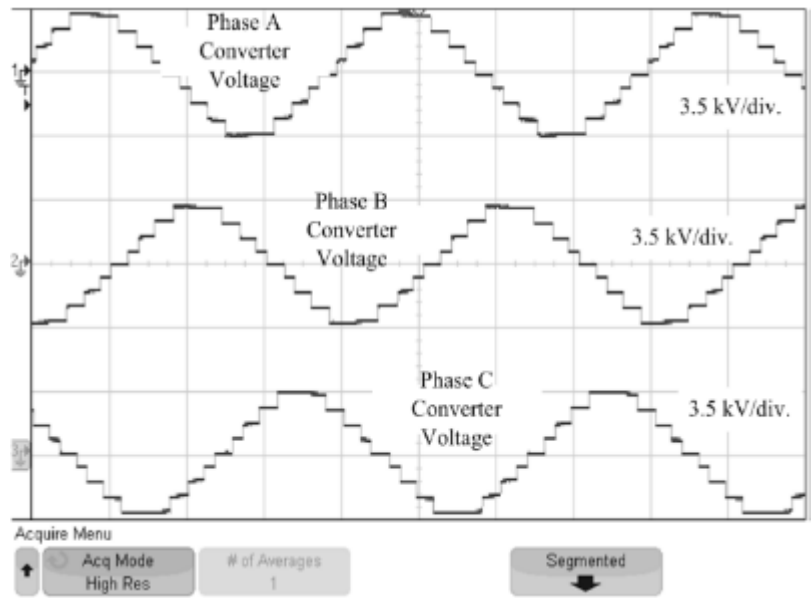


Fig.4.21 Waveforms and harmonic spectra for supply current for (a) SHE (b) PSPWM (c) NLM

The steady state and dynamic performances and converter output THD are also validated in HIL on OPAL-RT simulator. The obtained results are shown in Figs. 4.22, 4.23 and 4.24. Figs. 4.22 (a)-(b) show the steady state real-time performance. PV voltage and current of array are shown with maximum power operation. The grid voltage and grid current maintain unity power factor. Moreover, three phase converter voltages with nine level output are achieved in Fig. 4.22 (b). Figs. 4.23 (a)-(b) show the steady state and dynamic performance of PV arrays of each phase. Moreover, THD of phase and line voltages are achieved as 9.14% and 6.26% respectively under the SHE scheme. Fig. 4.24 (a) and (b) show the THDs for converter phase voltage and line voltage for SHE-PWM, whereas Fig. 4.24 (c) and (d) show the THDs for phase voltage for NLM-PWM and PS PWM respectively. Grid current THD is 0.53% as shown in Fig. 4.25. Fig. 4.26 (a) – (b) show the real time converter line voltage THD for NLM-PWM and PS PWM, whereas Fig. 4.26 (c) – (d) show the grid current THDs for NLM-PWM and PS-PWM. The simulation results of converter voltage and grid current THDs and their real time results are in close agreement.

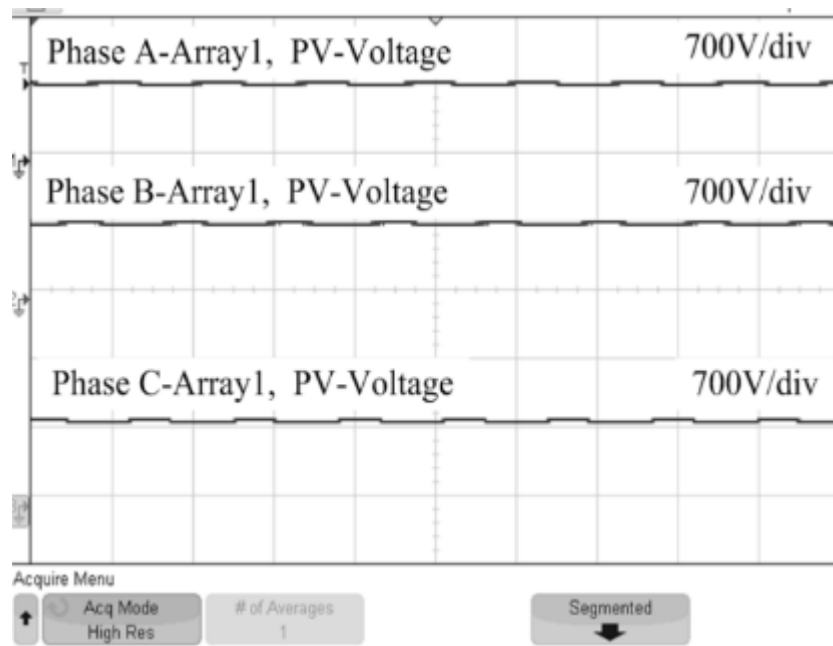


(a)

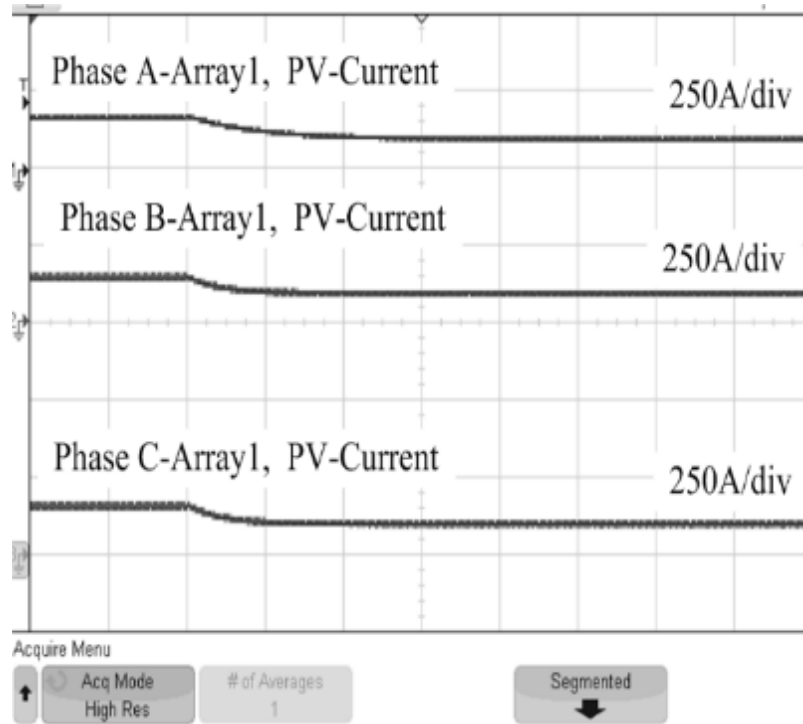


(b)

Fig.4.22 Steady-state response (a) PV voltage, PV current, grid current and grid voltage (b) Converter voltage

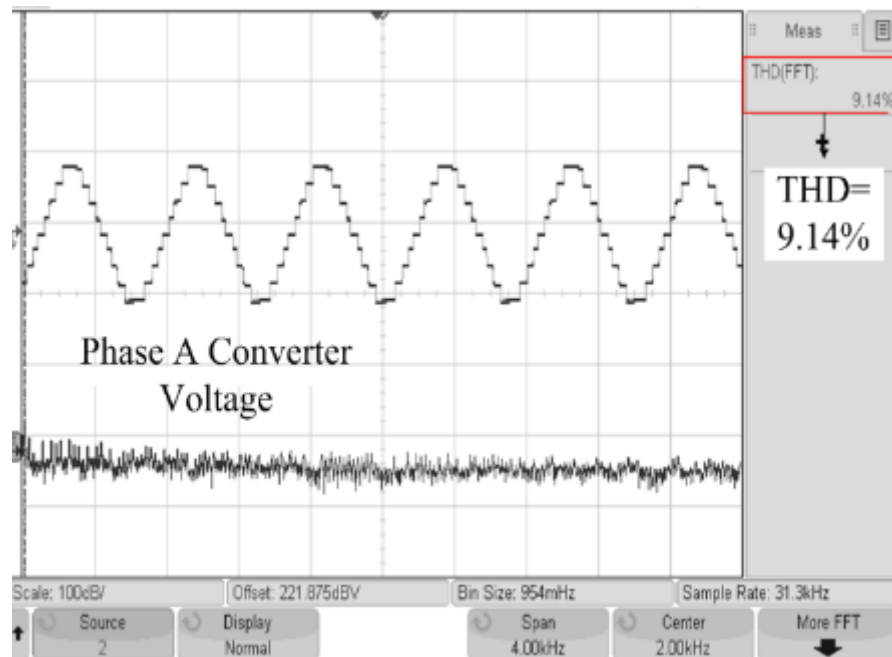


(a)

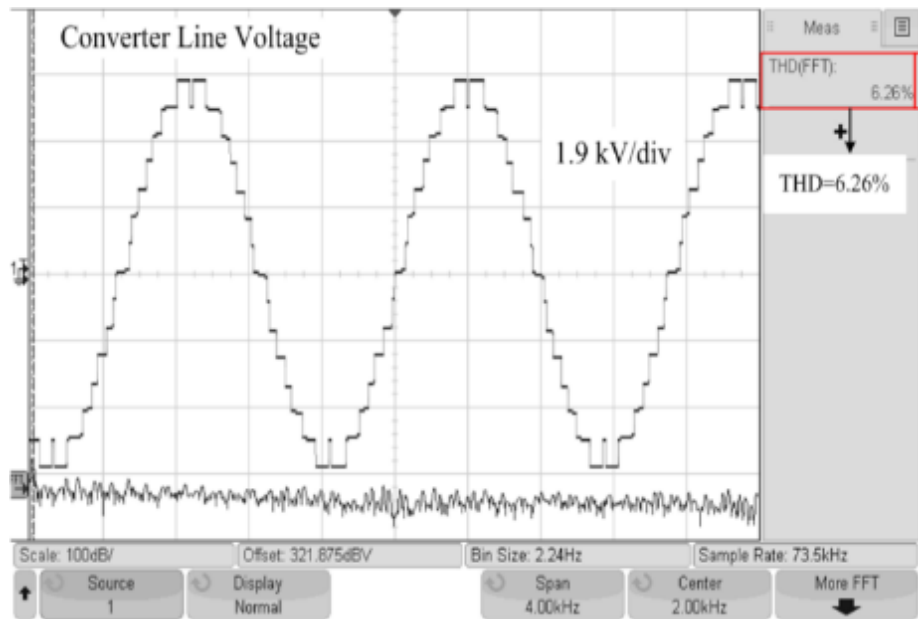


(b)

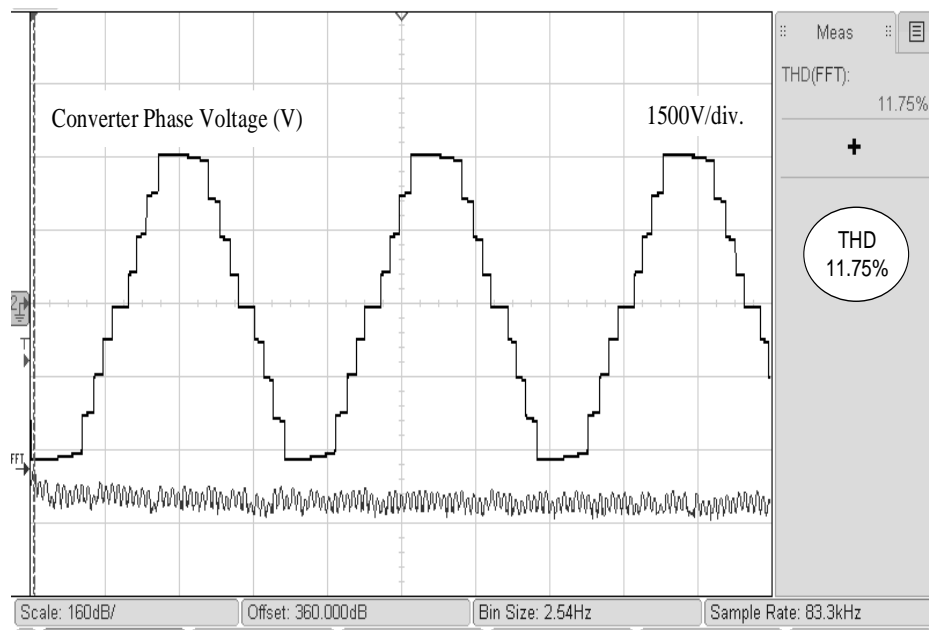
Fig 4.23 Dynamic response (a) PV voltage for three phase array1 (b) PV current for three phase array1



(a)

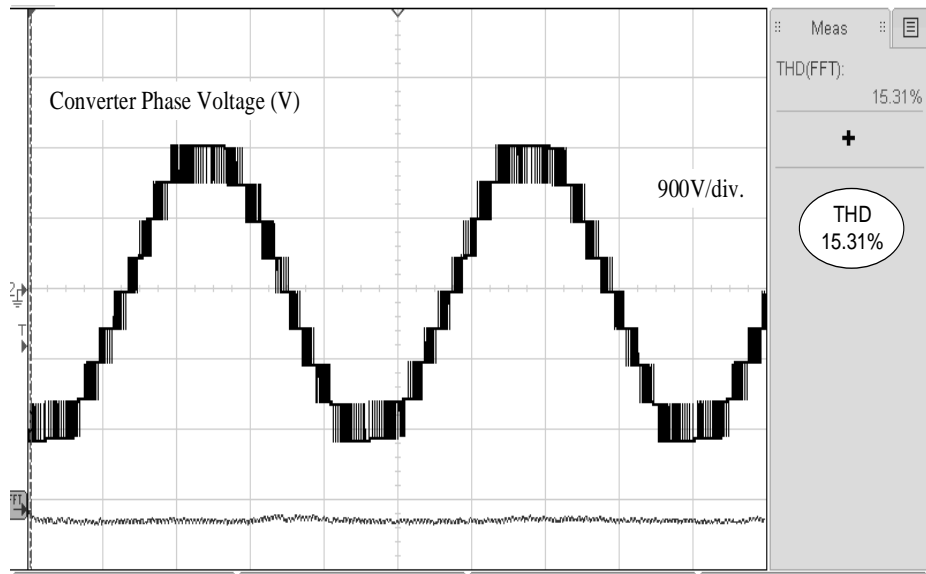


(b)



(c)





(d)

Fig 4.24 Converter voltage THDs (a) SHE-PWM phase voltage (b) SHE-PWM line voltage (c) NLM-PWM phase voltage and (d) PS PWM phase voltage

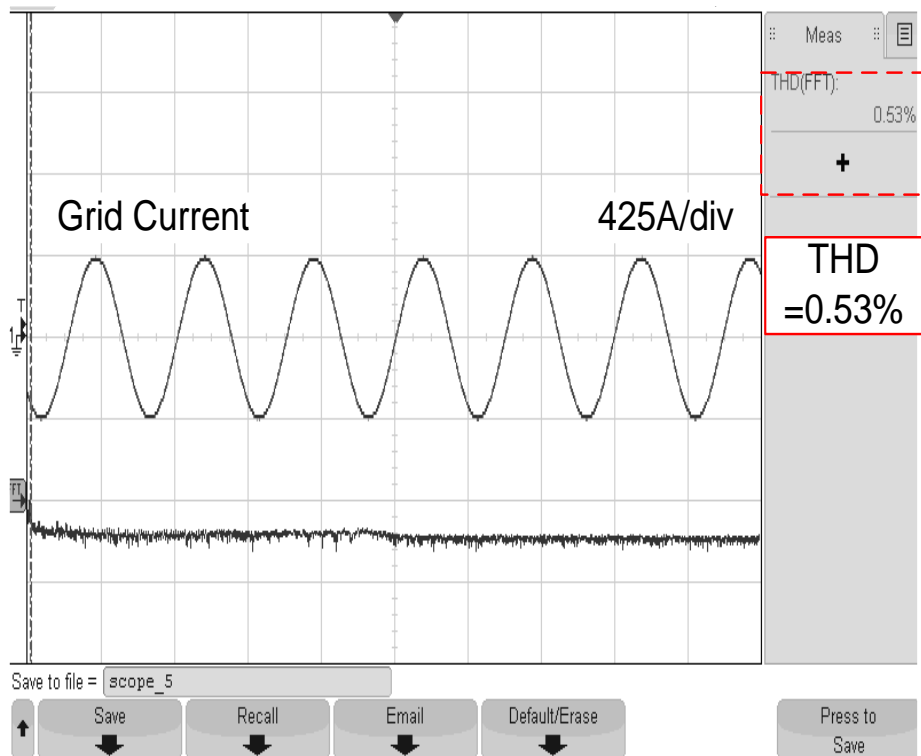
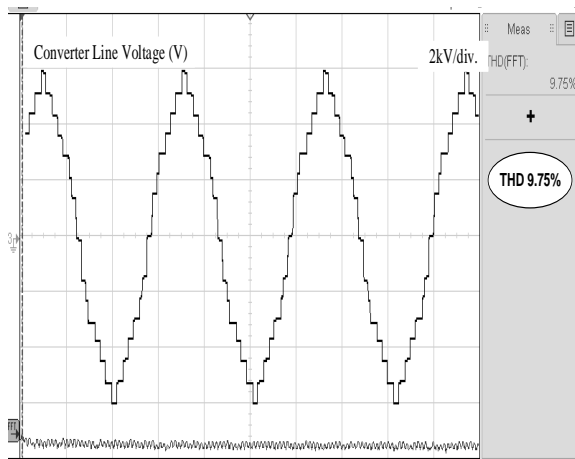
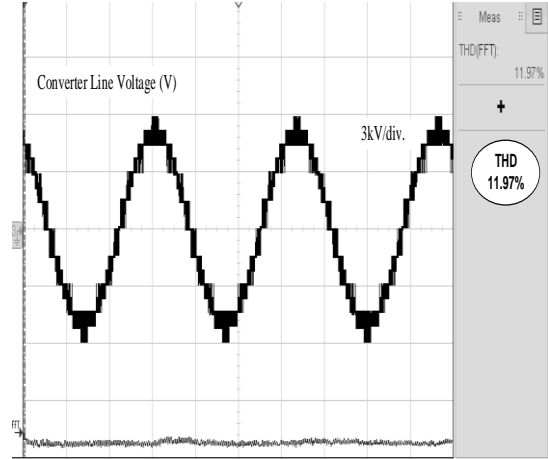


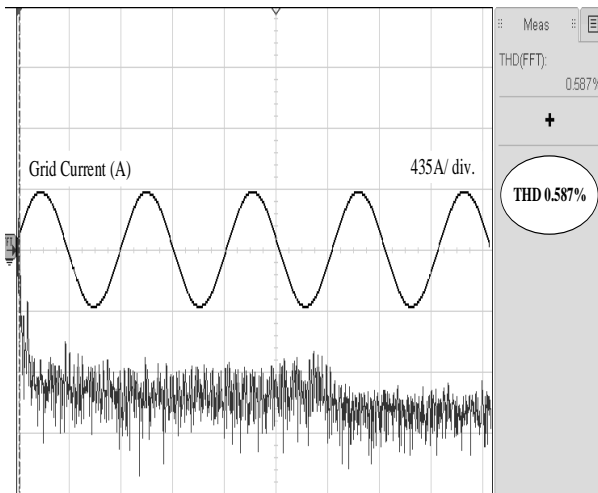
Fig. 4.25 Grid current THD



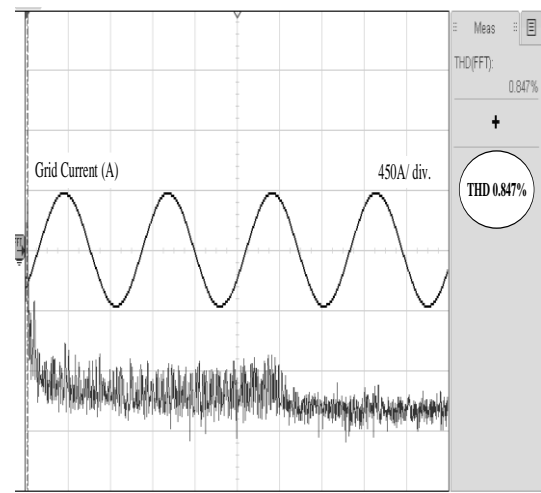
(a)



(b)



(c)



(d)

Fig.4.26 OPAL-RT results (a) & (b) Converter line voltage THD of NLM-PWM and PS PWM, (c) and (d) Grid current THD for NLM-PWM and PS PWM

## 4.7 CONCLUSIONS

The design, modelling, and control of transformerless single-stage nine-level H-bridge cascaded multilevel converters for the photovoltaic grid-tied plant have been carried out with the improved P&O MPPT, decoupled current controller based on SRF-PLL with phase-shifted PWM, SHE-PWM, and NLM modulation techniques. To solve nonlinear transcendental equations obtained from Fourier transform in SHE-PWM, the resultant theory algebraic method is employed, which eliminates lower order harmonics, i.e., fifth,

seventh, and eleventh in this work. Higher-order harmonics are reduced by using an inductive filter. The THD of grid current obtained by these modulation techniques is validated as per the IEEE-519 standard. The system's performance is observed satisfactory at  $1000 \text{ W/m}^2$  insolation level and  $25^\circ\text{C}$  temperature and validated as per the IEEE-519 standard [17].

## **CHAPTER-V**

### **CONTROL AND DESIGN OF NINETEEN LEVEL CASCADED MULTILEVEL CONVERTER BASED PV SYSTEM**

#### **5.1 GENERAL**

This chapter deals with design, modeling, and control of a medium voltage symmetrical CHB multilevel converter for the direct grid integration of a large photovoltaic (PV) system. It presents the design considerations for selecting an optimum number of levels in the multilevel converter, which are to be both efficient and economical. This system is designed for the medium voltage of 11 kV, hence it can be directly interfaced with the grid without a step-up transformer. It contributes considerable cost savings in the installation, operation, and maintenance of the large solar plant. With the increased number of levels, the converter output voltage waveform is a close to the sine waveform. The control employed is a decoupled control with the synchronous reference frame – phase-locked loop (SRF-PLL), and a 19-level cascaded converter is operating at the low switching frequency. The separate improved perturb and observe (P&O) maximum power point tracking (MPPT) algorithm is used to track the maximum power from each array of multi-string solar photovoltaic (SPV) system. Simulated results are obtained both for steady-state and dynamic performances of the system by using the FFT tool of MATLAB and validated in accordance with the IEEE-519 standard. Simulation results are validated in hardware-in-loop (HIL) on OPAL-RT platform. The system configuration, design, modelling, control, simulation, and results are discussed in detail in different sections of this chapter.

Earlier chapter 3 is focussed on design and development of a seven-level cascaded converter whereas chapter 4 is focussed on nine-level CHB converter and its performance

analysis using various PWM techniques. In this chapter, the focus is on an optimum selection of number of levels and use of low-voltage rating devices.

## 5.2 SELECTION CRITERIA FOR OPTIMUM NUMBERS OF LEVELS

In high voltages (3.3, 4.5, 6.5 kV), costly IGBTs are available in the market, but the lower voltage (0.6, 0.9, 1.2, 1.7, and 2.5 kV) IGBTs are comparatively low in cost and have better technology. Hence, a cascaded connection of low voltage IGBTs for achieving medium voltage can be used to develop a low-cost inverter. The designed system can facilitate a direct connection to the medium voltage AC network, with an improved output power quality. At the same time, this leads to a linear increase in the component number and control complexity. Hence, to achieve an improved performance versus price ratio, finding the optimum value for the number of levels is essential [68-72]. Usually, the 7-level to 21-level multilevel inverters for 11 kV are considered suitable for feeding the power at the given system voltage [68].

As the cost of a semiconductor device is significant for a medium voltage system, a higher device voltage utilization factor (DVUF) is necessary for making the system design a cost-effective one. The DVUF for an 11kV system with different levels is summarized in Table 5.1 [68].

Table-5.1 DVUF in an 11 kV system for different levels [68]

<b>Number of levels</b>	<b>Rated Device voltage in kV</b>	<b>DVUF (%)</b>
11	3.3	90
15	2.5	96
19	1.7	99
21	1.7	90

In semiconductor devices, the inverter section losses are the sum of conduction losses and switching losses. As one increases the number of levels in a multilevel converter, the carrier frequency reduces, and the active switching device count rises linearly. Hence, switching losses are reduced, and at the same time, conduction losses are increased. Moreover, the device voltage ratings determine an IGBT's on-state voltage drops and diode's forward voltage. For these reasons, total losses in the inverter section are almost constant and, therefore, despite the change in the number of levels, multilevel inverter's efficiency remains virtually constant. Thus, the efficiency is not a consideration in the selection of levels while designing multilevel inverter.

Table 5.2 [68] gives the count of arithmetic and logical operations (ALOs) required in a switching section, the count of IGBTs for different levels, THD (%), and the cost in US\$ for an 11 kV system for comparing the performance, cost, and complexity of the system.

Table-5.2 An 11kV system [68]

<b>Number of levels</b>	<b>11</b>	<b>15</b>	<b>19</b>	<b>21</b>
IGBTs	60	84	108	120
ALOs	55	77	99	110
THD(%)	8.55	6.00	4.27	4.25
Cost (US\$)	142080	198912	8748	9720

For comparing the variety of the inverter system based on the cost, performance, and control complexity comprehensively, a normalized index is defined as [68],

$$I_{dw} = (w - w_{\min}) / (w_{\max} - w_{\min}) \quad (5.1)$$

where  $w$  is a scored value and  $w_{\min}$ , and  $w_{\max}$  are the lowest and highest indicators.

The normalized index values for 11kV are given in Table 5.3 [68].

Table-5.3 Normalized index for 11kV system [68]

Number of levels	11	15	19	21
Performance	1.00	0.41	0.01	0.00
IGBT Cost (US\$)	0.70	1.00	0.00	0.005
Complexity	0	0.17	0.5	1.00
Total Index	1.7	1.58	0.51	1.005

For an 11kV inverter, the total index value is lowest for the 19-level, so a 19-level is an appropriate choice for an 11kV PV system. Beyond a 19-level, power quality improvements and the reduction in semiconductor cost are negligible, and it only increases parts (components) count and control complications as their increase are linear with the increase in the number of levels [68-72].

### 5.3 SYSTEM CONFIGURATION

Fig.5.1 shows the system's configuration with a 19-level, 3-phase grid interfaced multilevel converter of power rating of 1MW and 11kV with 50 Hz power frequency and a switching frequency of 500 Hz. This PV system is connected to the grid through an interfacing inductor for reducing ripple content in the current. If the  $L$  is the number of levels in the cascaded multilevel converter, the H-bridge per phase selected is calculated as [10].

$$L = (2 * \text{number of H-bridge per phase} + 1) = 19 \quad (5.2)$$

$$\text{Number of H-bridges per phase (s)} = 9$$

So for a 19-level symmetric CHB converter, 9 H-bridges per phase are required, and each H-bridge is fed by the separate and equal PV array, which is easily available in a large

multi-string SPV system. The variables measured for implementing the control algorithm are the grid voltages ( $v_{abc}$ ), the grid currents ( $i_{sabc}$ ), the converter line voltages ( $v_{cabc}$ ), the DC link voltage ( $V_{dc}$ ), PV array voltage ( $V_{pv}$ ), and PV current ( $I_{pv}$ ). The designed system includes design of the PV array, the DC link capacitor, and the DC link voltage. Other design specifications of the system are given in Table 5.4.

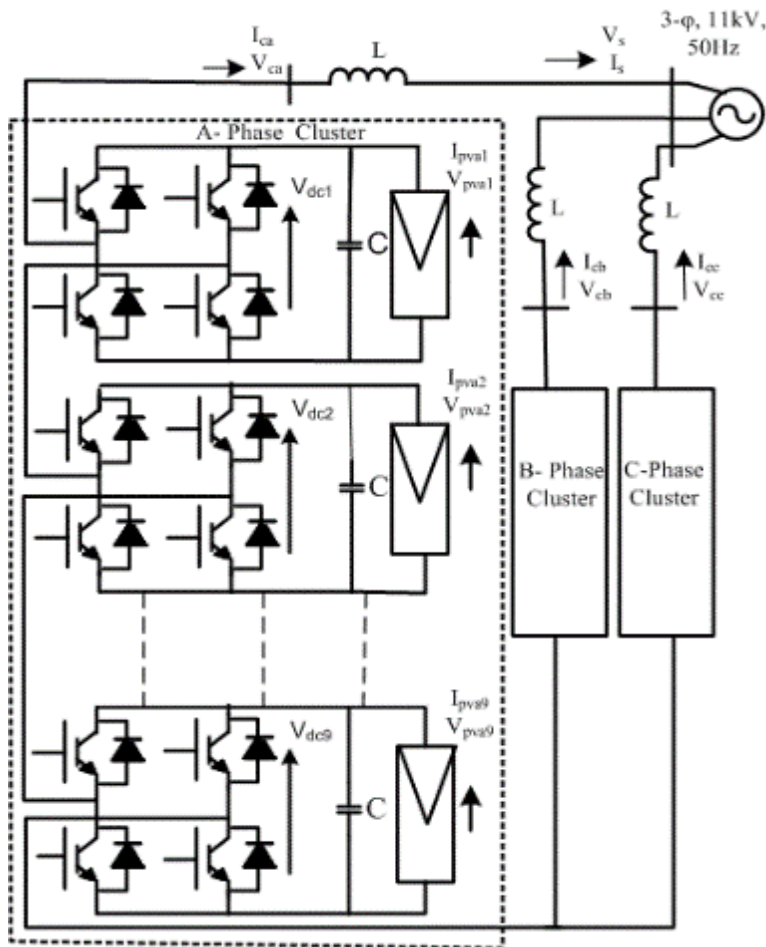


Fig. 5.1 19-level grid interfaced converter PV system

#### 5.4 DESIGN OF 19-LEVEL SYMMETRICAL CHB MULTILEVEL CONVERTER FOR GRID INTEGRATED PV SYSTEM

The system includes the design and modeling of the PV array, DC-link capacitor, DC-link voltage, and coupling inductor for a nineteen-level multilevel converter. As per the parameter obtained, the PV module is selected from the PV library. Depending on the PV



module chosen, the number of series and parallel connected PV modules in a PV array is selected. The other design specifications of the system are given in Table 5.4.

Table-5.4 Component specifications for a 19 level system

<b>Component</b>	<b>Value</b>
Power	1MW
Voltage ( $V_{rms}$ )	11 kV
Frequency	50 Hz
Switching Frequency	500 Hz
Inductor ( $L_c$ )	4 mH
No of parallel paths in SPV array ( $N_p$ )	6
No of series paths in SPV array ( $N_s$ )	25
The voltage of the PV module at maximum power ( $V_{mmp}$ )	40.5 V
The current of PV module at maximum power ( $I_{mmp}$ )	6.05 A
Open circuit voltage PV module ( $V_{oc}$ )	48.8V
Short circuit current of PV module ( $I_{sc}$ )	6.43 A
DC link capacitance ( $C_{dc}$ )	2000 $\mu$ F
DC link voltage ( $V_{dc}$ )	1010 V

#### 5.4.1 Selection of $V_{dc}$ Voltage for 19-Level Converter

For L-level CHB multilevel converter, the DC-link voltage ( $V_{dc}$ ) for each H-bridge connected to the PV array is calculated as [10],

$$V_{rms} = 0.612*(L-1)*V_{dc} \quad (5.3)$$

$$V_{dc} = 998.5V.$$

$V_{dc}$  is chosen as 1010 V

#### 5.4.2 Design Calculations and Selection of PV Array for 19-Level Converter

The required power rating of each PV array for a 19-level CHB converter consisting of nine PV array for feeding 1MW power to the grid is calculated as,

$$P_{mmp} = \frac{(\text{power rating of the system})}{(\text{number of total PV array})} \quad (5.4)$$

$$= 1\text{MW}/27 = 37.04\text{kW}$$

To obtain the PV array of 37.04 kW power ( $P_{mmp}$ ) and  $V_{dc}$  of 1010V, a Sun Power SPR-245NE-WHT-D model is chosen from the PV array library. The numbers of PV modules connected in parallel and series in PV array are selected as,

$$N_s = V_{dc}/V_{mmp} \quad (5.5)$$

$$= 1010/40.5 = 25$$

$$N_p = P_{mmp}/(N_s * I_{mmp} * V_{mmp}) \quad (5.6)$$

$$= 37.04 \times 10^3 / (25 * 6.05 * 40.5) = 6$$

#### 5.4.3 Design of Capacitor for 19-Level Converter

The DC-link capacitance ( $C_{dc}$ ) for each H-bridge connected to the PV array is obtained following the principle of conservation of energy. As per this principle, for  $V_{dc}$  recovery in 5 ms and 1.2 overloading factor  $a$ , and  $K_1$  denotes variation of energy during dynamics, taken as 10% ( $K_1 = 0.1$ ) as [11],

$$\frac{1}{2} * C_{dc} (V_{dc}^2 - V_{dc1}^2) = K_1 * 3 * V * a * I * t \quad (5.7)$$

$$C_{dc} = (0.1 * 37.04 * 10^3 * 1.2 * 0.005) / (0.5 * (1010 * 1010 - 998.5 * 998.5))$$

$$C_{dc} = 1924.35 \mu\text{F}.$$

It is selected as  $C_{dc}$  (C) = 2000  $\mu\text{F}$ .

#### 5.4.4 Design of Interfacing Inductance for 19-Level Converter

The 4mH inductor is selected for getting the required result of THD of grid current waveform for 19-level as per IEEE-519 standard for phase shifted PWM modulation. The per unit value of inductor corresponding to 4mH is calculated as [13]

$$L_c(\text{p.u.}) = (2 \cdot \pi \cdot f \cdot L \cdot P) / V_s^2$$

$$= (314 \times 4 \times 10^{-3} \times 1 \times 10^6) / (11 \times 10^3 \times 11 \times 10^3)$$

$$= 0.01 \text{ p.u.}$$

#### 5.5 CONTROL OF 19-LEVEL SYMMETRICAL CHB MULTILEVEL CONVERTER FOR GRID INTEGRATED PV SYSTEM

The algorithm for controlling the SPV system integrated to the three-phase AC grid is shown in Fig.5.2. The maximum power tracking from the array using converter voltages and currents, is necessitated. A decoupled current control having a feed-forward term, the control for the DC-link capacitor, synchronous reference frame (SRF), and phase-locked loop (PLL) for synchronization are used for controlling VSC [115-116].

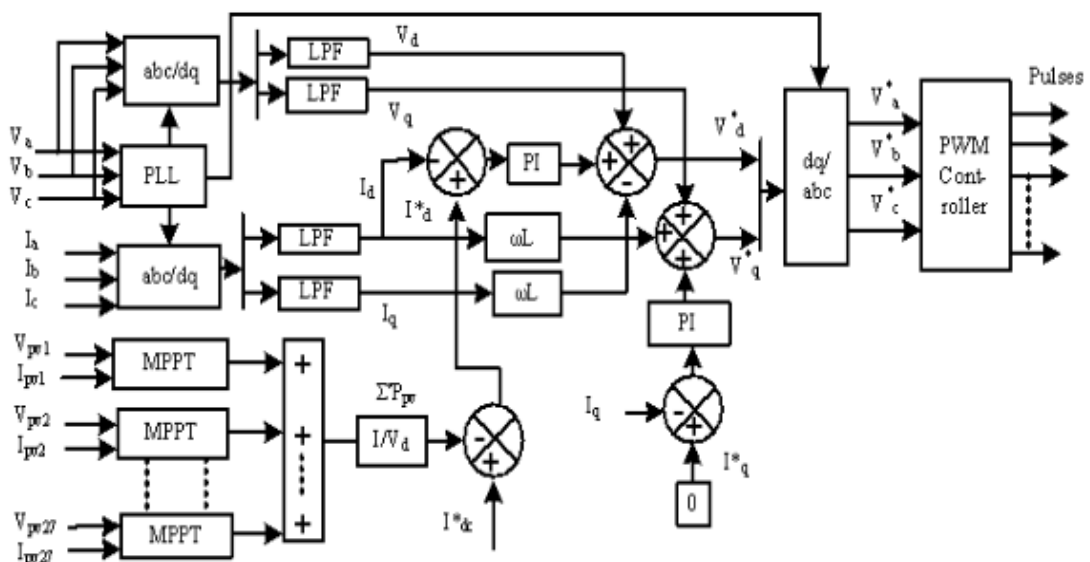


Fig. 5.2 Control algorithm for 19-level CHB multilevel converter

### 5.5.1. Implementation of Improved P&O MPPT Algorithm

The maximum power is extracted from the PV array, and a suitable  $V_{dc\_ref}$  is generated by using the MPPT algorithm. Out of many reported MPPT algorithms, the improved P&O algorithm is preferred owing to its superiority vis-à-vis other algorithms. In the literature [54-58], it is reported that the P&O algorithm is PV array independent. It is a true MPPT algorithm and implementable in both digital and analog forms, devoid of periodic tuning requirements, and easy to implement. As far as an improved P&O algorithm is concerned, apart from the P&O algorithm's benefits, it also takes care of the drift effect due to increased insolation by taking into account the change in the current apart from the change in voltage and power. The MPPT governing equations are as follows,

$$V_{pv}^*(k) = V_{pv}^*(k-1) + \Delta V_{pv}, \text{ if } dP_{pv} < 0 \text{ and } dV_{pv} < 0 \text{ or } dP_{pv} > 0, dV_{pv} > 0 \text{ and } dI_{pv} < 0 \quad (5.8)$$

$$V_{pv}^*(k) = V_{pv}^*(k-1) - \Delta V_{pv}, \text{ if } dP_{pv} < 0 \text{ and } dV_{pv} > 0 \text{ or } dP_{pv} > 0, dV_{pv} > 0 \text{ and } dI_{pv} > 0 \text{ or } dP_{pv} > 0 \text{ and } dV_{pv} < 0 \quad (5.9)$$

### 5.5.2. Implementation of VSC Control Algorithm

The voltages obtained from the measurement of each DC link ( $V_{dc}$ ) and given by each MPPT algorithm ( $V_{dc\_ref}$ ), are compared, and the error voltage ( $V_e$ ) between the two is processed by a proportional-integral (PI) controller as shown in Fig. 5.3, which is given to the improved P&O MPPT algorithm. To integrate the solar PV power generating system with the grid synchronization of the grid voltages and currents with the value of  $I_{dc}^*$ , the reference DC-link current, expressed at  $k$  and  $(k-1)$  instant as,

$$I_{dc}^*(k) = I_{dc}^*(k-1) + K_p \{V_e(k) - V_e(k-1)\} + K_i * V_e(k) \quad (5.10)$$

Where  $K_p$  &  $K_i$  are the proportional and integral gain constants for the PI controller. The sum of all reference DC-link current along with the feed-forward term is compared with the direct current component obtained by the Park's transformation from the grid currents [9,115-116] as given earlier in chapter 3.

The grid detection angle ( $\theta$ ) for the Park's transformation is obtained from a three-phase PLL.  $I_q^*$  the reference quadrature current (set to zero for feeding the grid current at unity power factor) is compared with the quadrature current component obtained from the Park's transformation.

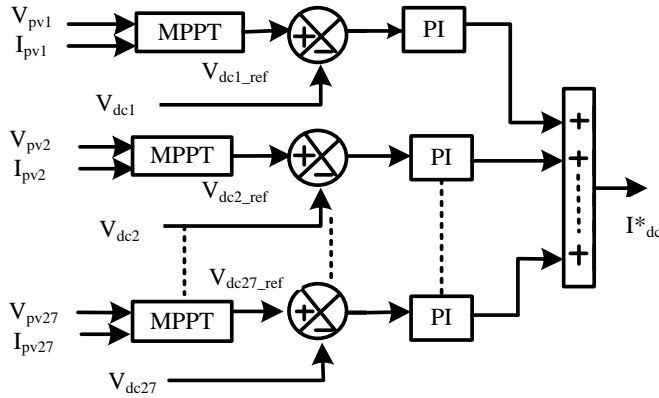


Fig. 5.3 Generation of  $I_{dc}^*$  for 19-level CHB multilevel converter

Similarly, the direct ( $V_d$ ) and the quadrature ( $V_q$ ) components of the grid voltages are calculated using the Park's transformation as given in the earlier chapter.

The reference direct-axis and quadrature-axis voltages at instants  $k$  and  $(k-1)$  are estimated as follows,

$$V_d^*(k) = V_d^*(k-1) + K_{p2} \{ I_{de}(k) - I_{de}(k-1) \} + K_{i2} * I_{de}(k) + V_d - I_q^* \omega L \quad (5.12)$$

$$V_q^*(k) = V_q^*(k-1) + K_{p3} \{ I_{qe}(k) - I_{qe}(k-1) \} + K_{i3} * I_{qe}(k) + V_q + I_d^* \omega L \quad (5.13)$$

where  $I_{de} = (I_d^* - I_d)$ ,  $I_{qe} = (I_q^* - I_q)$  and  $\omega L$  is the coupling reactance.  $K_{p2}$ ,  $K_{i2}$ ,  $K_{p3}$  and

$K_{i3}$  are the respective proportional and integral gains of the direct axis PI current controller and the quadrature axis PI current controller.

### 5.5.3 Implementation of Phase Shifted Multi-Carrier PWM Control for 19-Level Converter

A multicarrier PWM technique is most widely used in the multilevel converter. The phase-shifted PWM technique with a low switching frequency (500Hz) is used for modulation. For a 19-level CHB, a total of 27 H-bridges are used; hence a total of 108 pulses are generated. The phase shift between the carrier signals in case of CHB is calculated as

$$360^\circ / (L-1) = 360^\circ / (19-1) = 20^\circ, \quad (5.14)$$

where 'L' denotes the number of levels. For a 19-level, the phase shift between the carrier signals is  $20^\circ$  [10]. The modulating signal is compared with the carrier signal to generate the pulses for three phases, as shown in Fig. 5.4.

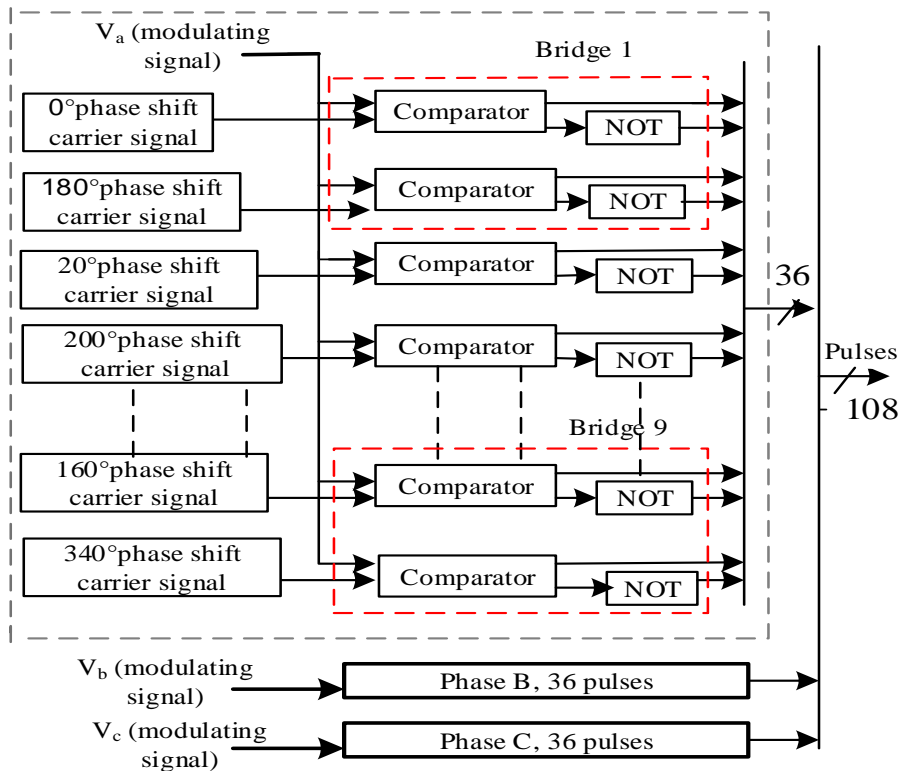


Fig.5.4: Scheme for the generation of PWM signals for 19-level CHB multilevel converter

## **5.6 MODELLING OF 19-LEVEL SYMMETRICAL CHB MULTILEVEL CONVERTER FOR GRID INTEGRATED PV SYSTEM**

This section presents the MATLAB based modelling of a nineteen-level symmetrical CHB multilevel converter for grid interfaced SPV system. Simulation software, MATLAB R2015a, is used for simulation. MATLAB modelling of the grid-connected converter, PV array fed 19-level CHB multilevel converter for phase A, MPPT block, control algorithm, and phase-shifted sinusoidal PWM is also developed. MATLAB model is designed for phase A only. Phase B and Phase C modelling are similar as phase A. MATLAB model is implemented by selecting a block from both Simulink and Simscape SimPowerSystems specialized technology library of MATLAB.

### **5.6.1 Model of Grid Connected Converter**

The developed MATLAB model of grid-connected multilevel converter for the three-phase system is shown in Fig. 5.5. The grid voltages ( $v_{sabc}$ ), grid currents ( $i_{sabc}$ ), converter voltages ( $v_{cabc}$ ), and converter currents ( $i_{cabc}$ ) are measured from three-phase VI-measurement. A three-phase source block of rating 11kV is chosen from the same library for the grid. Discrete powergui environmental block is selected from Simscape SimPowerSystems specialized technology library. The sampling time is set at 5e-06 s.

### **5.6.2 Model of PV Array Connected Nineteen-Level H-Bridge Converter**

For getting a nineteen-level converter, nine H-bridges are connected in a cascade. Each PV array is fed by a separate H-bridge, as shown in Fig. 5.6. For the photovoltaic system, the insolation level is taken as 1000W/m<sup>2</sup> and given through a limiter block, and temperature of 25°C is provided through a saturation block. Both are selected from the Simulink library. A Sun Power SPR-245NE-WHT-D array is selected from Simscape

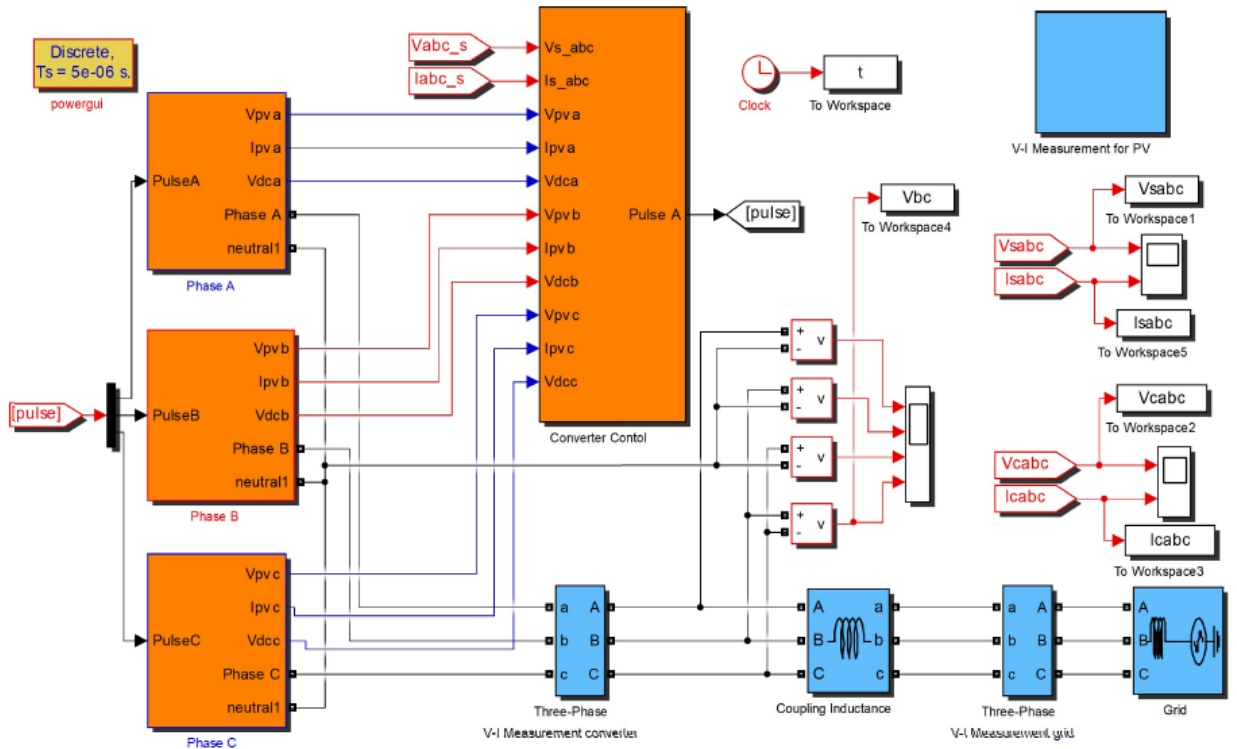


Fig. 5.5 MATLAB model of PV array fed 19-level CHB multilevel converter

simpowersystems specialized technology PV array library. The photovoltaic voltage and current of array 1 ( $V_{a1\_PV}$  &  $I_{a1\_PV}$ ), array 2 ( $V_{a2\_PV}$  &  $I_{a2\_PV}$ ), ..., array 8 ( $V_{a8\_PV}$  &  $I_{a8\_PV}$ ) and array 9 ( $V_{a9\_PV}$  &  $I_{a9\_PV}$ ) are measured for MPPT.  $V_{dc1}$ ,  $V_{dc2}$ , ...,  $V_{dc8}$  and  $V_{dc9}$  are the DC-link voltages across the DC-link capacitor, measured to control the DC-link.

### 5.6.3 Model of Control Algorithm

Fig.5.7 shows the developed model of control algorithm for VSC control. To implement the decoupled current scheme, the abc to dq0 transformation block and PLL block are selected from simpower systems specialized technology library. The reference direct current obtained from the MPPT block and the feed-forward term are compared by a comparator block selected from Simulink library with direct current  $I_d$  and error signal given to a PI-controller. Similarly, the quadrature-component of current is compared with zero-reference (unity pf), and the error voltage is passed through a PI-controller with a



saturation limit fixed at the output. The reference dq-component of voltage so obtained is transformed to  $V_{abc}^*$  (modulation signal) by a dq0 to abc transformation block and given to the PWM block. The synchronous signal ( $\omega t$ ) is provided by the PLL to abc to dq0 and dq0 to abc transformation.

#### **5.6.4 Model of MPPT Controller**

Each PV array is provided with a separate MPPT algorithm controlled by a separate PI-controller, as shown in Fig.5.8. The MPPT algorithm is implemented by writing the algorithm on a user-defined block selected from the Simulink library. Param block gives the upper and lower limit of  $V_{dc\_ref}$  and increment step for implementing the algorithm. This MPPT block provides the  $V_{dc\_ref}$  for controlling DC-link.  $V_{dc\_ref}$  is compared with  $V_{dc}$  by a comparator, and the output is controlled by a PI-controller (with saturation limit) to obtain the  $I_{dc}^*$ .

#### **5.6.5 Model of Phase-shifted PWM**

The eighteen carrier signals of 500 Hz switching frequency are generated by selecting a triangle generator block from simpowersystems specialized technology control and signal generation library for implementing the phase-shifted PWM for a 19-level CHB multilevel converter. The triangle generator block generates a symmetrical triangle waveform with a peak amplitude of +/-1 for implementing carrier signal. The phase shift is kept  $20^\circ$  between the carrier signal for implementing a 19-level converter. These carrier signals are compared with the modulating signal, as shown in Fig. 5.9, and a total of 36 pulses are generated for switching of phase-A switches. Switching pulses for

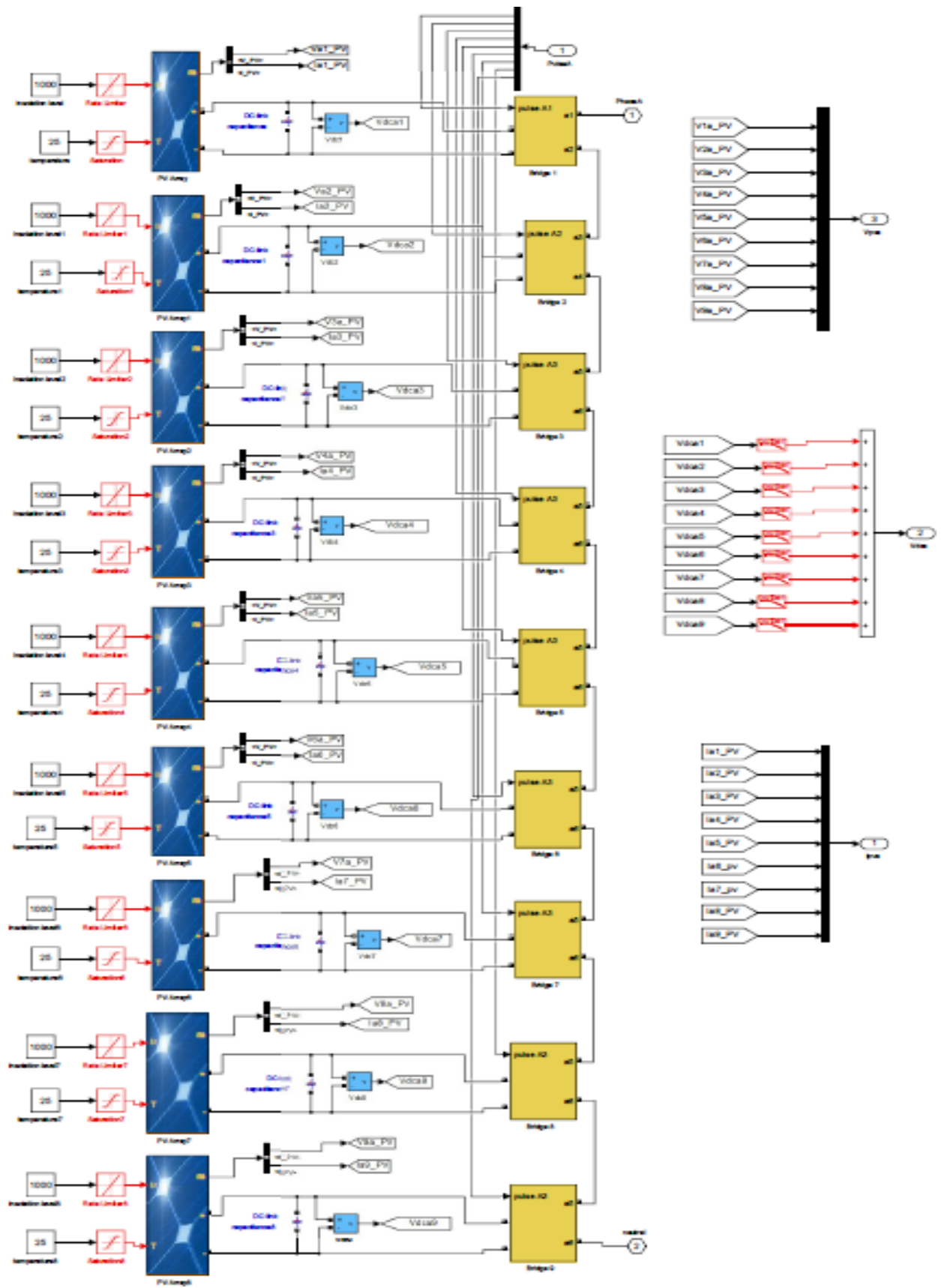


Fig. 5.6 PV array fed 19-level CHB multilevel converter

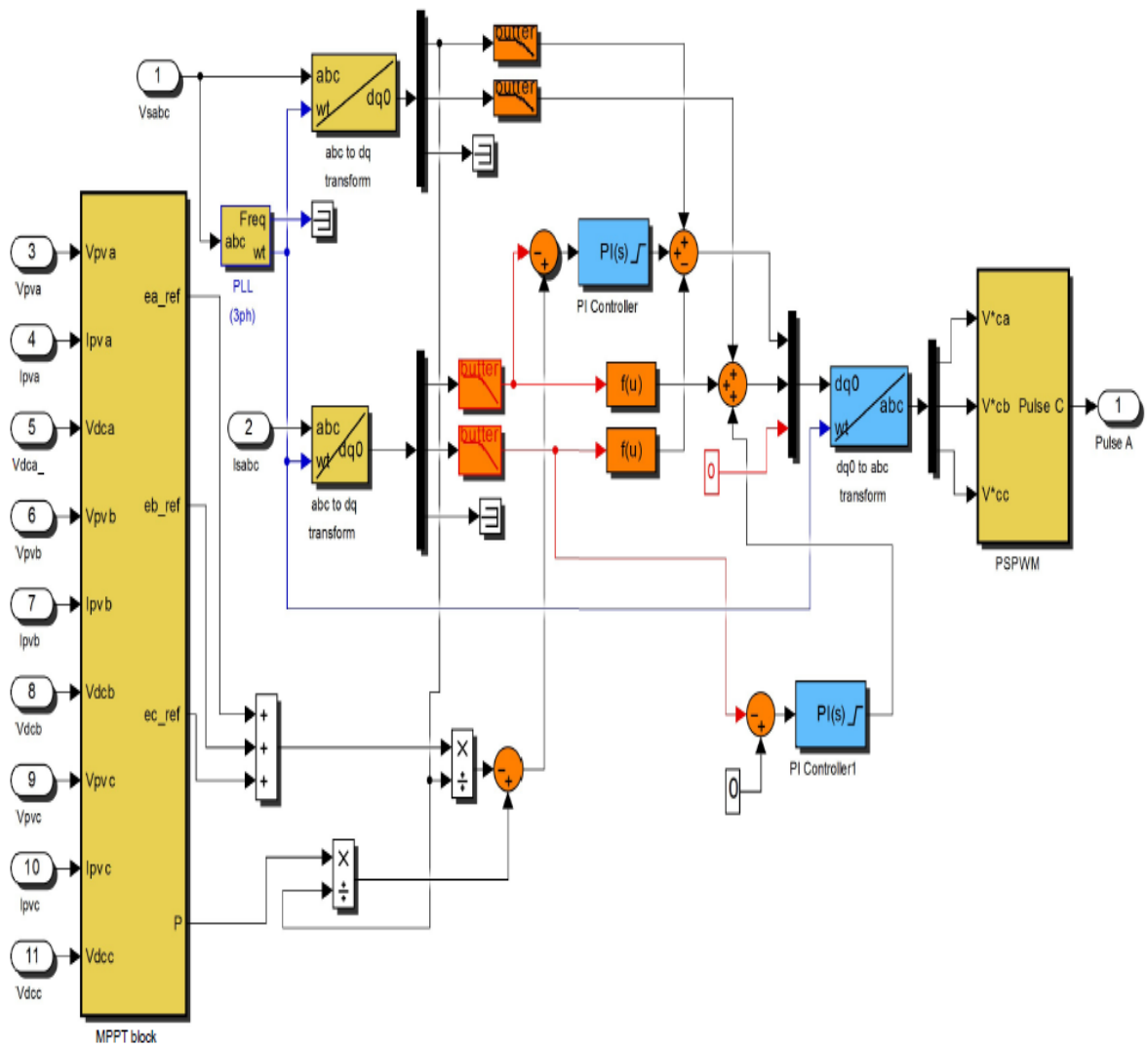


Fig.5.7: MATLAB model of control algorithm for 19-level CHB multilevel converter

the remaining two phases are generated in the similar way. Comparator and NOT-gate block are selected from the Simulink library for the generation of pulses.

## 5.7 RESULTS AND DISCUSSION

A 19-level CHB based MLC for an 11kV grid interfaced PV system with an optimum selected number of levels is designed, modelled, and analysed in a MATLAB environment and validated in HIL on OPAL RT simulator. The results obtained are as follows.

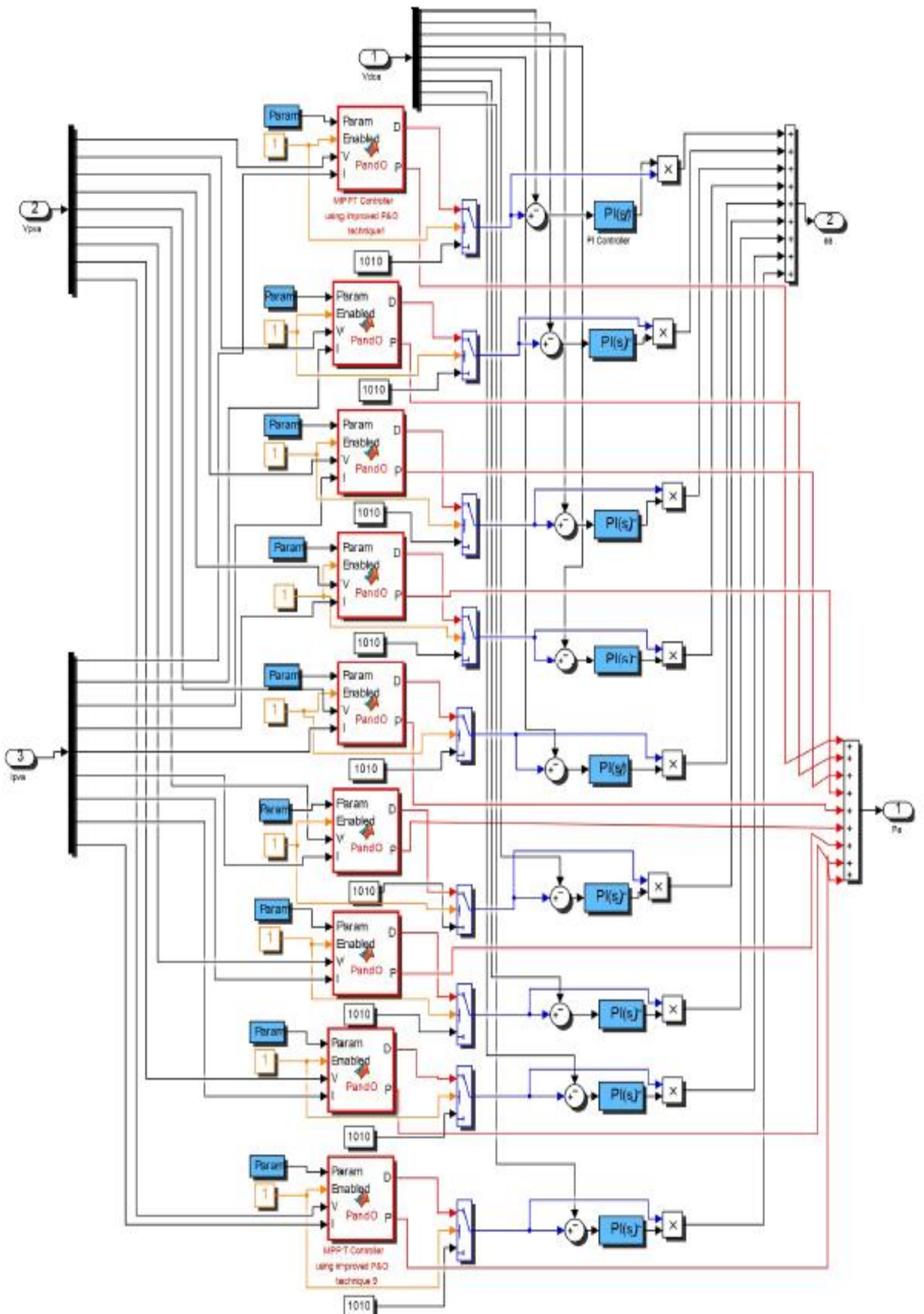


Fig.5.8 MATLAB model of MPPT controller for 19-level converter

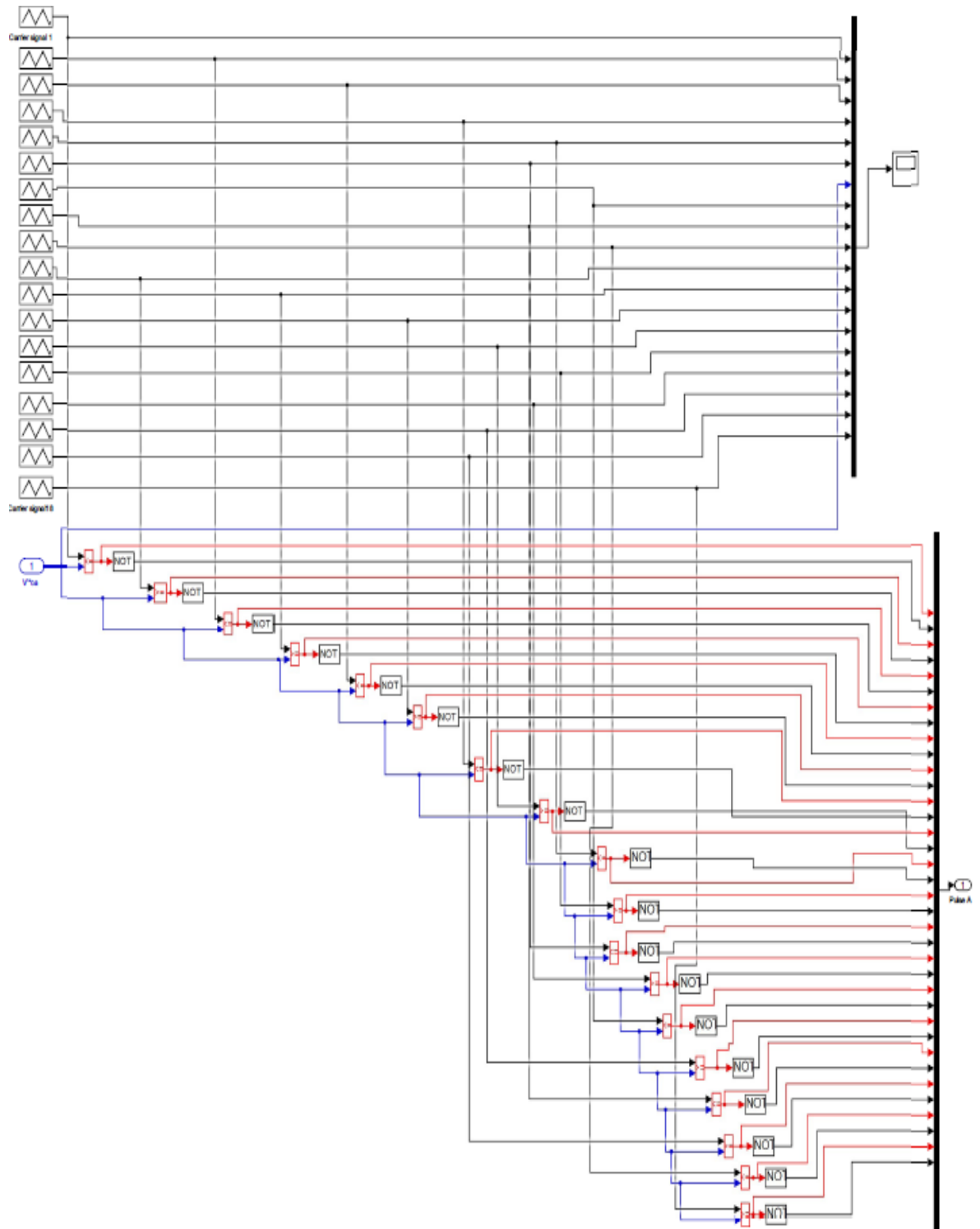


Fig. 5.9 MATLAB model for Phase shifted PWM for 19-level CHB multilevel converter

### 5.7.1 Steady-state Performance for 19-level Converter

The system's steady-state response is studied at an insolation level of  $1000 \text{ W/m}^2$  and temperature  $25^\circ\text{C}$ , and the results are depicted in Fig. 5.10. Simulated results consisting of the grid voltages ( $v_{sabc}$ ), the grid currents ( $i_{abc}$ ), the AC line voltages of VSC ( $v_{cabc}$ ), SPV voltage ( $V_{pv}$ ), SPV current ( $I_{pv}$ ), and power ( $P$ ) are obtained to validate the system performance. As the grid voltage and the grid current are in phase in steady-state response hence the maximum active power transfer is evident at a power factor of unity. PV array generates almost constant voltage and delivers almost constant current and power as shown in figure.

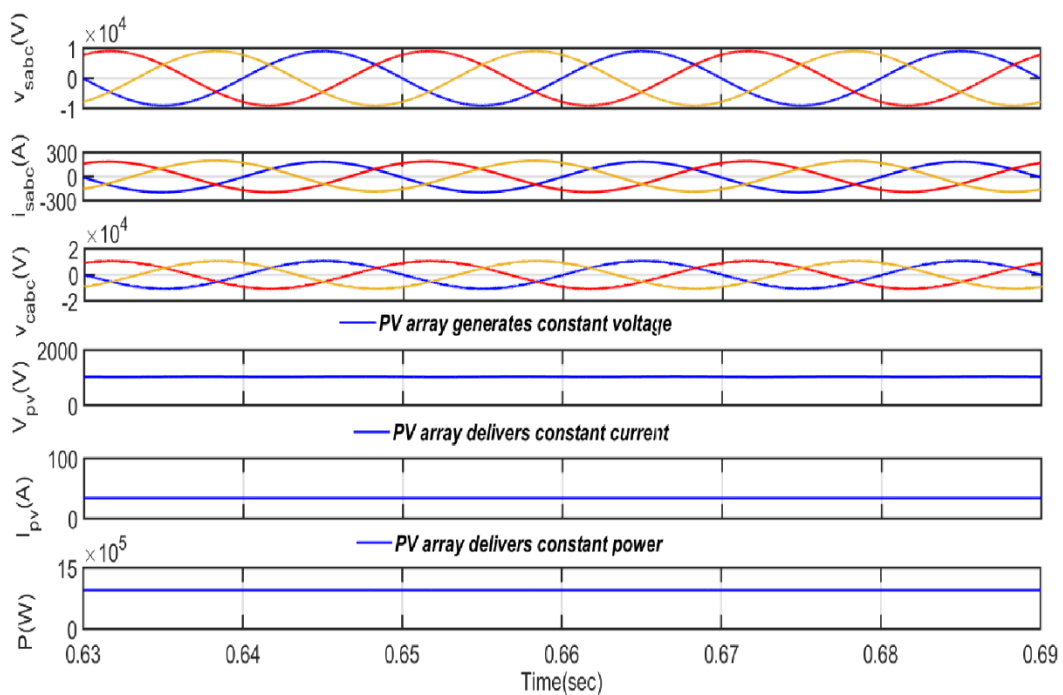
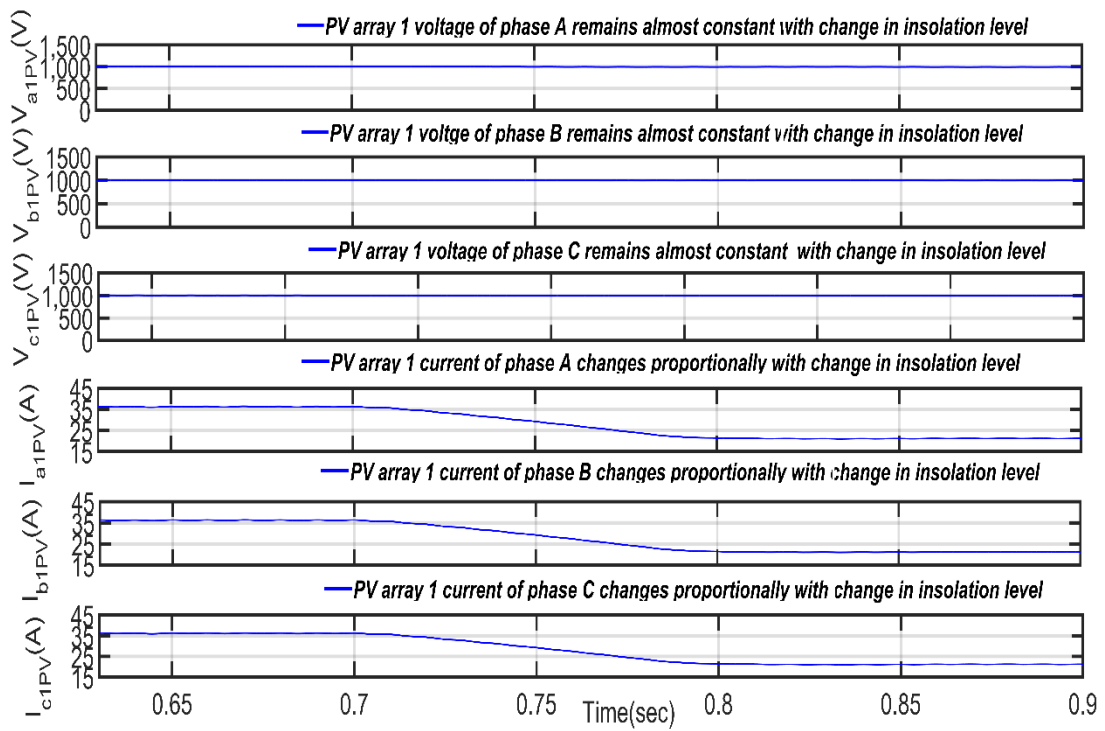


Fig.5.10: Steady-state response of PV system with a 19-level CHB multilevel converter

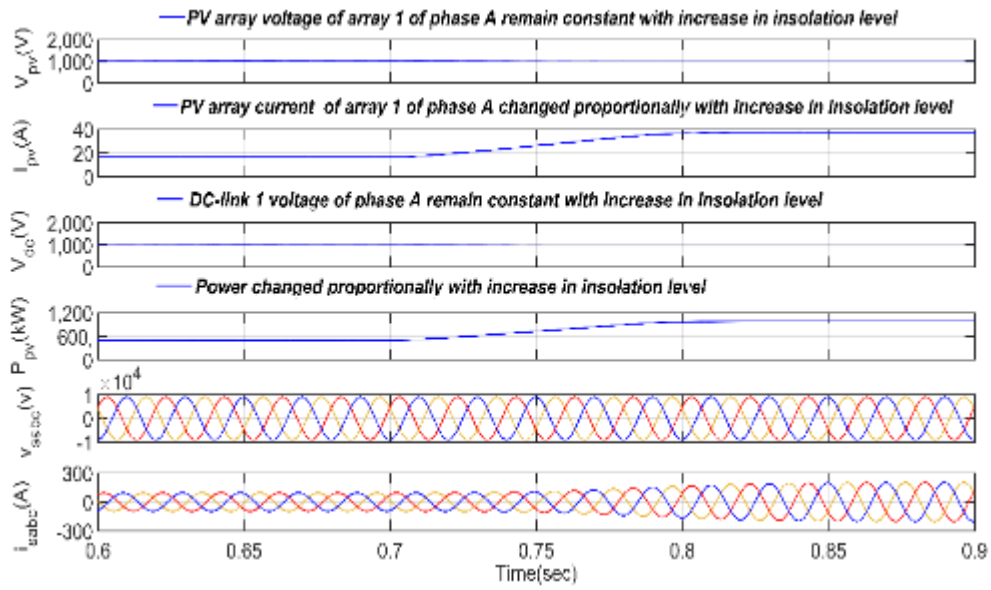
### 5.7.2 Dynamic Performance for 19-level Converter

As shown in Figs. 5.11 (a) and (b), the dynamic response is studied with a constant temperature of  $25^\circ\text{C}$  and an insolation change from  $1000 \text{ W/m}^2$  to  $500 \text{ W/m}^2$  at  $0.7\text{s}$ ,

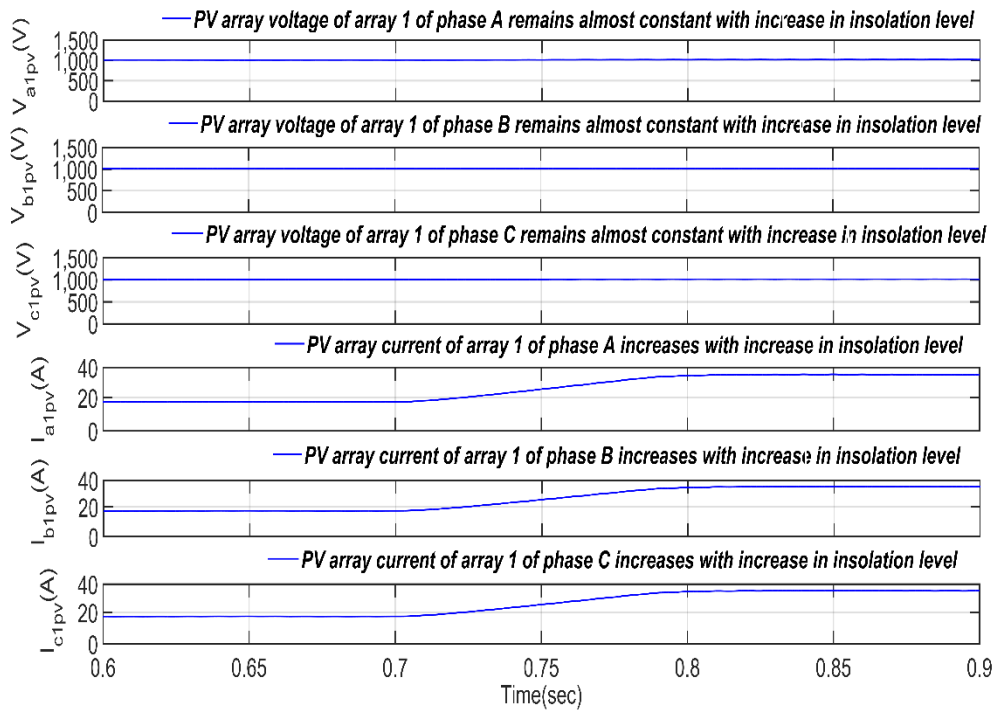
whereas Fig. 5.11 (c) and (d) show the system response for increased insolation from 500 W/m<sup>2</sup> to 1000 W/m<sup>2</sup> at 0.7 s. Simulated results consist of the voltage & the current for a PV array 1 of A-phase ( $V_{a1pv}$  &  $I_{a1pv}$ ), B- phase  $V_{b1pv}$  &  $I_{b1pv}$ ), C- phase ( $V_{c1pv}$  &  $I_{c1pv}$ ). In dynamic response, with the decrease of the insolation level, the PV current's remarkable change is observed, while there is no significant change seen in the PV voltage. The PV voltage and the change in PV current are same for three phase array 1 which verifies that the distributed MPPT control of each array is achieved as shown in Fig. 5.11 (a) and (c). The grid current, PV Power and PV current are changed proportionally and PV voltage and grid voltage remains constant with change in insolation level as shown in Fig. 5.11 (b) and (d).



(a)

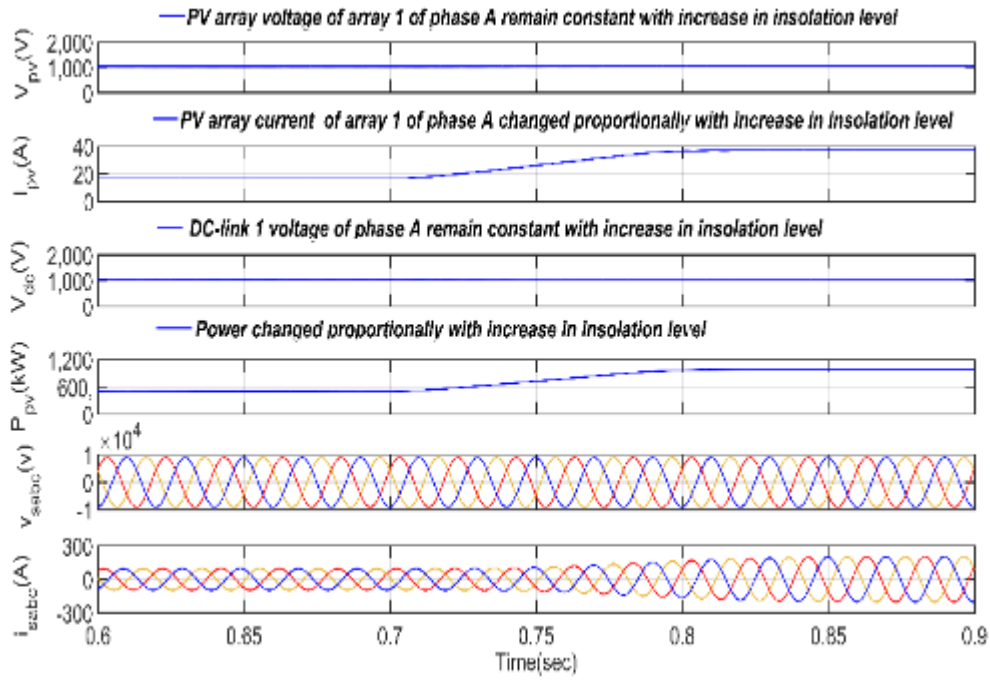


(b)



(c)



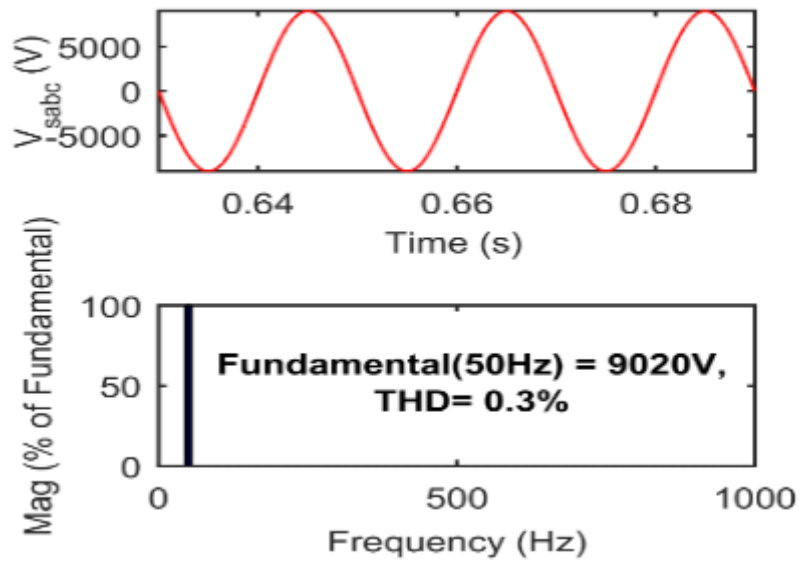


(d)

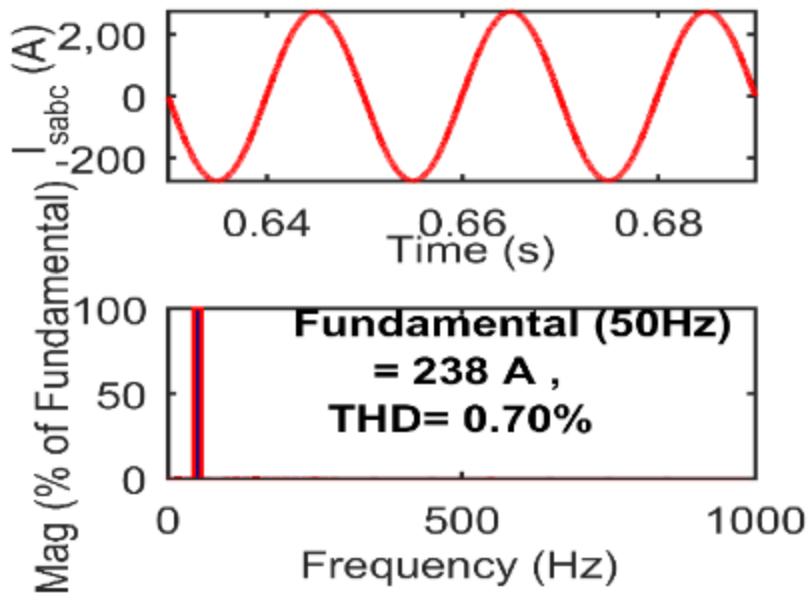
Fig.5.11 Dynamic response for the SHE-PWM technique for (a) and (b) decrease in insolation level from 1000 W/m<sup>2</sup> to 500 W/m<sup>2</sup>, (c) and (d) increase in insolation level from 500 W/m<sup>2</sup> to 1000 W/m<sup>2</sup> at 0.7 s

### 5.7.3 Power Quality Performance for 19-level Converter

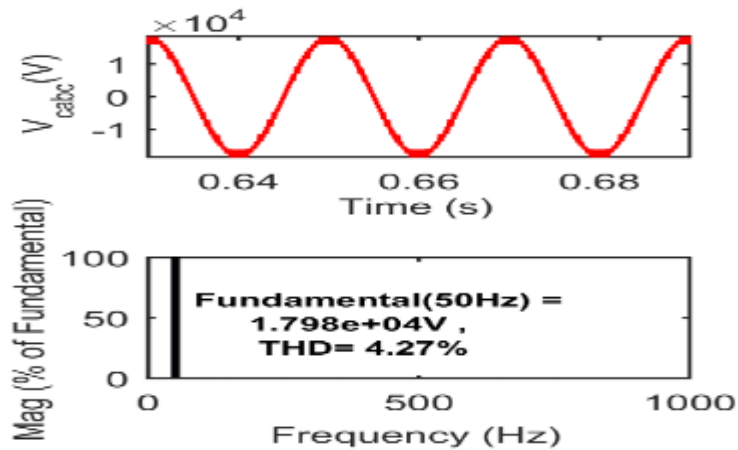
Fig. 5.12 shows the waveforms for the line voltage ( $v_{sabc}$ ), the line current ( $i_{sabc}$ ), and the converter line voltage ( $v_{cabc}$ ) and harmonic spectra along with THD levels at 1000 W/m<sup>2</sup> and 25°C temperature levels. The THD values of 0.30%, 0.79% and 4.27%, respectively are observed for the line voltage, the line current, and the converter line voltage for a 19-level grid interfaced 11 kV SPV system. The supply current THD is well within limits set by the IEEE-519 standard [17].



(a)



(b)



(c)

Fig. 5.12 Waveform and harmonic spectra of 19-level and 11kV system (a) line voltage (b) line current (c) converter voltage

#### 5.7.4 Validation of Results in HIL on OPAL-RT Simulator

Fig.5.13 to Fig. 5.16 show the steady state performance of the system at  $1000\text{W}/\text{m}^2$  and  $25^\circ\text{C}$  temperature. Fig. 5.13 and Fig. 5.14 give the PV array1 voltage of phase A ( $V_{pv}$ ), PV array1 current of phase A ( $I_{pv}$ ), phase A converter voltage ( $v_{ca}$ ), phase A grid voltage ( $v_{sa}$ ). Fig. 5.15 and Fig. 5.16 give phase A, B and C of grid currents ( $i_{sa}$ ,  $i_{sb}$  and  $i_{sc}$ ) and converter voltages ( $v_{ca}$ ,  $v_{cb}$  and  $v_{cc}$ ) respectively. Fig.5.17 to Fig.5.21 show the dynamic performance of the system with increase, decrease and both increase and decrease in irradiance. Fig. 5.17 to Fig. 5.21 show the change in  $V_{pv}$ ,  $I_{pv}$ ,  $i_{sa}$ ,  $v_{sa}$  and converter voltage with the change in irradiance.  $V_{pv}$ ,  $v_{sa}$  and converter voltage remains constant and  $i_{sa}$  and  $I_{pv}$  changes with the change in irradiance as shown in Fig. 5.17 to Fig. 5.21. Fig. 5.22 to Fig. 5.24 show the THD of converter phase voltage, converter line voltage and grid current are 6.9%, 4.6% and 0.75% respectively. THDs values of convertor line voltage and grid current are similar to the values obtained through MATLAB simulation, thus validating the performance of the designed system and the developed MATLAB model.

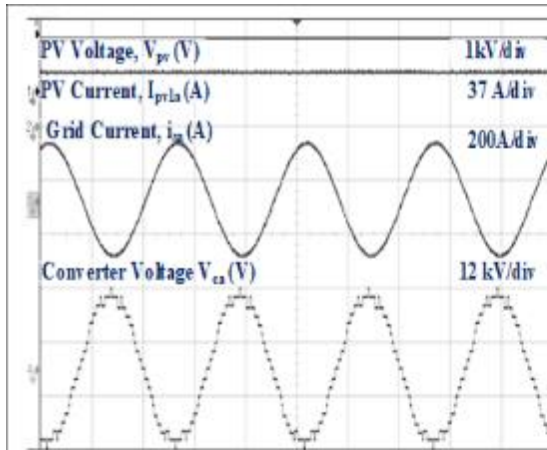


Fig. 5.13 Steady state performance of  $V_{pv}$ ,  $I_{pv}$ ,  $i_{sa}$ ,  $V_{ca}$  at Converter 25°C and 1000W/m<sup>2</sup>

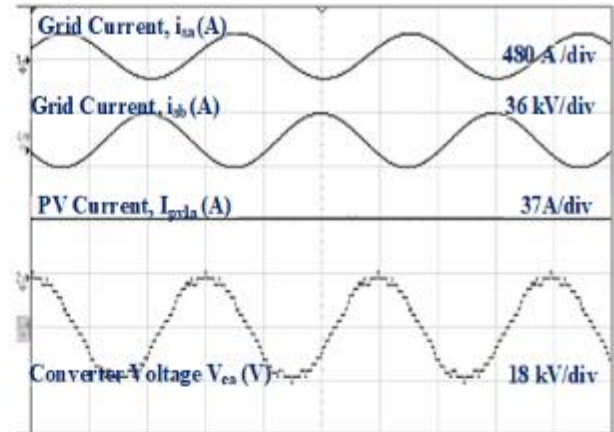


Fig. 5.14 Steady state performance of  $i_{sa}$ ,  $V_{ca}$ ,  $I_{pv}$ , voltage at 25°C and 1000W/m<sup>2</sup>

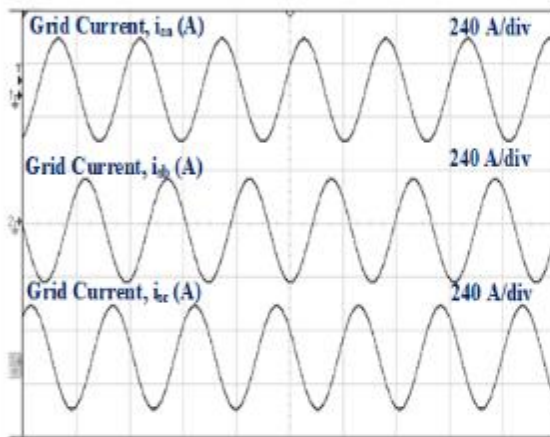


Fig. 5.15 Steady state performance of  $i_{sa}$ ,  $i_{sb}$  and  $i_{sc}$  at  $V_{\infty}$  at 25°C and 1000W/m<sup>2</sup>

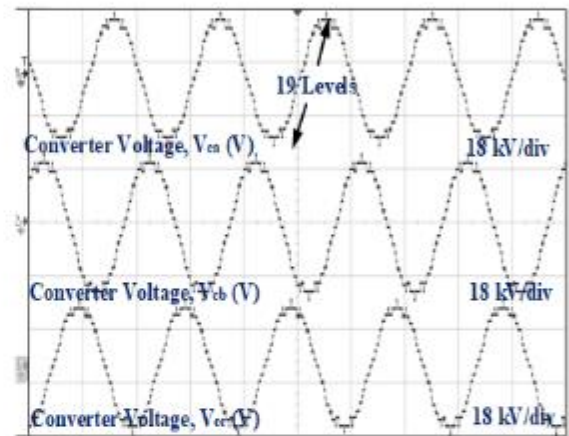


Fig. 5.16 Steady state performance of  $V_{ca}$ ,  $V_{cb}$  and  $V_{cc}$  at 25°C and 1000W/m<sup>2</sup>

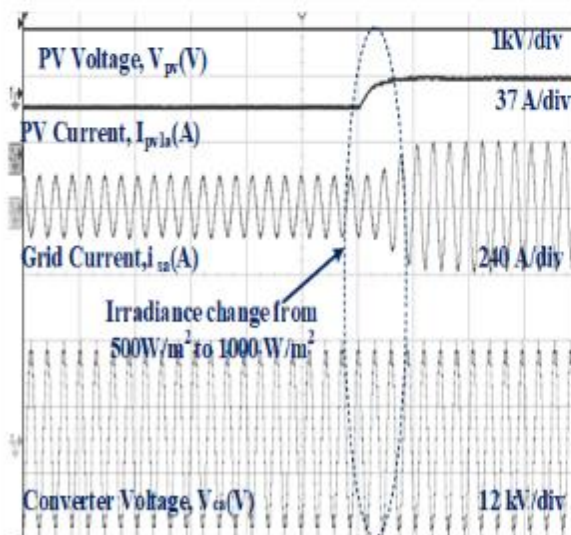


Fig. 5.17 Dynamic performance of  $V_{pv}$ ,  $I_{pv}$ ,  $i_{sa}$  and  $V_{ca}$  at irradiance change from 500W/m<sup>2</sup> to 1000 W/m<sup>2</sup> and 25°C

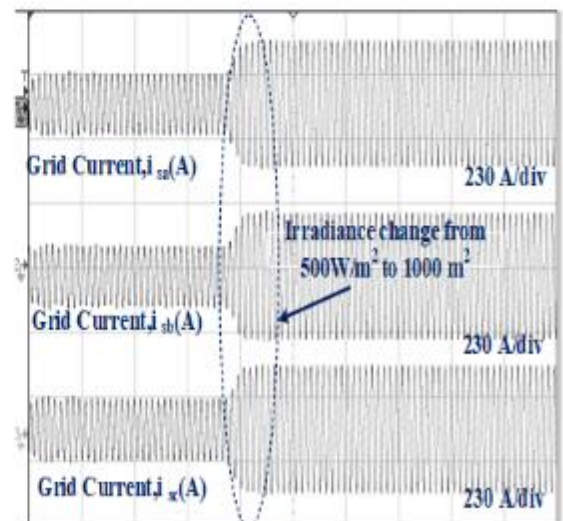


Fig. 5.18 Dynamic performance of  $i_{sa}$ ,  $i_{sb}$  and  $i_{sc}$  at irradiance change from 500W/m<sup>2</sup> to 1000 W/m<sup>2</sup> and 25°C

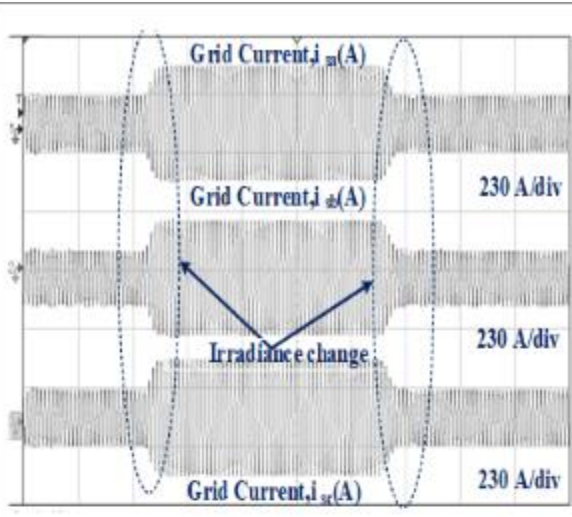


Fig. 5.19 Dynamic performance of  $i_{sa}$ ,  $i_{sb}$  and  $i_{sc}$  at converter at irradiance change from  $500\text{W/m}^2$  to  $1000\text{W/m}^2$ ,  $1000\text{W/m}^2$  to  $500\text{W/m}^2$  and  $25^\circ\text{C}$

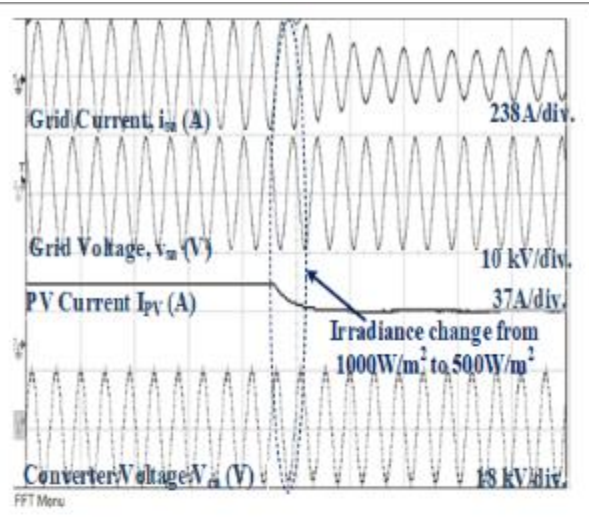


Fig. 5.20 Dynamic performance of  $i_{sa}$ ,  $v_{sa}$ ,  $I_{PV}$  and voltage change from  $1000\text{W/m}^2$  to  $500\text{W/m}^2$  and  $25^\circ\text{C}$

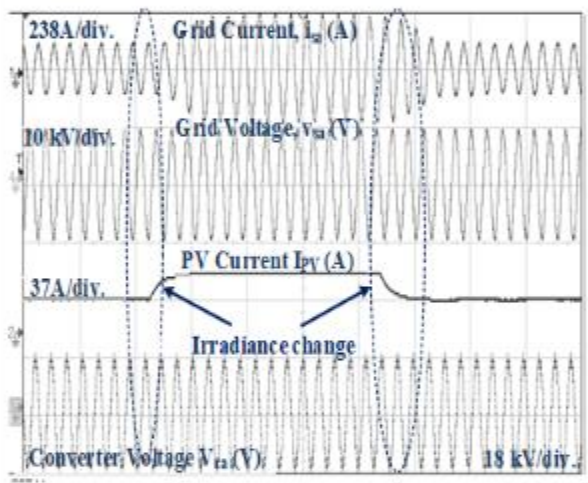


Fig. 5.21 Dynamic performance of  $i_{sa}$ ,  $v_{sa}$ ,  $I_{PV}$  and converter voltage at irradiance change from  $500\text{W/m}^2$  to  $1000\text{W/m}^2$ ,  $1000\text{W/m}^2$  to  $500\text{W/m}^2$  and  $25^\circ\text{C}$

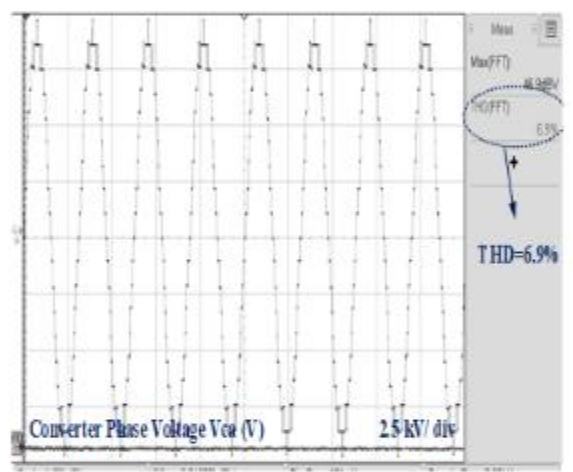


Fig. 5.22 Converter phase voltage THD

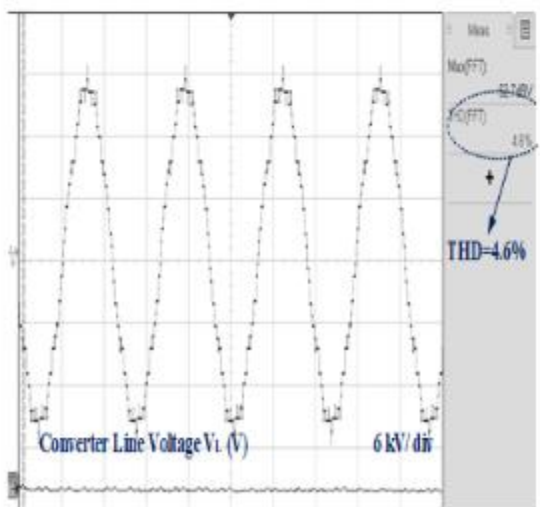


Fig. 5.23 Converter phase voltage THD

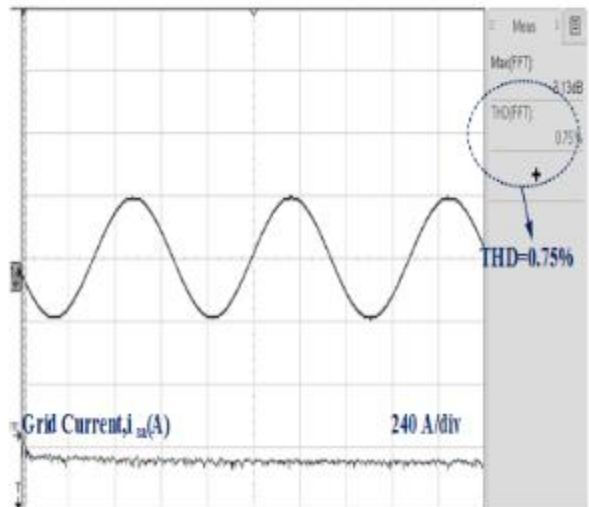


Fig. 5.24 Grid current THD

## **5.8. CONCLUSIONS**

The modelling and design of a medium voltage grid interfaced cascaded multilevel converter for PV system with selected number of levels have been carried out with decoupled current controller based on SRF-PLL and phase-shifted PWM at low switching frequency for a medium voltage and large scale PV direct grid integrated plant. Eliminating step-up transformers from the traditional system for integration with the grid contributes to large cost savings in installation, operation, and maintenance of such a large solar plant. The cost of IGBTs and voltage stress on each switching device are reduced at an optimum level. The low switching frequency employed minimizes the switching losses and lowers the acoustic noise. The converter line voltage THDs for a different number of levels is compared. The improved power quality of the system owing to reduced THDs is observed. The system performance is found satisfactory as per the IEEE standard 519 [17].

## CHAPTER-VI

### CONTROL AND DESIGN OF FORTY-THREE LEVEL CASCADED MULTILEVEL CONVERTER BASED PV SYSTEM

#### 6.1 GENERAL

Megawatt solar plants are the reality now, with nations looking for GW installed capacity. This is possible because of increased power levels in photovoltaic (PV) energy conversion systems. The multilevel converter is the emerging technology for interfacing medium and higher voltage grid. Various topologies of multilevel converters are available, but because of the natural availability of separate DC sources in multi-string large solar plants, a cascaded multilevel converter is most suitable. This chapter presents the design and control of a single-stage, transformerless grid interfaced 43-level CHB cascaded multilevel converter for integrating large solar PV plants with an improved THD (Total Harmonic Distortion) of the grid current. The control scheme comprises VOC (Voltage Oriented Control) with SRF (Synchronous Reference Frame) and PLL (Phase Locked Loop). Fundamental frequency employed for phase-shifted PWM (Pulse Width Modulation) suitable for the cascaded multilevel converter is used for modulation. The incremental conductance MPPT (Maximum Power Point Tracking) algorithm is used to track the solar PV array. The simulation is carried out in MATLAB/Simulink software platform and validated in HIL on OPAL RT simulator. The considered system's steady-state and dynamic performances are evaluated at 1000 W/m<sup>2</sup> and 25°C in this chapter. The THD of converter output voltage and the current waveform are evaluated on MATLAB's FFT tool in this chapter. The selection criteria for the number of levels, system configuration, design, modelling, control, simulation, and results of a 43-level converter are discussed in detail in different sections of this chapter.

## 6.2 SELECTION CRITERIA FOR OPTIMUM NUMBER OF LEVELS

A cascaded connection of low voltage IGBTs for achieving medium voltage helps to develop a low-cost inverter. At the same time, this leads to a linear increase in the component number and control complexity. Hence, to realize an improved performance versus price ratio, finding the optimum value for the number of levels is essential. Usually, the 15-level to 55-level multilevel inverters for 33 kV are considered suitable for feeding the power at the given system voltage [68-72].

Since semiconductor devices' cost is significant for a medium voltage system, a higher DVUF is necessary to make the system design a cost-effective one. The DVUF for a 33kV system with different levels is summarized in Table 6.1 [68].

Table-6.1 DVUF in a 33 kV system for different levels [68]

Number of levels	Rated device voltage (kV)	DVUF (%)
23	4.5	98
29	3.3	96
43	2.5	96
55	1.7	100

In semiconductor devices, the inverter section losses ( $P_{\text{loss\_ivr}}$ ) are the sum of conduction losses ( $P_{\text{c\_ivr}}$ ) and switching losses ( $P_{\text{sw\_ivr}}$ ). The approximated value of  $P_{\text{sw\_ivr}}$  is given as [68]

$$P_{\text{sw\_ivr}} = (AI_{\text{dv}} + BI_{\text{dv}}^2)F_c \quad (6.1)$$

Where  $F_c$  and  $I_{\text{dv}}$  are the carrier frequency and device current, respectively, as one increases the number of levels in a multilevel converter, the carrier frequency reduces; hence, switching losses are reduced. Simultaneously, the active switching device count



increases linearly, resulting in increased conduction losses. For an L-level multilevel converter, the total conduction losses can be approximately given as, [68]

$$P_{c\_ivr} = 6(L-1) (P_{c\_swi} + P_{c\_Dv}) \quad (6.2)$$

$P_{c\_swi}$  and  $P_{c\_Dv}$  are the conduction losses for switching device and antiparallel diode, respectively, of the multilevel converter. Moreover, the device voltage ratings determine an IGBT's on-state voltage drops and diode's forward voltage. For these reasons, total losses in the inverter section are almost constant and, therefore, despite the change in the number of levels, multilevel inverter's efficiency remains practically constant. Thus, the efficiency is not a consideration in the selection of levels while designing multilevel inverter.

Table 6.2 [68] gives the count of THD(%), the cost, ALOs required in a switching section and the count of IGBTs for different levels for a 33kV system to compare the system's

Table-6.2 A 33kV system [68]

<b>Number of levels</b>	<b>23</b>	<b>29</b>	<b>43</b>	<b>55</b>
IGBTs	132	168	252	324
ALOs	121	154	231	297
THD(%)	4.54	4.12	3.28	3.17
Cost (US\$)	301356	233016	150696	100764

performance, cost, and complexity. To enable comparison between a variety of the inverter system based on the cost, performance, and control complexity comprehensively, a normalized index is defined as follows [68],

$$I_{dw} = (w - w_{\min}) / (w_{\max} - w_{\min}) \quad (6.3)$$

Where  $w$  is a scored value and  $w_{\min}$ , and  $w_{\max}$  are the lowest and highest indicators. The normalized index values for 33kV are given in Table 6.3 [68].

Table-6.3 Normalized index for 33kV system [68]

<b>Number of levels</b>	<b>23</b>	<b>29</b>	<b>43</b>	<b>55</b>
Performance	1.00	0.69	0.08	0.00
IGBT Cost (US\$)	1	0.66	0.25	0.00
Complexity	0.00	0.19	0.625	1.00
Total Index	2	1.54	0.955	1

As shown from Table 6.3, for a 33kV inverter, the total index value is lowest for 43-level MLC, so a 43-level MLC is an appropriate choice for a 33kV PV system. Beyond 43-levels of MLC, power quality improvements and the reduction in semiconductor cost are negligible, and it only increases parts (components) count and control complications. Their increase is linear, with an increasing number of levels.

### 6.3 SYSTEM CONFIGURATION

Fig.6.1 shows the system's configuration with a 43-level, 3-phase grid interfaced multilevel converter of power rating of 10MW and 33kV with 50 Hz power frequency

and a switching frequency of 50 Hz. This PV system is connected to the grid through an interfacing inductor for reducing ripple content in the current. As the PV system is designed for medium and higher power ratings, so the SPV system is feeding power to the grid.

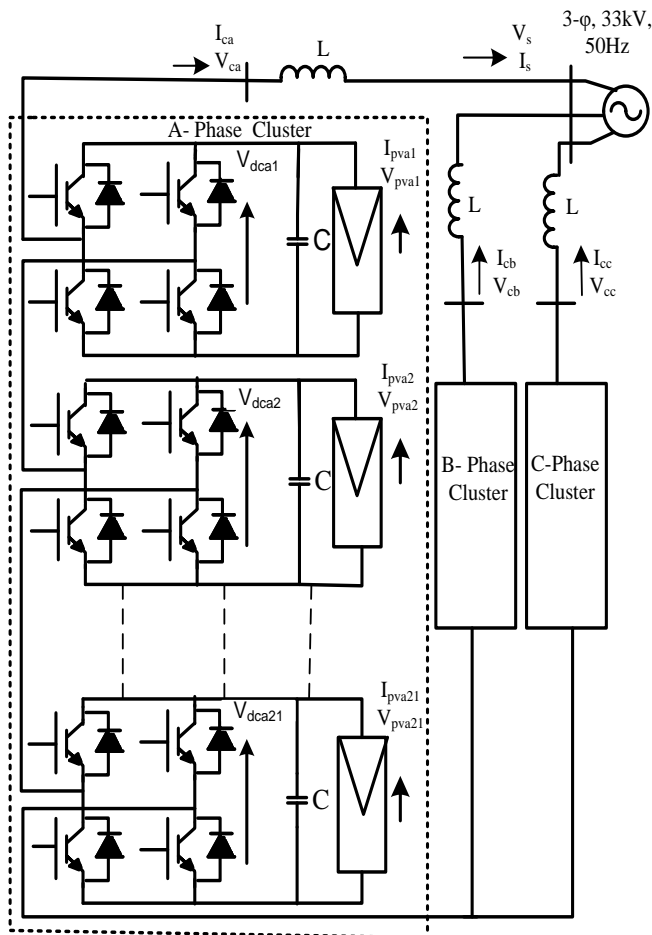


Fig 6.1 43-level grid interfaced CHB multilevel converter

In CHB multilevel converter, the number of H-bridges required is obtained as [10],

$$\text{Number of levels} = (2 * \text{H-bridges per phase} + 1) \quad (6.4)$$

$$\text{H-bridges per phase} = 21$$

So for a 43-level CHB converter, 21 H-bridges are required per phase, and a separate PV array is connected to each H-bridge, which is readily available in a large-scale multi-

string PV system. An incremental conductance MPPT algorithm is used to extract the maximum power of the PV array. The variables measured for implementing the control algorithm are the grid voltages ( $v_{sabc}$ ), the grid currents ( $i_{sabc}$ ), the converter line voltages ( $v_{cabc}$ ), the DC link voltage ( $V_{dc}$ ), PV array voltage ( $V_{pv}$ ), and PV current ( $I_{pv}$ ).

#### **6.4 DESIGN OF 43-LEVEL SYMMETRICAL CASCADED H-BRIDGE MULTILEVEL CONVERTER FOR GRID INTEGRATED PV SYSTEM**

This section of PV system includes the design and modeling of the PV array, DC link capacitor, DC link voltage, and coupling inductor for a 43-level of the multilevel converter. As per the parameter obtained, the PV module is selected from the PV library. Depending on the PV module chosen, the number of series and parallel connected PV modules in a PV array is selected. The other design specifications of the system are given in Table 6.4

##### **6.4.1. Selection of $V_{dc}$ Voltage for 43-Level Converter**

For L-level CHB multilevel converter, the DC-link voltage ( $V_{dc}$ ) for each H-bridge connected to the PV array is calculated as [10],

$$V_{rms} = 0.612*(L-1)*V_{dc} \quad (6.5)$$

$$V_{dc} = 1284V.$$

$V_{dc}$  is taken as 1300V.

##### **6.4.2. Design Calculations and Selection of PV Array for 43-Level Converter**

The required power rating of each PV array for a 43-level CHB converter consisting of 63 PV array (21 per phase) for feeding 10MW power to the grid is calculated as,

$$P_{mmp} = \frac{\text{(power rating of the system)}}{\text{(number of total PV array)}} \quad (6.6)$$

$$=10 \text{ MW} / 63=158.73 \text{ kW}$$

To obtain the PV array of 158.73kW power ( $P_{mmp}$ ) and  $V_{dc}$  of 1300V, an LG Electronics LG295N1C-G3 model is chosen from the PV array library. The numbers of PV modules connected in parallel and series in PV array are selected as,

$$N_s = V_{dc}/V_{mmp} \quad (6.7)$$

$$= 1300/31.8 = 41$$

$$N_p = P_{mmp}/(N_s * I_{mmp} * V_{mmp}) \quad (6.8)$$

$$= 158.73 * 10^3 / (41 * 9.34 * 31.8) = 13$$

#### 6.4.3 Design of DC-Link Capacitor for 43-Level Converter

The DC-link voltage ( $V_{dc}$ ) for each H-bridge connected to the PV array is obtained following the principle of conservation of energy. As per this principle, for  $V_{dc}$  recovery in 5 ms and 1.2 overloading factor a, as [11],

$$\frac{1}{2} * C_{dc} (V_{dc}^2 - V_{dc1}^2) = K_1 * 3 * V * a * I * t \quad (6.9)$$

Where  $K_1$  denotes variation of energy during dynamics, taken as 10% ( $K_1 = 0.1$ ).

Therefore,

$$C_{dc} = (0.1 * 158.73 * 10^3 * 1.2 * 0.005) / (0.5 * (1300 * 1300 - 1284 * 1284))$$

$$C_{dc} = 4700.33 \mu\text{F}.$$

It is selected as,  $C_{dc} (C) = 4700 \mu\text{F}$ .

#### 6.4.4 Design of Interfacing Inductor for 43-Level Converter

A 2.5mH inductor is selected for getting the required result of THD of grid current waveform for 9-level as per IEEE-519 standard for phase shifted PWM modulation. The per unit value of inductor corresponding to 2.5mH is calculated as [13]

$$\begin{aligned}
 L_c(\text{p.u.}) &= (2 * \pi * f * L * P) / V_s^2 \\
 &= (314 * 2.5 \times 10^{-3} * 10 * 10^6) / (33 \times 10^3 * 33 \times 10^3) \\
 &= 0.0072 \text{ p.u.}
 \end{aligned}$$

Table-6.4 Component specifications for 43-level system

Component	Value
Power	10MW
Voltage	33 kV
Frequency	50 Hz
Switching frequency	50 Hz
Inductor ( $L_c$ )	2.5 mH
No of parallel paths in SPV array( $N_p$ )	13
No of series paths in SPV array ( $N_s$ )	41
The voltage of PV module at maximum power ( $V_{mmp}$ )	31.8 V
The current of PV module at maximum power ( $I_{mmp}$ )	9.34 A
Open circuit voltage of PV module ( $V_{oc}$ )	39.3 V
Short circuit current of PV module ( $I_{sc}$ )	9.94 A
DC link capacitance ( $C_{dc}$ )	4700 $\mu$ F
DC link voltage( $V_{dc}$ )	1300 V

## 6.5 CONTROL OF 43-LEVEL SYMMETRICAL CASCADED H-BRIDGE MULTILEVEL CONVERTER FOR GRID INTEGRATED PV SYSTEM

Fig. 6.2 shows the control scheme for the 43-level MLC based three-phase AC grid integrated SPV system. An incremental conductance algorithm is used for tracking maximum power from the PV array, as shown in Fig. 6.3. A voltage-oriented control with a feed-forward term, the controller for DC-link capacitor, SRF, and PLL for synchronization with the grid, controls the VSC [115-116].

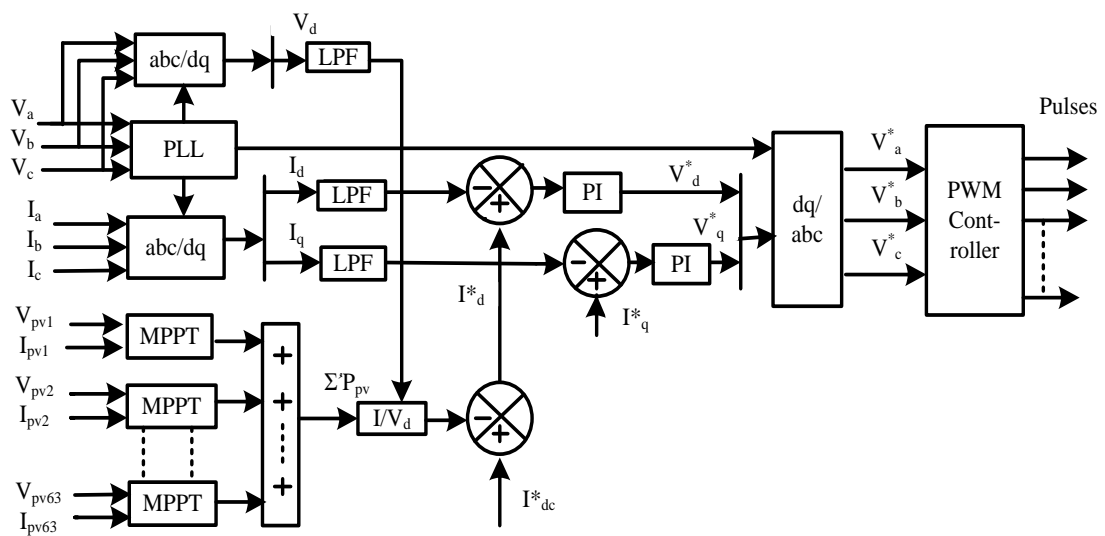


Fig.6.2 Control algorithm for 43-level CHB multilevel converter

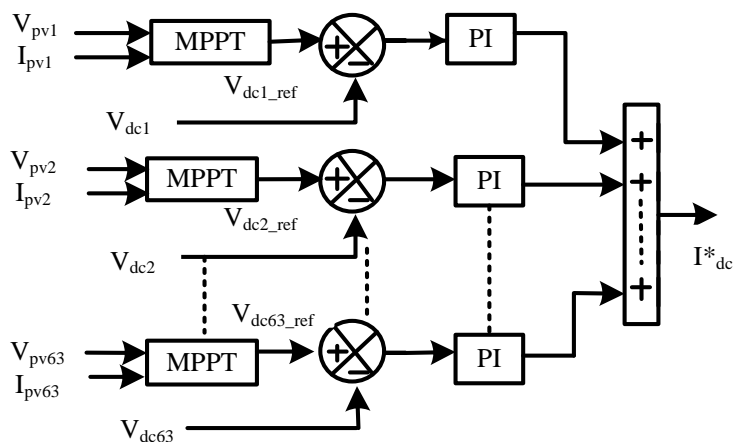


Fig.6.3 Control algorithm for generating  $I_{dc}^*$  for 43-level CHB multilevel converter

### 6.5.1 Implementation of Incremental Conductance Algorithm

In this InC algorithm, the change in maximum power output and voltage for PV array is given as [60-61],

$$\frac{dp_{pv}}{dv_{pv}} = \frac{di_{pv}v_{pv}}{dv_{pv}} = i_{pv} + v_{pv} \frac{di_{pv}}{dv_{pv}} = i_{pv} + v_{pv} \frac{\Delta i_{pv}}{\Delta v_{pv}} \quad (6.10)$$

Using above equations, the solution for MPPT is given as,

maximum power point,  $\frac{dp_{pv}}{dv_{pv}} = 0$

$$\frac{\Delta i_{pv}}{\Delta v_{pv}} = - \frac{i_{pv}}{v_{pv}} \text{ at MPP} \quad (6.11)$$

$$\frac{\Delta i_{pv}}{\Delta v_{pv}} > - \frac{i_{pv}}{v_{pv}} \text{ on left side of MPP, and} \quad (6.12)$$

$$\frac{\Delta i_{pv}}{\Delta v_{pv}} < - \frac{i_{pv}}{v_{pv}} \text{ on right side of MPP} \quad (6.13)$$

Thus, for tracking MPPT incremental conductance  $\Delta i_{pv}/\Delta v_{pv}$  and instantaneous conductance  $i_{pv}/v_{pv}$  is compared.

### 6.5.2 VSC Control Algorithm

The control scheme used in this work is shown in Figure 6.2. The voltage oriented control is used to regulate interactions between the CHB and the grid. It is based on the transformation of three-phase co-ordinates to a grid voltage oriented synchronous frame. The outer control loop determines the reference for the overall active power (P) required for controlling the system. In this voltage loop, the voltage obtained from each DC-link measurement is compared with reference voltage  $V_{dc\_ref}$  received from each MPPT algorithm, as shown in Figure 6.3.

The controller gives the value of  $I_d^*$ , which is the reference DC-link current for the active



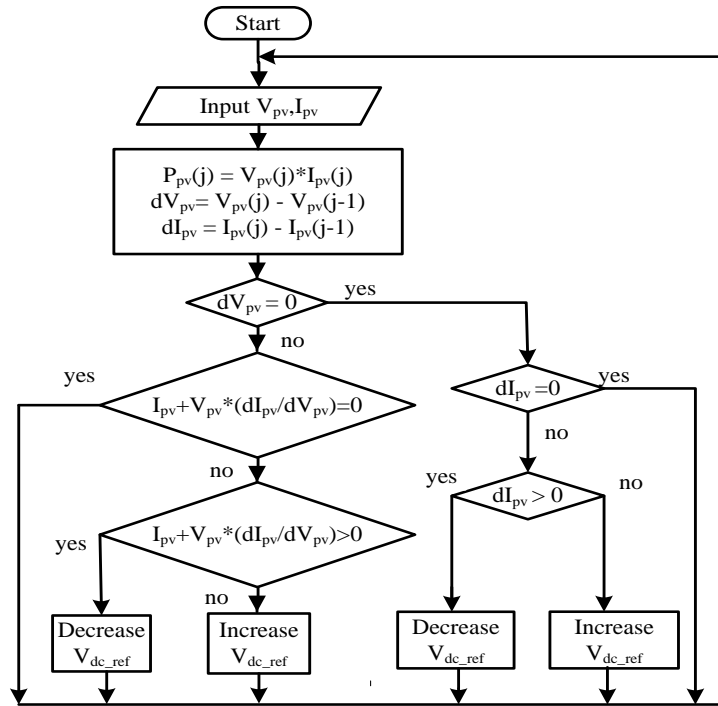


Fig.6.4 Flowchart for incremental conductance algorithm

power control of the system expressed at  $j$  and  $(j-1)$  instant as,

$$I_d^*(j) = I_d^*(j-1) + K_p \{V_e(j) - V_e(j-1)\} + K_i * V_e(j) \quad (6.14)$$

Where  $K_p$  &  $K_i$  are proportional and integral gain constants for the controller. The direct current component ( $I_d^*$ ) is obtained by Park's transformation. Three-phase PLL is used to find the grid voltage angle ( $\theta$ ) for Park's transformation.

Similarly, the direct ( $V_d$ ) component of the grid voltage is calculated using the Park's transformation. The sum of all  $I_d^*$ , along with the feed-forward term, is compared with the  $I_d$ . Quadrature currents,  $I_q^*$  (set zero for unity power factor), and  $I_q$  are compared where the ' $I_q^*$ ' component represents the reference quantity, and the component  $I_q$  is obtained from Park's transformation. The reference direct-axis and quadrature-axis voltages calculations are as follows.

$$V_d^*(j) = V_d^*(j-1) + K_{p2} \{I_{de}(j) - I_{de}(j-1)\} + K_{i2} * I_{de}(j) \quad (6.15)$$

$$V_q^*(j) = V_q^*(j-1) + K_{p3} \{ I_{qe}(j) - I_{qe}(j-1) \} + K_{i3} * I_{qe}(j) \quad (6.16)$$

$K_{p2}$ ,  $K_{i2}$ ,  $K_{p3}$ , and  $K_{i3}$  are the respective proportional and integral gains of the direct axis current controller and quadrature axis current controller. The inverse Park's transformation is used for getting reference voltage for the PWM controller.

### 6.5.3 Phase Shifted Multi-Carrier PWM Control for 43- Level MLC

The modulation of 43-level MLC is realised using phase-shifted PWM [10,129-133], in which, for 43-level (L) converters, 42 (i.e. (L-1)), carrier signals are displaced by  $8.57^\circ$  (i.e.  $360^\circ / (L-1)$ ), each carrier is compared with  $V_{ref}$  signal, respectively [10].

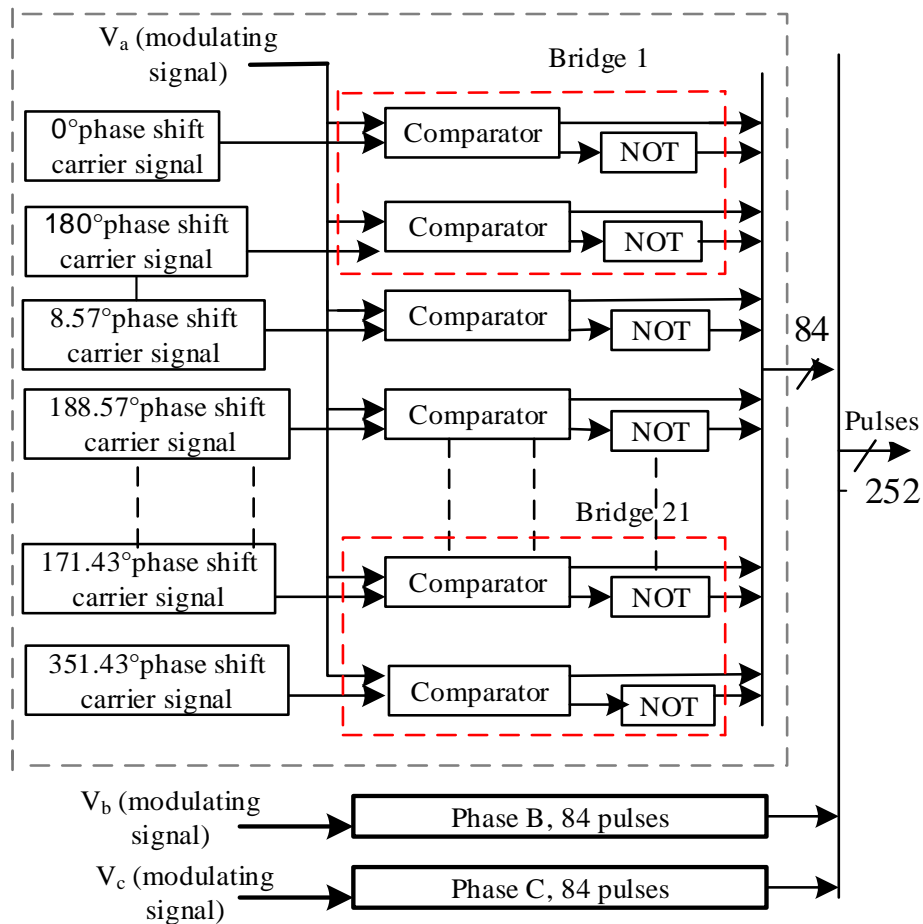


Fig.6.5 Scheme for the generation of PWM signals for 43-level CHB multilevel converter

## **6.6 MODELLING OF 43-LEVEL SYMMETRICAL CASCADED H-BRIDGE MULTILEVEL CONVERTER FOR GRID INTEGRATED PV SYSTEM**

This section presents the MATLAB based modelling of a 43-level CHB multilevel converter for grid interfaced SPV system. MATLAB R2015a is used for simulation. MATLAB modeling of the grid-connected converter, PV array fed 43-level CHB multilevel converter for phase A (remaining phase modeling is similar as phase A) is done. MATLAB models for MPPT block, control algorithm, and phase-shifted sinusoidal PWM are also developed. MATLAB model is implemented by selecting a block from both Simulink and Simscape SimPowerSystems specialized technology library of MATLAB.

### **6.6.1 Model of Grid Connected Converter**

The developed MATLAB model of grid-connected multilevel converter for the three-phase system is shown in Fig. 6.6. The grid voltages ( $v_{sabc}$ ), grid currents ( $i_{sabc}$ ), converter voltages ( $v_{cabc}$ ), and converter currents ( $i_{cabc}$ ) are measured from three-phase VI-measurement. A three-phase source block of rating 33 kV is chosen from the same library for the grid. Discrete Powergui environmental block is selected from Simscape SimPowerSystems specialized technology library. The sampling time is set at 5e-06 seconds.

### **6.6.2 Model of PV Array Connected 43-Level H-Bridge Converter**

For developing a model of a 43-level converter, 21 H-bridges are connected in a cascade. Each PV array feeds a separate H-bridge, as shown in Fig. 6.7. In the figure, only one PV array with a single H-bridge is shown. For a 43-level VSC, 21 modules per phase are connected in cascade. For this photovoltaic system, the insolation level is taken as

1000W/m<sup>2</sup> and given through a limiter block, and temperature of 25°C is provided through a saturation

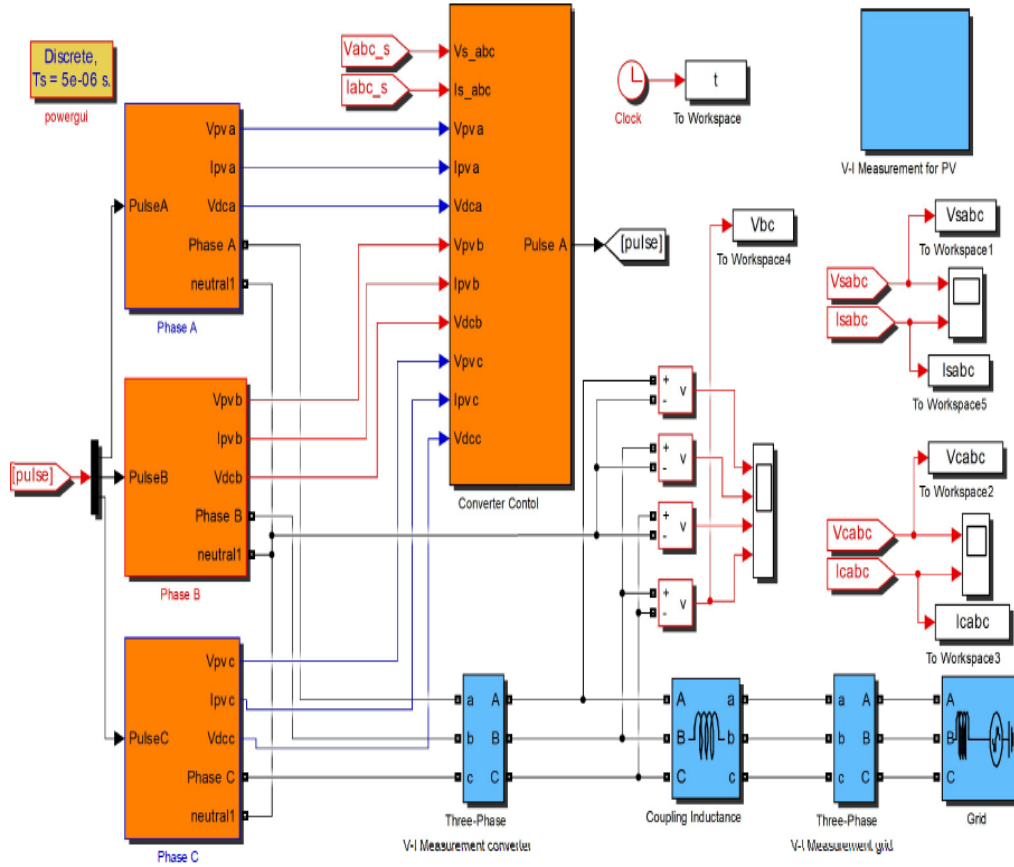


Fig. 6.6 MATLAB model of grid interfaced 43-level CHB multilevel converter

block, selected from the Simulink library. An LG Electronics LG295N1C-G3 PV module is selected from simscape simpowersystems specialized technology PV array library. The photovoltaic voltage and current of array1 ( $V_{a1\_PV}$  &  $I_{a1\_PV}$ ), array2 ( $V_{a2\_PV}$  &  $I_{a2\_PV}$ ),....., array 20 ( $V_{a20\_PV}$  &  $I_{a20\_PV}$ ) and array 21 ( $V_{a21\_PV}$  &  $I_{a21\_PV}$ ) are measured for MPPT.  $V_{dc1}$ ,  $V_{dc2}$ ,.....,  $V_{dc20}$  and  $V_{dc21}$  are the DC-link voltages across the respective DC link capacitors, measured to control the DC-link.

### 6.6.3 Model of Control Algorithm

Fig.6.8 shows the developed model of control algorithm for VSC control. To implement the decoupled current scheme, the abc to dq0 transformation block and PLL block are selected from simpower systems specialized technology library. The reference direct current obtained from the

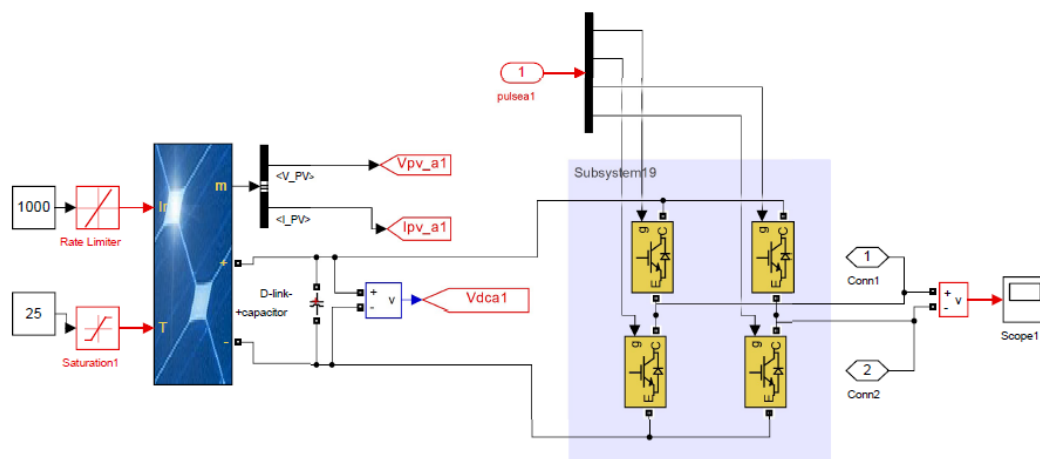


Fig.6.7 MATLAB model of Single PV array with H-bridge

MPPT block and the feed-forward term are compared by a comparator block selected from Simulink library with direct current  $I_d$  and error signal given to PI- controller. Similarly, the quadrature-component of current is compared with zero reference (unity pf), and error voltage is passed through PI- controller with a saturation limit fixed at the output. The reference dq-component of voltages so obtained are transformed to  $V_{abc}^*$  (modulation signal) by a dq0 to abc transformation block and given to the PWM block. The synchronous signal ( $\omega t$ ) is provided by the PLL to abc to dq0 and dq0 to abc transformation.

#### **6.6.4 Model of MPPT Controller**

The model of each PV array is provided with a separate MPPT algorithm controlled by a separate PI-controller, as shown in Fig.6.9. For a 43-level VSC, a total of 21 independent MPPTs are connected in cascade, whose output is added to give the  $V_{dc\_ref}$ . The MPPT algorithm is implemented by writing the algorithm on a user-defined block of Simulink library for obtaining the  $V_{dc\_ref}$ . Param block gives the upper and lower limit of  $V_{dc\_ref}$  and increment step for implementing the algorithm.

#### **6.6.5 Model of Phase-shifted PWM**

A set of 42 carrier signal of 50 Hz switching frequency is generated by selecting a triangle generator block from simpowersystems specialized technology control and signal generation library for implementing the phase-shifted PWM. The triangle generator block generates a symmetrical triangle waveform with a peak amplitude of +/-1 for implementing carrier signal. The phase shift between the two carrier signals is kept at  $8.57^\circ$ . These carrier signals are compared with the modulating signal, as shown in Fig. 6.10, and 84 pulses are generated. In the figure, pulse generation for the single H-bridge is shown for phase A. The remaining 20 H-bridge pulses of phase A are generated in similar way. Comparator and NOT-gate block are selected from the Simulink library for the generation of pulses.

### **6.7. RESULTS AND DISCUSSION**

A 43-level CHB MLC for 33 kV grid interfaced photovoltaic system is modelled and analysed in a MATLAB environment and its performance is validated in HIL on OPAL RT simulator, and the following results are obtained.

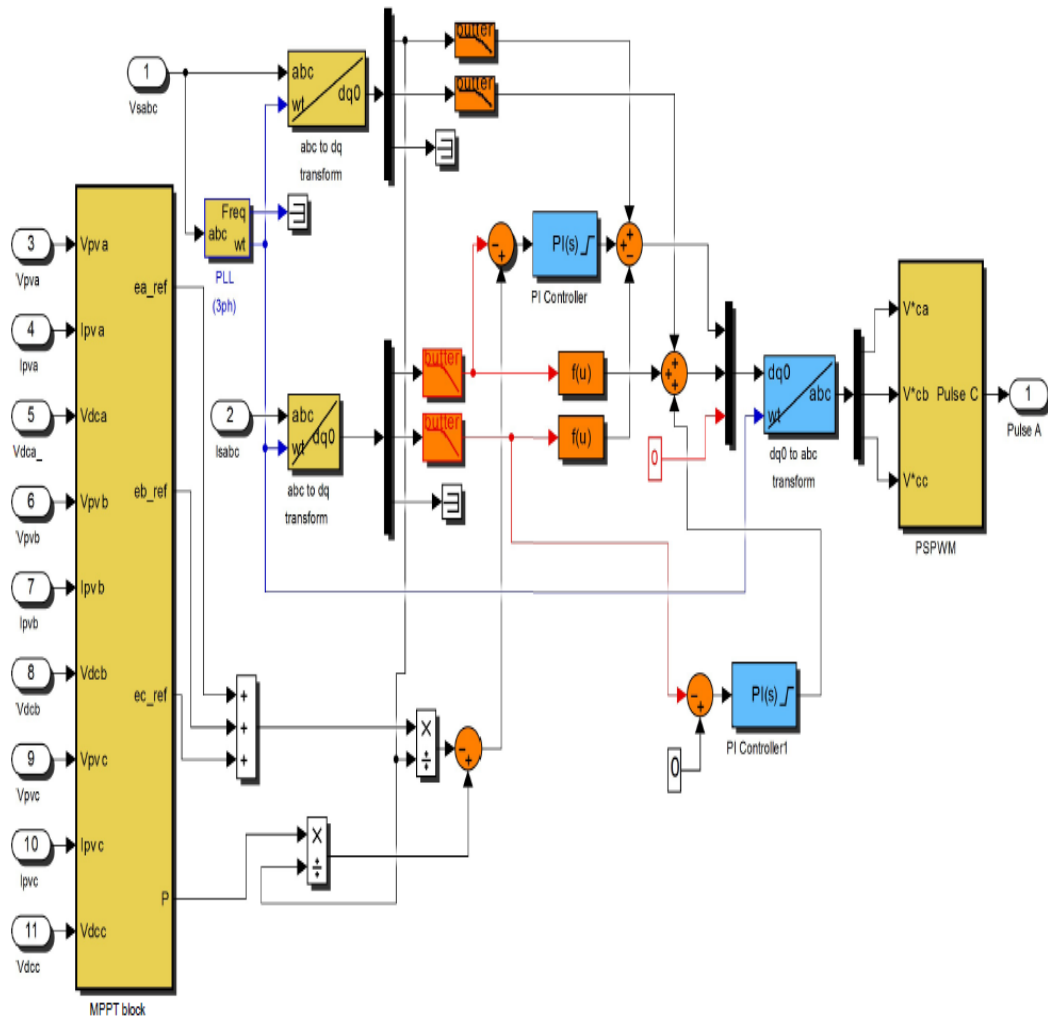


Fig.6.8 MATLAB model of Control algorithm of 43-level CHB multilevel converter

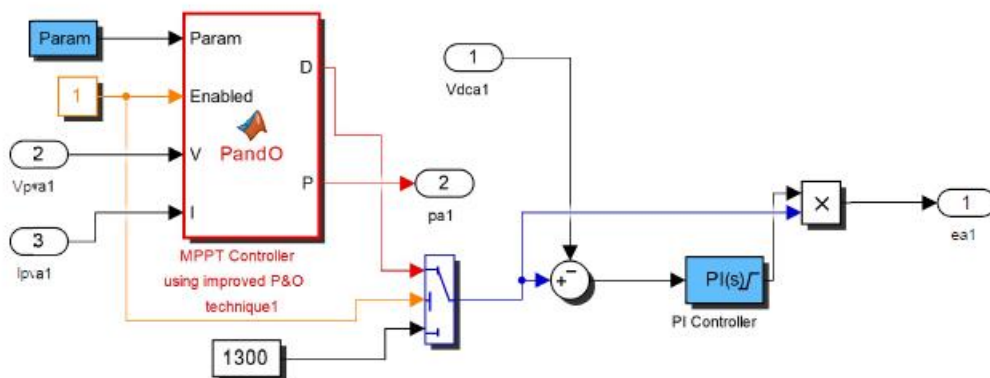


Fig.6.9 Single module of separate MPPT algorithm with PI controller.

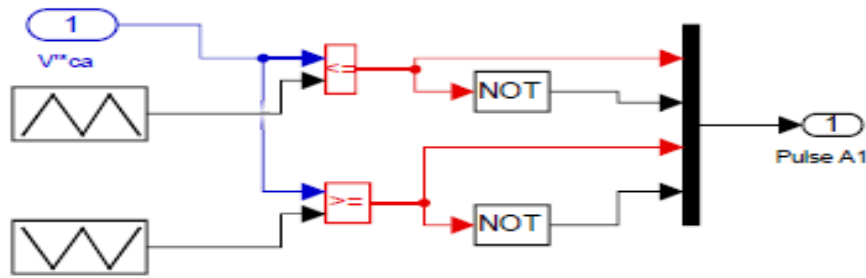


Fig.6.10 Pulse generation of single H-bridge

### 6.7.1 Steady-State Performances for 43-Level Converter

The system's steady-state response is studied at insolation level of  $1000 \text{ W/m}^2$  and temperature of  $25^\circ\text{C}$  and the results are depicted in Fig. 6.11. Simulated results consisting of the grid voltages ( $v_{sabc}$ ), the grid currents ( $i_{sabc}$ ), the AC line voltages of VSC ( $v_{cab}$ ), SPV voltage ( $V_{pv}$ ), SPV current ( $I_{pv}$ ), and power (P) are obtained to validate the system performance. As the grid voltage and the grid current are in phase in steady-state response; hence, the maximum active power transfer is evident at a unity power factor.

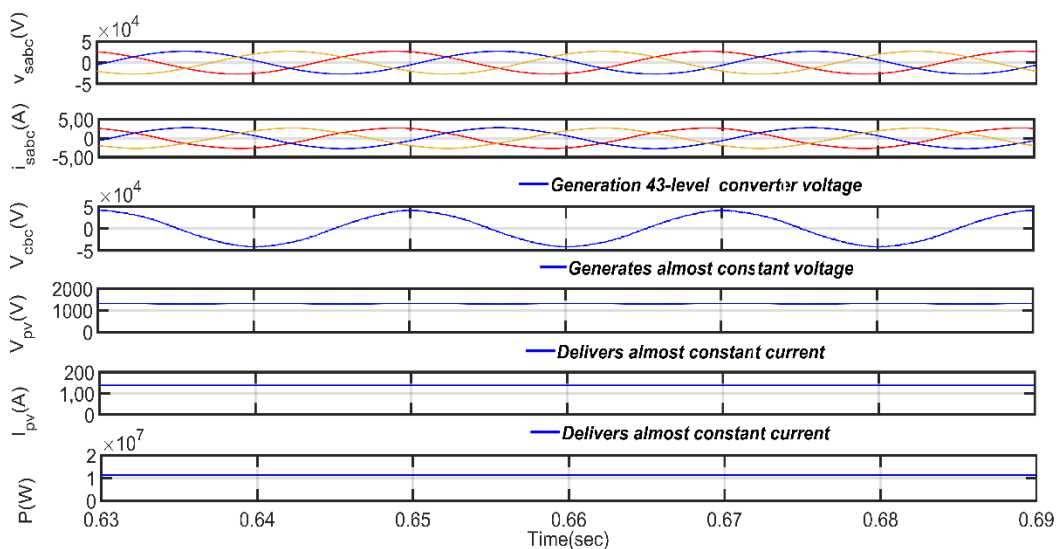
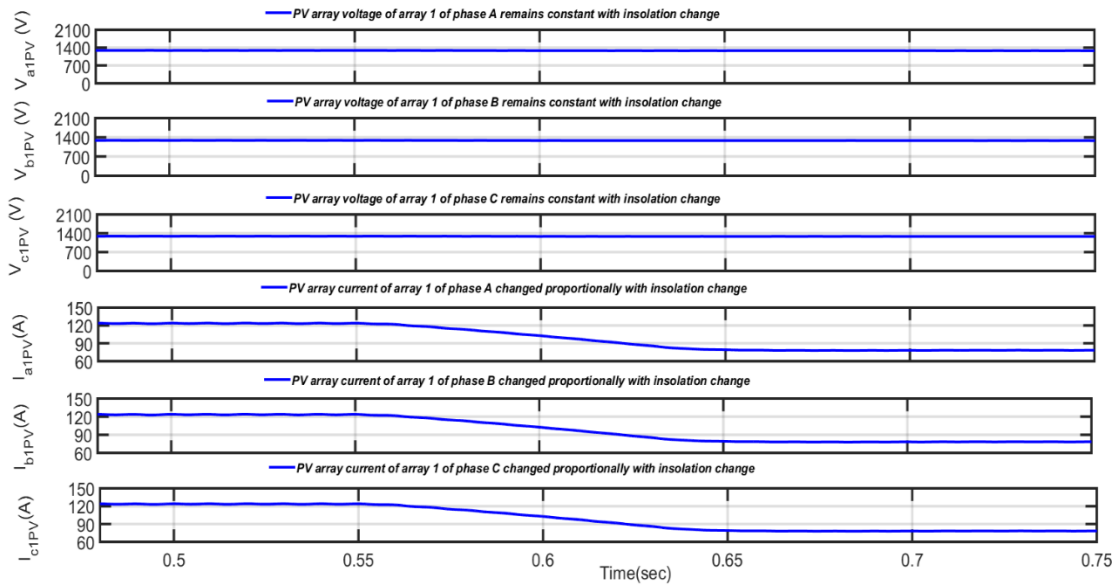


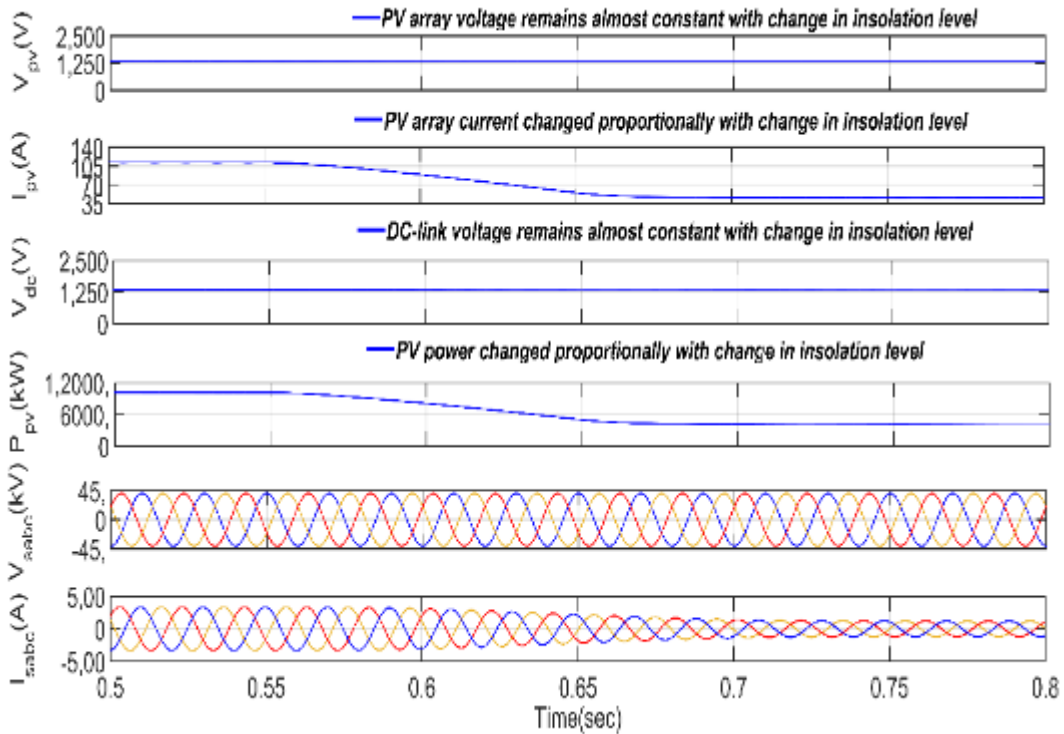
Figure 6.11 System steady-state performance at constant insolation level  $1000 \text{ W/m}^2$



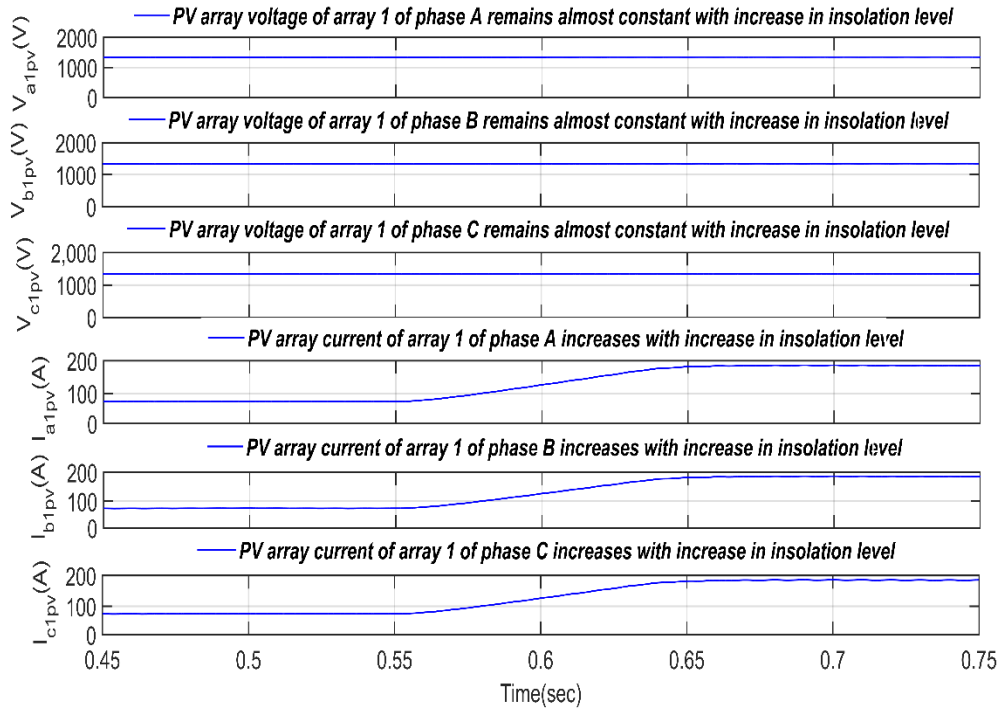
PV array generates almost constant voltage and delivers almost constant current and power as shown in figure.6.7.2 Dynamic Performances for 43-Level Converter as shown in Figs. 6.12 (a) and (b), the dynamic response is studied with a constant temperature of 25°C and an insolation change from 1000 W/m<sup>2</sup> to 400 W/m<sup>2</sup> at 0.55s.



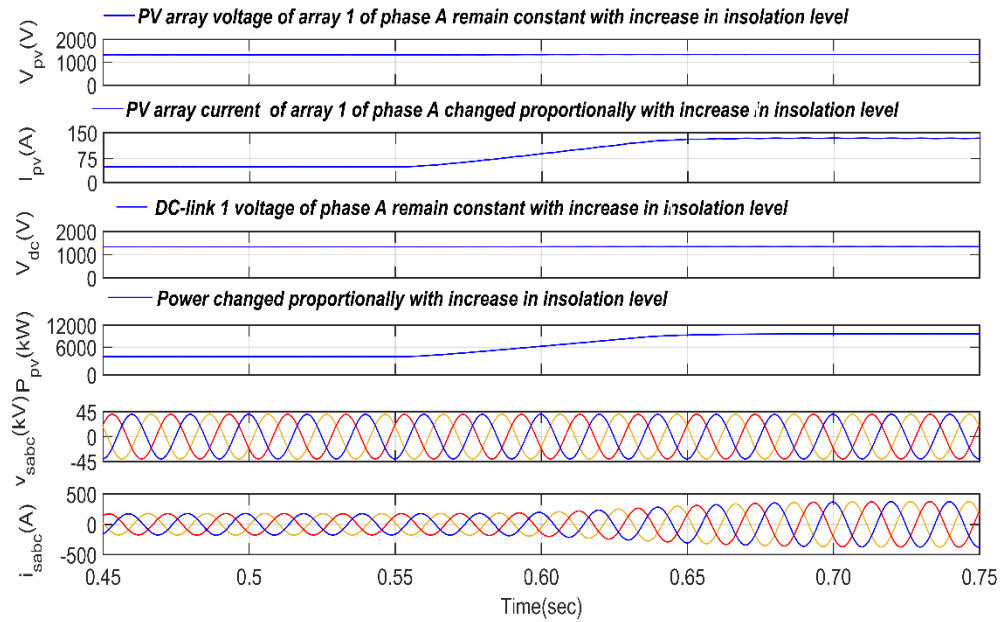
(a)



(b)



(c)



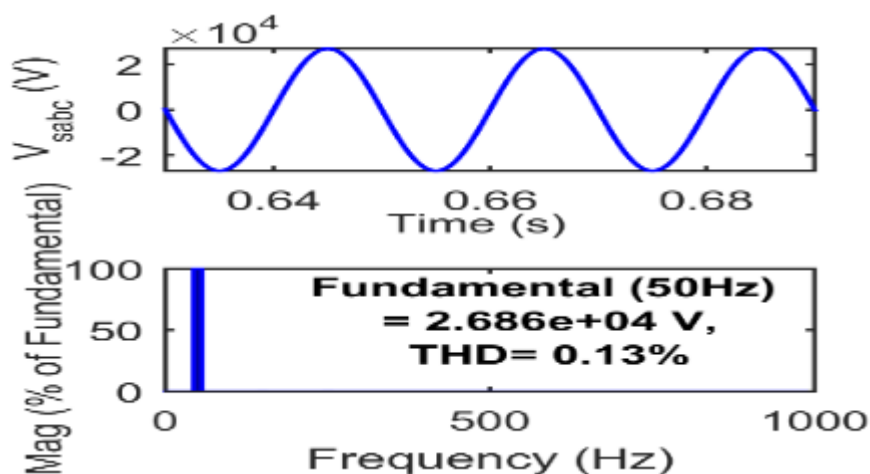
(d)

Figure 6.12 (a) and (b) System response to an insolation change from 1000 W/m<sup>2</sup> to 400 W/m<sup>2</sup> at 0.55 sec for 43-level CHB multilevel converter, (c) and (d) System response to an insolation change from 400 W/m<sup>2</sup> to 1000 W/m<sup>2</sup> at 0.55 sec for 43-level CHB multilevel converter

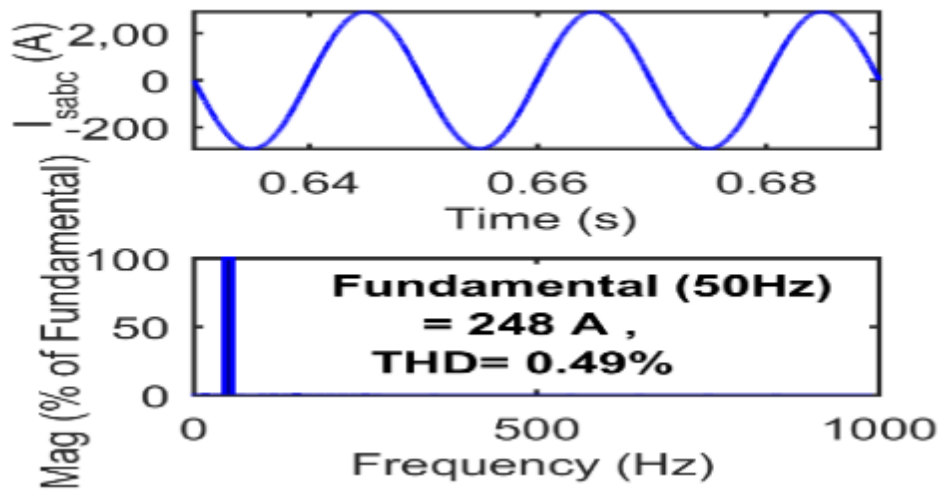
Whereas Fig. 6.12 (c) and (d) show the system response to increase in insolation from  $400 \text{ W/m}^2$  to  $1000 \text{ W/m}^2$  at 0.55 sec. Simulated results consist of the voltage & the current for a PV array 1 of A-phase ( $V_{a1pv}$  &  $I_{a1pv}$ ), B- phase ( $V_{b1pv}$  &  $I_{b1pv}$ ), C- phase ( $V_{c1pv}$  &  $I_{c1pv}$ ). In dynamic response, with the decrease of the insolation level, the remarkable change in PV current's is observed, while there is no significant change seen in the PV voltage. The PV voltage and the changes in PV current are same for three phase array 1 which verifies that the distributed MPPT control of each array is achieved as shown in Fig. 6.12 (a). The grid current, PV power and PV current are changed proportionally and PV voltage and grid voltage remain constant with change in insolation level as shown in Fig. 6.12 (b).

### 6.7.3. Power Quality Performances for 43-Level Converter

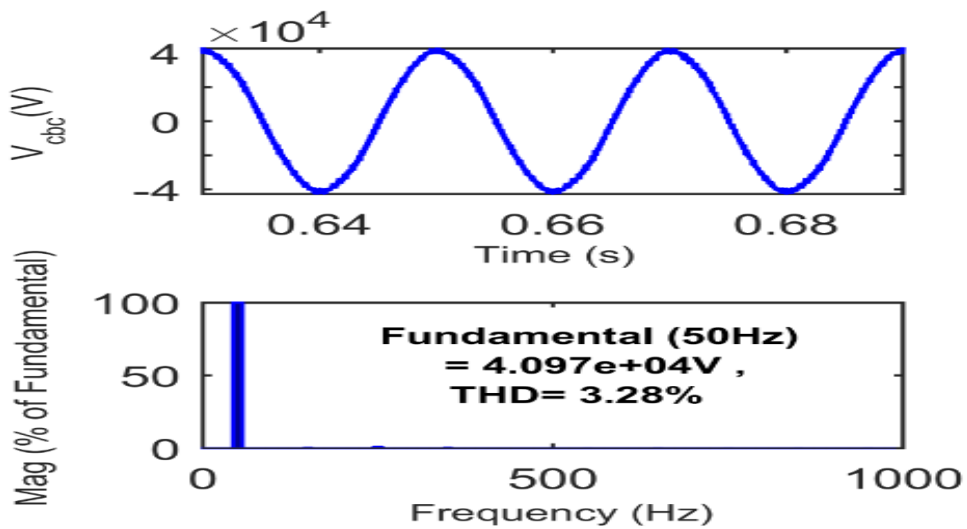
Figure 6.13 shows waveforms of grid voltage ( $v_{sabc}$ ), grid current ( $i_{sabc}$ ), and converter line voltage ( $v_{cbc}$ ) and harmonic spectrum along with the THD levels at isolation level of  $1000 \text{ W/m}^2$  and a temperature of  $25^\circ \text{ C}$  by using fast Fourier transform tool in MATLAB.



(a)



(b)



(c)

Fig.6.13: Waveforms and harmonic spectra of 43-level and 33 kV system (a) line voltage ( $V_{sabc}$ ) (b) line current ( $I_{sabc}$ ) (c) converter side voltage( $V_{cbc}$ ) at  $1000 \text{ W/m}^2$  and  $25^\circ\text{C}$

The observed THD values are presented in Table 6.5. The supply current THD is well within limits set by the IEEE-519 standard with reduced size of filter [17]. The power factor is observed near to unity.

Table-6.5 THD Values (%) at the insolation level of 1000 W/m<sup>2</sup> and ambient temperature 25°C

Quantity	% THD Values
Grid voltage	0.13
Grid current	0.49
Converter line voltage	3.28

#### 6.7.4 Validation of Results in HIL On OPAL-RT Simulator

Real time results of the 43 level MLC are obtained in HIL on OPAL-RT simulator as per the details given in appendix. Both the steady state and dynamic responses are obtained in real time. Fig. 6.14 to Fig. 6.17 show the steady state performance of the system at 1000W/m<sup>2</sup> and 25°C. Fig. 6.14 and Fig. 6.15 show the PV array1 voltage of phase A ( $V_{pv}$ ), PV array1 current of phase A ( $I_{pv}$ ), phase A converter voltage ( $v_{ca}$ ), phase A grid voltage ( $v_{sa}$ ) and phase A, B and C grid currents ( $i_{sa}$ ,  $i_{sb}$  and  $i_{sc}$ ). Fig. 6.16 gives the zoomed view of Fig.6.15. Fig.6.17 gives the 120°displaced phase A, B and C converter voltages ( $v_{ca}$ ,  $v_{cb}$  and  $v_{cc}$ ). Fig.6.18 to Fig. 6.22 show the dynamic performance of the system with an increase, and a decrease and both increase and decrease in irradiance at 25°C. Fig. 6.18 to Fig. 6.22 show the change in  $V_{pv}$ ,  $I_{pv}$ ,  $i_{sa}$ ,  $v_{sa}$  and converter voltage with the change in irradiance,  $V_{pv}$ ,  $v_{sa}$  remains constant and  $I_{pv}$ ,  $i_{sa}$  changes with the change in irradiance. Fig. 6.21 and 6.22 show the variation of phase A, B and C of grid currents with decrease and increase in irradiance respectively. Fig. 6.23, 6.24 and 6.25 give THD

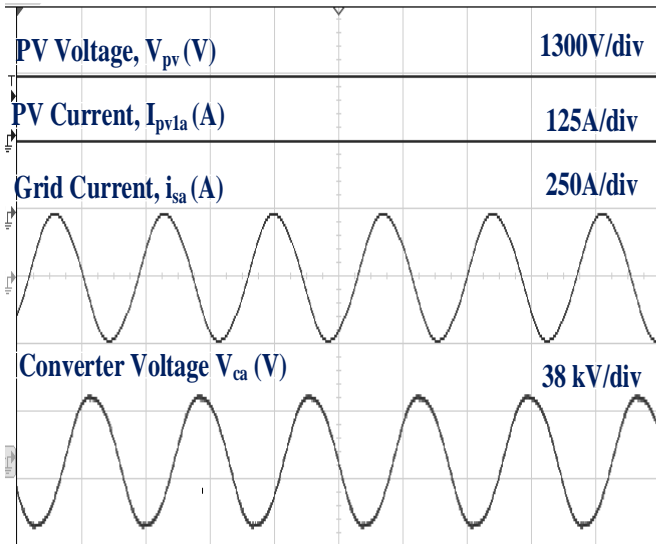


Fig.6.14 Steady state performance of  $V_{pv}$ ,  $I_{pv}$ ,  $i_{sa}$ ,  $V_{ca}$  at 25°C and 1000W/m²

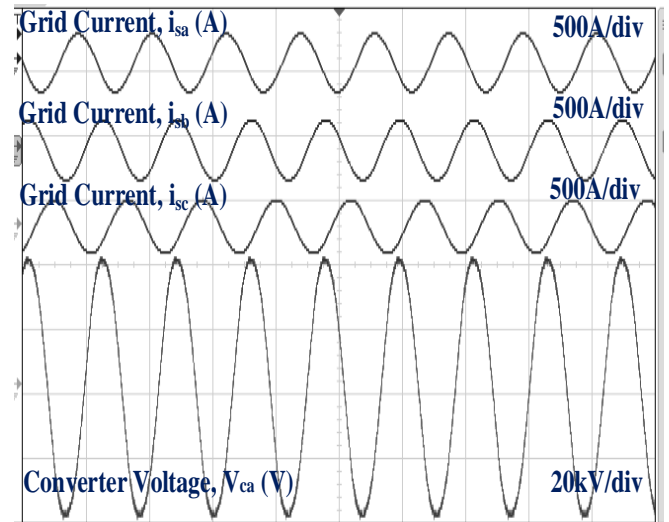


Fig. 6.15 Steady state performance of  $i_{sa}$ ,  $i_{sb}$ ,  $i_{sc}$  and Converter voltage at 25°C and 1000W/m²

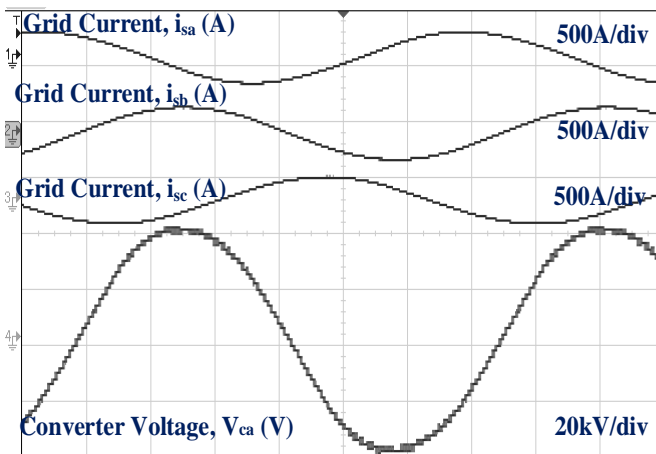


Fig 6.16. Zoomed view of Fig. 2

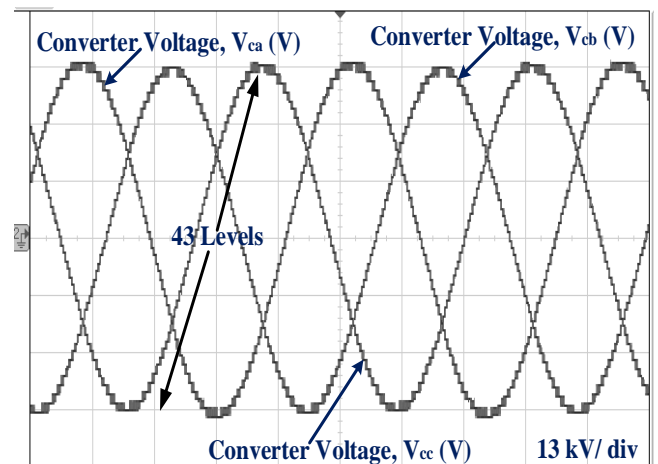


Fig.6.17 Three phase converter voltage at 25°C and 1000W/m²

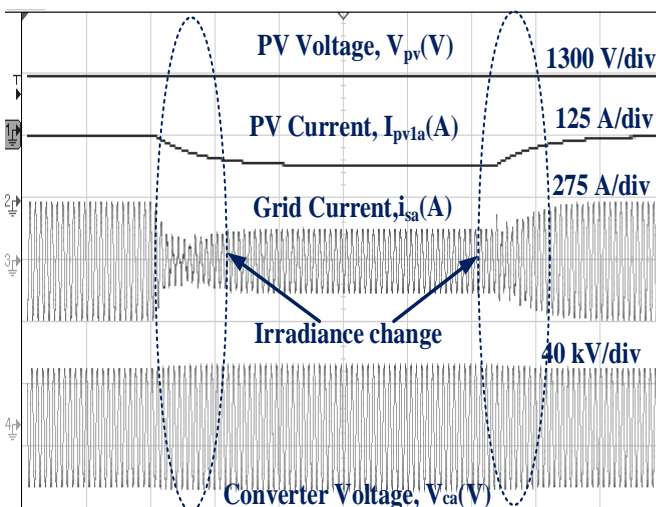


Fig. 6.18 Dynamic performance of  $V_{pv}$ ,  $I_{pv}$ ,  $i_{sa}$  and converter voltage at irradiance change from 1000W/m² to 500 W/m², and 500W/m² to 1000W/m² and 25°C

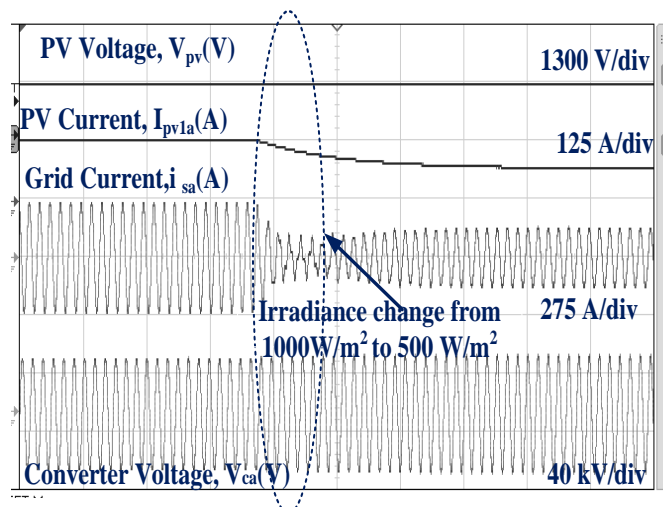


Fig. 6.19 Dynamic performance of  $V_{pv}$ ,  $I_{pv}$ ,  $i_{sa}$  and converter voltage change from 1000W/m² to 500 W/m² and 25°C

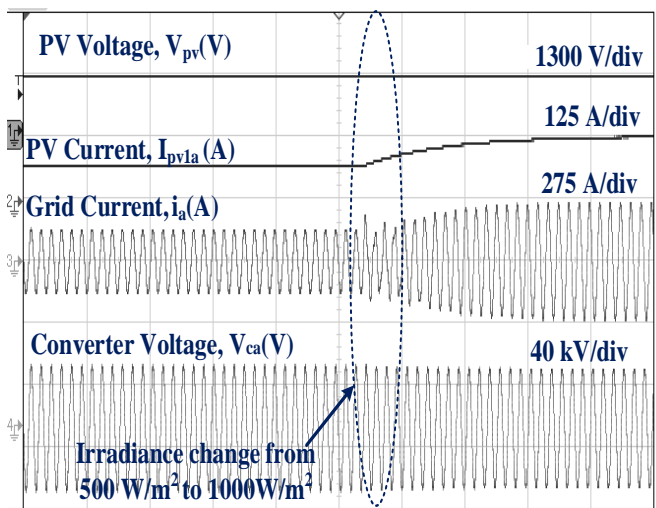


Fig. 6.20 Dynamic performance of  $V_{pv}$ ,  $I_{pv}$ ,  $i_{sa}$  and converter voltage irradiance at irradiance change from 500W/m<sup>2</sup> to 1000 W/m<sup>2</sup> and 25°C

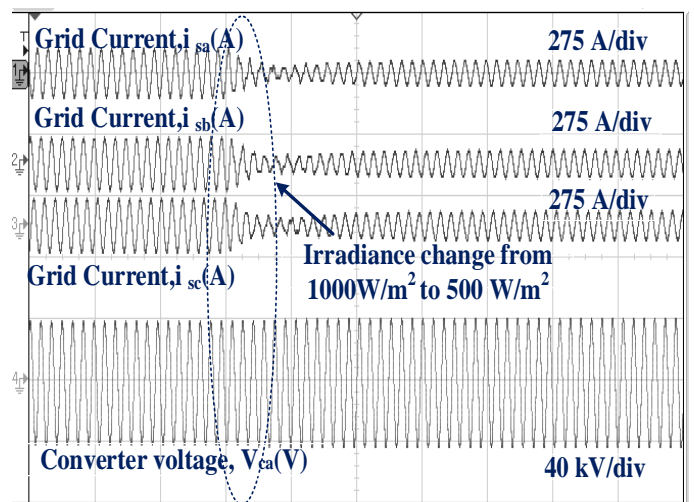


Fig.6.21 Dynamic performance of  $i_{sa}$ ,  $i_{sb}$  and  $i_{sc}$  at change from 1000W/m<sup>2</sup> to 500 W/m<sup>2</sup> and 25°C

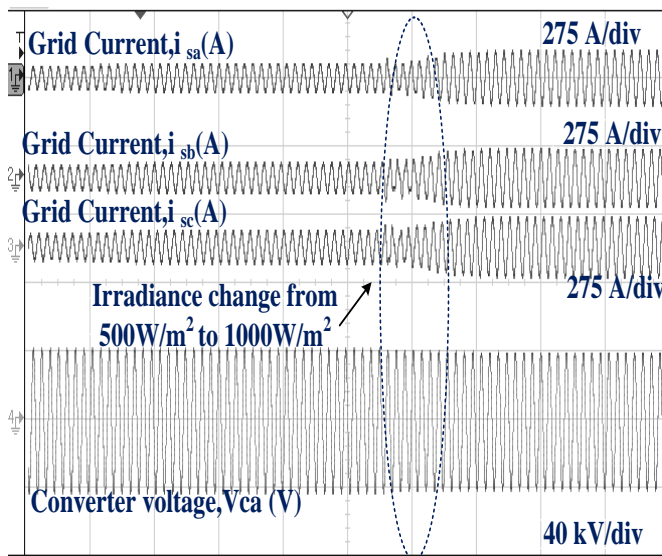


Fig.6.22 Dynamic performance of  $i_{sa}$ ,  $i_{sb}$  and  $i_{sc}$  at irradiance change from 500W/m<sup>2</sup> to 1000 W/m<sup>2</sup> and 25°C

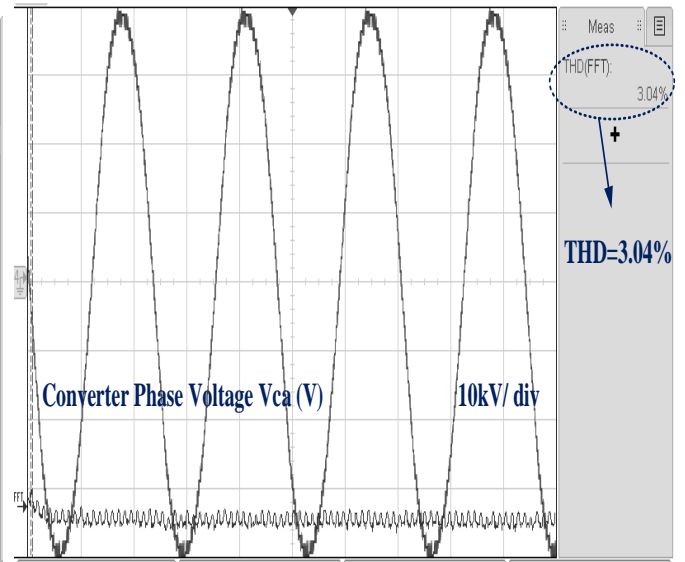


Fig. 6.23 Converter phase voltage THD

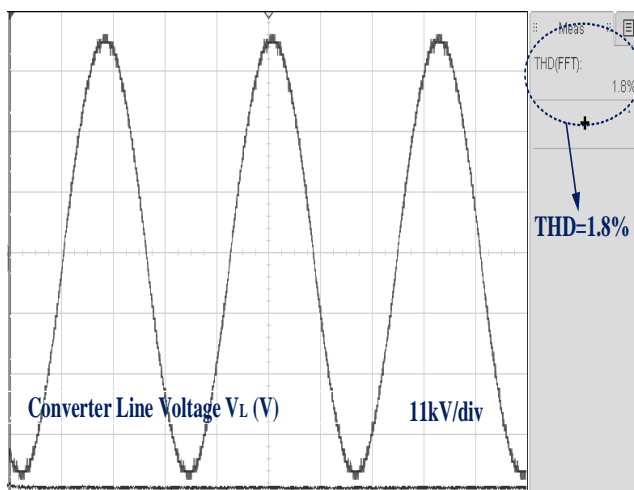


Fig. 6.24 Converter line voltage THD

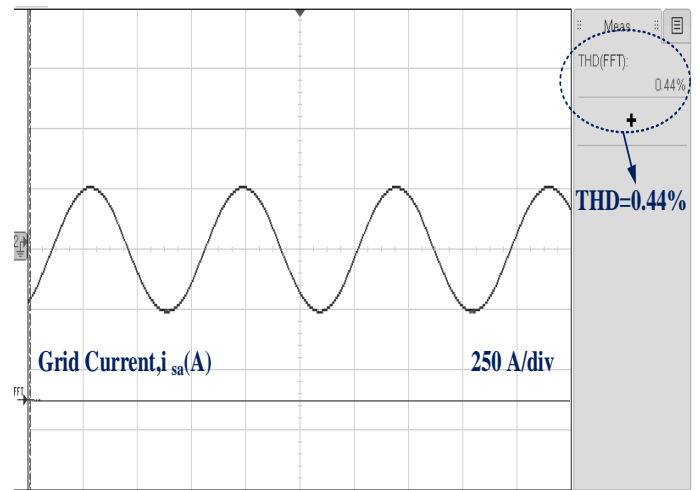


Fig. 6.25 Grid current THD

results, THD of converter phase voltage, converter line voltage and grid current are 3.04%, 1.8% and 0.44% respectively.

## **6.8 CONCLUSIONS**

The modelling and design of medium voltage grid interfaced CHB multilevel converter for a 10MW multi-string photovoltaic system with the selected number of levels have been carried out with voltage-oriented control based on SRF-PLL and phase-shifted PWM at the low switching frequency. The cost of IGBTs and voltage stress on each switching device are reduced with an optimum number of levels. The use of low switching frequency leads to reduced switching losses and lowers the acoustic noise. The system's improved power quality due to reduced THDs of supply current is observed. The elimination of step-up transformer from the conventional system for integration with the grid contributes appreciable savings in the CapEx (capital expenditure) and O&M (operation and maintenance) cost of such large solar plants. The system's performance is found to be satisfactory as per the IEEE standard 519 [17].



## CHAPTER-VII

### COMPARATIVE STUDY OF DIFFERENT CONVERTERS

#### 7.1 GENERAL

This chapter presents a comparative study of the output voltage waveform of different symmetrical CHB multilevel converter based on the number of levels and modulation techniques employed for modulation. Multilevel converters have the advantage of low total harmonic distortion (THD) of output voltage, and selecting a suitable modulation technique further improves its THD. This chapter compares the results of different modulation techniques such as phase-shifted multicarrier pulse width modulation (PWM), selected harmonic elimination (SHE), and nearest level modulation (NLM) employed for symmetric cascaded H-bridge (CHB) multilevel converter for THD and switching frequency. The implementation of these modulation techniques for a nine-level CHB multilevel converter is already given in chapter 4.

With an increase in the number of steps (corresponding to the number of levels achieved) in the AC voltage output waveform in the multilevel converter, the THD in the output grid current waveform is improved. This chapter also compares the result of the CHB multilevel converter for the different number of levels, 7-level, 9-level, 19-level, and 43-level, to study the effect of an increased number of levels on the multilevel converter. The graphical results of the comparison of number of levels and PWM technique are also given. The design, modelling, control, and MATLAB based simulation modelling of the grid-tied CHB multilevel converter for photovoltaic application with 7-level, 9-level, 19-level, and 43-level converters have already been mentioned in the previous chapters.

This chapter gives in its various sections, the comparison based on the number of levels used, comparison on modulation technique employed, results, and conclusion.

## **7.2 COMPARISON OF CONVERTERS FOR DIFFERENT LEVELS**

The selection of the optimum number of levels for a given voltage rating in a multilevel converter is a necessary consideration for designing the multilevel converter.

With the increase in the number of levels in a multilevel converter, each device's voltage stress is reduced for a given voltage rating. The multilevel converter is used for medium or high voltage applications, so the reduction in voltage stress on switching devices is remarkable.

A low voltage rating device is more matured in construction and readily available in the market at a low cost. Using more cascade devices for getting the required voltage rating increases the scalability and, hence, the system's reliability. The multilevel converter can operate even in case of a fault in a single unit of switching device with the reduced voltage rating.

As the number of levels increases, the number of steps in the staircase waveform increases, and the output waveform reaches nearer to the sine wave with improved THD. With improved THD of the converter's output voltage waveform, the filter's size for required filtering also reduces and further contributes to lowering the filter's cost.

The increase in the number of levels definitely enhances the system performance, but the number of components and hence cost and control complexity increases. Therefore, while selecting the number of levels in a multilevel converter, a proper trade-off between performance and complexity is made. Criteria for choosing the optimum number of levels for a given voltage rating are already given in the earlier chapter. The 7-level, 9-level, 11-level, 19-level, 25-level, and 43-level grid interfaced CHB multilevel converter for photovoltaic application with phase-shifted PWM are considered for comparison.

### **7.3 COMPARISON OF CONVERTER ON DIFFERENT PWM TECHNIQUES**

Multilevel converters have the advantage of low total harmonic distortion (THD) of output voltage and employed a low switching frequency. Selecting a suitable modulation technique further improves the THD and reduce switching frequency. However, the low switching frequency employed in a multilevel converter at a high power-rating reduces the switching losses. Moreover, the multilevel converter is used for medium or high power applications; hence switching losses are the significant parameter for the selection of converter.

A comparison of different modulation techniques such as phase-shifted multicarrier pulse width modulation (PWM), selective harmonic elimination (SHE), and nearest level modulation (NLM), usually employed for symmetric cascaded H-bridge (CHB) multilevel converter, is made as follows.

#### **7.3.1 Frequency Based Comparison**

The phase shifted SPWM is a high-frequency PWM method. The higher switching frequency employed in the PSPWM method has high switching losses and, consequently, low efficiency. As the multilevel converter is used for medium or high power applications; hence switching losses are the significant parameter for the converter selection. Moreover, high switching frequency produces high acoustic noise, which increases the size of the filter for filtering the high noise, and further, it adds up the cost component of the system.

SHE-PWM and NLM are the fundamental switching frequency methods and the fundamental frequency employed reduces the switching losses and enhances efficiency.

### **7.3.2 THD Based Comparison**

A converter with low THD enhances power quality. A multilevel converter has low THD compared to the two-level converter, which can be improved by opting for a good modulation technique. The THD converter output voltage and grid current of SHE-PWM is better than NLM and NLM is having better THD compared to PSPWM. In the SHE-PWM, higher-order harmonic are easily filtered using a low-pass filter. The third harmonic and its multiples are canceled out in line voltages. Hence, the better power quality is achieved by SHE-PWM, which further contributes to the reduction of the filter size and also the cost.

### **7.3.3 Complexity Based Comparison**

The PSPWM is a simple modulation method that can be employed for symmetric CHB up to any level. To implement the SHE strategy for cascaded inverter, one must solve the complex transcendental equations to get the turn ON and OFF angles. It is implemented only to eliminate lower order harmonics as with the increase of levels, the size of transcendental equations is increased that complicates the solution of equations. For the elimination of higher-order harmonics, a filter is used. NLM is simpler than SHE-PWM, as it is not involved with transcendental equations. It is applicable for any number of levels for symmetric CHB multilevel converter.

## **7.4 RESULTS AND DISCUSSION**

A comparative study of different CHB multilevel converters based on the number of levels used in the converter and modulation technique implemented is carried out here. The following results are obtained using the MATLAB software platform's FFT tool.

#### 7.4.1 Different Number of Levels

The converter output waveform along with their THD of 7-level, 9-level, 11-level, 19-level, 25-level, and 43-level CHB multilevel converters for photovoltaic system applications are shown in Fig.7.1(a)-(f). The grid current waveform with harmonic spectra is shown in Fig. 7.2 for a 7-level, 9-level, 11-level, 19-level, 25-level and 43-level converters. The THD result is shown in Table 7.1 for different number of levels of CHB multilevel converter. From these results obtained for various converter levels, it is clearly depicted that the THD is improved with the increase in the number of levels.

Table-7.1 THD for different number of levels

<b>Number of levels</b>	<b>Converter voltage THD(%)</b>	<b>Grid current THD(%)</b>
7-level	12.55	1.15
9-level	11.7	0.8
11-level	8.55	0.75
19-level	4.27	0.7
25-level	3.98	0.64
43-level	3.28	0.49

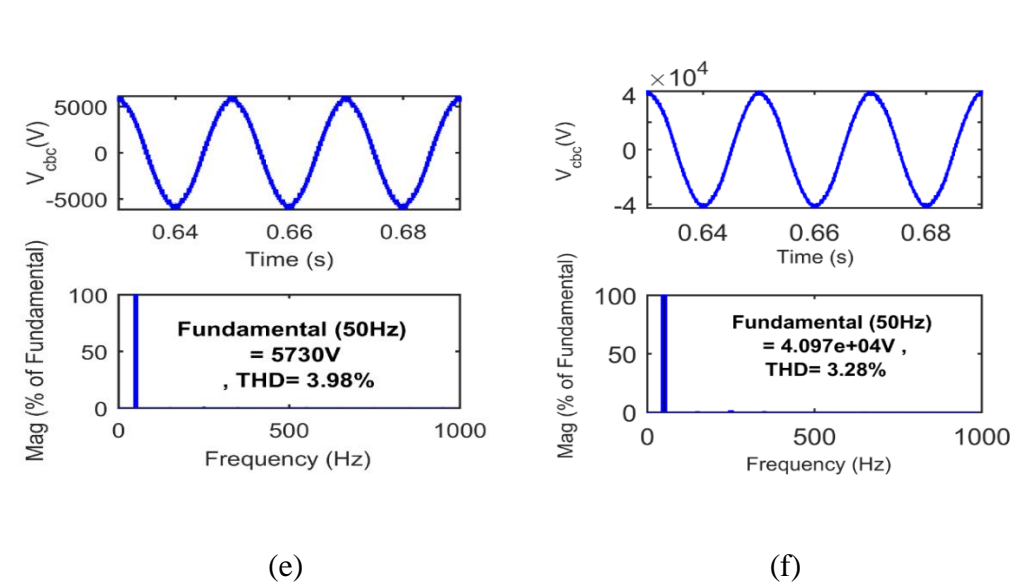
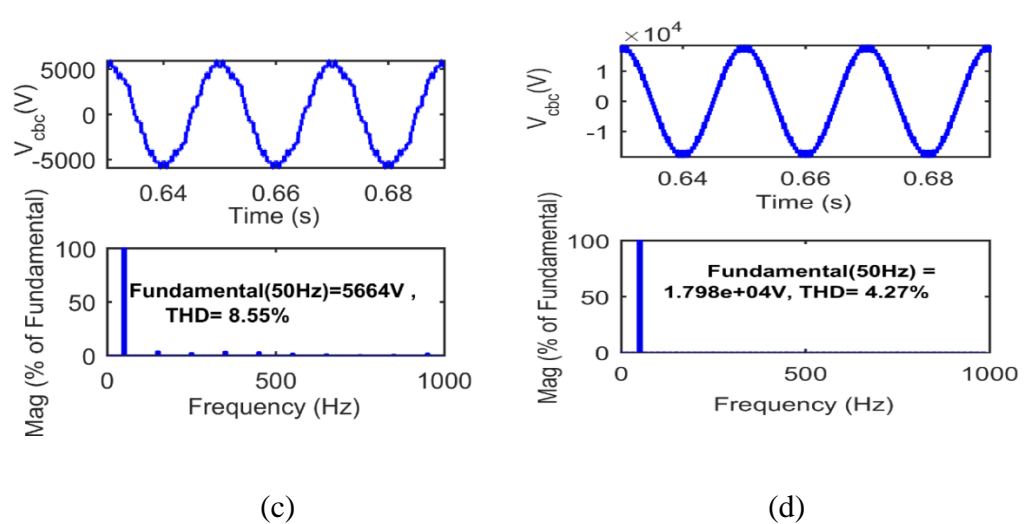
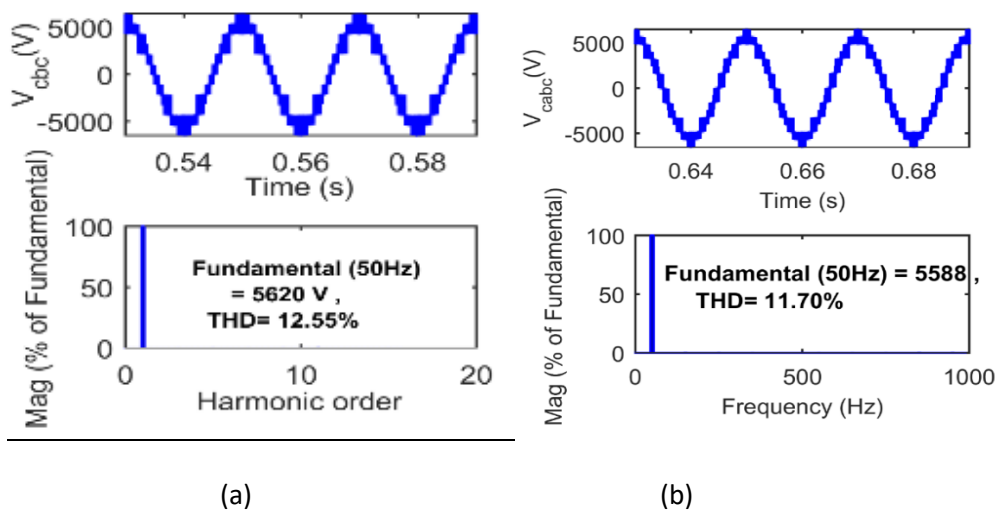
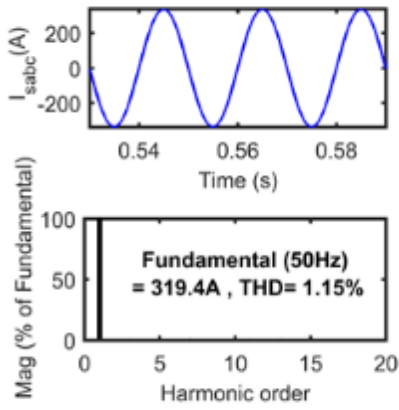
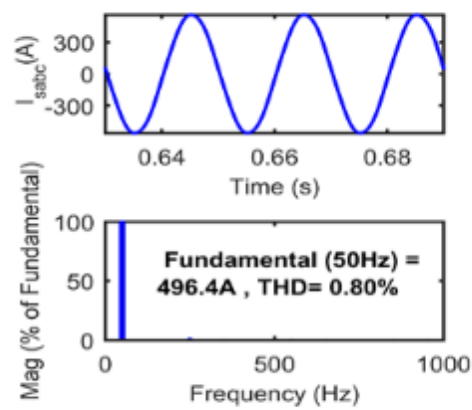


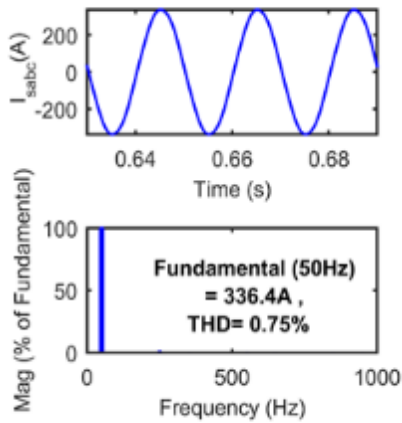
Fig 7.1 Converter output voltage and harmonic spectra for (a) 7-level, (b) 9-level, (c) 11-level, (d) 19-level, (e) 25-level and (f) 43-level



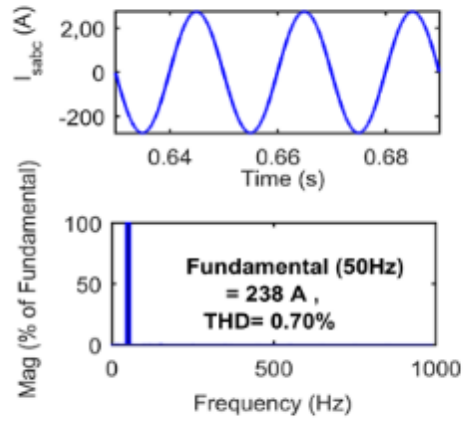
(a)



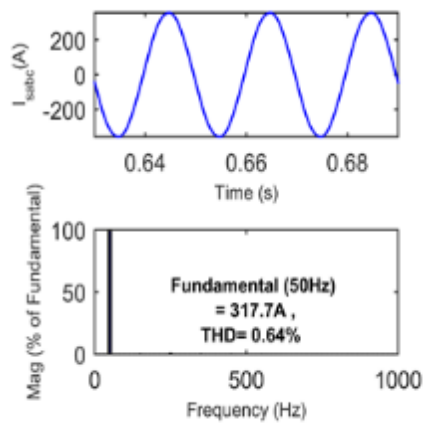
(b)



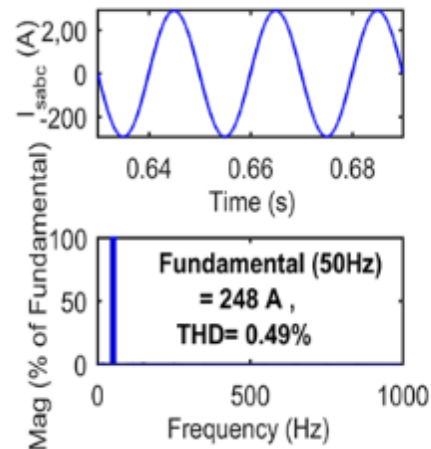
(c)



(d)



(e)



(f)

Fig. 7.2 Grid current waveform and harmonic spectra (a) 7-level (b) 9-level  
(c) 11-level (d) 19-level (e) 25-level (f) 43-level converter

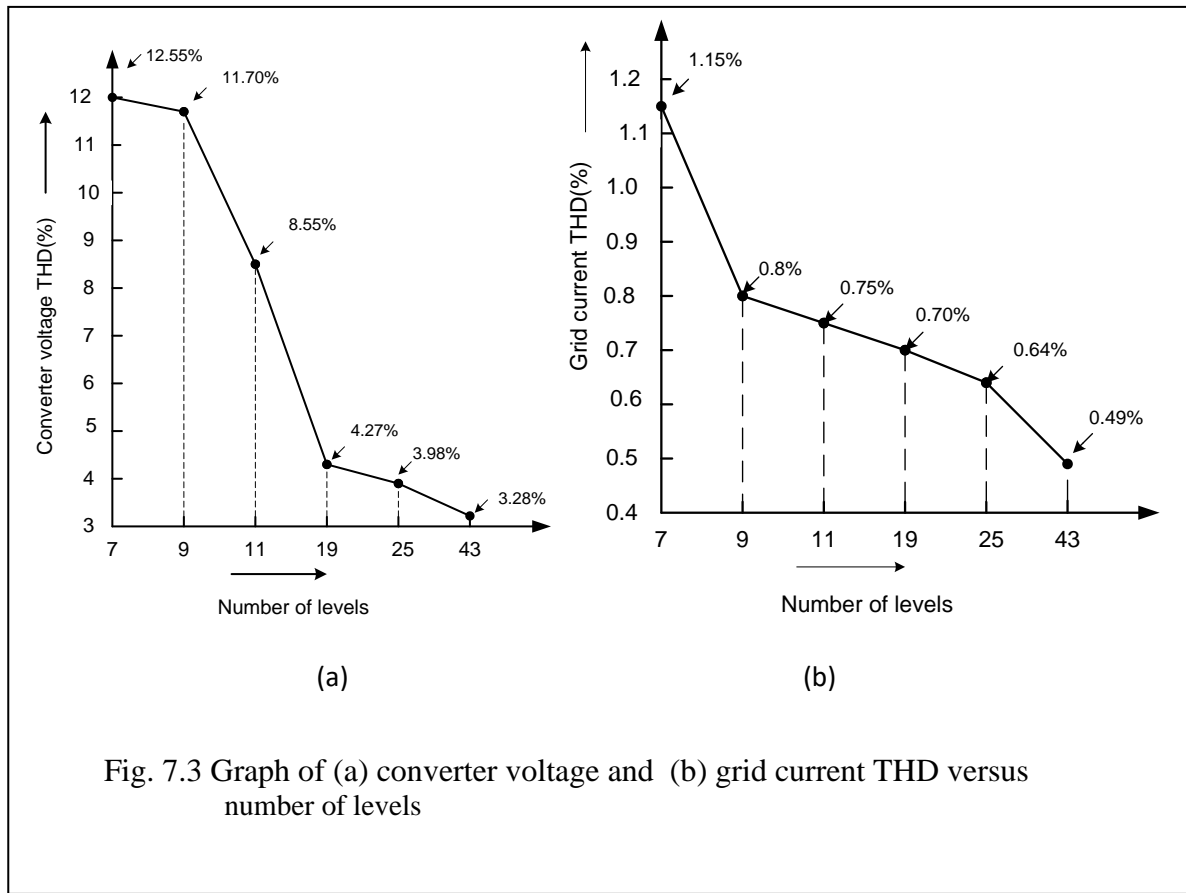


Fig. 7.3 Graph of (a) converter voltage and (b) grid current THD versus number of levels

The graphs of converter voltage and grid current THD versus number of level are shown in Fig. 7.3.

## 7.4.2 Different Modulation Techniques

The modulation techniques, phase shifted PWM, SHE-PWM, and NLM, suitable for the 9-level symmetric multilevel CHB multilevel converter, are implemented in chapter 4 and compared in this chapter for unity modulation index. The following results are obtained by using the FFT tool of the MATLAB software platform.

### 7.4.2.1 PWM strategies

In PSPWM, the modulating signal is compared with eight carriers in the PSPWM modulation technique, and the output waveform is shown in Fig.7.4.



This figure shows the pulse generation after comparison, voltage waveform across each H- bridge ( $V_{dc1}$ ,  $V_{dc2}$ ,  $V_{dc3}$ , and  $V_{dc4}$ ), and the resultant waveform across the series-connected bridge. The bipolar PWM method is used for modulation [10]. In SHE-PWM, the switching angle is calculated offline, and switching is selected from the flowchart (given in chapter 4); accordingly, switching for different levels is done as given in switching Table 4.2 (given in chapter 4). In NLM, the switching is done by first obtaining the nearest level by calculation. Then, switching is done as per switching Table 4.2 for the corresponding level by using the logic of the flowchart given in chapter 4.

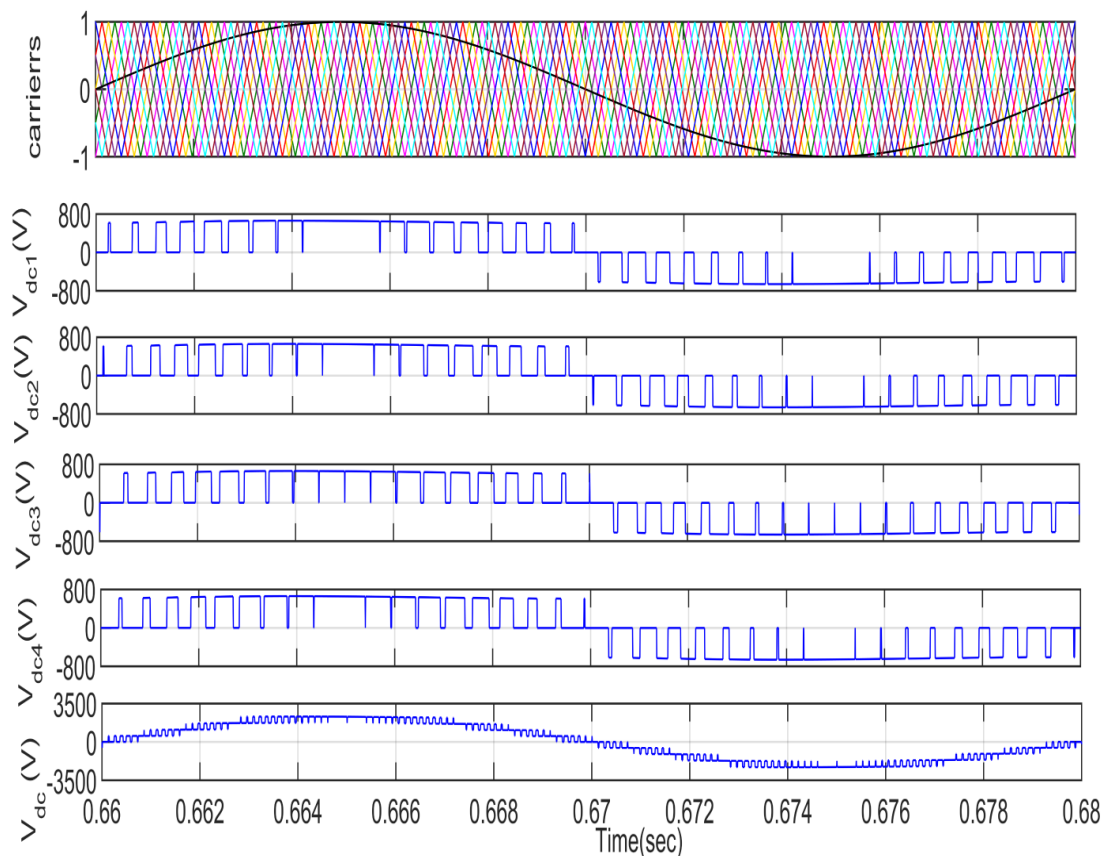


Fig.7.4 Switching pulses generated in PSPWM

### 7.4.2.2 Power quality

Fig. 7.5 shows waveforms of the converter voltages ( $v_{cabc}$ ), and harmonic spectra along with THD levels for (a) SHE-PWM, (b) PSPWM, and (c) NLM modulation techniques by using the fast Fourier transform tool in MATLAB. Fig. 7.6 shows waveforms of the supply voltages ( $v_{sabc}$ ) and harmonic spectra along with THD levels for (a) SHE-PWM, (b) PSPWM, and (c) NLM modulation techniques. Fig.7.7 shows waveforms of the supply currents ( $i_{sabc}$ ) and harmonic spectra along with THD levels for (a) SHE-PWM, (b) NLM, and (c) PSPWM modulation techniques by using the fast Fourier transform tool in MATLAB. The THD values of  $v_{cabc}$ ,  $v_{sabc}$ , and  $i_{sabc}$  for three modulation techniques at modulation index unity are given in Table 7.2 for comparison.

These results shown in Figs. 7.5, 7.6, and 7.7 confirm that the THD for SHE-PWM is lower than PSPWM and NLM, and also THD for NLM is lower than PSPWM. The graph of grid current, grid voltage and converter voltage versus PWM techniques is shown in Fig. 7.8.

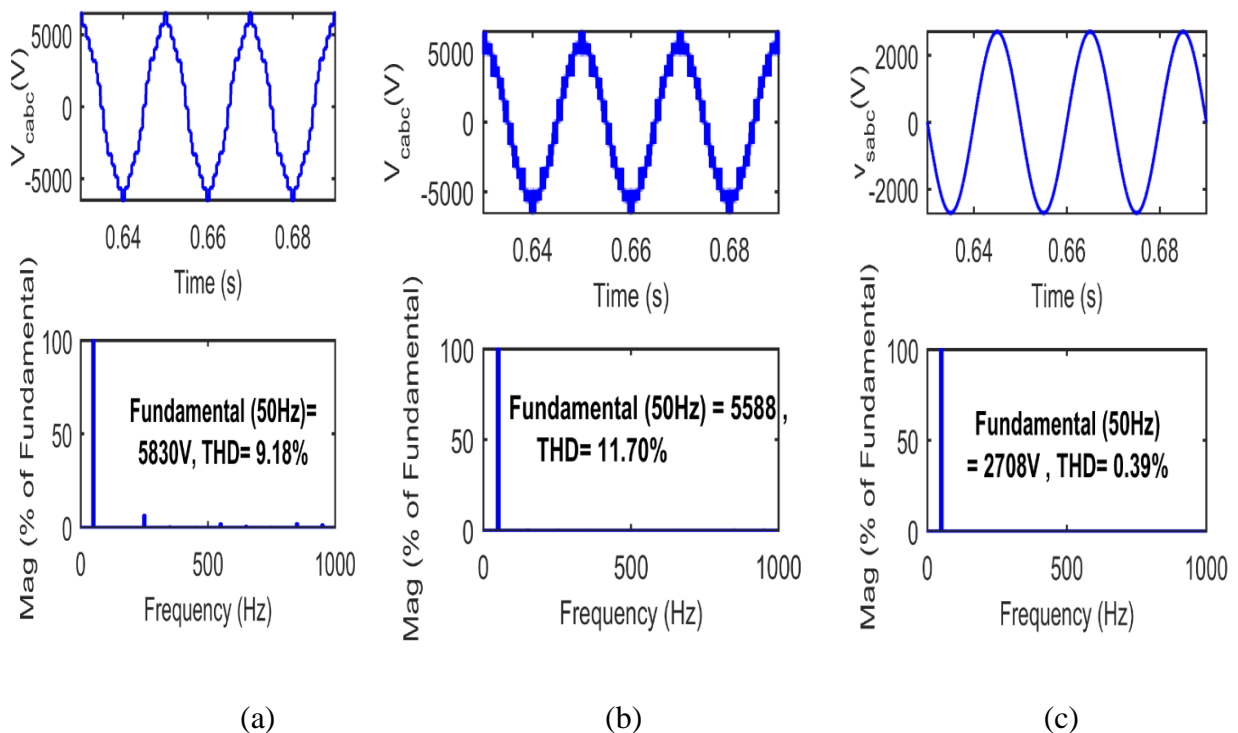


Fig. 7.5 Waveforms and harmonic spectra for converter side voltage for (a) SHE-PWM (b) PSPWM (c) NLM

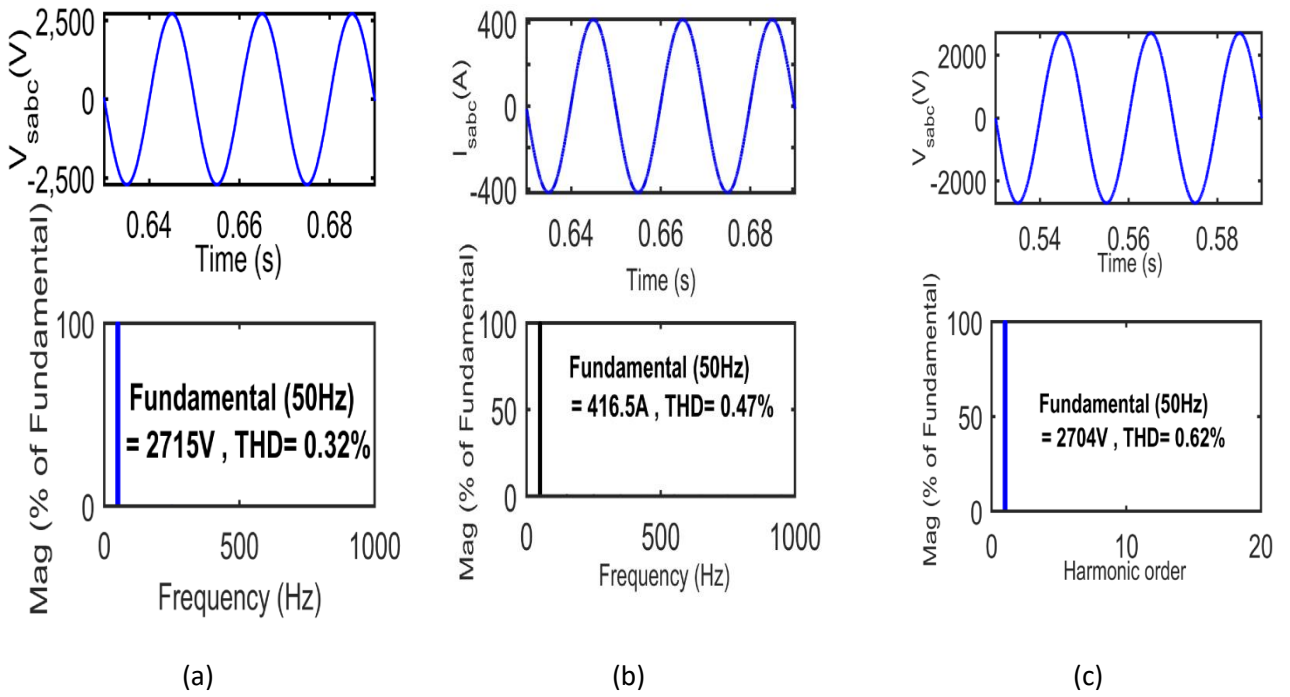


Fig.7.6 Waveforms and harmonic spectra for supply Voltage for (a) SHE-PWM (b) NLM (c) PSPWM

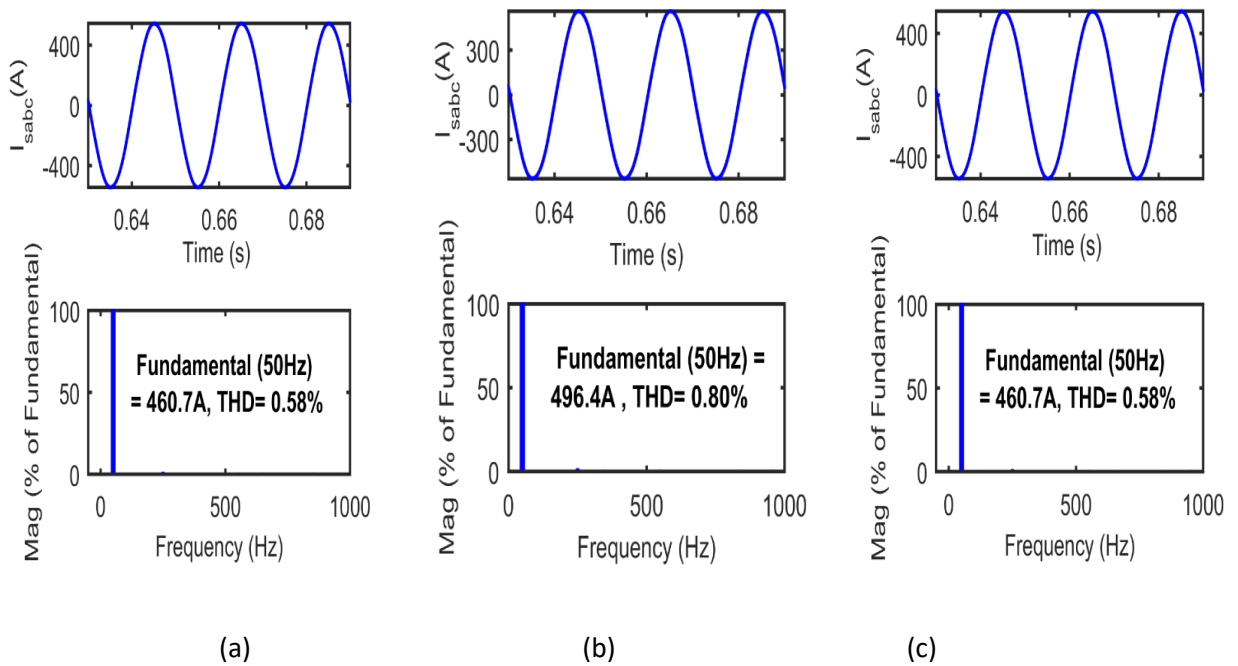


Fig. 7.7 Waveforms and harmonic spectra for supply current for (a) SHE (b) PSPWM (c) NLM

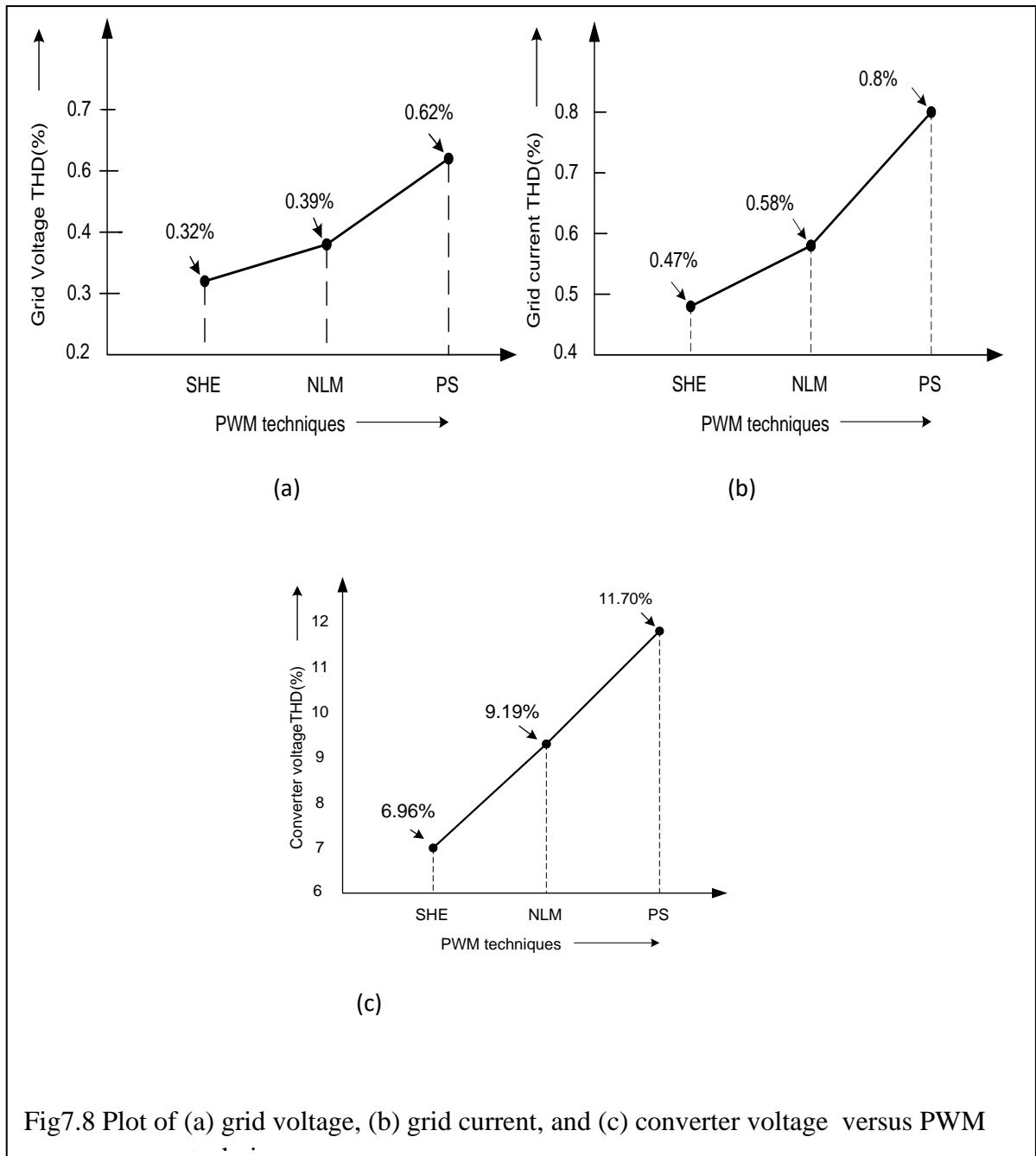


Table 7.2 Modulation techniques and corresponding THD values for a 9-level converter

S.No.	Modulation Technique	$v_{cabc}$ THD (%)	$v_{sabc}$ THD (%)	$i_{sabc}$ THD (%)
1.	PSPWM	11.70	0.62	0.8
2.	NLM	9.19	0.39	0.58
3.	SHE-PWM	6.96	0.32	0.47

### 7.4.3 Reduction in Filter Size

The size of filter in p.u. for various level is shown in Table 7.3 and from the table the reduction of the size of filter with number of levels is clearly observed.

Table 7.3 Inductor value (p.u.) corresponding to number of levels

Number of levels	Inductor value (p.u.)
7-level	0.192
9-Level(PS)	0.17
9-level(SHE & NLM)	0.1
19-level	0.01
43-level	0.0072

## 7.5 CONCLUSIONS

The THDs of converter output voltage and grid current for the different number of levels are compared. The number of steps in the staircase waveform increases with the increase of level, and the waveform reaches close to sinusoidal waveform with improved power quality. Even a 19-level converter is having THD 4.27%, which is sufficient for feeding the grid as per the IEEE-519 standard with a small size filter, which further saves the filter cost.

The modulation technique used in the converter affects the performance of the system. PSPWM, SHE-PWM, NLM are some suitable modulation techniques usually employed for symmetric CHB multilevel converter. PSPWM is a more straightforward technique but it has a high switching frequency and higher switching losses. The multilevel converter is used for medium or high power applications; hence switching losses are the significant parameter. SHE-PWM and NLM are the fundamental frequency methods. Due to the fundamental switching frequency employed, the switching losses are reduced, and also the acoustic noise is reduced in these modulation techniques. Lower acoustic noise further contributes to reduced size filter resulting in lower cost. In the SHE-PWM method for finding the switching angle for the corresponding level, the complex

transcendental equation is to be solved. It increases the system's complexity, increasing further with the increase in the multilevel converter levels. Moreover, SHE-PWM is eliminating only the lower order harmonics. For removing the higher-order harmonics, the number of the transcendental equations to be solved increases, or higher-order harmonics are removed by using an inductive filter. In SHE-PWM, the better THD is obtained; hence a better quality output waveform is obtained. NLM has the advantage of the fundamental frequency and being simple than SHE-PWM, but the THD of SHE-PWM is better than NLM.

Among the three techniques, the SHE-PWM is the best technique. It is having lowest THD with elimination of lowest harmonics, having fundamental switching frequency (hence reduced switching losses).

## **CHAPTER-VIII**

### **MAIN CONCLUSIONS AND SUGGESTIONS FOR FURTHER WORK**

#### **8.1 GENERAL**

For enhancing the power quality, reliability, and efficiency of power to be fed to the grid, designing the converter used for grid integration is a challenging task for the researcher. Conventionally, a two-level converter is employed for the grid integration. However, for medium or high voltage grid in the two-level converter case, the entire high voltage stress is transferred on a single device. Moreover, for improving the THD of the MLC output AC voltage and the grid current, the switching frequency is increased, which ultimately increases the switching losses. Moreover, the switching losses are the significant component for medium and high power applications. The researchers have to design a multilevel converter with a low switching frequency, low THD of grid current, and low voltage device stress for medium or high voltage grid integration.

The main objective of this research work, has been to design, model, and control the multilevel converters for transformerless integration to high or medium voltage grid for the large photovoltaic plant. The multilevel converter has the advantage of low switching frequency and low THD due to the staircase output voltage waveform, which can be further improved by selecting an optimum number of levels and a suitable modulation scheme. The symmetrical CHB multilevel converter is selected for an integration as multi-string photovoltaic system naturally provides the independent DC sources. In this work, each string is provided with a separate MPPT and each controlled by the separate controller to remove the effect of partial shading, uneven temperature and insolation level, and other

unbalancing effects. The improved P&O and incremental conductance MPPT algorithms are employed to track the maximum power from the PV array, and the decoupled current control with SRF-PLL is used for VSC control. The phase-shifted PWM, SHE-PWM, and NLM modulation techniques are employed for modulation in this work, and their comparative study is also carried here. The low switching frequency reduces the switching losses and also reduces the acoustic noise. Low acoustic noise reduces the filter size, and only a small size inductive filter is sufficient for filtering. The transformerless integration and low-size filter increase the conversion efficiency and reduce the cost of installation and maintenance. The converter is designed for different levels; 7-level, 9-level, 11-level, 19-level, 25-level, and 43-level to study the effect of increasing levels on the THD of grid current and the voltage stress across each device. Simulated performance is achieved with MATLAB R2015a software. Performance validation for SHE-PWM based 9-level converter is also done on OPAL-RT platform. This chapter gives the main conclusions and further scope of the work.

## **8.2 MAIN CONCLUSIONS**

In this work, the transformerless grid interfaced single-stage multilevel CHB multilevel converters are designed, modelled, and controlled for photovoltaic application. The MATLAB modelling of the system designed for different levels and PWM carried out and the results are validated as per the IEEE-519 standard. Additional validation is also done on OPAL-RT platform. The multilevel converter is designed for both high switching frequency and fundamental switching frequency in this work. The developed system's performance is evaluated based on switching frequency, THD of output voltage and grid current, cost, and complexity of the control as follows.



- CHB multilevel converters have been designed for 7-level, 9-level, 19-level, and 43-level configurations. The optimum number of multilevel converter levels is selected for a given voltage rating with the proper performance and cost complexity ratio. The number of levels in the multilevel converter in this system is chosen with all design considerations like the cost of IGBTs, arithmetic and logical operations (ALOs), THDs, and device voltage utilization factor (DVUF). The results obtained for 7-level, 9-level, 11-level, 19-level, 25-level, and 43-level have shown that THDs are improved with an increase in the number of CHB multilevel converter levels, and voltage stress per device are reduced for the grid interfaced applications.
  
- For large PV plant applications, CHB converter topology is an exciting topology. It naturally needs a separate DC source for each H-bridge in CHB multilevel converter; hence CHB multilevel converter is employed in this work. Despite the increased hardware cost and complexity, multi-string topology is employed in this work, allowing individual MPPT control of each string. Each string is controlled by a separate controller to overcome the unpredictable irradiance level variations, ambient temperature, shading effect, and other relevant factors [18]. In this work, an improved P&O technique and an incremental conductance MPPT algorithms are employed, as these algorithms, although having low accuracy compared to intelligent algorithms but are fast to converge.
  
- The VSC is controlled in this work for feeding current to the grid at unity P.F. The control scheme employed is a decoupled current control with dq-transformation and PLL. It provides zero steady-state error with excellent dynamic performance. PLL is used in this work for the grid synchronization.

- The selection of a suitable modulation technique is a challenging task in designing the multilevel converter for improving the THD and reducing the switching losses. In this work, phase-shifted modulation, SHE-PWM and NLM are employed for modulation. The phase-shifted modulation is a high switching frequency modulation technique suitable for CHB multilevel converter. SHE-PWM is a fundamental frequency switching modulation. A transcendental equation is written for eliminating selected harmonic, and on solving these equations, the switching angle is obtained. NLM is also a fundamental switching frequency method used in these MLCs.
  
- A comparative analysis of different modulation techniques suitable for the CHB multilevel converter is also carried out in this work. The phase-shifted PWM is a high switching frequency method that has high switching losses, which is a significant parameter for a multilevel converter used for medium or high power applications. SHE-PWM and NLM are the fundamental frequency method, which are having low switching losses. The THD obtained in the SHE-PWM method is found superior as compared to phase-shifted PWM and NLM. The THD of the NLM is better to phase-shifted PWM. The phase-shifted PWM and NLM are found simple in implementation and can be employed to any level. Still, SHE-PWM is a complicated method in implementation involving solutions of the non-linear transcendental equations and cannot be employed up to any level. The PWM method, which has low THD and low fundamental switching frequency, requires a small size filter and contributes to cost reduction.

- The system considered in this work is the transformerless system as a multilevel converter system is designed for medium and high voltage. So, it saves the capital and maintenance cost of a bulky and expensive step-up transformer.
- The system considered in this work is a single-stage system to save the cost and reduce control complexity.
- The performance analysis of the designed system is validated as per the IEEE-519 standard by using the MATLAB and OPAL RT simulator.

### **8.3. SUGGESTIONS FOR FURTHER WORK**

In this research work, MLCs are designed, modelled and controlled in this the single stage CHB multilevel converter for transformerless integration of the grid for large photovoltaic system with optimum number of levels. The research areas for further work are suggested as follows.

- Some advanced VSC control schemes like adaptive control, model predictive control method with the cost functions as stability and voltage balancing can be applied for improved results.
- Asymmetrical CHB multilevel converter can be taken if the multi-string photovoltaic system has devices of different voltage ratings.
- For a cost-effective solution, these multilevel converters can supply some reactive power together with the active power to the grid.
- Some new topologies with reduced switches and other components can be designed to feed the grid with the same THD.

## REFERENCES

- **Power Quality Books, Thesis, Reports and Review Articles**
- [1] Ministry of New and Renewable Energy Annual Report 2019-20 available at: [https://mnre.gov.in/img/documents/uploads/file\\_f-1597797108502.pdf](https://mnre.gov.in/img/documents/uploads/file_f-1597797108502.pdf)
- [2] Solar Power Europe and LUT University (2020): 100% Renewable Europe: How To Make Europe's Energy System Climate-Neutral Before 2050, [https://www.solarpowereurope.org/wpcontent/uploads/2020/04/LUT-100-Renewable-Europe-150420-3.pdf?cf\\_id=11443](https://www.solarpowereurope.org/wpcontent/uploads/2020/04/LUT-100-Renewable-Europe-150420-3.pdf?cf_id=11443).
- [3] Earnest and Young, "The Paris agreement; What it means for India" [online] available: [https://www.ey.com/Publication/vwLUAssets/EY-the-paris-agreement-2017/\\$FILE/EY-the-paris-agreement.pdf](https://www.ey.com/Publication/vwLUAssets/EY-the-paris-agreement-2017/$FILE/EY-the-paris-agreement.pdf).
- [4] "107 Sunshine countries..." [online] Available: <https://web.archive.org/web/20151208071012/http://liveindia.in/107-sunshine-countries-may-shape-pms-vision>.
- [5] <https://www.pv-magazine.com/2020/03/20/saudi-arabia-reveals-pre-qualified-bidders-for-1-2-gw-pv-tender/>.
- [6] <https://www.saurenergy.com/solar-energynews/saudi-arabia-lists-49-pre-qualified-bidders-1-2-gw-solar-tender>.
- [7] D. A. Paice, *Power Electronics Converter Harmonics: Multipulse Methods for Clean Power*, IEEE, 1996.
- [8] S. Khomfoi, L. M. Tolbert, "Multilevel Power Converters," *Power Electronics Handbook*, 3rd Edition, Butterworth-Heinemann, 2011, USA, Chapter 17, pp. 455-486.
- [9] R. Teodorescu, M. Liserre and P. Rodríguez, *Grid Converters for Photovoltaic and Wind Power Systems*, First Edition, John Wiley & Sons, Ltd., Sussex, UK, 2011.
- [10] Bin Wu, *High-Power Converters and AC Drives*, IEEE, NJ, 2006.
- [11] B. Singh, A. Chandra and K. Al-Haddad, *Power Quality: Problems and Mitigation Techniques*, John Wiley & Sons Ltd., Sussex, UK, 2015.
- [12] B. Xiao, "Cascaded Inverters for Grid-Connected Photovoltaic Systems," PhD diss., University of Tennessee, 2014. [https://trace.tennessee.edu/utk\\_graddiss/2744](https://trace.tennessee.edu/utk_graddiss/2744)
- [13] Y. Yu, "Multilevel Cascaded H-Bridge Converters for Large-Scale Photovoltaic Power Plants," PhD diss., University of New South Wales, 2016. <http://unsworks.unsw.edu.au/fapi/datastream/unsworks:42472/SOURCE02?view=true>
- [14] X. Zhang, "Control Strategy of Cascaded H-Bridge Multilevel Inverter With PV system as Separate DC Source Degree project in Control Strategy of Cascaded H-Bridge Multilevel Inverter With PV system as Separate DC Source," Master of Science Thesis in Power Electronics, School of Electrical Engineering, Royal Institute of Technology, Stockholm, Sweden, 2011.
- [15] D. Zhong, "Active Harmonic Elimination in Multilevel Converters," Ph.D. diss., University of Tennessee, 2005. [https://trace.tennessee.edu/utk\\_graddiss/1944](https://trace.tennessee.edu/utk_graddiss/1944).
- [16] M. T. Ahmad, "Intelligent Control Algorithms for DSTATCOM and its Applications", Ph.D. Thesis, Department of Electrical Engineering, Delhi Technological University, 2018.

- [17] "IEEE Recommended Practices and Requirements for Harmonic Control in Electrical Power Systems," *IEEE Standard 519-1992*, 2014.
- [18] A. J. Morrison, "Global Demand Projections for Renewable Energy Resources," *2007 IEEE Canada Electrical Power Conference*, Montreal, Que., 2007, pp. 537-542.
- **Power Electronics for Grid Integration**
- [19] R. Dogga, M. Pathak, "Recent trends in solar PV inverter topologies," *Solar Energy*, vol. 183, pp. 57-73, 2019.
- [20] J. M. Carrasco, L. G. Franquelo, J. T. Bialasiewicz, E. Galvan, R. C. P. Guisado, Ma. A. M. Prats, J. I. Leon and N. Moreno-Alfonso, "Power-Electronic Systems for the Grid Integration of Renewable Energy Sources: A Survey", *IEEE Transactions on Industrial Electronics*, vol. 53, no. 4, pp. 1002-1016, June 2006.
- [21] F. Blaabjerg, R. Teodorescu, M. Liserre and A.V. Timbus, "Overview of control and grid synchronization for distributed power generation systems," *IEEE Transactions on Industrial Electronics*, vol. 53, no. 5, pp.1398-1409, October, 2006.
- [22] F. Blaabjerg, K. Ma and Y. Yang, "Power Electronics for Renewable Energy Systems - Status and Trends," *CIPS 2014; 8th International Conference on Integrated Power Electronics Systems*, Nuremberg, Germany, 2014, pp. 1-11.
- [23] F. Blaabjerg, Z. Chen and S. B. Kjaer, "Power electronics as efficient interface in dispersed power generation systems," *IEEE Transactions on Industrial Electronics*, vol. 19, no 5, pp.1184-1194, September, 2006.
- [24] J. T. Bialasiewicz, "Renewable energy systems with photovoltaic power generators: operation and modeling," *IEEE Transactions on Industrial Electronics*, vol. 55, no. 7, pp.2752-2758, July 2008.
- [25] B. Kroposki, C. Pink, R. DeBlasio, H. Thomas, M. Simões, and P. K. Sen, "Benefits of Power Electronic Interfaces for Distributed Energy Systems," *IEEE Transactions on Energy Conversion*, vol. 25, no. 3, pp. 901-908, September 2010.
- **Grid Interfaced Two Level Converters**
- [26] B. Yang, W. Li, Y. Zhao, and X. He, "Design and analysis of a grid connected photovoltaic power system," *IEEE Trans. Power Electron.*, vol. 25, no. 4, pp. 992-1000, Apr. 2010.
- [27] A. K. Verma, B. Singh and D. T. Shahani, "Grid interfaced solar photovoltaic power generating system with power quality improvement at AC mains", *IEEE Third International Conference on Sustainable Energy Technologies (ICSET)*, Kathmandu, 2012, pp. 177-182.
- [28] B. Singh, C. Jain and S. Goel, "A UVT based control for single-stage grid interfaced SPV system with improved power quality," *2014 6th IEEE Power India International Conference (PIICON)*, Delhi, 2014, pp. 1-6.
- [29] C. Jain, S. Goel and B. Singh, "A distribution grid tied multifunctional SPV system operating with control approach based on decoupled adaptive neural network," *IEEE Industry Applications Society Annual Meeting*, Addison, TX, 2015, pp. 1-8.
- [30] A. K. Verma, C. Jain, B. Singh and D. T. Shahani, "Adaptive noise cancellation based harmonic elimination in grid integrated photovoltaic system," *IET Renewable Power Generation*, vol. 10, no. 8, pp. 1096-1104, 9 2016.

- [31] B. Singh, S. Goel, A. Singhal, A. Garg and C. Jain, "Power quality enhancement of grid integrated solar PV system based on adaptive noise reduction control," *2015 IEEE Power & Energy Society General Meeting*, Denver, CO, 2015, pp. 1-5.
- [32] A. Verma, B. Singh and D. Shahani, "Modified EPLL based control to eliminate DC component in a grid interfaced solar PV system," *2014 6th IEEE Power India International Conference (PIICON)*, Delhi, 2014, pp. 1-6.
- [33] Faa-Jeng Lin, Kuang-Chin Lu, Ting-Han Ke, Bo-Hui Yang, and Yung-Ruei Chang, "Reactive Power Control of Three-Phase Grid-Connected PV System During Grid Faults Using Takagi-Sugeno-Kang Probabilistic Fuzzy Neural Network Control," *IEEE Transactions on Industrial Electronics*, vol. 62, no. 9, pp. 5516-5528, September 2015.
- [34] C. Jain and B. Singh, "Luenberger observer based control algorithm for single-phase two-stage multifunctional grid connected solar energy conversion system," *2014 9th International Conference on Industrial and Information Systems (ICIIS)*, Gwalior, 2014, pp. 1-6.
- [35] B. Singh, C. Jain, S. Goel, A. Chandra and K. Al-Haddad, "A Multifunctional Grid-Tied Solar Energy Conversion System With ANF-Based Control Approach," *IEEE Transactions on Industry Applications*, vol. 52, no. 5, pp. 3663-3672, Sept.-Oct. 2016.
- [36] C. Jain and B. Singh, "A Three-Phase Grid Tied SPV System With Adaptive DC Link Voltage for CPI Voltage Variations" *IEEE Transactions on Sustainable Energy*, vol. 7, no. 1, pp. 337-344, January 2016.
- [37] C. Jain and B. Singh, "An Adjustable DC Link Voltage-Based Control of Multifunctional Grid Interfaced Solar PV System," *IEEE Journal of Emerging and Selected Topics in Power Electronics*, vol. 5, no. 2, pp. 651-660, June-2017.
- [38] B. Singh, S. Kumar, and C. Jain, "Damped-SOGI-Based Control Algorithm for Solar PV Power Generating System," *IEEE Transactions on Industry Applications*, vol. 53, no. 3, pp. 1780-1787, May/June 2017.
- [39] B. Singh and C. Jain, "A Decoupled Adaptive Noise Detection Based Control Approach for a Grid Supportive PV System," *IEEE Transactions on Industry Applications*, vol. 53, no. 5, pp. 4894-4902 September/October, 2017.
- [40] S. Kumar, C. Jain and B. Singh, "Adaptive pseudo-linear control for grid-supportive PV system," *IET Generation, Transmission & Distribution*, vol. 13, no. 9, pp. 1653-1660, May 2019.
- **Maximum Power Point Tracking Algorithms**
- [41] S. Jain and V. Agarwal, "Comparison of the performance of maximum power point tracking schemes applied to single-stage grid-connected photovoltaic systems," *IET Electr. Power Appl.*, vol.1, no.5, p.p. 753-762, Sept. 2007
- [42] B. Subudhi and R. Pradhan, "A comparative study on maximum power point techniques for photovoltaic power systems," *IEEE Trans. Sustainable Energy*. vol. 4, no.1, pp. 89-98, Jan. 2013.
- [43] M.A.G. De Brito, L. Galloto, L. P. Sampaio, G.E. de Azevedo Melo and C. A. Caesin, "Evaluation of the main MPPT techniques for photovoltaic applications," *IEEE Trans. Ind. Electron.*, vol. 60, no. 3, pp. 1156-1167, Mar. 2013.
- [44] M. I. Hossain, S. A. Khan, M. Shafiullah, M. J. Hossain, "Design and Implementation of MPPT Controlled Grid Connected Photovoltaic Systems", *IEEE Symposium on Computer and Informatics*, pp.284-289, 2011.

- [45] Q. Mei, M. Shan, L. Liu, and J. M. Guerrero, "A Novel Improved Variable Step-Size Incremental-Resistance MPPT Method for PV Systems," *IEEE Trans. Ind. Electron.* vol. 58, no. 6, pp. 2427–2434, June 2011.
- [46] K. H. Hussein, I. Muta, T. Hoshino and M. Osakada, "Maximum photovoltaic power tracking: an algorithm for rapidly changing atmospheric conditions," *IEE Proceedings - Generation, Transmission and Distribution*, vol. 142, no. 1, pp. 59-64, Jan. 1995.
- [47] J. Ahmad, "A Fractional Open Circuit Voltage Based Maximum Power Point Tracker for Photovoltaic Arrays," *2010 2nd International Conference on Software Technology and Engineering*, San Juan, PR, 2010, pp. V1-247-V1-250.
- [48] Y. Chen and K.M. Smedley, "A cost-effective single-stage inverter with maximum power point tracking," *IEEE Transactions on Power Electronics*, vol.19, no.5, pp.1289-1294, Sept. 2004.
- [49] J. S. C. M. Raj and A. E. Jeyakumar, " A novel maximum power point technique for photovoltaic module based on power plane analysis of I-V characteristics," *IEEE Trans. Ind. Electron.*, vol. 61, no.9, pp. 4734-4745, Sep 2014.
- [50] M. Adly, H. El-Sherif and M. Ibrahim, "Maximum power point tracker for a PV cell using a fuzzy agent adapted by the fractional open circuit voltage technique," *2011 IEEE International Conference on Fuzzy Systems (FUZZ-IEEE 2011)*, Taipei, 2011, pp. 1918-1922.
- [51] M. Farhat, A. Flah, and L. Sbita, "Photovoltaic maximum power point tracking based on ANN control," *Int. Rev. Model. Simul.*, vol. 7, no. 3, pp. 474-480, June 2014.
- [52] J. Ghazanfari and M. M. Farsangi, "Maximum power point tracking using sliding mode control for photovoltaic array," *Iran. J. Elect. Electron.* Vol. 9, No. 3, pp. 189-196, Sep. 2013.
- [53] Q. Shihong, W. Min, C. Teng and Y. Xiangling, "Comparative analysis of incremental conductance and perturb-and-observation methods to implement MPPT in photovoltaic system," *International Conference on Electrical and Control Engineering (ICECE)*, 16-18 Sept. 2011, pp. 5792-5795.
- [54] N. Femia, G. Petrone, G. Spagnuolo and M. Vitelli, "Optimization of perturb and observe maximum power point tracking method," *IEEE Transactions on Power Electronics*, vol. 20, no. 4, pp. 963-973, July 2005.
- [55] M. Killi and S. Samanta, "Modified Perturb and Observe MPPT Algorithm for Drift Avoidance in Photovoltaic Systems," *IEEE Transactions on Industrial Electronics*, vol. 62, no. 9, pp. 5549-5559, Sept. 2015.
- [56] J. Ahmed and Z. Salam, "A modified P&O maximum power point tracking method with reduced steady state oscillation and Improved tracking efficiency ," *IEEE Transactions on Sustainable Energy*, vol. 22, no. 2, pp. 1506-1514, Oct. 2016.
- [57] A. K. Singh, I. Hussain and B. Singh, "An improved P&O MPPT algorithm for single stage three-phase grid integrated solar PV system," *IEEE 7<sup>th</sup> Power India International Conference(PIICON)*, Bikaner, 2016, pp. 1-6.
- [58] G. J. Kish, J. J. Lee and P. W. Lehn, "Modelling and control of photovoltaic panels utilising the incremental conductance method for maximum power point tracking," *IET Renewable Power Generation*, vol.6, no.4, pp.259-266, July 2012.

- [59] D. Menniti, A. Burgio, N. Sorrentino, A. Pinnarelli, and G. Brusco, "An Incremental Conductance Method with Variable Step Size for MPPT: Design and Implementation," presented at the *10th International Conference on Electrical Power Quality and Utilization*, Lodz, Poland, 2009.
- [60] X. Zhou, D. Song, Y. Ma, and D. Cheng, "The Simulation and Design for MPPT of PV System Based on Incremental Conductance Method", presented at the *WASE International Conference on Information Engineering*, Beidaihe, China, 2010, Hebei, 2010, pp. 314-317.
- [61] M. A. Elgendy, B. Zahawi and D.J. Atkinson, "Assessment of the Incremental Conductance Maximum Power Point Tracking Algorithm," *IEEE Trans. On Sustainable Energy*, vol. 4, no. 1, pp. 108-117, Jan. 2013.
- [62] S. S. Mohammed and D. Devaraj, "Simulation of Incremental Conductance MPPT based two phase interleaved boost converter using MATLAB/Simulink," *2015 IEEE International Conference on Electrical, Computer and Communication Technologies (ICECCT)*, Coimbatore, 2015, pp. 1-6.
- [63] O. Alonso, P. Sanchis, E. Gubia, and L. Marroyo, "Cascaded h-bridge multilevel converter for grid connected photovoltaic generators with independent maximum power point tracking of each solar array," *Power Electronics Specialist Conference, 2003. PESC '03*, Acapulco, Mexico, 2003, pp. 731-735 vol.2.
- [64] B. Xiao, L. Hang, J. Mei, C. Riley, L. M. Tolbert and B. Ozpineci, "Modular Cascaded H-Bridge Multilevel PV Inverter With Distributed MPPT for Grid-Connected Applications," *IEEE Transactions on Industry Applications*, vol. 51, no.2, pp.1722-1731, 2015.
- [65] E. Pouresmaeil, M. Mehrasa, M. A. Shokridehaki, E. M. G. Rodrigues and J. P. S. Catalão, "Control of Modular Multilevel Converters for integration of distributed generation sources into the power grid," *2015 IEEE International Conference on Smart Energy Grid Engineering (SEGE)*, Oshawa, ON, 2015, pp. 1-6.
- **Multipulse Converter**
- [66] I. Hussain and B. Singh, "Investigations on solar PV grid interfaced power generating system using two-level twelve-pulse double bridge converter," *9<sup>th</sup> International Conference on Industrial and Information Systems (ICIIS)*, Gwalior, 2014, pp. 1-6.
- [67] B. Singh and I. Hussain, "Grid integration of single stage solar PV power generating system using 12-pulse VSC," *IEEE 6<sup>th</sup> India International Conference on Power Electronics (IICPE)*, Kurukshetra, 2014, pp. 1-6.
- **Multilevel Converter**
- [68] M. R. Islam, Y. G. Guo, and J. G. Zhu, "A multilevel medium-voltage inverter for step-up-transformer-less grid connection of photovoltaic power plants," *IEEE J. Photovoltaics*, vol. 4, no. 3, pp. 881-889, May 2014.
- [69] M. R. Islam, Y. G. Guo, and J. G. Zhu, and D. Dorrell, "Design and comparison of 11 kV multilevel voltage source converters for local grid based renewable energy systems," in *Proc. the 37th Annual Conf. IEEE Ind. Electron. Society (IECON 2011)*, Melbourne, Australia, 7–10 Nov., 2011, pp. 3596–3601.
- [70] M. R. Islam, Y. G. Guo and J. G. Zhu, "H-bridge multilevel voltage source converter for direct grid connection of renewable energy systems," *IEEE PES Innovative Smart Grid Technologies*, Perth, WA, 2011, pp. 1-7.



- [71] M. R. Islam, Y. Guo and J. Zhu, "A High-Frequency Link Multilevel Cascaded Medium-Voltage Converter for Direct Grid Integration of Renewable Energy Systems," *IEEE Transactions on Power Electronics*, vol. 29, no. 8, pp. 4167-4182, Aug. 2014.
- [72] T. Kerekes, E. Koutroulis, D. Sera, R. Teodorescu and M. Katsanevakis, "An optimization method for designing large PV plants," *IEEE Journal of Photovoltaics*, vol. 3, no. 2, pp. 814-822, April 2013.
- [73] R. Gonzalez, E. Gubia, J. Lopez and L. Marroyo, "Transformerless single-phase multilevel-based photovoltaic inverter," *IEEE Trans. Industrial Electronics*, vol. 55, no. 7, pp. 2694-2702, July 2008.
- [74] T. Kerekes, R. Teodorescu, M. Liserre, C. Klumpner and M. Sumner, "Evaluation of Three-Phase Transformerless Photovoltaic Inverter Topologies," *IEEE Transactions on Power Electronics*, vol. 24, no.9, pp. 2202-2211, Sept. 2009
- [75] G. Buticchi, D. Barater, E. Lorenzani, C. Concari and G. Franceschini, "A Nine-Level Grid-Connected Converter Topology for Single-Phase Transformerless PV Systems," in *IEEE Transactions on Industrial Electronics*, vol. 61, no. 8, pp. 3951-3960, Aug. 2014.
- [76] J. S. Lai and F. Z. Peng, "Multilevel Converters-A new Breed of Power Converters," *IEEE Transactions on Industry Applications*, vol.32, pp. 509-517, May/June 1996.
- [77] M. Manjreker and G. Venkataramanan, "Advanced topologies and modulation strategies for multilevel inverters," in *Proc. IEEE Power Electronics Specialists Conf. (PESC)*, Baveno, Italy, 1996, pp. 1013-1018.
- [78] L. M. Tolbert, F. Z. Peng, "Multilevel Converters as a Utility Interface for Renewable Energy Systems," *IEEE Power Engineering Society Summer Meeting*, Seattle, Washington, pp. 1271-1274, July 15, 2000.
- [79] J. Rodriguez, J. S. Lai, and F. Z. Peng, "Multilevel inverters: A survey of topologies, controls, and applications," *IEEE Trans. Ind. Electron.*, vol. 49, no. 4, pp. 724-738, Aug. 2002.
- [80] H. Akagi, "Multilevel Converters: Fundamental Circuits and Systems," *Proceedings of the IEEE*, vol. 105, no. 11, pp. 2048-2065, Nov. 2017.
- [81] S. Kouro, M. Malinowski, K. Gopakumar, J. Pou, L. G. Franquelo, B. Wu, J. Rodriguez, M. A. Perez and J. L. Leon, "Recent advances and industrial applications of multilevel converters", *IEEE Transactions on Industrial Electronics*, vol. 57, no 8, August 2010.
- [82] S. Amamra, K. Meghriche, A. Cherifi and B. Francois, "Multilevel Inverter Topology for Renewable Energy Grid Integration," *IEEE Transactions on Industrial Electronics*, vol. 64, no. 11, pp. 8855-8866, Nov. 2017.
- [83] A. Dekka, B. Wu and M. Narimani, "A Series-Connected Multilevel Converter: Topology, Modeling, and Control," *IEEE Transactions on Industrial Electronics*, vol. 66, no. 8, pp. 5850-5861, Aug. 2019.
- [84] F. Z. Peng, J. W. McKeever, D. J. Adams, "Cascade multilevel inverters for utility applications," *Proc. of 23rd Int. Conf. on Industrial Elect. Control, and Inst.*, 1997, pp. 437-442.
- [85] A. Mortezaei, M. G. Simões, T. D. C. Busarello, F. P. Marafão and A. Al-Durra, "Grid-Connected Symmetrical Cascaded Multilevel Converter for Power Quality Improvement," *IEEE Transactions on Industry Applications*, vol. 54, no. 3, pp. 2792-2805, May-June 2018.

- [86] H. Akagi, "Classification, terminology, and application of the modular multilevel cascaded converter (MMCC)," *IEEE Trans. Power Electron.*, vol. 26, no. 11, pp. 3119–3130, Nov. 2011.
- [87] D. Zhu, M. Ding, "Research on the Topology and Control Scheme of an Innovative Modular Multilevel Converter," *Energy and Power Engineering*, 2013, vol. 5, no. 4B, pp 1512-1516.
- [88] F. Z. Peng, J. S. Lai, J. W. McKeever, J. VanCoevering, "A Multilevel Voltage-Source Inverter with Separate DC Sources for Static Var Generation," *IEEE Transactions on Industry Applications*, vol. 32, no. 5, pp. 1130-1138, Sept. 1996.
- [89] G. Joos, X. Huang, B. T. Ooi, "Direct-Coupled Multilevel Cascaded Series VAR Compensators," *Conference Record – IEEE Industry Applications Society 32nd Annual Meeting*, 1997, pp. 1608-1615.
- [90] W. Xiang, R. Yang, C. Lin, J. Zhou, J. Wen and W. Lin, "A Cascaded Converter Interfacing Long Distance HVDC and Back-to-Back HVDC Systems," *IEEE Journal of Emerging and Selected Topics in Power Electronics*, vol. 8, no. 4, pp. 4109-4121, Dec. 2020.
- [91] A. Nabae, I. Takahashi and H. Akagi, "A New Neutral-Point-Clamped PWM Inverter," *IEEE Transactions on Industry Applications*, vol. IA-17, no. 5, pp. 518-523, Sept. 1981.
- [92] J. Rodriguez, S. Bernet, P. K. Steimer and I. E. Lizama, "A Survey on Neutral-Point-Clamped Inverters," *IEEE Transactions on Industrial Electronics*, vol. 57, no. 7, pp. 2219-2230, July 2010,
- [93] S. Busquets-Monge, J. Rocabert, P. Rodriguez, S. Alepuz, J. Bordonau, "Multilevel Diode-clamped Converter for Photovoltaic Generators with Independent Voltage Control of Each Solar Array," *IEEE Transactions on Industrial Electronics*, vol. 55, pp. 2713-2723, July 2008.
- [94] X. Liu, J. Lv, C. Gao, Z. Chen and S. Chen, "A Novel STATCOM Based on Diode-Clamped Modular Multilevel Converters," *IEEE Transactions on Power Electronics*, vol. 32, no. 8, pp. 5964-5977, Aug. 2017.
- [95] A. A. Abdel-Aziz, K. H. Ahmed, S. Wang, A. M. Massoud and B. W. Williams, "A Neutral-Point Diode-Clamped Converter With Inherent Voltage-Boosting for a Four-Phase SRM Drive," *IEEE Transactions on Industrial Electronics*, vol. 67, no. 7, pp. 5313-5324, July 2020,
- [96] U. V. Patil, H. M. Suryawanshi and M. M. Renge, "Direct torque control of induction motor: Simulation results using two-level and diode clamped multilevel inverter," *2010 Joint International Conference on Power Electronics, Drives and Energy Systems & 2010 Power India*, New Delhi, 2010, pp. 1-5.
- [97] T. Zheng, C. Gao, X. Liao, X. Liu, B. Sun and J. Lv, "A medium-voltage motor drive based on diode-clamped modular multilevel converters," *20th International Conference on Electrical Machines and Systems (ICEMS)*, Sydney, NSW, 2017, pp. 1-6.
- [98] T. A. Meynard, H. Foch, "Multi-Level Conversion: High Voltage Choppers and Voltage-Source Inverters," *PESC '92 Record. 23rd Annual IEEE Power Electronics Specialists Conference*, Toledo, Spain, 1992, pp. 397-403.
- [99] S. Du, B. Wu, N. R. Zargari and Z. Cheng, "A Flying-Capacitor Modular Multilevel Converter for Medium-Voltage Motor Drive," *IEEE Transactions on Power Electronics*, vol. 32, no. 3, pp. 2081-2089, March 2017.

- [100] T. Modeer, N. Pallo, T. Foulkes, C. B. Barth and R. C. N. Pilawa-Podgurski, "Design of a GaN-Based Interleaved Nine-Level Flying Capacitor Multilevel Inverter for Electric Aircraft Applications," *IEEE Transactions on Power Electronics*, vol. 35, no. 11, pp. 12153-12165, Nov. 2020.
- [101] G. Ramya, R. Ramaprabha and K. N. Dinesh Babu, "Analysis of synchronization algorithm for grid connected photovoltaic modular multilevel converter using positive sequence detector and phase locked loop," *Trends in Industrial Measurement and Automation (TIMA)*, Chennai, 2017, pp. 1-7.
- [102] Nikhil Bhugra, and Ketan P. Detroja, "Sliding Mode control based Power Balancing For Grid Connected PV System," *2013 IEEE International Conference on Control Applications (CCA)*, Hyderabad, 2013, pp. 673-678.
- [103] J. Negroni, F. Guinjoan, C. Meza, D. Biel, and P. Sanchis, "Energy sampled data modeling of a cascade H-bridge multilevel converter for grid-connected pv systems," *2006 IEEE International Power Electronics Congress*, Puebla, 2006, pp. 1-6.
- [104] J. Chavarría, D. Biel, F. Guinjoan, C. Meza, and J. J. Negroni, "Energy-Balance Control of PV Cascaded Multilevel Grid-Connected Inverters Under Level-Shifted and Phase-Shifted PWMs" *IEEE Transactions on Industrial Electronics*, vol. 60, no. 1, pp. 98-111, January 2013.
- [105] P. Cortés, A. Wilson, S. Kouro, J. Rodriguez, and H. Abu-Rub, "Model Predictive Control of Multilevel Cascaded H-Bridge Inverters," *IEEE Transactions on Industrial Electronics*, vol. 57, no. 8, pp. 2691-2699, August 2010.
- [106] L. Tarisciotti, P. Zanchetta, A. Watson, S. Bifaretti, and J. C. Clare, "Modulated Model Predictive Control for a Seven-Level Cascaded H-Bridge Back-to-Back Converter," *IEEE Transactions on Industrial Electronics*, vol. 61, no. 10, pp.5375-5383, October 2014.
- [107] D. Zhou , S. Yang, and Y. Tang , "Model-Predictive Current Control of Modular Multilevel Converters With Phase-Shifted Pulsewidth Modulation," *IEEE Trans.on Ind. Electr.*, vol. 66, no. 6, pp. 4368-4377, June 2019.
- [108] Y. Han, H. Chen, Z. Li, P. Yang, L. Xu and J. M. Guerrero, "Stability Analysis for the Grid-Connected Single-Phase Asymmetrical Cascaded Multilevel Inverter With SRF-PI Current Control Under Weak Grid Conditions," *IEEE Trans. Power Electronics*, vol. 34, no. 3, pp. 2052-2069, March 2019.
- [109] N. Mishra and B. Singh, "Performance of single stage cascaded H-bridge multilevel converter based grid interfaced PV system," *2016 IEEE 1st International Conference on Power Electronics, Intelligent Control and Energy Systems (ICPEICES)*, Delhi, 2016, pp. 1-6.
- [110] N. Mishra, P. Kant and B. Singh, "An asymmetric seven level multilevel converter for grid Integrated systems," *8th IEEE India International Conference on Power Electronics (IICPE)*, Jaipur, India, 2018 pp. 1-6.
- [111] S. Kuncham, K. Annamalai and S. Nallamothu, "Single phase two stage seven-level power conditioner for photovoltaic power generation system," *IEEE Journal of Emerging and Selected Topics in Power Electronics*, vol.8, no.1, pp. 794-804, 2020.
- [112] E. Villanueva, P. Correa, J. Rodriguez, "Control of a Single-Phase Cascaded H-Bridge Multilevel Inverter for Grid-Connected Photovoltaic Systems," *IEEE Transactions on Industrial Electronics*, vol. 56, no. 11, PP. 4399-4406, November 2009.

- [113] S. Alepuz, S. Busquets-Monge, J. Bordonau, "Interfacing renewable energy sources to the utility grid using a three-level inverter" *IEEE Transactions on Industrial Electronics*, vol. 53, no 5, pp 1504-1511, October 2006.
- [114] S. A. Gonzalez, M. I. Valla and C. F. Christiansen, "Five-level cascade asymmetric multilevel converter," *IET Power Electronics*, vol. 3, no. 1, pp. 120-128, January 2010.
- [115] B. Singh, M. Kandpal and I. Hussain, "Grid integration of single stage SPV system using asymmetric cascaded 7-level VSC," *39th National Systems Conference (NSC)*, Noida, 2015, pp. 1-6.
- [116] M. Mehtani, I. Hussain, M. Kandpal and B. Singh, "Integration of multiple source SPV grid tied system using 27-level cascaded H-bridge converter," *2016 IEEE 7th Power India International Conference (PIICON)*, Bikaner, 2016, pp. 1-5.
- [117] M. Hagiwara and H. Akagi, "Control and experiment of pulse-width modulated modular multilevel converters," *IEEE Trans. Power Electron.*, vol. 24, no. 7, pp. 1737-1746, Jul. 2009.
- [118] M. A. Perez, S. Bernet, J. Rodriguez, S. Kouro, and R. Lizana, "Circuit Topologies, Modeling, Control Schemes, and Applications of Modular Multilevel Converters" *IEEE Transactions on Power Electronics*, pp. 4-17, vol. 30, no. 1, January 2015
- [119] A. Acharya, M. Rico, D. Sera, R. Teodorescu, and L. Norum, "Performance analysis of medium-voltage Grid Integration of PV plant using modular multilevel converter," *IEEE Transactions of Energy Conversion*, vol. 34, no.4, pp.1731- 1740, 2019.
- [120] S. Kouro, B. Wu, A. Moya, E. Villanueva, P. Correa, and J. Rodriguez, "Control of a cascaded h-bridge multilevel converter for grid connection of photovoltaic systems," *2009 35th Annual Conference of IEEE Industrial Electronics*, Porto, 2009, pp. 3976-3982.
- [121] N. Jaalam, N.A. Rahim, A.H.A. Bakar, C. Tan, and A. M.A. Haidar, "A comprehensive review of synchronization methods for grid-connected converters of renewable energy source," *Renewable and Sustainable Energy Reviews*, vol. 59, Pages 1471-1481, June 2016.
- [122] V. Valouch, M. Bejvl, P. Simek, and J. R. Skramlik, "Power Control of Grid-Connected Converters Under Unbalanced Voltage Conditions," *IEEE Transactions on Industrial Electronics*, vol. 62, no.7, pp. 4241-4248, July 2015.
- [123] S. Rivera, B. Wu, S. Kouro, H. Wang, and D. Zhang, "Cascaded H-bridge multilevel converter topology and three-phase balance control for large scale photovoltaic systems," *Power Electronics for Distributed Generation Systems (PEDG), 3rd IEEE International Symposium*, pp. 690-697, 2012 .
- [124] H. S. Krishnamoorthy, S. Essakiappan, P. N. Enjeti, R. S. Balog and S. Ahmed, "A new multilevel converter for Megawatt scale solar photovoltaic utility integration," *2012 Twenty-Seventh Annual IEEE Applied Power Electronics Conference and Exposition (APEC)*, Orlando, FL, 2012, pp. 1431-1438.
- [125] Y. Yu, G. Konstantinou, B. Hredzak and V. G. Agelidis, "Operation of Cascaded H-Bridge Multilevel Converters for Large-Scale Photovoltaic Power Plants Under Bridge Failures," *IEEE Transactions on Industrial Electronics*, vol. 62, no. 11, pp. 7228-7236, Nov. 2015.

- [126] Y. Yu, G. Konstantinou, C. D. Townsend, R. P. Aguilera and V. G. Agelidis, "Delta-Connected Cascaded H-Bridge Multilevel Converters for Large-Scale Photovoltaic Grid Integration," *IEEE Transactions on Industrial Electronics*, vol. 64, no. 11, pp. 8877-8886, Nov. 2017.
- [127] C. Zhang, S. Du and Q. Chen, "A Novel Scheme Suitable for High-Voltage and Large-Capacity Photovoltaic Power Stations," *IEEE Transactions on Industrial Electronics*, vol. 60, no.9, pp. 3775-3783, Sept. 2013.
- [128] K. Wang, R. Zhu, C. Wei, F. Liu, X. Wu and M. Liserre, "Cascaded Multilevel Converter Topology for Large-Scale Photovoltaic System With Balanced Operation," *IEEE Transactions on Industrial Electronics*, vol. 66, no. 10, pp. 7694-7705, Oct. 2019.
- **PWM Techniques**
- [129] B. McGrath and D. Holmes, "Multicarrier PWM strategies for multilevel inverters," *IEEE Trans. Industrial Electronics*, vol. 49, no. 4, pp. 858-867, August 2002.
- [130] A. Edpuganti, A. K. Rathore, "A survey of low switching frequency modulation techniques for medium-voltage multilevel converters," *IEEE Transactions on Industry Applications*, vol.51, no. 5, pp. 4212-4228, Sept.-Oct. 2015.
- [131] K. Ilves, L. Harnefors, S. Norrga, and H. Nee, "Analysis and operation of modular multilevel converters with phase-shifted carrier PWM," *IEEE Transactions on Power Electronics*, vol. 30, no. 1, pp. 268-283, Jan. 2015.
- [132] A. Elmelegi, M. Aly, E. Ahmed, A. Alharbi, "A simplified phase shift PWM-based feedforward distributed MPPT method for grid-connected cascaded PV inverters," *Solar Energy*, vol.187, pp.1-12, 2019.
- [133] Y. Li, Y. Wang and B. Q. Li, "Generalized Theory of Phase-Shifted Carrier PWM for Cascaded H-Bridge Converters and Modular Multilevel Converters," *IEEE Journal of Emerging and Selected Topics in Power Electronics*, vol. 4, no. 2, pp. 589-605, June 2016.
- [134] Y.M. Chen, C.H. Hsieh and Y.M. Cheng, "Modified SPWM control schemes for three-phase inverters", *4th IEEE International Conference on Power Electronics and Drive Systems. IEEE PEDS 2001 - Indonesia. Proceedings (Cat. No.01TH8594)*, Denpasar, Indonesia, 2001, , vol. 2, pp. 651-656.
- [135] Z. Pa and F.Z. Peg, "A novel SPWM method with voltage balancing capability for multilevel rectifier and inverter systems", *APEC 07 - Twenty-Second Annual IEEE Applied Power Electronics Conference and Exposition*, Anaheim, CA, USA, 2007, pp. 1109-1115.
- [136] W. Yao, H. Hu, and Z. Lu, "Comparisons of space-vector modulation and carrier-based modulation of multilevel inverter," *IEEE Transactions on PowerElectronics*, vol. 23, no. 1, pp. 45-51, Jan. 2008.
- [137] H. Iman-Elini, M. Bakhshizadeh, A. Moeini, "Selective harmonic mitigation-pulse-width modulation technique with variable DC link voltages in single and three-phase cascaded H-bridge inverters," *IET Power Electron.*, vol.7, no.4, pp. 924-32, April 2014.
- [138] Y. Deng, K. H. Teo, C. Duan, T. G. Habetler and R. G. Harley, "A fast and generalized space vector modulation scheme for multilevel Inverters," *IEEE Transaction on Power Electronics*, vol. 29, no. 10, pp.5204-5217, Oct. 2014.
- [139] I. Ahmed, V.B. Borghate, A. Matsa, P. M. Meshram, H. M. Suryawanshi and M.A. Chaudhari, "Simplified space vector modulation techniques for

- multilevel converters,” *IEEE Transactions on Power Electronics*, vol. 31, no.12, pp. 8483-8498, Dec. 2016.
- [140] H. S. Patel, and R. G. Hoft, “Generalized Techniques of Harmonic Elimination and Voltage Control in Thyristor Inverters: Part I--Harmonic Elimination,” *IEEE Transactions on Industry Applications*, vol. IA-9, no.3, pp. 310-317, May 1973.
- [141] H. S. Patel, and R. G. Hoft, “Generalized Techniques of Harmonic Elimination and Voltage Control in Thyristor Inverters: Part II --- Voltage Control Techniques,” *IEEE Transactions on Industry Applications*, vol. IA-10, no. 5, pp. 666-673, Sept. 1974.
- [142] M. Al-Hitmi, S. Ahmad, A. Iqbal, A., S. Padmanaban, “Selective harmonic elimination in a wide modulation range using modified Newton-Raphson multilevel inverter,” *Energies*, vol. 11, no. 2, 458, pp. 1-16, Feb. 2018.
- [143] S. Ahmad, M. Meraj, A. Iqbal, and I. Ashraf, “Selective harmonics elimination in multilevel inverter by a derivative-free iterative method under varying voltage condition,” *ISA Transactions*, vol. 92, pp. 241-256, Sept. 2019.
- [144] B. Ozpinci, L. M. Tolbert, J. Chiasson, “Harmonic optimization of multilevel converters using genetic algorithms,” *IEEE Power Electronics Letters*, vol. 3, no. 3, 92-95, Sept. 2005.
- [145] M. T. Hagh, H. Taghizadeh, K. Razi, “Harmonic minimization in multilevel inverters using modified species based particle swarm optimization,” *IEEE Transactions on Industrial Electronics*, vol. 57, no. 11, pp. 3678-84, Nov. 2010.
- [146] F. J. Filho, L. M. Tolbert, B. Ozpineci, “Real-time selective harmonic minimization for multilevel inverters using genetic algorithm and artificial neural network angle generation,” *IEEE Transactions on Industry Applications*, vol. 47, no. 5, pp. 2117-24, Sept.-Oct. 2011.
- [147] K. Sundareswaran, K. Jayant, and T. N. Shanavas, “Harmonic elimination through a colony of continuously exploring ants,” *IEEE Transactions on Industrial Electronics*, vol. 54, no.5, pp. 2558-65, Oct. 2007.
- [148] A. Kavousi, “Application of the Bee algorithm for selective harmonic elimination strategy in multilevel inverters,” *IEEE Transactions on Power Electronics*, vol.27, no. 4, pp. 1689-96, April 2012.
- [149] M. Balasubramonium, and V. Rajamani, “Design and real-time implementation of SHEPWM in single-phase inverter using generalized Hopfield network,” *IEEE Transaction on Industrial Electronics*, vol. 61, no. 11, pp.6327-6334, Nov. 2014.
- [150] A. Siadatan, M. Fakhari, B. Taheri, and M. Sedaghat, “New Fundamental Modulation Technique with SHE using Shuffled Frog Leaping Algorithm for Multilevel Inverters,” *Evolving Systems*, vol. 11, no. 4, pp. 541-557, Dec. 2020.
- [151] M. Ahmed, A. Sheir, and M. Orabi, “Real-Time Solution and Implementation of Selective Harmonic Elimination of Seven-Level Multilevel Inverter,” *IEEE Journal of Emerging and Selected Topics in Power Electronics*, vol. 5, no. 4, pp. 1700-1709, Dec. 2017.
- [152] S. Kundu, A. D. Burman, S. K. Giri, S. Mukherjee, and S. Banerjee, “Comparative study between different optimisation techniques for finding precise switching angle for SHE-PWM of three-phase seven-level cascaded

- H-bridge inverter,” *IET Power Electronics*, vol.11, no.3, pp. 600-609, March 2018.
- [153] P. Kant, and B. Singh, “Multi-winding transformer Fed CHB Inverter with online switching angle calculation based SHETechnique for VCIMD,” *2019 IEEE International Electric Machines & Drives Conference (IEMDC)*, San Diego, CA, USA, 2019, pp. 1256-1261.
- [154] B. Singh and P. Kant, “Multipulse AC–DC Converter Fed 15-Level Cascaded MLI-Based IVCIMD for Medium-Power Application,” *IEEE Transactions on Industry Applications*, vol. 55, no. 1, pp. 858-868, Jan.-Feb. 2019.
- [155] C. L. Xiong, X. J. Wu, F. Diao, and X. Y. Feng, “Improved nearest level modulation for cascaded H-bridge converter,” *Electron. Lett.*, vol. 52, no. 8, pp. 648–650, Apr. 2016.
- [156] Y. Wang, C. Hu, R. Ding, L. Xu, C. Fu, and E. Yang, “A nearest level PWM method for the MMC in DC distribution grids,” *IEEE Trans. Power Electron.*, vol. 33, no. 11, pp. 9209–9218, Nov. 2018.
- [157] M. H. Nguyen and S. Kwak, “Nearest-Level Control Method With Improved Output Quality for Modular Multilevel Converters,” *IEEE Access*, vol. 8, pp. 110237-110250, 2020.
- [158] X. Chen, J. Liu, S. Song and S. Ouyang, “Circulating Harmonic Currents Suppression of Level-Increased NLM Based Modular Multilevel Converter With Deadbeat Control,” *IEEE Transactions on Power Electronics*, vol. 35, no. 11, pp. 11418-11429, Nov. 2020.
- [159] P. Hu and D. Jiang, “A Level-Increased Nearest Level Modulation Method for Modular Multilevel Converters,” *IEEE Transactions on Power Electronics*, vol. 30, no. 4, pp. 1836-1842, April 2015.
- [160] B.Xiao, L. Hang, J. Mei, C. Riley, L. M. Tolbert, and B. Ozpineci, “Modular Cascaded H-Bridge Multilevel PV Inverter With Distributed MPPT for Grid-Connected Applications,” *IEEE Transactions on Industry Applications*, vol.51, no.2, pp.1722-1731, March-April 2015.

## APPENDIX

The plant and controller of a MATLAB model acts as master and console in RT-LAB environment and OPAL-RT enables it to run at physical clock time. The schematic of the same is shown in Fig.1. Fig. 2 shows auto generated real-time window after successful execution. The high sampling speed of OPAL-RT, makes it a dynamic real time system. Moreover, Table I shows specifications of the real time OPAL-RT simulator.

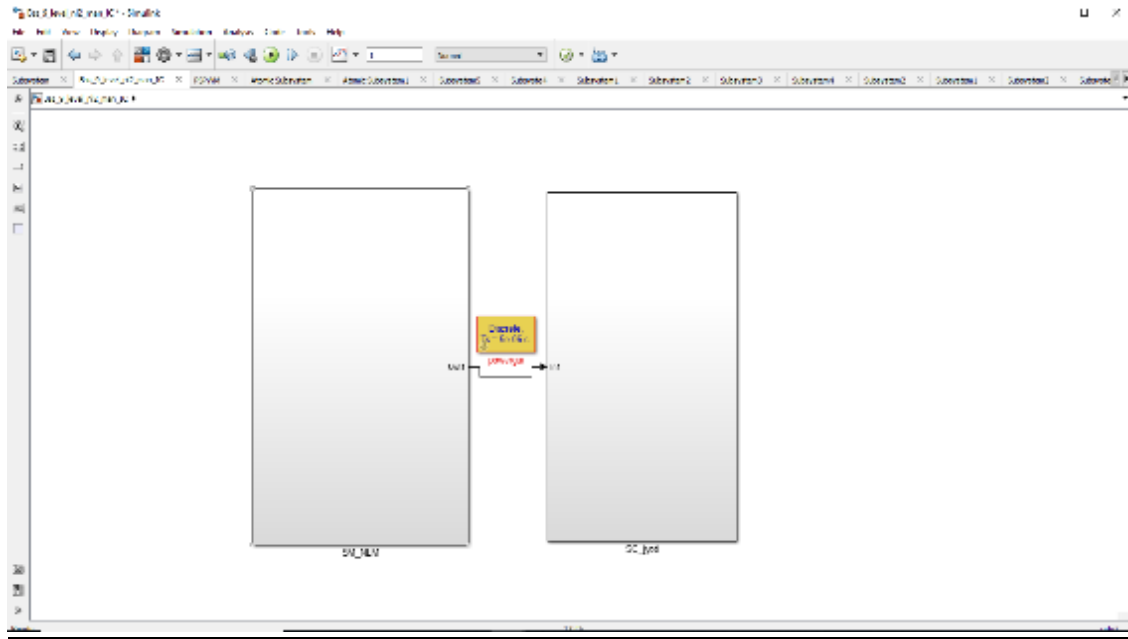


Fig. 1 Schematic of master slave RT-LAB model execution

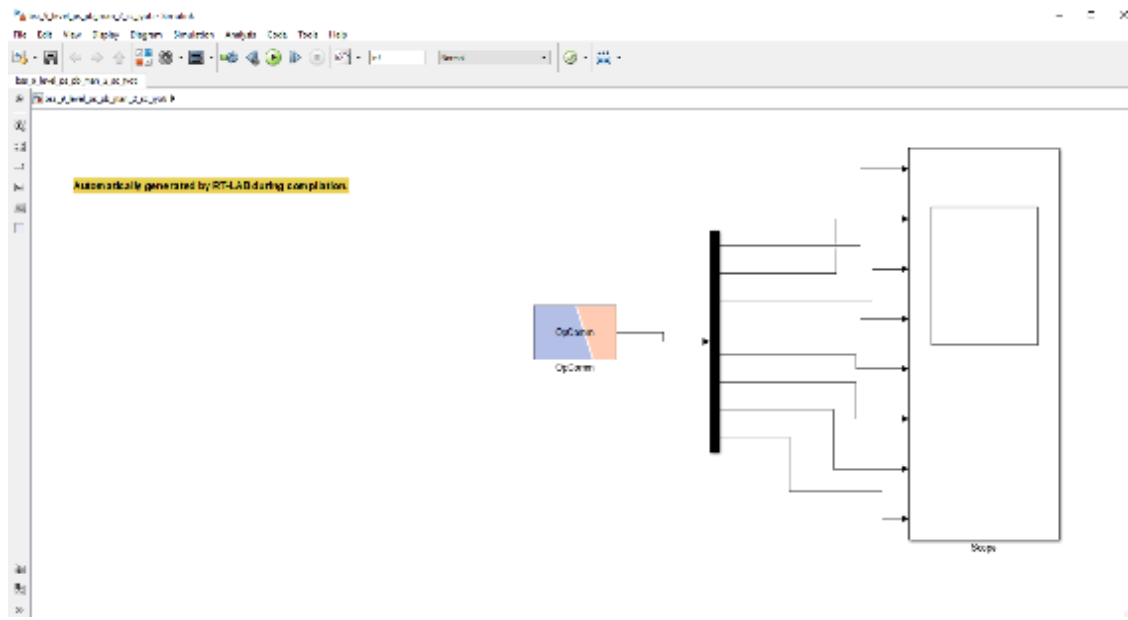


Fig.2 Successfully generated real-time window

**Table 1 : OPAL-RT Specifications**



Features	Hyper-sim Mode	Phasor-sim Mode	FPGA-sim Mode	Mega-sim Mode
Research Areas	Power Sector	Power Sector	Power Sector	Power electronics and Power Sector
Network Size	9000 real time nodes	-	-	9000 real-time nodes
Processing Speed	200 ns-100 $\mu$ s	1-10 ms	200 ns-2 $\mu$ s	200 ns-100 $\mu$ s
Simulation Type	EMT	Phasor	EMT	EMT
Compatible	Simulink and Sim-scape	Simulink, CYME	PLECS, NI-sim, Simulink	Simulink and Sim-scape

Fig.3 shows flowchart of the execution in real time environment. The real time controller blocks named as “OPComm” and “OPController” provide real time acquisition. The large scale solar PV plant is built and code generation is adopted for assessment in real-time.

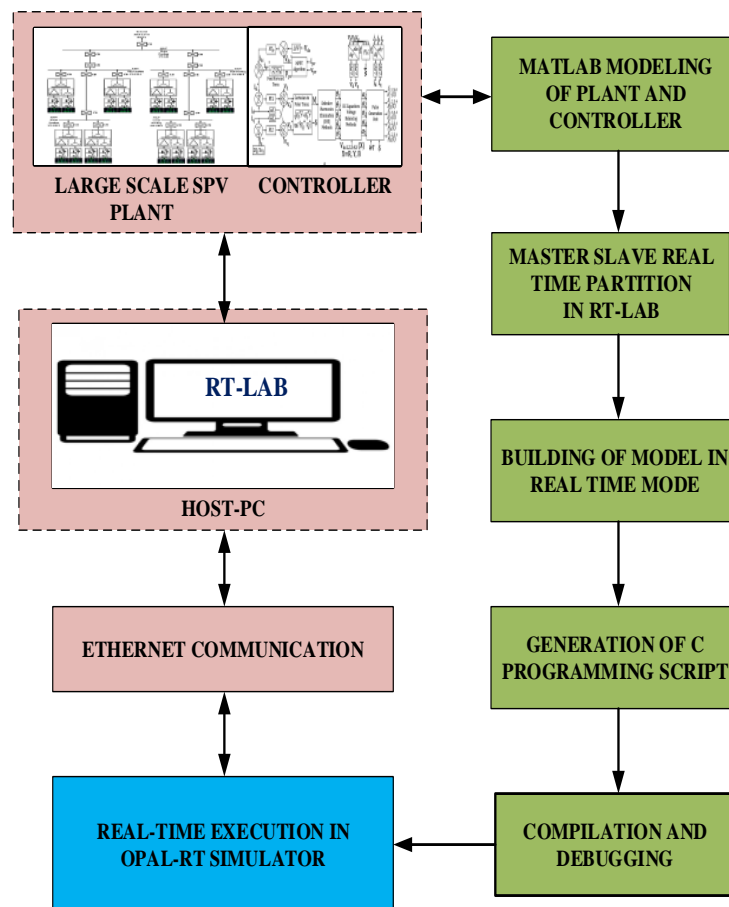


Fig.3 Flowchart of real-time execution

## LIST OF PUBLICATIONS

### ❖ Publications in National/International Journals

1. “Design and Control of Medium-Voltage Multilevel Converter for Direct Grid Integration of Photovoltaic Systems,” Accepted for publication in *J. Inst. Eng. India Ser. B*. Published online: 10<sup>th</sup> November, 2020.
2. “Control and Design of Seven Level Cascaded Multilevel Converter for Transformer-less Large-scale Photovoltaic Integration,” Accepted for publication in *J. Inst. Eng. India Ser. B*. Published online: 27<sup>th</sup> July, 2020. In print now: *J. Inst. Eng. India Ser. B*, Vol. 101, No. 6, pp 623–629 (2020).

### ❖ Under Review

1. “Design and Analysis of Grid Interfaced 43-level CHB Converter for Integrating 10 MW Solar PV Plant” communicated to *IETE Journal of Research*.
2. “Power Quality Improvement of Grid Integrated CHB Multilevel Converter for a SPV Plant by SHE-PWM” communicated to *IETE Journal of Research*.

## **BIODATA**

**NAME:** JYOTI KULKARNI

**DATE OF BIRTH:** 8<sup>TH</sup> SEPTEMBER 1975

**NATIONALITY:** INDIAN

### **QUALIFICATIONS:**

<b>EDUCATIONAL QUALIFICATION</b>	<b>UNIVERSITY/BOARD</b>
M.E (ELECTRICAL – CONTROL SYSTEMS)	PUNE UNIVERSITY
B.E. (ELETRICAL ENGG.)	GWALIOR UNIVERSITY